Long-Term Simulation of Coastal Evolution

Le Xuan, Hoan

2010

LUND UNIVERSITY

ISSN 1101-9824
ISBN 978-91-7473-031-9

Printed by ***MEDIA-TRYCK***, Lund 2010

Le Xuan Hoan

Long-Term Simulation of Coastal Evolution

Report No 1050

WATER RESOURCES ENGINEERING
Lund University, Sweden

Long-Term Simulation of Coastal Evolution

Le Xuan Hoan

Report No. 1050
Lund, Sweden, 2010

Long-Term Simulation of Coastal Evolution

Le Xuan Hoan

Akademisk avhandling som för avläggande av teknologie doktorsexamen vid tekniska fakulteten vid Lunds Universitet kommer att offentligen försvaras vid Institutionen för Bygg- och Miljöteknologi, John Ericssons väg 1, Lund, hörsal V:B, fredagen den 19 november 2010, kl. 10:15.

Academic thesis submitted to Lund University in partial fulfillment of the requirements for the Degree of Doctor of Philosophy (Ph.D. Engineering) will be publicly defended at the Department of Building and Environmental Technology, John Ericssons väg 1, lecture hall V:B, Friday, November 19, 2010, at 10.15 a.m.

Fakultetsopponent/Faculty Opponent: Dr. Nalin Wikramanayake, Department of Civil Engineering, Open University, Sri Lanka.

Organization:	Document name:
LUND UNIVERSITY Water Resources Engineering Box 118, SE-221 00, Lund, Sweden	DOCTORAL DISSERTATION
	Date of issue: October 10, 2010
	Coden: LUTVDG/TVVR-1050 (2010)
Author:	**Sponsoring organization**
Le Xuan Hoan	
Title:	
Long-Term Simulation of Coastal Evolution	

Abstract

There is a strong relationship between regional sediment transport and the local processes at tidal inlets and around coastal structures. Many coastal projects require quantitative understanding of these processes and interactions between them. Regional sediment transport and shoreline evolution models, which include fully important coastal processes at local scale, are lacking at present. The overall aim of this thesis is to develop a new numerical model of regional sediment transport and shoreline evolution for complex conditions with a simulation domain that may extend over hundreds of kilometers and cover several inlets and river mouths, including development of flood shoal and ebb shoal complexes, shoreline response in the vicinity of inlets, barrier elongation, and different shore protection measures.

The new numerical modeling tool is composed of a one-line model of shoreline change, an inlet reservoir model, and a spit growth model. The shoreline change model is based on the one-line theory (Pelnard-Considere, 1956), employing algorithms for the numerical solution developed by Hanson (1987) and including regional shoreline features introduced by Larson *et al.* (2002a). The inlet reservoir model is based on a reservoir analogy approach developed by Kraus (2000, 2002) and then refined by Larson *et al.* (2006) through the introduction of the flood shoal and associated coupling coefficients describing the transfer of sediment between the morphological units. A mathematical model of spit growth and barrier elognation supplied by sediment coming from the longshore sediment transport (LST) was developed based on the spit growth model suggested by Kraus (1999).

In order to realistically reproduce the coastal evolution at local scales, an attempt was made by this study through the introduction of several new methods and modifications to improve the above mentioned models. Fine grain size sediment lost into the deep water was included in the shoreline change model. Wave sheltering effects from the bars was included in the empirical formula for longshore sediment transport. The direction of the ebb jet at inlets was taken into account. Onshore movement of sediment from attachment bars was included in the inlet reservoir model. Relationship between maximum depth of the channel and the depth of active LST was used to estimate LST rate bypassing the spit.

The model was validated against measurements at Hai Hau beach in Vietnam, at the south coast of Long Island in the United States, and at the Badreveln Spit in Sweden. The modeled simulations were generally in good agreement with measurements. The modified formulas and new methods introduced by this study were performing well at these study sites. The model applications show the capability of the model to simulate regional sediment transport and shoreline evolution for complex conditions including several inlets and river mouths, different coastal protection measures, barrier elongation, and shoreline response in the vicinity of inlets.

Key words: Numerical modeling, sediment transport, shoreline response, tidal inlet, inlet shoal, sand bypassing, spit growth

Classification system and/or index terms (if any):

Supplementary bibliographical information — Language: English

ISSN and key title: 1101-9824 — ISBN: 978-91-7473-031-9

Recipient's notes — Number of pages 150 — Price:

Security classification:

Distribution by Division of Water Resources Engineering, Lund University, Box 118, SE-221 00, Lund, Sweden.

WATER RESOURCES ENGINEERING, FACULTY OF ENGINEERING,
LUND UNIVERSITY
CODEN: LUTVDG/TVVR-1050 (2010)

Doctoral Thesis

Long-Term Simulation of Coastal Evolution

By

Le Xuan Hoan

November 2010

Long-Term Simulation of Coastal Evolution

Doktorsavhandling
Teknisk Vattenresurslära
Lunds Tekniska Högskola, Lunds Universitet

Doctoral Thesis
Water Resources Engineering
Department of Building and Environmental Technology
Faculty of Engineering
Lund University

Box 118
SE-221 00 Lund
Sweden

http://aqua.tvrl.lth.se

Cover photo: An image of Hai Hau Beach, Vietnam
Photo: Satellite Image (2001)

CODEN: LUTVDG/(TVVR-1050) (2010)
ISBN: 978-91-7473-031-9
ISSN: 1101-9824
Report No. 1050
Printed in Sweden by Media-Tryck, Lund 2010

ACKNOWLEDGEMENTS

First and foremost I would like to thank my supervisors, professors Hans Hanson and Magnus Larson. Without their continuous support and patient guidance, my scientific knowledge would not have grown to the level where I am today. I learned so much from them during my doctoral study. I am forever deeply indebted for their help.

To the memory of professor Pham Van Ninh who gave me the opportunity to be involved in the Sida /SAREC project as a PhD student at Lund University.

My deep appreciation goes to Prof. Zbigniew Pruszak, Dr. Rafal Ostrowski, Dr. Grzegorz Rozynski, Dr. Shigeru Kato, Dr. Dang Huu Chung, Prof. Do Ngoc Quynh, Prof. Tran Gia Lich, Prof. Dinh Van Uu, Dr. Pham Thanh Nam, Dr. Nguyen Thi Viet Lien, Dr. Dinh Van Manh, and Dr. Phan Ngoc Vinh for their useful discussion and comments; to Dr. Chantal Donnelly, Dr. Bas Van Maren, Prof. Guohong Fang, M.S. Nguyen Van Moi, and M.S. Nguyen Thi Kim Nga for providing measured data and literatures.

I would like to thank all my colleagues at the Institute of Mechanics in Hanoi, the colleagues at Water Resources Engineering, Lund University, and all my friends who helped and encouraged me so much during my doctoral study.

Financial support from the Swedish International Cooperation Development Agency (Sida); the Åke och Greta Lissheds Foundation; and the Ångpanneföreningens Forskningsstiftelse (foundation) are gratefully acknowledged.

I wish to express my heartfelt gratitude to my parents, my brothers, and sisters for their help, encouragement, and continuing support.

Finally, I owe a lot of thanks to Giang Huong, my dear wife, for her extra patience and motivation. To my sweethearts Ngoc Linh and Bao Long, for making my life so joyful. Your love has kept me going. I love you all very much.

ABSTRACT

There is a strong relationship between regional sediment transport and the local processes at tidal inlets and around coastal structures. Many coastal projects require quantitative understanding of these processes and the interactions between them. Regional sediment transport and shoreline evolution models that fully include important coastal processes at local scale are lacking at present. The overall aim of this thesis is to develop a new numerical model of regional sediment transport and shoreline evolution for complex conditions with a simulation domain that may extend over hundreds of kilometers and cover several inlets and river mouths including development of flood shoal and ebb shoal complexes, shoreline response in the vicinity of inlets, barrier elongation and different shore protection measures.

The new numerical modeling tool is composed of a one-line model of shoreline change, an inlet reservoir model, and a spit growth model. The shoreline change model was based on the one-line theory (Pelnard-Considere, 1956), employing algorithms for the numerical solution developed by Hanson (1987) and including regional shoreline features introduced by Larson *et al.* (2002a). The inlet reservoir model is based on a reservoir analogy approach developed by Kraus (2000, 2002) and then refined by Larson *et al.* (2006) through the introduction of the flood shoal and associated coupling coefficients describing the transfer of sediment between the morphological units. A mathematical model of spit growth and barrier elognation supplied by sediment coming from the longshore sediment transport (LST) was developed based on the spit growth model suggested by Kraus (1999).

In order to realistically reproduce the coastal evolution at local scales, an attempt was made in this study through the introduction of several new methods and modifications to improve the above mentioned models. Fine grain size sediment lost into the deep water was included in the shoreline change model through a loss parameter combined with gradients in the LST rate (Donnelly *et al.* 2004). Wave sheltering effects from the bars was included in the empirical formula for LST through an attenuation parameter for breaking wave height in lee of the bars. Direction of ebb jet at inlets was taken into account in the empirical formulas for the distances from the inlet to the downdrift and updrift attachment bars. Onshore movement of sediment from attachment bars was also included in the inlet reservoir model. For the spit growth and barrier elongation model, a relationship between maximum depth of the channel and the depth of active LST was used to estimate LST rate bypassing the spit.

The model was validated against measurements at Hai Hau beach in Vietnam, at Long Island coast in the United States, and at the Badreveln spit in Sweden. At the Hai Hau beach, a 20-year time series of offshore waves hindcasted from the recorded wind data was used to reproduce the nearshore wave climate; measured shorelines in 1910, 1965, and 2000 were employed to calibrate and validate the model. At the Long Island coast, hindcast wave data of 20-year time series from three WIS stations along the coast was used as input for the model; measured shorelines in 1933 and 1983, measured volume growth of the flood shoals and ebb shoal complexes at several occasions between 1931 and 1998, net longshore transport estimated from measurements, and measured barrier elongation, were used to compare with the modelled simulations. At the Badreveln spit, measured spit

locations at a number of occasions from 1860 to 1994 were used to compared with the analytical solution of the model.

The model simulations were generally in good agreement with the measurements. The modified formulas and new methods introduced by this study were performing well at these study sites. The modelled results show that fine sediment lost into the deep water and gradients of the LST are main causes of the severe erosion at Hai Hau beach; onshore sediment transfer and wave sheltering effects from the attachment bars are main contributions to produce the salient-type feature in the downdrift areas of the inlets; dredging work to maintain the navigational channel at the Fire Island Inlet located at the south end of the Long Island coast is the main reason for the barrier stable period connected with the period of dredging from 1954 to 1994. The model applications show the capability of the model to simulate regional sediment transport and shoreline evolution for complex conditions including several inlets and river mouths, different coastal protection measures, barrier elongation, and shoreline response in the vicinity of inlets.

APPENDED PAPERS

I. **Hoan, L.X.,** Hanson, H., Larson, M., Donnelly, C., and Nam, T.P. (2010). Modeling Shoreline Evolution at Hai Hau Beach, Vietnam. *Journal of Coastal Research,* 26(1), 31-43.

II. **Hoan, L.X.,** Hanson, H., Larson, M., and Nam, T.P. (2010). Modeling regional sediment transport and shoreline response in the vicinity of tidal inlets on the Long Island coast, United States. *Coastal Engineering.* (Submitted)

III. **Hoan, L.X.,** Hanson, H., and Larson, M. (2010), A mathematical model of spit growth and barrier elongation. *Marine geology.* (Submitted)

IV. Larson, M., **Hoan, L.X**., and Hanson, H. (2010). A direct formula to compute wave height and angle at incipient breaking. *Journal of Waterway, Port, Coastal, and Ocean Engineering*, 136(2), 119-122.

V. Nam, T.P., Larson, M., Hanson, H., and **Hoan, L.X**. (2009). A numerical model of nearshore waves, currents and sediment transport. *Coastal Engineering* 56(2009), 1084-1096.

VI. Nam, T.P., Larson, M., Hanson, H., and **Hoan, L.X**. (2010). A numerical model of beach morphological evolution due to waves and currents in the vicinity of coastal structures. *Coastal Engineering.* (Submitted)

RELATED PUBLICATIONS

I. **Hoan, L.X.,** Hanson, H., Larson, M., and Nam, P.T. (2010). Modeling shoreline response and inlet shoal volume development on the Long Island coast, United States. *The 32nd International Conference on Coastal Engineering* (Shanghai, China).

II. **Hoan, L.X,** Hanson, H., and Larson, M. (2007). Numerical modeling of sediment transport and long-term shoreline evolution at Hai Hau beach, Vietnam. *Proceeding of 8th National Conference on Fluid Mechanics* (Hanoi, Vietnam), Vol. 3, p. 245-258.

III. **Hoan, L.X**. (2006). Some results of comparison between numerical and analytic solutions of the one-line model for shoreline change. *Vietnam Journal of Mechanics,* Vol. 28, No.2, pp. 94-102.

IV. **Hoan, L.X**., and Nam, P.T. (2005). Two dimension numerical modeling of wave and wind induced currents and bed morphology evolution at Phan Ri-Binh Thuan coastal zone. *Vietnam Journal of Mechanics,* Vol. 27, No.2, pp. 96-106.

V. **Hoan, L.X**., and Hung, N.M. (2003). A two dimension numerical model for waves induced currents in coastal zone, *Vietnam Journal of Mechanics,* Vol. 26, No.2, pp. 113-121.

AUTHOR'S CONTRIBUTION TO THE APPENDED PAPERS

All the work described in this thesis was performed under the supervision of professor Hans Hanson and professor Magnus Larson.

Paper 1: performed the numerical modeling work, collected measured data, ran the model, analyzed the modeled results and wrote all sections of the paper.

Paper 2: performed the numerical modeling work, collected measured data together with co-authors, ran the model, analyzed the modeled results and wrote all sections of the paper.

Paper 3: performed development of the mathematical model and numerical modeling work, collected measured data together with co-authors, analyzed the modeled results and wrote all sections of the paper.

Paper 4: performed the model calculation, analyzed the results and wrote the paper together with co-authors.

Paper 5 and 6: checked the papers, discussed the modeled results, and provided comments on the modeling approach.

CONTENTS

1. Introduction

1.1 Background and identification of the problem

Coastal regions are home to a large and growing proportion of the world's population. They provide significant natural resources, transportation, commercial, and tourism benefits to communities and the nation. However, many coastal regions are being subjected to many attacks from the ocean as well as interaction between the land and the sea. One of the most striking impacts are sediment transport and coastal evolution, resulting in risks to the ecosystem, natural resources, and economic operations. Coastal projects aiming at developing a strategy for sustainable development in coastal regions and barrier islands call for long-term simulation of coastal evolution covering fully primary interactions between processes at regional and local scales.

Under wave action combined with longshore currents in the coastal zone, sediment transport and shoreline evolution may occur at regional scale extending from tens of kilometers to hundreds of kilometers. Gradients in the LST rate alter the shoreline shape, resulting in areas of erosion and accretion (Larson *et al.*, 2002b). The gradients and character of the regional LST may be modified by processes at local scale. For example, the LST may be trapped by inlet or river flows and then transferred to the downdrift through the flood shoal and ebb shoal complexes; jetties and groins can block the LST resulting in an accretion on the updrift side and erosion on the downdrift side. Morphology change and shoreline response at local scale are, in turn, governed by the magnitude and direction of the regional net transport rate such that an inlet navigation channel may be shoaling from deposited sediment coming from the LST; depending on direction and magnitude of the net sediment transport, a spit can occur at one side or both side of a inlet, resulting in migration of the inlet channel; and so on. Thus, there are strong interactions between the processes at regional and local scales. Many coastal projects call for regional sediment transport and shoreline change models covering a coastal stretch with several inlets and different engineering activities. This model class is lacking, and some important processes at local scales have not been investigated in existing regional shoreline change models.

A wide range of models to calculate sediment transport and morphological evolution has been developed during the last 20 years and successfully applied in engineering studies conducted to solve a variety of problems in coastal areas. Such problems include:

- sedimentation in navigation channels,
- beach topography change in the vicinity of coastal structures,
- scour adjacent to coastal structures,
- impact on dunes during severe storms,
- overwash of dunes and barrier islands,
- design of beach nourishment operations,
- assessment of large-scale coastal evolution,
- sediment bypassing inlets and inlet shoal complex development,

- spit growth and inlet channel migration.

To address these problems, several prominent numerical models of sediment transport and morphological evolution have been developed as joint research efforts between the Water Resources Engineering (WRE), Lund University (LU), Sweden, and the Coastal and Hydraulics Laboratory (CHL), US Army Engineer Research and Development Center, USA. Examples of such models are the shoreline change model GENESIS, the profile response model SBEACH, and the large-scale coastal evolution model CASCADE. Furthermore, WRE has assisted CHL in the development of a basic sediment transport model that has been included in the Coastal Modeling System (CMS) for detailed analysis of the morphological evolution around inlets. The Coastal Inlets Research Program (CIRP) being conducted at CHL has also developed a three-dimensional version of this model. Researchers at WRE have provided several of the fundamental components in the RMAP (Regional Morphology Analysis Package) model, which is used to analyze data on shorelines and beach profiles. GENESIS and SBEACH have been employed in numerous engineering projects by the US Army Corps of Engineers, as well as by researchers and consultants in projects world-wide. Both these models are regarded as being among the foremost for their particular type of application. CASCADE and CMS are at the cutting edge of modeling technology and it is expected that they will be frequently used in projects in the near future.

Although significant progress has been made in mathematical modeling of sediment transport and morphological evolution in recent years through the above-mentioned models, further development and validation of the models are needed to extend capabilities and improve predictive skills. GENESIS and SBEACH represent models that apply mature, well-proven technology that has been validated through many research studies and engineering projects. However, development of various modeling capabilities is still needed and useful to enhance the applicability of the models. CASCADE and CMS are models under development and testing that need more validation before they can yield reliable and robust predictions in complex coastal environments such as around inlets. The RMAP model is frequently used to manipulate and analyze survey data from coastal areas. So far, the focus of the RMAP development has been on shorelines and beach profiles, whereas only limited effort has been directed towards analyzing complete topographies.

In the following, a summary is provided for each of the above mentioned models focusing on the purpose of the model and its present state of development.

1.2 Model review

GENESIS

Kraus *et al*. (1984) and Hanson and Kraus (1986) developed a one-line model with the overall aim to arrive at a model which could be used as an engineering tool. This was the first step towards a general shoreline evolution model that was named GENESIS (Hanson 1989). A shoreline-change model predicts shoreline position changes that occur over a period of several years. Cross-shore transport effects, such as storm-induced erosion and cyclical movement of shoreline position as associated with seasonal variation in wave climate, are assumed to cancel over a long simulation period. The model is generalized in

that it allows simulation of a wide variety of user-specified offshore wave inputs, initial beach configurations, coastal structures, bypassing operations, and beach fills. Input to the model is the nearshore bathymetry and a time series of wave height, period, and direction. Based on these data, the model calculates breaking wave conditions, sediment transport rates, and shoreline positions.

Most GENESIS applications involve analysis and design of structures or beach nourishments, although in recent applications the model has been extended to describe the transport pattern and shoreline response around inlets. GENESIS has become a standard tool applied by the U.S. Army Corps of Engineers (USACE), consulting engineering companies, and universities world wide. The model is incorporated into two of CHL's software packages: the *Coastal Engineering Design and Analysis System* (CEDAS) and the *Shoreline Modeling System* (SMS), both developed for the PC environment. GENESIS has been applied at numerous project sites including stretches of coasts in Alaska, California, Louisiana, New Jersey, New York, Texas, and Florida (Chu *et al.* 1987; Kraus *et al.* 1988, Gravens *et al.* 1989, Hanson *et al.* 1990). A full compilation of all GENESIS applications would be impossible to assemble because of the large number copies distributed. However, GENESIS is only applicable where the boundary conditions can be specified, namely, at a groin, jetty, or a uniformly (known) changing shoreline position. Recently, a modified version of GENESIS was developed where sediment transport by tidal currents and/or wind induced current are included (Hanson *et al.* 2001, Bayram *et al.* 2007, Hanson *et al.* 2006).

SBEACH

Mathematical modeling of beach-profile change has seen substantial advances since the first attempts by Swart (1974, 1976) and Vellinga (1982). Major advances were made by Kriebel (1982) and Kriebel and Dean (1985) in modeling storm-induced beach erosion and by Larson and Kraus (1989) in development of the SBEACH model supported by CHL. This model has undergone substantial refinement (Larson *et al*. 1990), including detailed description of waves and sediment transport under random waves (Wise *et al*. 1996), the capability to model hard bottoms (Larson and Kraus 1998), dune overtopping (Kraus and Wise 1993, Wise and Kraus 1993, Larson *et al*. 2004, Donnelly *et al*. 2005), and extensive comparisons with laboratory and field data (Wise *et al*. 1996). The SBEACH model is also a standard tool applied by the USACE, consulting engineering companies, and universities world wide. SBEACH is not applicable to beaches near inlets because the profile there is irregular and not solely molded by waves. However, equilibrium concepts as frequently employed in cross-shore sediment transport and profile evolution may often be transferred to other, more complex, morphological systems (Larson *et al*. 1999).

SBEACH was primarily developed to calculate the profile response during a storm, although the model can qualitatively reproduce post-storm recovery and seasonal changes in the profile shape. The model also describes the formation and movement of longshore bars, at least the bar associated with the main break point of the waves. SBEACH has been widely used both as an analysis tool in studies on coastal processes and as an instrument for design of beach nourishment operations to protect against erosion and flooding. The model is under constant development and model components are being replaced and introduced as research

on nearshore processes and beach profile change progresses. SBEACH was originally developed and validated using data from large wave tank experiments (prototype-size; see Larson and Kraus 1989). Then, extensive model testing has been performed against field data, primarily from the US East Coast (Larson and Kraus 1989, Larson *et al*. 1990, Wise *et al*. 1996). High-quality field data sets involving the effect of severe storms, such as hurricanes or northeasters, on several different beaches have been used in the model testing. SBEACH has been shown to produce reliable predictions of storm impacts in terms of the nearshore profile shape, eroded sediment volume, and contour recession. The model has often been employed in studies on coastal processes where the impact of large storms needs to be assessed. Another principal application of SBEACH has been in the design of beach fills and the response of the beach to hard structures such as seawalls and revetments (Larson and Kraus 1998). SBEACH is used to calculate beach profile response of alternative design configurations to storms of varying intensity. Model predictions of beach erosion are used to estimate with- and without-project storm damages over the project design life. In the design process, storm erosion, flooding, and wave damage estimates are utilized in economic analyses to compare total project costs and total project benefits for each design alternative.

CASCADE

CASCADE simulates longshore sediment transport and coastal evolution at the regional and local scale (Larson *et al*. 2002a, Larson and Kraus 2003, Larson *et al*. 2006). A typical coastal setting to which CASCADE may be applied is barrier islands separated by inlets with and without jetties, where the sediment is transferred around inlets through the inlet-shoal complex. Sediment sources and sinks can be included, such as cliff erosion and wind-blown sand. The shoreline of the barrier island chain may display a curved trend at the regional scale with local variations in between the inlets. At present, the CASCADE model contains modules to simulate shoreline evolution (taking into account regional trends), evolution of flood shoal and ebb-shoal complexes and bypassing of sediment at inlets (Kraus 2000), and sediment supplies and losses (e.g., beach nourishment, cliff erosion, wind-blown sand, and sediment mining). Several of its modules have required development of new theory and numerical approaches (e.g., rapid calculation of breaking wave properties, generalized longshore sediment transport formula, and bypassing algorithms). The model has been validated for the eastern reach of Long Island, New York, containing three inlets (Larson *et al.* 2002a), and for the Delmarva Peninsula where two inlets are present (Larson and Kraus 2003). Recently the model was enhanced with respect to the inlet shoal modeling and to the simulation of dune erosion and overwash (Larson *et al*. 2006).

CMS-FLOW

The two-dimensional depth-averaged circulation model (CMS-FLOW) was developed under the CIRP with the purpose of being able to conduct practical projects at coastal inlets (Militello *et al*. 2004, Buttolph *et al*. 2006). CMS-FLOW is a hydrodynamic model intended for local applications, primarily at inlets, the nearshore, and bays. CMS-FLOW is computationally efficient, easy to set up, and has features required for many coastal engineering applications. CMS-FLOW can be coupled to regional circulation models, such as the ADvanced CIRCulation (ADCIRC) model (Luettich *et al*. 1992), through boundary conditions, providing flexibility for large-scale applications and connectivity between

models. At the same time, the code is accessible to CIRP researchers with expertise in areas other than computational fluid dynamics, as expected in interdisciplinary teams. Recently, sediment transport was added in CMS-FLOW, including the option of selecting between several different formulas and the possibility to employ the advection-diffusion equation for simulating horizontal exchange of suspended material (Buttolph *et al*. 2006). One of the formulas available in CMS-FLOW with sediment transport (denoted as CMS-SED) is the Lund-CIRP formulas developed in a research project sponsored by CHL (Camenen and Larson, 2005, 2007, 2008). A capability to represent non-erodible bottom was recently introduced to CMS-SED, making the model applicable to coastal inlets where the sea bottom may be covered by hard or non-erodible material, which in turn may or may not be covered by a layer of sediment (Hanson and Militello 2005). Work is also underway to include swash-zone sediment transport and shoreline change in CMS-SED, which is essential for modeling topographic evolution in coastal areas. Algorithms as described above can be readily ported to the 3D version of CMS-SED.

1.3 Objectives of the research

The overall objective of this study was to develop a general numerical model of regional sediment transport and coastal evolution for complex conditions including inlet shoal development, cross-sectional area of inlets varying substantially with time, shoreline response in vicinity of inlets, barrier island elongation, and different coastal protection measures. Main focuses of the model are to simulate:

- regional sediment transport and shoreline evolution with simulation domains that extend over hundreds of kilometers and cover several inlets and river mouths,
- shoreline response in vicinity of inlets and river mouths,
- sand volume growth of flood shoals and ebb shoal complexes,
- spit growth and barrier elongation supplied by sediment coming from the LST.

1.4 Thesis structure and appended papers

This thesis consists of two parts: a summary and six appended papers. In the summary overall background, identification of the problems, model review, methodology, and the model applications are presented. Details of the study sites, model setup, results and discussion can be found in the appended papers. Finally, conclusions from this study are given at the end of the summary.

The study results are presented in the following papers:

Paper 1: presents the numerical modeling of shoreline change and the model application for simulating the shoreline evolution at Hai Hau beach, Vietnam. Detailed environmental conditions at the study site and nearshore wave calculation are discussed in this paper. In this study, the major aim of the model application was to investigate the causes of the severe erosion here. Some conclusions regarding the reasons for the erosion were drawn in this paper.

Paper 2: documents the numerical modeling of shoreline change combined with the inlet reservoir model. Model applications to simulate regional sediment transport, shoreline response in vicinity of the tidal inlets, and inlet shoal volume development at the Long island coast, United States, are presented. Several modifications and new methods to realistically simulate erosion and accretion in the downdrift areas of the inlets were introduced in this paper. Details concerning natural conditions and model setup for the study site are also described.

Paper 3: presents the mathematical model of spit growth and barrier elongation. Ratio of maximum depth of the inlet channel and depth of active longshore transport used to estimate LST rate bypassing the spit was introduced. Model applications to reproduce the barrier elongation at Fire Island Inlet on south Long Island coast in the United States, and at Badreveln spit in Sweden are discussed in this paper.

Paper 4: introduces a direct formula to compute wave height and angle at incipient breaking. Comparison of calculation time between the new formula and the standard iterative method is presented.

Paper 5 and paper 6: discussed simulation of wave propagation, currents, sediment transport, and morphology change using a 2-D numerical model.

2. Methodology

The numerical model development mainly focused on simulating regional sediment transport and shoreline evolution due to waves and currents, local shoreline response in the vicinity of inlets, development of the inlet shoal volumes as well as spit growth and barrier elongation supplied by sediment coming from the LST. Thus, main components of the model were composed from three sub-models: a one-line model of shoreline change, an inlet reservoir model, and a spit growth model. In addition, a 2-D wave transformation model was employed to simulate the inshore wave climate used as input for the model. The basics of the model components are described below where some of the components were developed as a part of this thesis, whereas others were based on previous work.

2.1 Nearshore 2-D wave transformation

In this study, a 2-D wave transformation model called EBED was applied to calculate the inshore wave climate. The EBED model was developed by Mase (2001) based on the energy-balance equation for multidirectional random waves taking into account wave shoaling, refraction, diffraction, and wave breaking. Advantages of using the EBED model include the ability to reproduce wave transformation over complicated bathymetry and the facilities for setting up the input and output for many different wave spectra. The long-time hindcast time series of offshore waves was used as input data for the EBED model in order to reproduce the nearshore wave climate at the study sites. The output from the EBED model includes significant wave height, significant wave period, and wave direction.

2.2 Shoreline change model

2.2.1 Basic assumptions and governing equations

Hanson (1987) documented that a common observation recognizes that the beach profile maintains an average shape that is characteristic of the particular coast. For example, beaches retain their average slope in a comparative sense and in the long term. Although seasonal changes in wave climate cause the shoreline position to move shoreward and seaward with corresponding changes in shape and average slope of the profile, the deviation from an average beach slope over the total active profile is relatively small over a long-term period of consideration. Pelnard-Considere (1956) was the first to formulate a mathematical model of shoreline response to wave action under the assumption that the beach profile maintains a constant shape at all times. If the profile shape does not change, any point on it can be employed to specify the location of the entire profile with respect to a baseline. Thus, one contour line can be used to describe changes in the beach plan shape, and the model is therefore called the “one-line” model. The theoretical work of Pelnard-Considere is the basis for many numerical models that have been successfully applied to simulate shoreline response to wave and current actions (Hanson, 1987; Hanson and Kraus, 1989; Hanson *et al*., 2006). To derive the governing equation of shoreline change from the one-line theory, the following standard assumptions are employed (Hanson, 1987):

- the shape profile shape is constant,

- the shoreward and seaward limits of the profile are constant,
- sand is transported alongshore by the action of breaking waves,
- the detailed structure of the nearshore circulation is ignored,
- there is a long-term trend in shoreline evolution.

In this study, the shoreline change modeling is based on the one-line theory, employing algorithms for the numerical solution developed by Hanson (1987). Conservation of sediment volume yields the fundamental equation to be solved for obtaining the shoreline change. A local coordinate system is employed, where the *y*-axis points offshore and the *x*-axis is oriented parallel to the main trend of shoreline (see Fig. 1). It is assumed that the beach profile moves parallel to itself seaward or shoreward depending on the net rate of sand entered or exited a cross section over a time interval Δt. The change in shoreline position is Δy, the length of shoreline segment is Δx, and the profile moves within a vertical extent defined by the berm elevation D_B, and the depth of closure D_C, both measured from a vertical datum. The net volume change due to the gradient in the LST rate over the time interval unit is $\Delta Q\Delta t = \left(\partial Q/\partial x\right)\Delta x\Delta t$. Another contribution may come from a line source or sink of sand $q = q_s + q_o$, where q_s and q_o represent for a volume of sand added or removed per unit width of beach from shoreward side and offshore side, respectively. These produce a volume change of the beach that gives $\Delta V_{beach} = \Delta x\Delta y\left(D_B + D_C\right) = \left(\partial Q/\partial x\right)\Delta x\Delta t + q\Delta x\Delta t$. Rearrangement of the terms and taking the limit as $\Delta t \to 0$ yields the governing equation for the rate of change in shoreline position (Hanson, 1987):

$$\frac{\partial y}{\partial t} + \frac{1}{(D_B + D_C)}\left[\frac{\partial Q}{\partial x} + q\right] = 0 \qquad (1)$$

In order to solve Eq. 1, the initial shoreline position together with boundary conditions and values for D_B, D_C, q, and Q must be specified.

The quantity D_B and D_C can be estimated based on a long-term measurement of the beach profile or based on empirical parameters determined from statistical wave parameters at the study site (see Hanson, 1987).

The quantity q represents a line source or sink of the sand in the system such as wind-blown sand, sand discharge from rivers and tidal inlets, cliff erosion, and sand lost into the deep water.

Hanson *et al.* (2006) developed a general relationship for the total LST rate that includes currents generated by tide and wind based on the Inman and Bagnold (1963) formula. Suspended sediment is assumed to be the dominant mode of transport. Breaking waves in the surf zone stir up sediment and maintain an average concentration determined through a balance between the energy supplied from breaking waves and the work required to keep the sediment suspended. The product of the longshore current and the sediment concentration integrated across the profile yields the total longshore transport. The

empirical predictive formula for the total longshore sand transport employed in this study is expressed as follows (Hanson *et al.,* 2006),

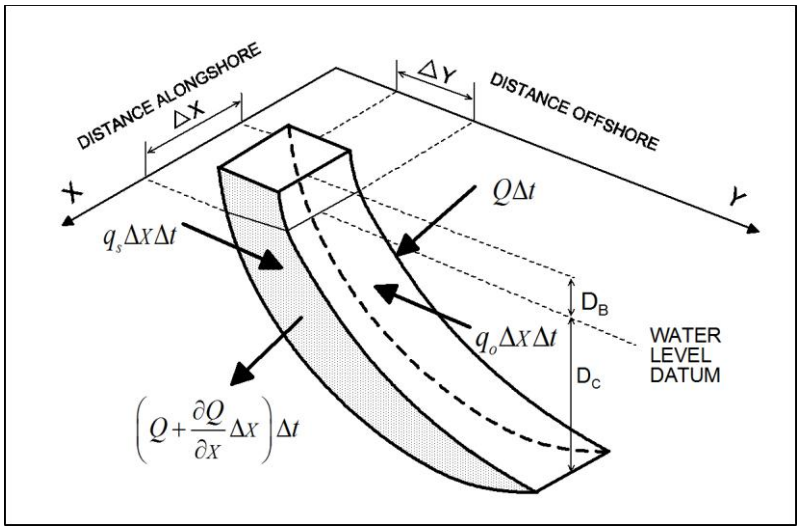

Fig. 1. Definition sketch for shoreline change calculation (Hanson, 1989).

$$Q = \frac{\varepsilon}{8(\rho_s/\rho - 1)(1-p)w_s} H_b^2 C_{gb} \cos\alpha_0 \left[K_1 \left(a_1 \sin\alpha_0 + \overline{V_{ex}} \right) - K_2 a_2 \right] \tag{2}$$

in which, $a_1 = \frac{5}{32}\frac{\pi\chi}{c_f}\sqrt{g}A^{\frac{3}{2}}$; $a_2 = \frac{\pi}{C_f \chi^2}\sqrt{g d_b}\frac{\partial H_b}{\partial x}$ and $A = 2.25\left(\frac{w_s^2}{g}\right)^{\frac{1}{3}}$

where: H = wave height; d = water depth; C_g = wave group celerity; b = subscript denoting breaking wave condition; K_1, K_2 = empirical coefficients (treated as calibration parameters); ρ_s = density of sand; ρ = density of water; p = porosity of sand on the bed; w_s = fall velocity; $\overline{V_{ex}}$ = external surf-zone average longshore current velocity generated by tide or/and wind; A = shape parameter; χ = breaker index; g = acceleration due to gravity; c_f = bottom friction coefficient; ε = transport coefficient expressing efficiency of the waves keeping sand grains in suspension, which can be estimated through physical parameters as (Bayram *et al.*, 2007), $\varepsilon = \left(4.0 + 9.0\frac{H_b}{w_s T_p}\right)\times 10^{-5}$; T_p = peak wave period; and α_0 = angle of breaking waves to the local shoreline orientation given by (see Fig. 2),

$$\alpha_0 = \alpha_b - \alpha_s = \alpha_b - \arctan\left(\partial y/\partial x\right) \tag{3}$$

where α_b is the angle between breaking wave crests and the x-axis, α_s is the angle between the shoreline and the x-axis.

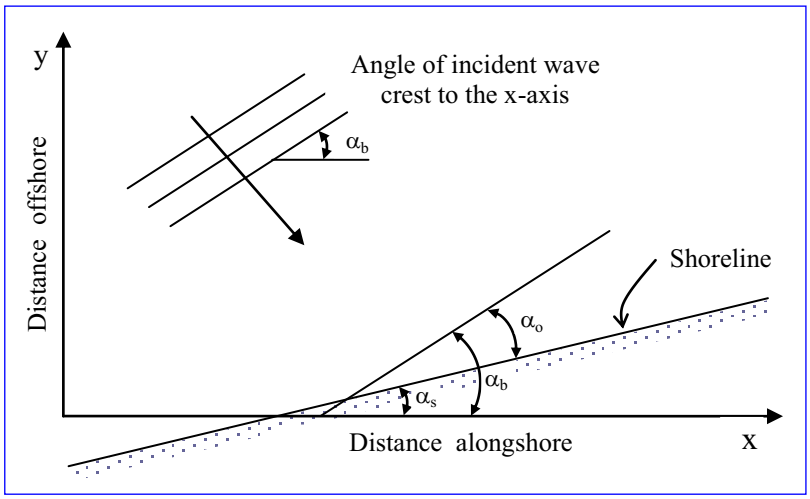

Fig. 2. Definition of breaking wave angle (Hanson, 1989).

2.2.2 Analytic solution technique

Under certain idealized wave conditions and simple shoreline configurations, Eq. 1 can be reduced to the one-dimensional heat diffusion equation, which can be solved analytically. Application of the analytical solution for a real environment may involve considerable errors due to violation of these limitations. However, the analytical solutions are often used to investigate the qualitative features and the properties of shoreline change. A numerical model of shoreline change would be more useful to satisfy the requirements for real situations.

If we neglect the external longshore current ($\overline{V_{ex}}$) and the LST component produced by gradient of longshore breaking wave height ($\partial H_b / \partial x$), Eq. 2 is reduced to a simple form as,

$$Q = Q_0 \sin(2\alpha_0) \tag{4}$$

where

$$Q_0 = \frac{\varepsilon K_1 a_1}{16(\rho_s/\rho - 1)(1-p)w_s}\left(H_b^2 C_{gb}\right) \tag{5}$$

For beaches with mild slope, it can be assumed that the breaking wave angle to the shoreline is small. In this case, $\sin(2\alpha_o) \approx 2\alpha_o$. If also the angle between the shoreline

and the x-axis, is assumed to be small, then $\arctan(\partial y/\partial x) \approx \partial y/\partial x$. From Eq. 3, $\alpha_0 \approx \alpha_b - \partial y/\partial x$. Eq. 4 can be rewritten as (Larson *et al.*, 1987),

$$Q = 2Q_0\left(\alpha_b - \frac{\partial y}{\partial x}\right) \tag{6}$$

If the amplitude of the longshore sand transport rate Q_0 as well as the breaking wave angle α_b is assumed independent of x and t, and with negligible contributions from sources or sinks ($q = 0$), Eqs. 1 and 6 can be rewritten as,

$$\frac{\partial y}{\partial t} = \xi \frac{\partial^2 y}{\partial x^2} \tag{7}$$

where $\xi = \frac{2Q_0}{(D_B + D_C)}$ (8)

Eq. 7 is analogous to the one-dimensional heat diffusion equation and it can be solved analytically for different initial and boundary conditions. The coefficient, ξ, can be interpreted as a diffusion coefficient expressing the time scale of shoreline change following a disturbance (wave action). A high value of the amplitude of the sand transport rate results in a rapid shoreline response, while a larger depth of closure, meaning that the longshore transport will be distributed over a larger portion of the beach profile, leads to a slower shoreline response.

2.2.3 Numerical solution technique

The Eqs. 1-2 can also be solved numerically. Then, the limitations in the analytical solution will be avoided, making it possible to apply the numerical model for complex conditions of coastal configuration and a more realistic wave climate.

Eqs. 1-2 are discretized on a staggered grid in which shoreline positions y_i are defined at the centre of the grid cells and transport rates Q_i at the cell walls (see fig. 3). The Crank-Nicholson implicit scheme is used in which the derivative $\partial Q/\partial x$ at each grid point is expressed as an equally weighted average between the present time step and the next time step (Hanson, 1987),

$$\frac{\partial Q_i}{\partial x} = \frac{1}{2}\left[\frac{Q'_{i+1} - Q'_i}{\Delta x} + \frac{Q_{i+1} - Q_i}{\Delta x}\right] \tag{9}$$

where the prime ($'$) is used to denote a quantity at the new time level, whereas the unprimed quantity indicates a value at the present time step, which is known.

Substituting of Eq. 9 into Eq. 1 and linearizing the wave angle in Eq. 2 in terms of $\partial y/\partial x$ results in two systems of coupled equations for the unknowns y'_i and Q'_i:

$$y_i' = M'\left(Q_i' - Q_{i+1}'\right) + yc_i \tag{10}$$

$$Q_i' = E_i\left(y_{i+1}' - y_i'\right) + F_i \tag{11}$$

where $M' = \Delta t/2(D_B + D_C)\Delta x$ and yc_i are the functions of known quantities, including Q_i, q_i and y_i, and where F_i and E_i are functions of wave height, wave angle, and other known quantities.

Substituting Eq. 10 into Eq. 11 results in three-diagonal system, and it can be solved by the Thomas method:

$$-F_i Q_{i-1}' + S_i Q_i' - F_i Q_{i+1}' = G_i \tag{12}$$

where $S_i = 2F_i - \dfrac{\Delta x}{B'}$ and $G_i = \dfrac{\Delta x}{M'}\left[\dfrac{y_{i+1} - y_i}{\Delta x}F_i - E_i - \dfrac{F_i}{\Delta x}\left(yc_i - yc_{i-1}\right)\right]$

The initial condition is taken to be $y_i = y_{(x_i,0)}$ where $y_{(x_i,0)}$ is the initial shoreline position.

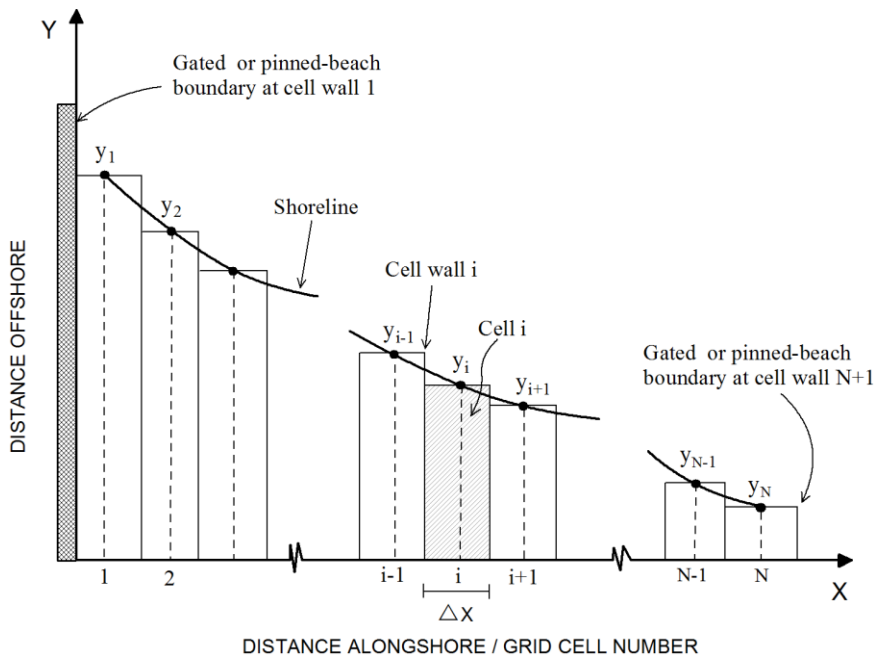

Fig. 3. A coordinate system and grid used by the numerical model (Hanson, 1987).

The most commonly used boundary condition at both lateral boundaries is expressed as $\partial Q/\partial x = 0$ (Hanson, 1987) or $Q = 0$. By Eq. 1, if $\partial Q/\partial x = 0$ at the boundaries and with

negligible sources or sinks, then $\partial y/\partial t = 0$, indicating that y does not change. The above boundaries should be located far away from the project to assure that the conditions in the vicinity of the boundary are unaffected by changes that take place in the project.

2.2.4 Regional scale effect

The effect of a regional shoreline shape enters in Eq. 3 by assuming that the local shoreline evolves with respect to the regional shoreline (Larson *et al.*, 2002a), (see Fig. 4), yielding a new expression for α_0,

$$\alpha_0 = \alpha_{br} + \alpha_b - \arctan\left(\partial y/\partial x\right) \tag{13}$$

where $\alpha_{br} = \arctan\left(\partial y_r/\partial x\right)$ and y_r denotes the regional shoreline, which is taken to be constant over the simulation period.

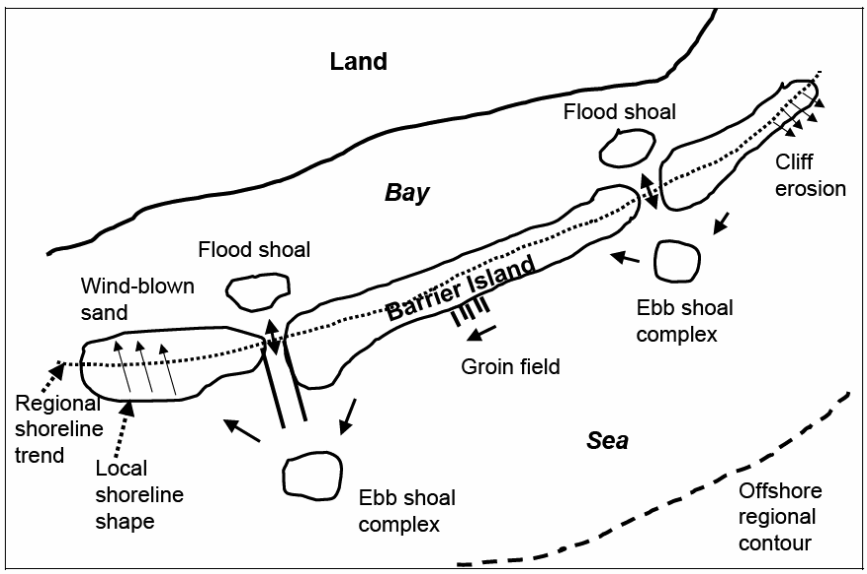

Fig. 4. Overview of local shoreline shape with respect to the regional shoreline trend (Larson *et al.* 2002a).

2.2.5 Cross-shore sediment lost

Under wave influence, eroded material is picked up from the seabed and transported in two directions: the longshore and the cross-shore direction. The former is expected to contain coarser sediment that is transported alongshore. This component is represented by the term of $\partial Q/\partial x$ in Eq. 1. The latter contains a larger amount of fine-grained sediment that is transported offshore and deposited further out in the deep water. Such cross-shore sediment losses may be expressed in the one-line modeling through the term q (Eq. 1).

Because classical one-line models of shoreline change do not include more complex relationship for q, it was necessary to develop such a relationship. In this study, the cross-shore loss of fine sediment depends on the rate of erosion, directly proportional to the gradient of LST rate through an offshore loss parameter ϕ, which specifies the ratio of fine material in the eroded sediment. The relationships employed are given by (Donnelly *et al.,* 2004):

$$q = \frac{\phi}{1-\phi}\frac{\partial Q}{\partial x}, \qquad \frac{\partial Q}{\partial x} > 0 \tag{14}$$

$$q = 0, \qquad \frac{\partial Q}{\partial x} \le 0 \tag{15}$$

Eqs. 14 and 15 state that the loss of fine sediment only occur during erosive conditions when the resident sediment is being mobilized. These equations were substituted into Eq. 1 such that the sediment continuity equation is expressed in terms of ϕ as,

$$\frac{\partial y}{\partial t} + \frac{1}{\left(D_B + D_C\right)}\frac{1}{\left(1-\phi\right)}\frac{\partial Q}{\partial x} = 0 \tag{16}$$

In the present study, the value of the loss parameter was estimated by comparing equilibrium beach profiles for sediment samples taken in the delta and in the surf zone. If an equilibrium beach profile, as defined by Dean (1977) is constructed for each of these sediment samples (Fig. 5), it may be assumed that ϕ, the material loss, is the area difference in percent between the two profiles. This can then be expressed as (Donnelly *et al.,* 2004),

$$\phi = 1 - \left(\frac{A_{delta}}{A_{surf}}\right)^{3/2} \tag{17}$$

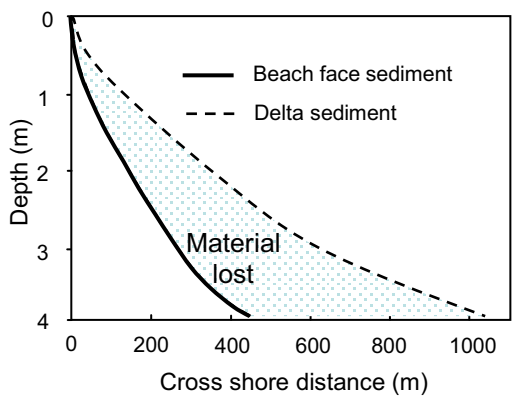

Fig. 5. Example of comparison between equilibrium beach profiles in the delta and in surf zone (Donnelly *et al.,* 2004).

where A_{delta} is the shape parameter in the equilibrium beach profile equation for deltaic sediments and A_{surf} is the shape parameter for the surf zone sediments.

2.3. Inlet Reservoir Model

2.3.1 General equations of the model

Larson *et al.* (2006) refined the inlet reservoir model by Kraus (2002) through the introduction of flood shoals and associated coupling coefficients, which analytically describe the transfer of sediment between the morphological units. The inlet morphology is schematically divided into distinct morphology units including ebb shoal, bypassing bars, attachment bars, and flood shoal (Fig. 6). Each morphological unit is assumed to have a certain equilibrium volume for fixed hydrodynamic and sediment conditions.

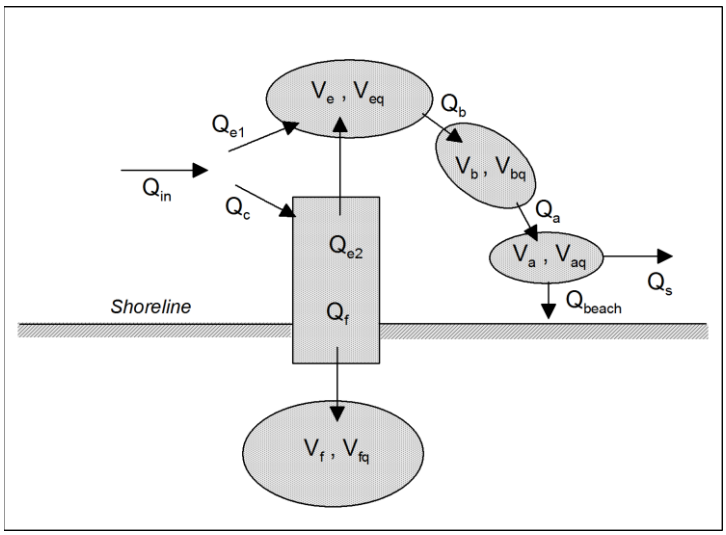

Fig. 6. Definition sketch for inlet morphological units with sediment transport occurring from the left-hand side (after Larson *et al.,* 2002a).

In order explain the inlet model employed in the present study, the simple case of sediment being transported from left-to-right is considered here, where Q_{in} is the incoming sediment transport rate around the jetty (if such a structure is present). The transport Q_{in} is split into one portion that goes to the ebb shoal, Q_{e1}, and one portion that goes into the channel, Q_c. Once in the channel, the sediment might be transported to the ebb shoal, Q_{e2} or to the flood shoal, Q_f. Sediment at a rate Q_b is leaving the ebb shoal and feeding the bypassing bar. The volume of the ebb and flood shoal at any given time is V_e and V_f, respectively, with the corresponding equilibrium values of V_{eq} and V_{fq}.

The mass conservation equation of sediment for the ebb shoal is,

$$\frac{dV_e}{dt} = Q_{e1} + Q_{e2} - Q_b \tag{18}$$

and for the flood shoal,

$$\frac{dV_f}{dt} = Q_f \tag{19}$$

Transport out of the ebb shoal is,

$$Q_b = \frac{V_e}{V_{eq}}\left(Q_{e1} + Q_{e2}\right) \tag{20}$$

Transport rates between elements are defined through the coupling coefficients,

$$Q_{e1} = \delta Q_{in} \;;\; Q_c = (1-\delta)Q_{in} \tag{21}$$

$$Q_{e2} = \beta\left(1-\delta\right)Q_{in} \;;\; Q_f = \left(1-\beta\right)\left(1-\delta\right)Q_{in} \tag{22}$$

where δ and β are coupling coefficients defined as follows (Larson *et al.* 2006),

$$\delta = \frac{V_e + V_f}{V_{eq} + V_{fq}},\ \beta = \frac{1 - V_e/V_{eq}}{2 - V_e/V_{eq} - V_f/V_{fq}} \tag{23}$$

Sediment at rate Q_a is leaving the bypassing bar and feeding the attachment bar. The volume of the bypassing and attachment bars at any given time is V_b and V_a, respectively, with the corresponding equilibrium values V_{bq} and V_{aq}.

The sediment volume conservation equation for the bypassing bar is,

$$\frac{dV_b}{dt} = Q_b - Q_a \tag{24}$$

whereas the transport from the bypassing bar is given by,

$$Q_a = \frac{V_b}{V_{bq}}Q_b \tag{25}$$

The transport out from the attachment bar and further along the shore, Q_s, is:

$$Q_s = \frac{V_a}{V_{aq}}Q_a \tag{26}$$

In the area of the bypassing and attachment bars, incident wave energy greatly exceeds ebb-directed tidal energy, allowing a portion of the ebb shoal to migrate towards the shore under accretionary wave conditions (Kana *et al.,* 1999; Rosati *et al.,* 1999; Gaudiano and

Kana, 2001). Thus, shoal bypassing is a natural form of beach nourishment (Gaudiano and Kana, 2001). This process is believed to contribute partly in the generation of a salient-type feature commonly observed on beaches downdrift inlets. In order to describe the process of onshore sand transport from the attachment bar to the shoreline in the numerical model, a macroscopic approach is taken where it is assumed that a certain fraction of the transport supplying the attachment bar volume is transferred to the beach at each calculation time step. Thus, sediment moves at a rate Q_{beach} from the attachment bar to the shoreline, expressed through a fraction, γ, of the total net sand transport being supplied to the attachment bar at any given time,

$$Q_{beach} = \gamma\left(Q_a - Q_s\right) = \gamma Q_a\left(1 - \frac{V_a}{V_{aq}}\right) \tag{27}$$

The sediment volume conservation equation for the attachment bar is:

$$\frac{dV_a}{dt} = Q_a - Q_s - Q_{beach} = \left(1-\gamma\right)\left(Q_a - Q_s\right) \tag{28}$$

Larson *et al.* (2002a) introduced a nonlinear relationship for releasing sediment from the ebb shoals when the inlet cross-sectional area is decreasing or closes completely. Thus, the above equations, (20), (25), (26) and (27) were changed to a nonlinear form, that is, $Q_{out} = Q_{in}(V/V_q)^n$, where Q_{out} and Q_{in} are sediment transport rates going out and entering a morphological unit, respectively, V and V_q are the volumes at a given time and at equilibrium of the unit, and n is an empirical power. By specifying a value of $n < 1$ for situations where sediment is released back to the beach, the release will be slower than for the linear model. Larson *et al.* (2002a) suggested a value of n between 0.1 and 0.2 when the shoal experienced reduction in volume.

2.3.2 Distance to attachment bars

According to Hicks and Hume (1996) and Carr and Kraus (2001), the tidal prism is expected to control the size and location of the ebb shoal. Carr and Kraus (2001) developed an empirical relationship between tidal prism and the distance from the centerline of the inlet to the downdrift and updrift attachment bars by examining 108 tidal inlets in the United States. The inlets were classified according to whether the inlets had two, one, or no jetties. The empirical relationships governing distance to the attachment bar was found to be a power function of the tidal prism (Carr and Kraus, 2001) according to,

$$Wi = zP^{\lambda} \tag{29}$$

where Wi = distance from centerline of the inlet to the downdrift or updrift attachment points where the ebb shoal complex attaches to the shoreline; P = the tidal prism; z and λ = coefficients determined by the regression analysis of the measured data set, however these coefficient differ considerably between the downdrift and updrift distances due to asymmetry of the ebb shoal complex.

The angle between the orientation of the ebb jet and the shoreline affects the size and shape of the delta (Hicks and Hume, 1996); thus, the above relationships could be modified for improved predictability by including the ebb jet angle. If the ebb jet is perpendicular to the local shoreline trend, the morphological asymmetry is mainly controlled by the magnitude and direction of net longshore transport, as well as wave refraction and diffraction over the bathymetry and ebb shoal. Thus, a straight channel is expected to promote morphological symmetry and a reduced distance to the downdrift attachment point (Carr and Kraus, 2001). However, if the ebb jet angle becomes more acute, the tidal and wave energy oppose each other less. An ebb jet flow more parallel to the wave crests implies that the waves can more efficiently return shoreward sand deposited from the ebb jet (Hicks and Hume, 1996), but at a location further downdrift. Thus, a more acute ebb jet angle is expected to promote more sand being transferred to the downdrift beach and a longer distance to the attachment bar. Thus, Eq. (29) was modified by including the angle between the ebb jet and the local shoreline, ψ , expressed as (see Fig. 7),

for downdrift attachment bars: $Wd = zP^{\lambda}(1+\cos\psi)$ (30)

for updrift attachment bars: $Wu = zP^{\lambda}(1-\cos\psi)$ (31)

For the case where the ebb jet is perpendicular to the shoreline, ψ takes on a value of 90 deg, implying no asymmetry due to ebb jet orientation.

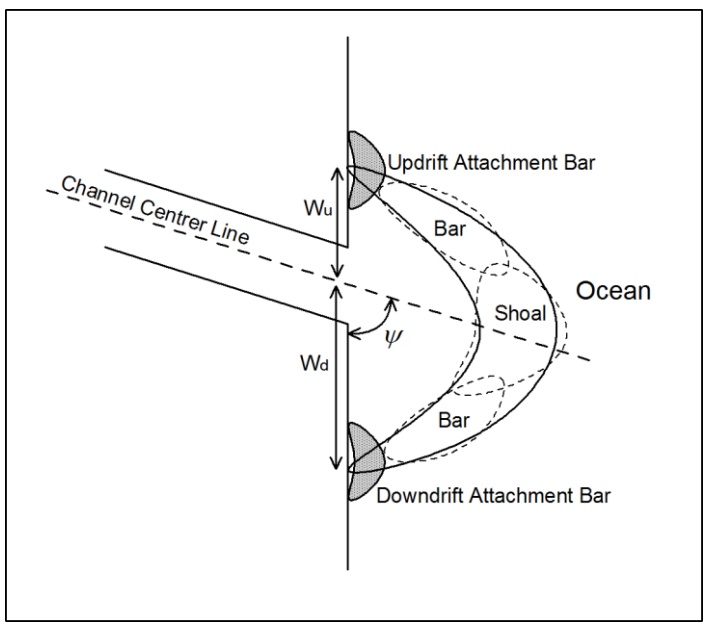

Fig. 7. Asymmetric ebb shoal and definitions of terminology used (after Carr and Kraus, 2001).

2.3.3 Wave sheltering effects from attachment bar

Beach erosion typically occurs along the shoreline on both sides of the attachment bar, whereas accretion occurs in its lee (Dean and Walton, 1975; Williams and Kana, 1987; Gaudiano and Kana, 2001) (see Figs. 8 and 9). The sheltered area behind the bar is gradually filled in, and finally the shoal attaches to the shore resulting in alongshore spreading of the bar in both directions from the point of attachment (Gaudiano and Kana, 2001). Thus, there are two mechanisms that cause sediment to gradually feed sand to the area behind the bar. The first mechanism is the onshore bypassing process of sand from the attachment bar due to landward flow associated with the waves (Williams and Kana, 1987; FitzGerald *et al.* 2000). The second mechanism is due to the sheltering from the wave activity provided by the bar, which produces a zone of low energy in which alongshore currents can deposit transported material (Dean and Walton, 1975). The onshore bypassing process is described through the coefficient, γ, which represents the fraction of the transport supplied to the attachment bar build-up that is transferred to the shore (see Eq. 27). The decrease in wave energy in the lee of the bar is expressed through a reduction in breaking wave height. In the numerical model, a calibration parameter for reduction of the breaking wave height in the lee of the bar was introduced. In principal, the value of this parameter depends on the size and shape of the bar, which are different on the downdrift and updrift sides of the inlet due to asymmetry in inlet morphology. The breaking wave height in the lee of the bar was multiplied by a spatially varying attenuation parameter, η, and thus, H_b in Eq. 2 was replaced with ηH_b, where $0 \le \eta \le 1$. The value of η is less than 1.0 behind the bars, and equals 1.0 outside the sheltered areas. In principal, η has a minimum value at the centre point of the sheltered area, and its value increases towards both sides of the bar. As a simplification for this study, the values of η within the

Fig. 8. Migration landward of attachment bar at Dewees Inlet (South Carolina) (Gaudiano and Kana, 2001).

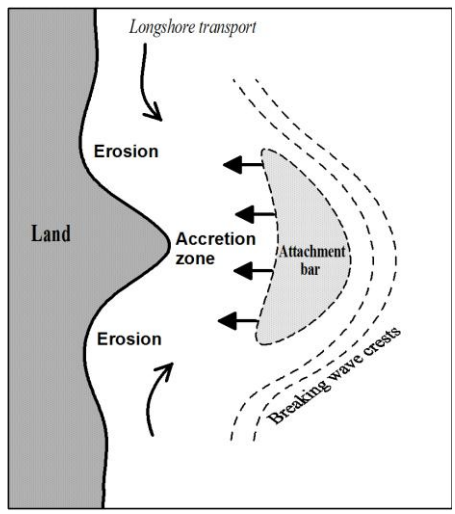

Fig. 9. Depiction of sand movement (after Kana *et al.,* 1985).

sheltered areas were obtained by linearly interpolating between a minimum value at the centre point of the respective sheltered area and 1.0 in areas not sheltered by the bar. The minimum values inside the bars were determined through a calibration procedure.

2.4 Spit growth and barrier elongation model

The governing equation of this model is primarily based on the sand volume conservation equation suggested by Kraus (1999). In this study, an attempt is made to estimate the amount of sand, coming from the LST and bypassing the spit, while taking also other sinks or sources of sand into account. The model mainly focuses on two typical types of spit growth. First, spit elongation is restricted by the presence of an inlet channel or by an obstacle, and second, the spit elongates without restriction over the time period of consideration.

2.4.1 Restricted spit growth

Under proper hydrodynamic forcing and availability of sediment, a spit may form and elongate over time. However, at inlets an equilibrium state is typically reached at some point controlled mainly by the flow through the inlet and the LST rate. Such a limitation to the spit development are known as restricted spit growth. If the inlet flow is too weak to prevent the navigation channel from filling in completely, the inlet will eventually close. Spits can form at the ocean and bay sides of inlets (Kraus, 1999), resulting in migration of the inlet channel and changes in the dynamic conditions at the inlet. Depending on the magnitude and direction of the net LST rate, spits can form at one side or both sides of the inlet.

In general, tidal inlets act as sinks for LST, although sediment is also bypassed from the updrift to the downdrift side. The magnitude of the bypassing depends on how close the morphological units of the inlet are to their equilibrium states. Natural bypassing of sediment at inlets occurs mainly through two processes: the LST can be bypassed through the ebb shoal complex or fall into the inlet channel and then be directly flushed out of the inlet to the downdrift beach (Bruun and Gerritsen, 1959). The hydrodynamic conditions at the inlet govern the fraction of the sediment falling into the channel. Weak hydrodynamic forces promote deposition of sediment in the channel, which may be the case at inlets or entrances with a large cross-sectional area or with a small tidal prism. This deposition results in spit development together with shoaling of the inlet channel. Spit elongation can decrease the inlet cross-sectional area, gradually increasing the hydrodynamic forces in the channel. The stability of a spit depends on the balance between other LST rate coming into the channel and the tidal (and/or river) flow that scours the channel.

In order to derive a spit growth model, the following assumptions are made (compare Kraus, 1999),

- spit growth is sustained by the LST,
- spit elongation is in the same direction as the regional shoreline trend,
- spit width is constant,

- contours of the spit move in parallel.

Assuming that the LST (Q) is coming to the inlet from the left (Fig. 10), the sand volume conservation equation that governs spit growth can be expressed as,

$$\frac{d}{dt}\left[\left(h+B_s\right)x\right]=\frac{1}{W}\left(Q_{cin}-Q_{cou}+Q_s\right) \tag{32}$$

where x = spit length; h = channel depth; B_s = average berm elevation of the spit; W = spit width; Q_{cin} = sediment transport entering the channel; Q_{cou} = sediment transport going out from the channel; and Q_s = sources or sinks of sand associated with the channel.

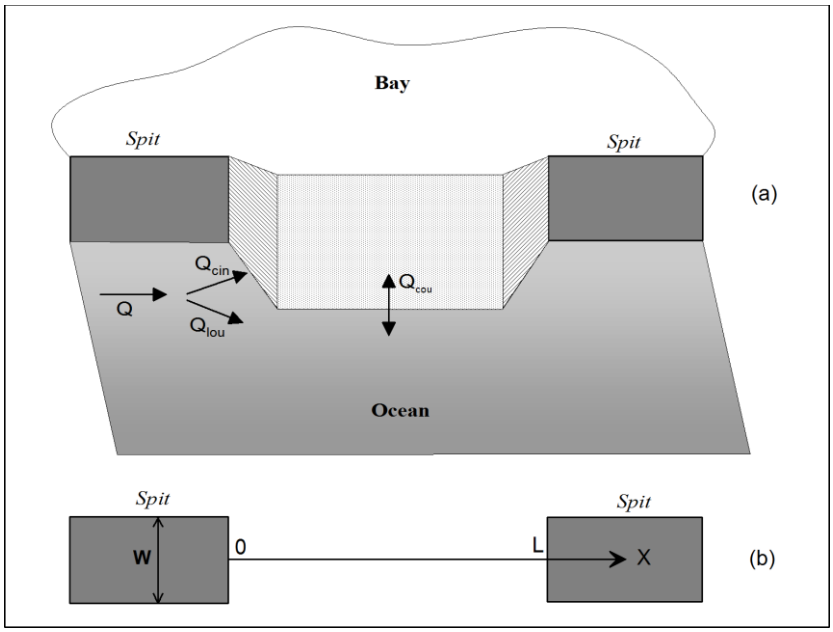

Fig. 10. Definition sketch for spit growth and sediment pathway: (a)- overview, (b)- plan view and coordinate axis.

Kraus and Seabergh (2002; see also Kraus, 1999) proposed an approach to calculate Q_{cin} for spit growth restricted by the presence of an inlet channel. In their approach, the portion of the LST rate that is transported away by the channel, Q_{lou}, depends on how far the spit is from the center line of the inlet channel with respect to an initial condition for the spit position located far updrift of the channel where the LST is unrestricted. Thus, the definition of the initial condition presents some difficulties and contains an element of subjectiveness.

In this study, another method is employed to calculate Q_{cin} and Q_{cou} in Eq. 32, where the sediment pathways are taken into account. The sediment that falls into the channel (Q_{cin}), contributing to the spit growth, is estimated based on the relationship between the maximum depth of the channel and the depth of active LST. If the maximum depth of the channel (D_M) is deeper than the depth of active LST (D_{LT}) it is expected that the entire LST falls into the channel (Fig. 10). Otherwise, if the maximum depth of the channel is smaller than the depth of active LST, a fraction of the LST is directly transferred to the ebb shoal complex and then bypassed downdrift (or possibly lost into deep water). If the cross-shore distribution of the LST is assumed to be uniform (Hanson, 1987), Q_{cin} is expressed through the ratio between D_M and D_{LT} according to,

$$Q_{cin} = \frac{D_M}{D_{LT}} Q \tag{33}$$

where D_{LT} is estimated from an empirical equation (Hanson, 1987) as $D_{LT} = 1.6 H_b$.

The sediment tranport rate produced by the inlet flow (Q_{cou}) is given by (Watanabe *et al.*, 1991; Kraus, 1998),

$$Q_{cou} = \omega \frac{\left(\tau_m - \tau_{cr}\right)}{\rho g} U_c w_c \tag{34}$$

where ω = an empirical coefficient (on the order of unity); τ_m = bottom shear stress; U_c = mean velocity of the inlet channel flow; w_c = channel width; and τ_{cr} = critical shear stress for sediment transport calculated from (Van Rijn, 1993),

$$\tau_{cr} = \theta_{cr} \left(\rho_s - \rho\right) g d_{50} \tag{35}$$

where d_{50} = medium grain size; and θ_{cr} = critical Shield's parameter given by (Soulsby, 1998),

$$\theta_{cr} = \frac{0.30}{1 + 1.2 D_*} + 0.055\left[1 - \exp\left(-0.020 D_*\right)\right] \tag{36}$$

where $D_* = d_{50}\left[\frac{\left(s-1\right) g}{\upsilon}\right]^{1/3}$; $s = \rho_s / \rho$; and υ = viscosity coefficient.

The bottom shear stress due to the mean current is expressed as (Kraus, 1998),

$$\tau_m = \rho c_f U_c^2 \tag{37}$$

with $c_f = g m^2 / \overline{h}^{1/3}$ (38)

where m = the Manning coefficient; and $\overline{h}$ = average depth of the channel. Mean current velocity in the inlet channel is calculated based on the tidal prism (P), the tidal period (T), and the cross-sectional area of the inlet (A_c) according to Keulegan and Hall (1950),

$$U_c = \frac{\pi C_k P}{T A_c} \tag{39}$$

where C_k = a coefficient to account for a non-sinusoidal tide, having a value in the range of 0.81 to 1.0 (Kraus, 1998), and

$$A_c = \int_{x_t}^{L} h dx \tag{40}$$

where x_t = length of the spit at any given time, and L = maximum length of the spit from the initial spit position (Fig. 10).

Using Eqs. (34), (37), and (38), Eq. (32) may be written,

$$\frac{d}{dt}\left[\left(h+B_s\right)x\right] = \frac{1}{W}\left[Q_{cin} - \omega U_c w_c \left(\frac{m^2}{\overline{h}^{1/3}}U_c^2 - \frac{\tau_{cr}}{\rho g}\right) + Q_s\right] \tag{41}$$

Spit elongation can gradually decrease the entrance cross-sectional area, increasing the mean current velocity in the inlet. Equilibrium conditions for the spit occur when $d/dt\left[\left(h+B_s\right)x\right] = 0$, that is,

$$Q_{cin} = \omega U_c w_{ce}\left(\frac{m^2}{\overline{h}^{1/3}}U_c^2 - \frac{\tau_{cr}}{\rho g}\right) - Q_s \tag{42}$$

where w_{ce} = width of the inlet at equilibrium. Under conditions of strong inlet flow at equilibrium, τ_{cr} may be neglected (Kraus, 1998). If the channel depth is assumed to be constant, and neglecting sand sources or sinks, substituting (39) and (40) into (42), the equilibrium length of the spit is obtained as:

$$x_e = L - \frac{\omega^{1/2} m}{h^{5/3}}\left(\frac{\pi C_k}{T}\right)^{3/2}\frac{P^{3/2}}{Q_{cin}^{1/2}} \tag{43}$$

Eq. (43) shows that the length of a spit at equilibrium is directly proportional to the LST rate supplied to the channel to a power 1/2 and inversely proportional to the tidal prism to a power 3/2. This means that, for the same magnitude of LST, a weaker inlet flow will produce a longer spit at equilibrium than that produced by a stronger flow.

An example of how a spit may grow depending on the tidal prism is shown in Paper 3.

2.4.2 Unrestricted spit growth

Unrestricted spit growth occurs if there is nothing preventing its elongation, for example, at a headland or a large entrance. In such cases, the cross-sectional area of the entrance is assumed to be large enough so that the inlet current velocity is causing negligible sediment transport, implying that $Q_{cou} \approx 0$. Thus, Eq. (32) simplifies to:

$$\frac{d}{dt}\left[\left(h+B_s\right)x\right]=\frac{1}{W}\left(Q_{cin}+Q_s\right) \tag{44}$$

If a spit grows without restriction in time, the entire LST is expected to fall into the channel and feed the spit (Kraus and Seabergh, 2002), yielding $Q_{cin}=Q$, and:

$$\frac{d}{dt}\left[\left(h+B_s\right)x\right]=\frac{1}{W}\left(Q+Q_s\right) \tag{45}$$

2.5 Overall calculation procedures

The overall calculation procedures in the model is shown in Fig. 11.

Input data for the model include:

- wind data input: wind velocity, direction, and fetch;
- inlet data input: inlet cross-sectional area or tidal prism, inlet position, and angle between ebb jet and the local shoreline;
- spit and barrier data input: width of spit, depth of inlet channel, inlet tidal prism, and maximum length of the spit.

In addition, historical shoreline position and boundary conditions must be specified.

Output data of the model include:

- breaking wave parameters: wave height, direction, period, and water depth at breaker line;
- shoreline response: large-scale shoreline evolution and shoreline response in vicinity of inlets;
- longshore sediment transport rate: positive, negative, and net LST rate;
- inlet shoal volume growth: volume growth of flood shoal, ebb shoal, bypassing bar, and attachment bar;
- spit growth: spit development, LST rate bypassing the spit, and LST rate feeding the spit.

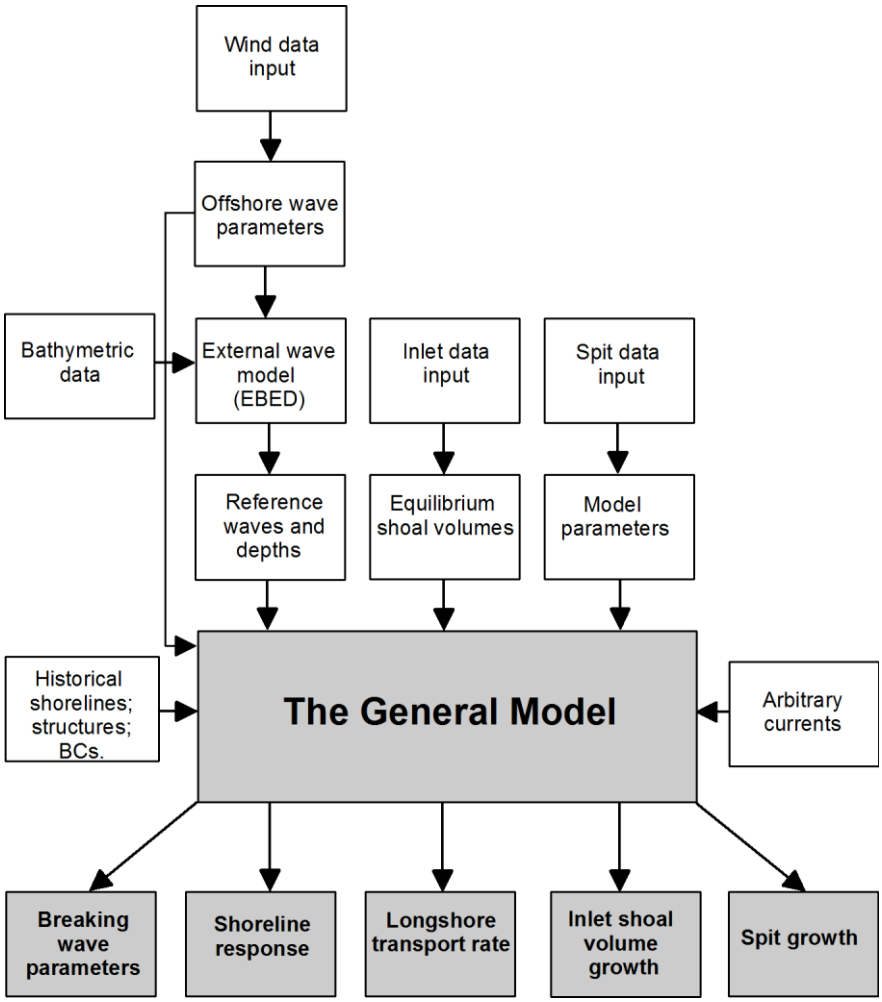

Fig. 11. Overall calculation flow of the model.

3. Study sites and employed data

Three different study sites with available measured data were selected as suitable locations to develop and validate the model, including: Hai Hau beach in Vietnam; south Long Island coast in the United states; and Badreveln spit in Sweden. At Hai Hau beach, the model was primarily applied to simulate shoreline evolution on the coastal stretch without inlets and river mouths. At the south Long Island coast, the model was applied to simulate regional sediment transport and shoreline response together with inlet shoal volume development and barrier elongation on the coastal stretch including two inlets. At the Badreveln spit, an analytical solution of the model was validated against the measured data of spit elongation.

3.1 Hai Hau beach, Vietnam

The main portion of the coastline of Nam Dinh and Thai Binh provinces, in the north part of Vietnam, particularly at the seven active river mouths (see Fig. 12), is stable or accreting while the coastline segment of Hai Hau beach, the area of interest between Ha Lan and Lach Giang estuaries on the coastal stretch of about 30 km, is seriously eroding. According to several recent studies, the erosion rate averaged along the coastline is about

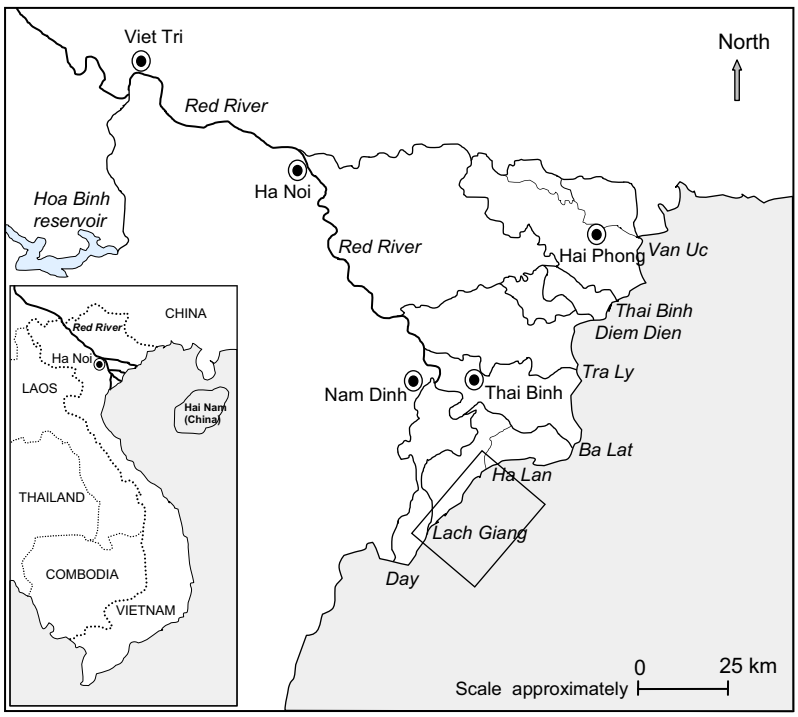

Fig. 12. Study site and the tributaries of Red River system.

5-10 m/year (Donnelly *et al*., 2004; Wijdeven, 2002), with a maximum rate reaching 19-35 m/year (Pruszak *et al*., 2002). The main objectives of this study are to establish the cause of the erosion at Hai Hau beach and to estimate the recession rate.

Long-term time series of offshore wave data are not available in Vietnam or at Hai Hau beach. Therefore, offshore waves were hindcasted from wind data recorded at the wind stations around the study area. Wind data at Bach Long Vi (BLV) station (see Fig. 13) were preferred to estimate offshore waves (Pruszak *et al*., 2002; Wijdeven, 2002). However, by comparing measured wave data with predictions from winds at Con Co (CC) station, Häglund and Svensson (2002) realized that the wind at CC station may significantly control the wave climate at Hai Hau beach under certain circumstances. In order to derive a more representative wind climate for the waves, the approach of combining wind data at BLV and CC was suggested by Häglund and Svensson (2002). Also in this study, a long-term time series of waves (20 years: from 1976 to 1996) was estimated by combining wind data at BLV and CC (see Fig. 13).

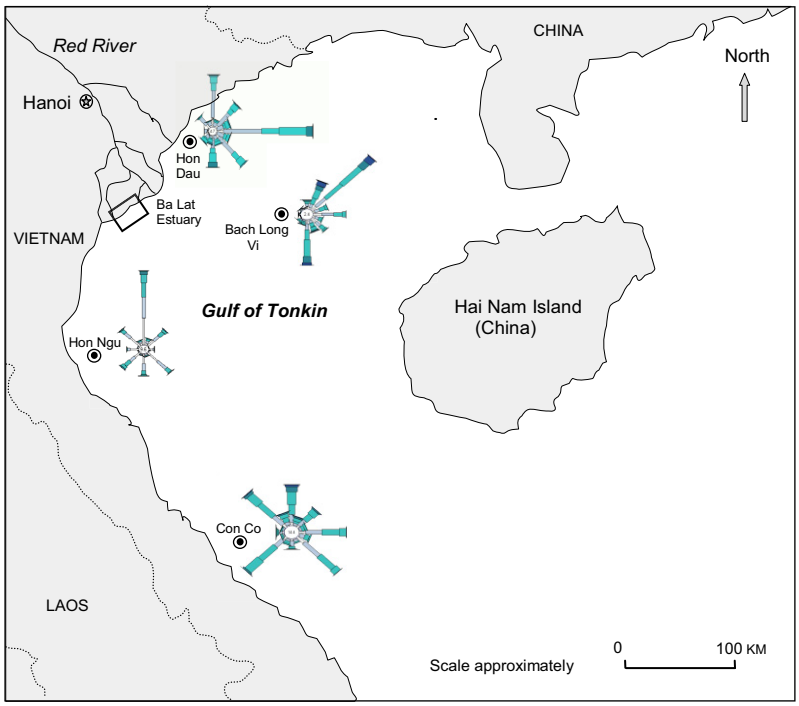

Fig. 13. Wind roses at the stations around Hai Hau beach, based on time series of 20 years (from 1976 to 1996).

Shoreline data were obtained from maps and satellite images. In this study, the shoreline in 1910, 1965 and 2000 were used to validate the model. The shoreline of Hai Hau beach was modeled between Ha Lan estuary in the north and Lach Giang estuary in the south (Fig. 12). For the sample taken at Hai Hau beach, the value of the loss parameter in Eq. 17 varied around 0.6-0.7 (Donnelly *et al.,* 2004). Sediment sampling shows the median grain size in this region, D_{50}, to be about 0.17 mm. The spatial and time steps were set at 200 m and 1 hours, respectively. More details on the environmental conditions are described in the Paper 1.

3.2 Long Island coast, United states

The Long Island shoreline has a length of about 135 km and it is oriented in a direction of about 67.5 deg northeast. The study area extended from Fire Island Inlet to Montauk Point because most available information originated from this coastal stretch (Larson *et al.*, 2002a), (see Fig. 14). The stretch includes many coastal features and processes such as sediment transport and evolution at regional scale, the cross-sectional areas of the inlets varied substantially with time including opening and closure of the inlets, substantial shoreline response in the vicinity of the jettied inlets, large amount of beach fill volumes placed at several locations along the coast (Larson *et al.,* 2002a), and a system of groins constructed to protect the beach.

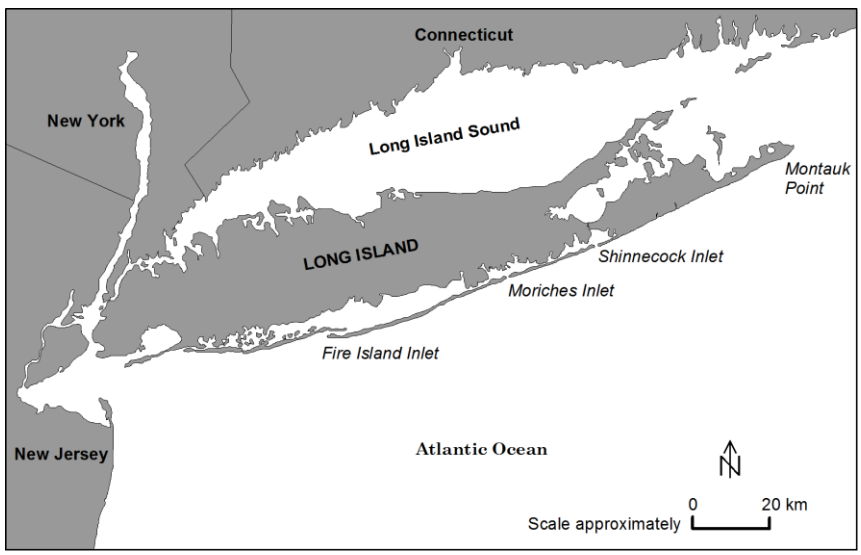

Fig. 14. Study site and locations of the inlets on the Long Island coast.

Hindcast wave data (a 20-years time series at an interval of 3 hours from 1976 to 1995) from three WIS Stations along the coast were used as input data for the modeling. The spatial step was set at 100 m, and the input wave parameters were linearly interpolated

based on the three stations corresponding to this spatial interval. The calculation time step was set at 3 hours, coinciding with the interval of measured wave data.

Measurements of inlet cross-sectional areas at Shinnecock and Moriches Inlet were performed at several occasions between 1931 and 1998, which includes the closure and subsequent opening of Moriches Inlet in the 1950's. These data were used to calculate the equilibrium volumes of the ebb shoal complexes, from which the equilibrium volumes of the individual morphological units at the inlets could be estimated (Larson *et al.,* 2002a). Equilibrium volume of the flood shoals were set to 4.10^6 m^3 for both inlets (Larson *et al.,* 2006).

Several structures were included in the simulations. Jetty lengths on each side of the inlets and the time of construction were specified according to information from the literature. The lengths of the east and west jetties at Moriches Inlet are 258 m and 445 m, respectively, and the jetties were constructed in 1953 (Vogel and Kana, 1984). For Shinnecock Inlet, the lengths of the east and west jetties are 280 m and 450 m, respectively, with construction carried out in 1953 (Smith *et al.,* 1999). Changes in the jetty lengths were not modeled, but they were kept constant during the simulation time after completion. The 15 groins comprising the Westhampton groin field were constructed in three phases, from March 1965 to October 1966, from 1969 to 1970, and in 1998 (Rosati *et al.,* 1999). These groins were included in the model at the proper times and the lengths and locations of the groins were specified based on available data.

Dredged material has typically been placed along adjacent beaches or within nearshore areas east and west of the inlets (Smith *et al.,* 1999). These beach fill volumes were included in the model as source terms in the sediment conservation equation that vary in time and space. A total volume of about 800,000 m^3 was placed west of Shinnecock Inlet between 1949 to 1983, and another 1,115,000 m^3 was put in this area between 1983 and 1995 (Larson *et al.,* 2002a). From 1955 to 1969, a total volume of about 661,000 m^3 was placed east of the inlet. Total quantities placed at Moriches Inlet between 1953 to 1996 were approximately 2.5 million cubic meters in which about 1.3 million cubic meters (52%) and 0.75 million cubic meters (30%) were placed to the east and west of the inlet, respectively (Smith *et al.*, 1999). Smaller beach fills have been placed at other locations, but they were neglected in the present modeling study.

In order to employ Eqs. (30) and (31), the angle between the ebb jet and the local shoreline must be specified. Based on satellite images, the angle between the ebb jet and local shoreline at Shinnecock and Moriches Inlet were set to 60 deg and 67 deg, respectively.

The equilibrium volumes, V_{eq}, V_{bq} and V_{aq}, of each morphology unit must be specified. Limited information exists on the equilibrium size of the individual morphological units described in the reservoir model. To simplify, the units are determined as being a constant fraction of the volume of the ebb shoal complex, which in turn is a function of inlet cross-sectional area (tidal prism). Militello and Kraus (2001) estimated sand bypassing to the attachment bar at a rate of about 19,000 m^3/yr for Shinnecock Inlet. The rate of ebb shoal growth, which is estimated to 117,000 m^3/yr (Williams *et al.*, 1998), implies that the ratio between the attachment bar and the ebb volume growth is 0.16. The ratio between

bypassing bar and the ebb shoal volume is assumed to be 0.25 following Larson *et al.* (2002a). In the present study, the same ratios were employed for the both inlets.

To employ Eqs. (27) and (28), the fraction of the transport causing deposition on the attachment bar transferred to the shore at any given time must be specified. Taking into consideration the ratio between the attachment bar and the ebb shoal complex volume, the sand volume percentage transferred to the shore is about 20.0. Thus, the coefficient γ in the Eqs. (27) and (28) was set to 0.20.

In order to employ Eqs. (39)-(41) to describe spit growth, the geometrical parameters of the spit must be specified. Based on available maps, Cedar Island to the west of Fire Island Inlet, which follows the regional shoreline trend of Fire Island, can be regarded as a stable point with respect to the Fire Island barrier elongation (see Fig. 15). Thus, the Fire Island barrier can be modeled as a spit where growth is restricted by an obstacle. The distance from the initial position to the Cedar Beach along the lengthening regional shoreline trend obtained from the Fire Island shoreline in 1825 (Kana, 1995) is about L = 10500 m. Futhermore, the average width of the Fire Island barrier is taken to be 500 m (W) (see Psuty *et al*., 2005). Based on the measured tophography reported by Smith *et al*. (1999), the depth of the entrance from the initial position to the Cedar Beach was taken as linearly decreasing from 8.5 m to 2.5 m. Tidal prism was specificied to be $52 \cdot 10^6$ m^3 (Jarrett, 1976) with a semi-diurnal oscillation of about 12 hours tidal period (Psuty *et al*., 2005). The empirical coefficients, ω and C_k, were set to 1.0 and 0.9, respectively, whereas the Manning coefficient m was given a value of 0.025 (Kraus, 1998).

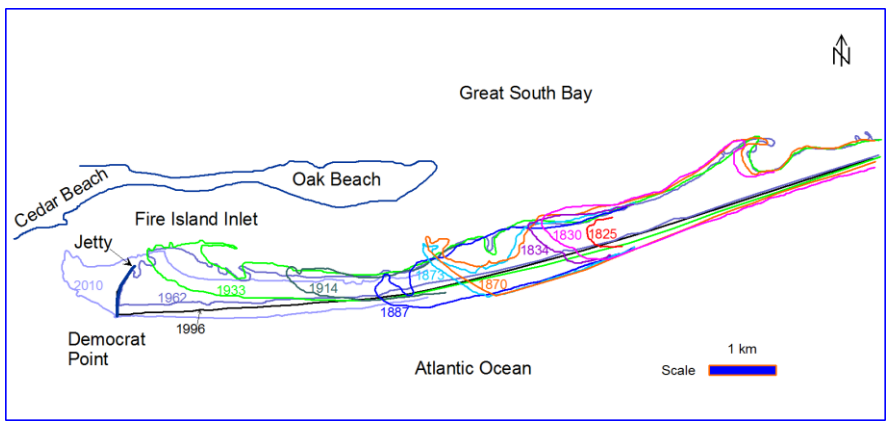

Fig. 15. Historical shoreline and spit growth at the Fire Island inlet (after Kana, 1995; Kraus and Seabergh, 2002; and satellite image in 2010).

3.3 Badreveln spit, Sweden

The Badreveln spit is formed in the northeast part of the Falsterbo Peninsula in southern Sweden (Fig. 16). The spit started to develop in the early 1860's after the Skanör Habor

was constructed (Blomgren and Hanson, 2000), and extended northward from the harbor into an open area in the southwest corner of the Baltic Sea (see Fig. 16). Therefore, the Badreveln spit elongation may be modeled as an unrestricted spit growth, and it was selected as a suitable location for validating the spit growth model.

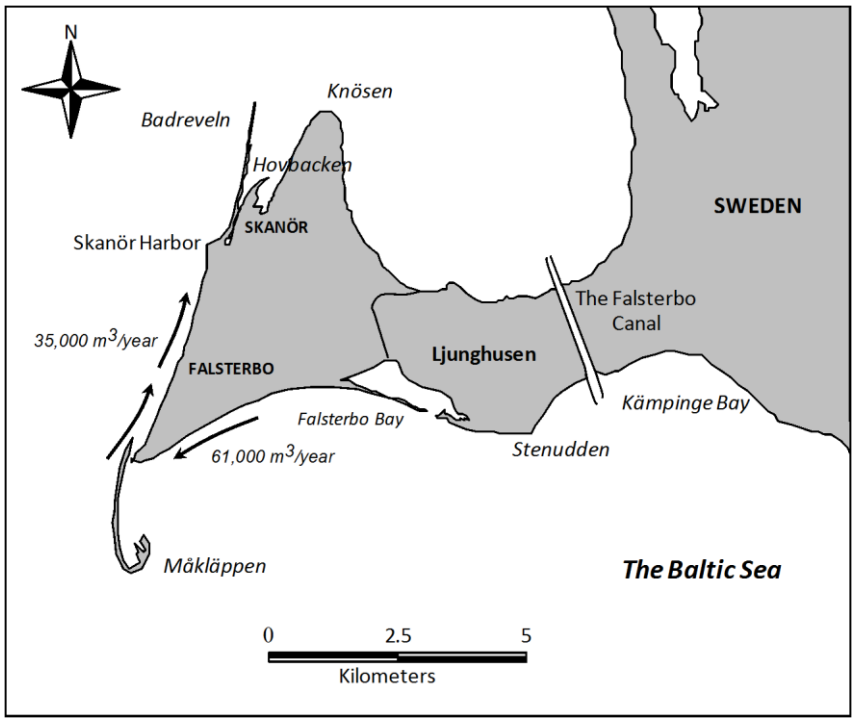

Fig. 16. Study site and calculated net sediment transport rates at the Falsterbo Peninsula in the south-west Baltic Sea (Blomgren and Hanson, 2000).

In order to employ the shoreline change model to represent the LST rate that feeds the spit, initial shoreline positions, offshore wave properties, and other boundary conditions must be specified. However, these necessary data are not available at the study site. As a simplification, the analytical solution to Eq. (45) was applied under the assumption that the sediment transport rate feeding the spit is constant (linear growth):

$$x = \frac{Q}{\left(h + B_s\right)W} t \tag{46}$$

The input LST rate was estimated from information in existing studies. Hanson and Larson (1993) applied the numerical shoreline change model GENESIS to estimated the potential sediment transport rates along the south and west coast of the Falsterbo Peninsula. Along the Falsterbo bay coast, the average net transport rate was calculated to be 61,000 m^3/year,

directed westward, and along the west coast, the average net transport rate was calculated to be 35,000 m^3/year, directed northward (see Fig. 16). The sediment transport along the west coast is expected to be partly blocked by Skanör harbor to build the south Skanör beach, and the remaining part is bypassed around the Skanör harbor to feed the Badreveln spit and the north Skanör beach. An average sediment transport rate feeding the spit was estimated to about 10,000 m^3/year. Based on the measured data, the depth of closure and the berm elevation were specified to be 4 m and 1 m, respectively. An average width of the spit was determined based from satellite images to be 70 m. Measured data of spit elongation at several occasions from 1860 to 1994 (see Fig. 17) were used to compare with the analytical solution.

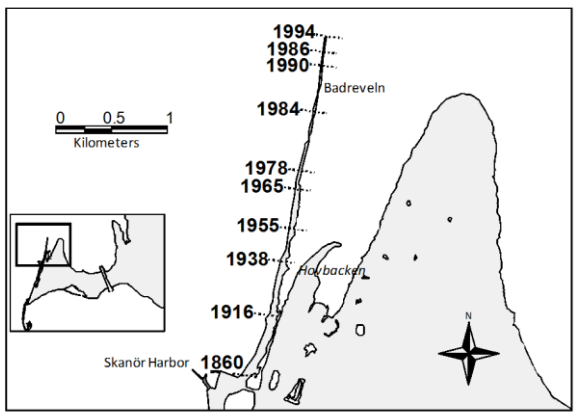

Fig. 17. The elongation of the Badreveln spit since 1860 (Blomgren and Hanson, 2000).

4. Results and discussion

Depending on the ready availability of the input data, the model application as well as comparison between the modeled results and measured data were focused on different processes at each study site. At the Hai Hau beach, the model application focused on shoreline evolution and LST rate, but only measured data of the historical shorelines are available for the comparison. At Long Island coast, the modeled results were compared with the measurements of regional shoreline evolution, anual net LST rate, sand volume growth of flood shoal and ebb shoal complexes, shoreline response in vicinity of the inlets, and barrier elongation. At the Badreveln spit, only measured spit elongation was used to compare with the analytical solution of the spit growth model.

4.1. Hai Hau beach, Vietnam

4.1.1 Modeled shoreline evolution

The measured shorelines from 1910 and 1965 were used to calibrate the model. The parameter values during calibration were optimized based on minimizing the errors (Fig. 18). The calibration parameters obtained are $\phi = 0.7$, $K_1 = 0.89$ and $K_2 = 0.50$. Employing the above calibration parameters, the model was validated from 1965 to 2000 using the 1965 measured shoreline as the initial shoreline. For the period from 1995 to 2000, two sea dike segments reinforced by stones and mortar constructed in 1995 were represented using a seawall boundary condition (Fig. 19).

The model does not simulate the fine details of the shoreline shape, however, the general trend and magnitude of shoreline change are well reproduced during both the calibration and the validation periods, including the influence of the seawalls through the boundary conditions. Annual shoreline retreat rates estimated from the measured shorelines have decreased from 8.7 m during the calibration period to 6.8 m during the validation period. This shows that the average erosion rate at Hai Hau beach has been slowing down during the recent decades.

4.1.2 Modeled sediment budget

The calculated values for the components in the sediment budget show that the total amount of sediment from sources is, $Q_{source} = Q^1_{south} + Q^n_{north} = 203\text{x}10^3$ m^3/year, and the total amount of sediment from sinks is, $Q_{\sin k} = Q^1_{north} + Q^n_{south} + Q_{off} = 1043\text{x}10^3$ m^3/year, where fine sediment lost offshore is $767\text{x}10^3$ m^3/year (70% of total sink volume). Thus, the annual sediment volume lost from the area is $Q_{lost} = Q_{\sin k} - Q_{source} = 840\text{x}10^3$ m^3/year (Fig. 20).

There is a large difference in the LST rates between the southward and northward directions. Overall, the southerly directed sediment transport rate is around $150\text{-}250\text{x}10^3$ m^3/year, whereas the northerly sediment transport rate is only about $30\text{-}50\text{x}10^3$ m^3/year, constituting about 15% of the gross sediment transport rate. The result is a significant net

sediment transport rate in the southward direction with values in the range of 100-200x10^3 m^3/year (Fig. 21).

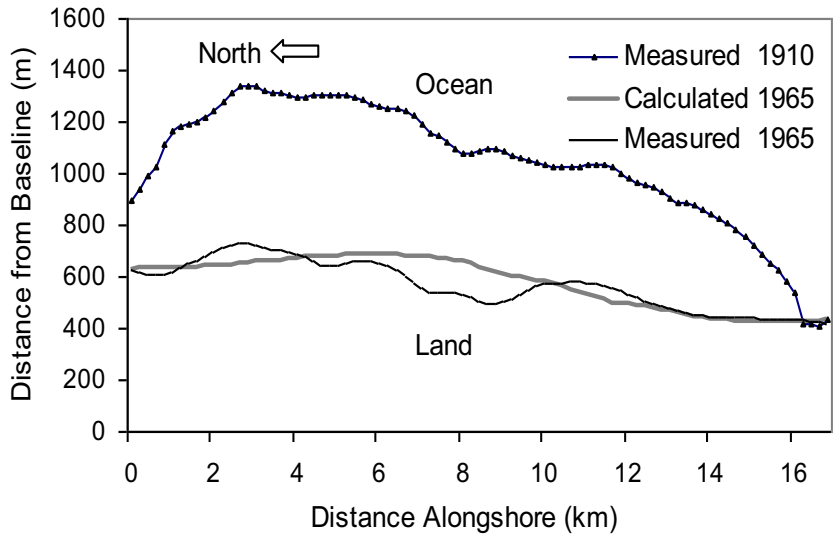

Fig. 18. Measured and modeled shorelines at Hai Hau beach, period of 1910 to 1965.

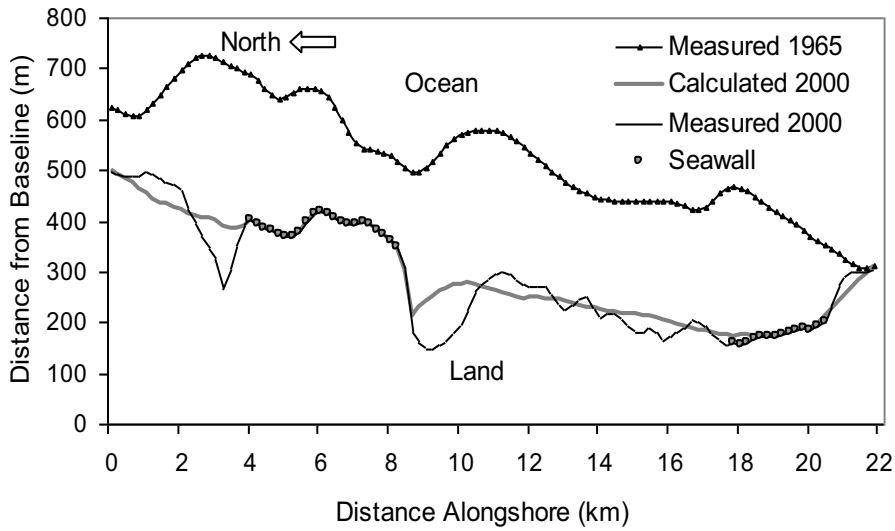

Fig.19. Measured and modeled shorelines at Hai Hau beach, period of 1965 to 2000.

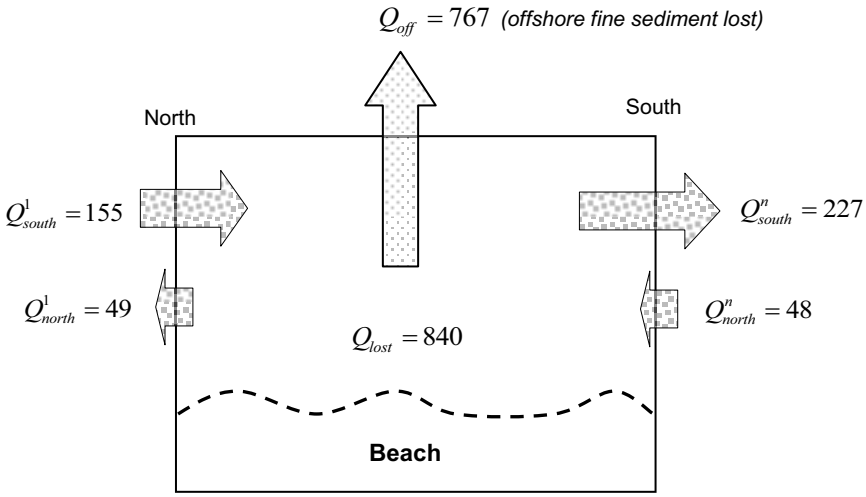

Fig. 20. Sketch of calculated sediment budgets, values multiplied by 10^3 (m^3/year).

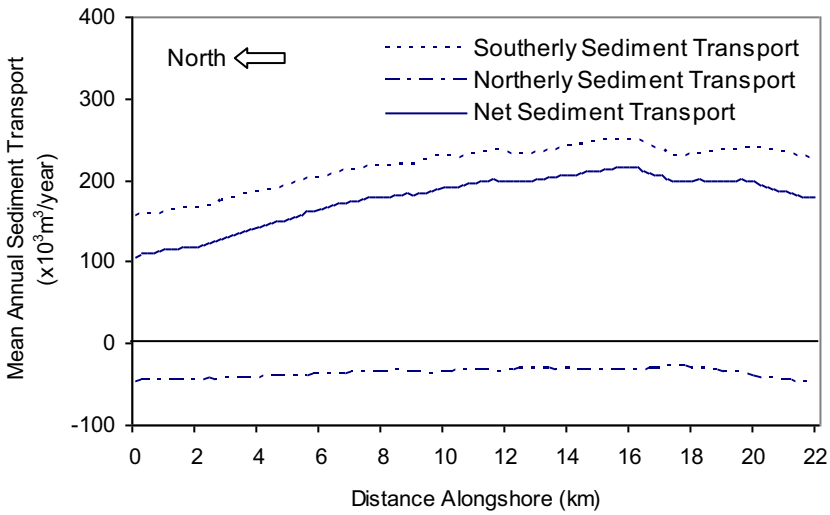

Fig. 21. Spatial distribution of annual longshore sediment transport rates at Hai Hau beach.

Because of the different wind energy supply between winter and summer, offshore wave energy in the winter (coming from the north) is much greater than that in the summer (coming from the south). Offshore wave energy estimated from the wave hindcast show that, in winter (from November to March) about 52.2% of the total offshore wave energy is supplied, while in summer (from May to September) it is only 29.3%. On the other hand, since the shoreline of Hai Hau beach runs in NE-SW direction (about 40 degrees with respect to N direction), (see Fig. 12), incoming wave angles from N to ESE, generating the LST in the southward direction, encompass about 81% of total offshore wave energy. Incoming wave angles from SE to SW, generating the LST in the northward direction, encompass only about 17% of total offshore wave energy. Thus, the southward sediment transport, encompassing about 85% of the gross transport, is much higher than the northward sediment transport, making up only about 15% of the gross transport (Fig. 20), which results in a large net sediment transport to the south. In addition, gradients in the LST rates to the south (in winter) are higher than in the transport to the north (in summer) (Fig. 21), and therefore there is a large amount of fine sediment being transported into deep water during the winter. This implies that the serious erosion at Hai Hau beach mainly occurs during the winter period.

4.2 Long Island coast, United States

4.2.1 Modeled shoreline response

The model was first run for the period 1933 to 1983 to compare with the measured shoreline in 1983. The simulated and measured shorelines, as well as the initial shoreline, are plotted in Fig. 22, in which Fig. 22a gives an overview and Fig. 22b and 22c the details at Shinnecock and Moriches Inlet, respectively. The shoreline plots provide a view "standing on shore" looking towards the ocean with Montauk Point on the left side and Fire Island Inlet on the right side. The wave height attenuation coefficient was set to $\eta = 0.85$, implying that the breaking wave height at centre point of the lee of the attachment bars decreases 15% compared to the height outside the sheltered areas. This value was held constant during the entire simulation time, as well as for the downdrift and updrift bars.

The simulated shoreline is overall in good agreement with the measured shoreline, particularly on the updrift side of the jetties and in the downdrift area where the salient-type feature appears. However, at Shinnecock Inlet, on both sides of this feature, the shoreline retreat was overestimated by the model, and south of the downdrift attachment bar at Moriches Inlet, the simulated shoreline retreat was underestimated. The reason for this discrepancy may be due to several factors, at regional and local scale, that were not included in the model. Overwash by storm waves could produce shoreward displacement of the shoreline, which may have been the case west of Moriches Inlet. During storm surge, waves may overtop the island, and overwash of sediment occurs. This sediment is deposited on the back of the island and it is lost from the nearshore system or transported back at a low rate by wind (Larson *et al.,* 2002b). Large storm events have contributed to significant alteration of the Fire Island shoreline. These storms generally cause rapid beach erosion, dune displacement, and coastal flooding (Psuty *et al.,* 2005).

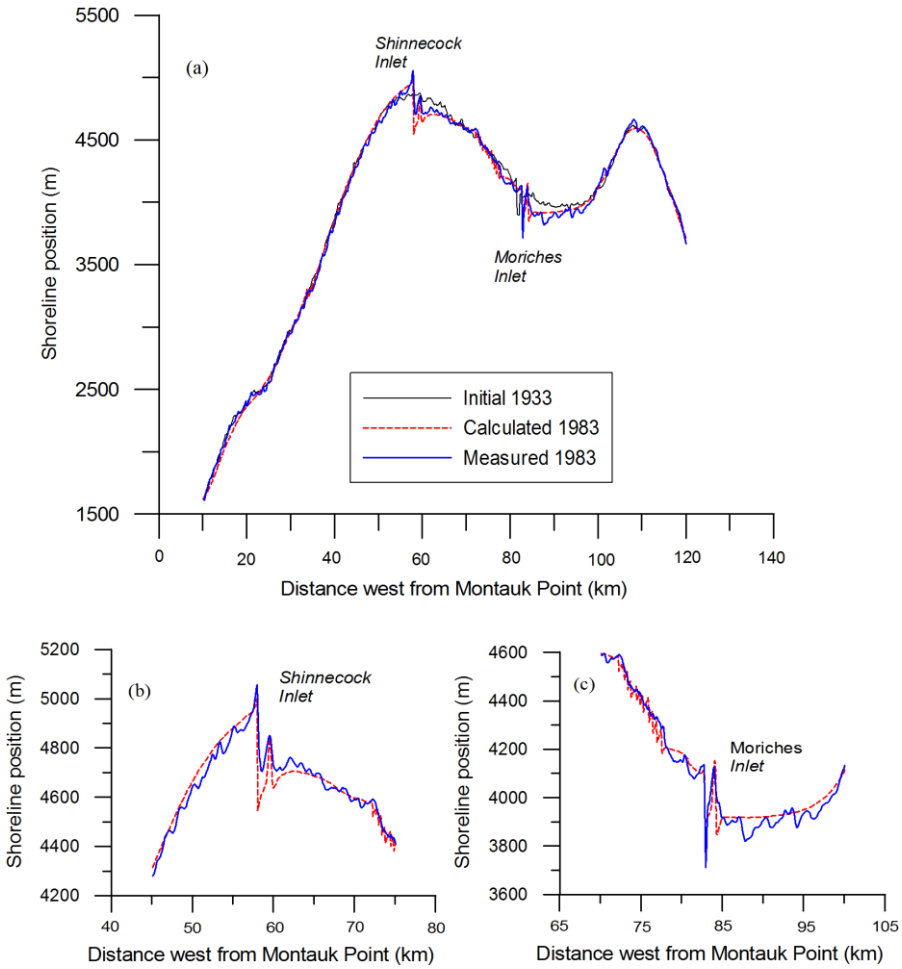

Fig. 22. Comparison between the measured and simulated shoreline in 1983 at the Long Island coast, (a): Overview and detail from (b) Shinnecock Inlet and (c) Moriches Inlet.

4.2.2 Modeled longshore transport

At Long Island coast, the simulated net transport rate together with the derived transport data reported by Rosati *et al.* (1999) is plotted in Fig. 23. The simulated annual net longshore transport rates were in good agreement with the analyzed data, except at Montauk Point where the rate was underestimated. The data from Rosati *et al.* (1999), for Montauk Point, included several important sinks and sources not described in the model, such as offshore losses due to sea level rise (76,000 m^3/yr), beach fill placement (from zero

to 170,000 m^3/yr), and bluff erosion (from 33,000 to 203,000 m^3/yr). This will affect net transport rates and cause a difference between the modeled and analyzed results at Montauk Point. The net annual longshore transport rate exhibits an increasing trend from Montauk Point to Fire Island Inlet. Since the tidal inlets act as sinks to the longshore transport as they evolve towards their equilibrium state, the net transport rate decreases significantly across the inlets. The average annual longshore net transport rate obtained in this study is 108,000 m^3/yr.

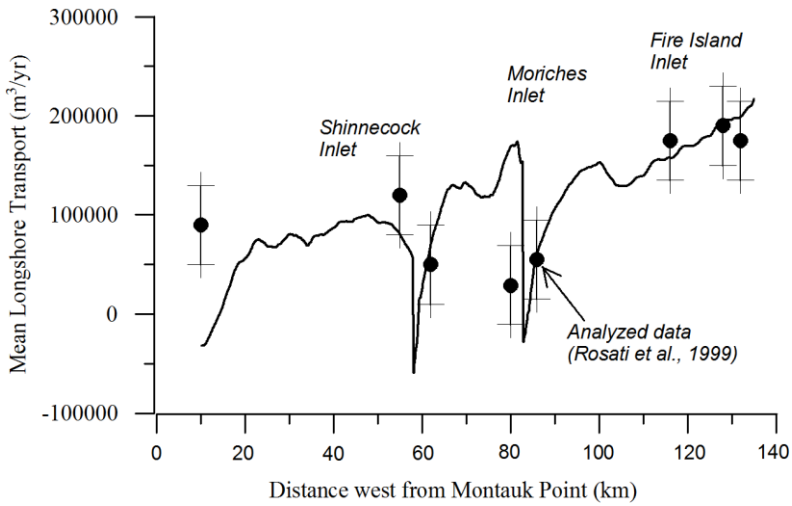

Fig. 23. Comparison between annual net transport rate and estimated data from measurements at Long Island coast.

4.2.3 Modeled flood and ebb shoal growth

The model was also run for the period 1933 to 2000 to compare with the measurements of ebb and flood shoal volume growth at Shinnecock and Moriches inlets on Long Island coast. Comparison between the calculated and measured ebb and flood shoal volumes are plotted in Figs. 24 and 25, respectively, where the total volume of the ebb shoal complex is displayed. Overall, the calculated and measured data are in good agreement, although specific individual points show more discrepancy.

4.2.4 Modeled barrier elongation

The model was run for a period between 1825 and 2010 to reproduce the barrier elongation at the Fire Island Inlet located at the south end of the Long Island coast (Fig. 14). Simulation results were compared with measured data reported by Kana (1995) and Kraus and Seabergh (2002), and the data based on satellite image in 2010 (Fig. 26). The measured position of the Fire Island barrier in 1825 was used as the initial condition in the model (Fig. 15). Overall, the calculated barrier elongation agreed well with the measured data, although some underestimation is observed between 1933 and 1962. These

differences may be caused by lack of detailed data on dredging as well as modifications to structures during this period. Also, the actual wave conditions were not known and the simulations were performed through the repetitive use of the 20-year hindcasted time series of waves.

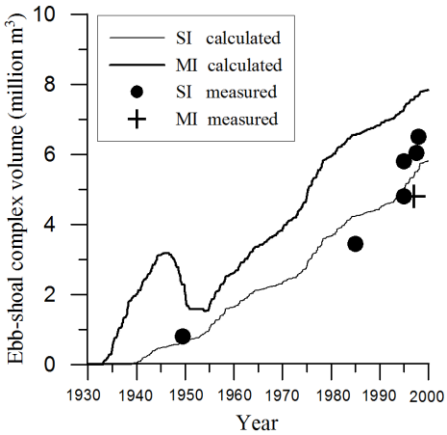

Fig. 24. Comparison between the measured and calculated volume of ebb-shoal complex (SI = Shinnecock Inlet, MI = Moriches Inlet).

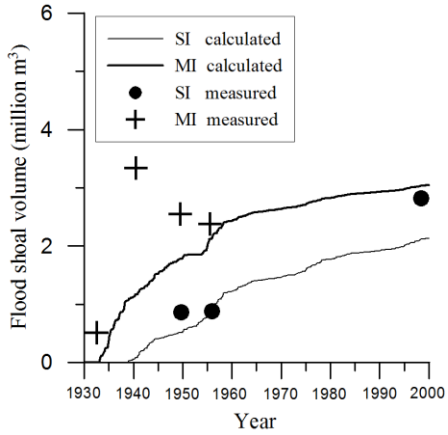

Fig. 25. Comparison between the measured and calculated volume of flood shoal (SI = Shinnecock Inlet, MI = Moriches Inlet).

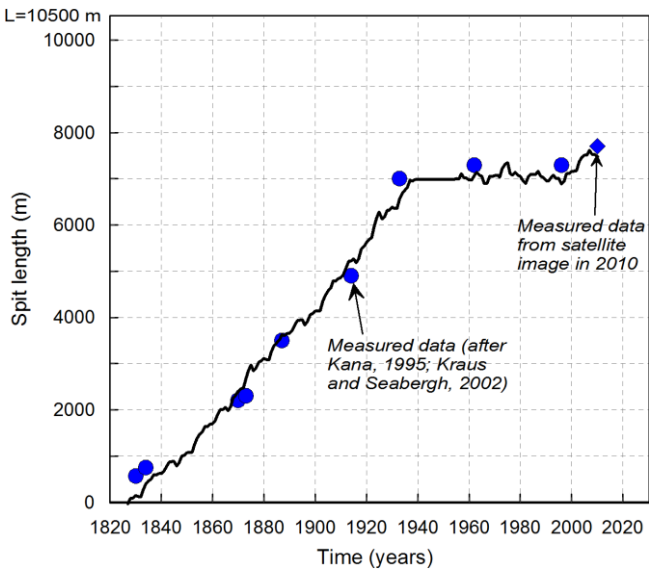

Fig. 26. Comparison between modeled and measured spit elongation at the Fire Island inlet.

4.3 Badreveln spit, Sweden

Comparison between the analytical solution and measured data of the spit elongation is plotted in the Fig. 27. The analytical solution employed the estimated incoming net LST at a rate of 10,000 m^3/yr. Overall, the analytical solution is in good agreement with the measured data.

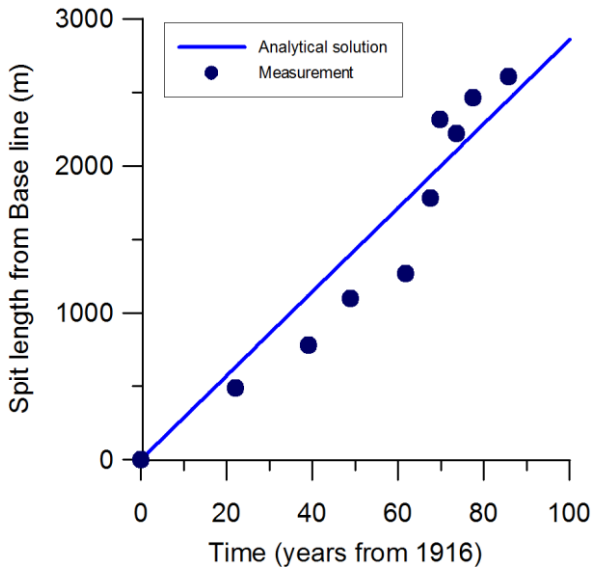

Fig. 27. Comparison between the analytical solution and measured data on spit elongation at the Badreveln spit, Sweden.

5. Conclusions

The new numerical model of regional sediment transport and shoreline change combined with the inlet reservoir model and spit growth model was developed and successfully applied to simulate: shoreline evolution at the Hai Hau beach, Vietnam; regional longshore transport rate, shoreline response in vicinity of the tidal inlets, sand volume growth of the flood shoals and ebb shoal complexes, and barrier elongation at the south Long Island coast, the United States; and spit growth at Badreveln spit, Sweden.

At the Hai Hau beach, the model simulation included the dike-seawall boundary condition, offshore sediment losses, and the complex morphology around the Ba Lat river mouth. The overall magnitude and trend of the simulated shoreline evolution was in good agreement with the measurements. The modeled results showed that: the net sediment transport is in the southward direction and a large amount of fine sediment is transported offshore into deep water; gradients in the LST and the fine sediment lost are the major causes of the erosion; and the severe erosion at Hai Hau beach occurs mainly in winter.

At the south Long Island coast, the modeled domain covered a stretch of coastline from Montauk Point to Fire Island Inlet that includes two tidal inlets and other complex conditions involving a wide range of structures and engineering activities such as jetties, groins, and beach fills. Model calculations were compared with measurements of shoreline evolution, annual net longshore transport rates, flood shoal and ebb shoal complex volumes, and barrier elongation. The simulated shoreline agreed well with the measured shoreline, including the accumulation updrift the inlets, the overall erosion and the formation of salient-type features downdrift the inlets. The annual net longshore transport rates were overall in good agreement with the reported data, showing an increase in transport rate going west from Montauk Point. The growths of the flood and ebb shoal complexes at the inlets were also well predicted. The barrier elongation at the Fire Island inlet was well adapted to the measured data. The modeled results show the modified formulas and the new methods suggested by this study were working well at this study site.

At the Badreveln spit, an analytical solution to the spit model for unrestricted growth was validated through measurements with an estimated incoming net LST rate of about 10,000 m^3/yr. The analytical solution yielded predictions in good agreement with the measured data.

Application of the model to the Hai Hau beach and the Long Island coast shows the capability of the model to simulate regional sediment transport and shoreline evolution for complex conditions. Thus, a simulation domain may extend over hundreds of kilometers and cover several inlets, development of flood shoals and ebb shoal complexes, elongation of barrier islands, different shore protection measures, and shoreline response in the vicinity of inlets.

6. References

Bayram, A., Larson, M., and Hanson, H. (2007). A new formula for the total longshore sediment transport rate. *Coastal Engineering*, 54, 700-710.

Blomgren, S., and Hanson, H. (2000). Coastal Geomorphology at the Falsterbo Peninsula, Southern Sweden. *Journal of Coastal Research* 16(1), 15-25.

Bruun, P., and Gerritsen, F. (1959). Natural by-passing of sand at coastal inlets. *Proceedings of the American Society of Civil Engineerings* (New York), Vol. 85, No. WW4, pp. 75-107.

Buttolph, A.M., Reed, C.W., Kraus, N.C, Ono, N., Larson, M., Camenen, B., Hanson, H., and Zundel, A.K. (2006). Two-Dimensional Depth-Averaged Circulation Model M2D: Version 3.0, Report 2, Sediment Transport and Morphology Change. *Technical Report* ERDC/CHL TR-06-09, Coastal and Hydraulics Laboratory, Vicksburg, MS.

Camenen, B., and Larson, M. (2005). A general formula for non-cohesive bed load sediment transport. *Estuarine, Coastal and Shelf Science,* 63(1-2), 249-260.

Camenen, B., and Larson, M. (2007). A unified sediment transport formulation for coastal inlet application. *Technical report* ERDC/CHL CR-07-1, US Army Engineer Research and Development Center, Vicksburg, MS.

Camenen, B., and Larson, M. (2008). A general formula for noncohesive suspended sediment transport. *Journal of Coastal Research,* 24(3), 615-627.

Carr, E.E., and Kraus, N.C. (2001). Morphologic Asymmetries at Entrances to Tidal Inlet. *Coastal and Hydraulics Engineering technical Note* IV-33, U.S. Army Engineer Research and Development Centre, Vicksburg, MS.

Chu, Y., Gravens, M.B., Smith, J.M., Gorman, L.T., and Chen, H.S. (1987). Beach Erosion Control Study, Homer Spit, Alaska. *Miscellaneous Paper* CERC-87-15, U.S. Army Engineer Waterways Experiment Station, Coastal Engineering Research Center, Vicksburg, MS.

Dean, R.G. (1977). Equilibrium Beach Profiles: U.S. Atlantic and Gulf Coasts. Department of Civil Engineering, Ocean Engineering, Report No. 12. Newark, Delaware: University of Delaware, 45p.

Dean, R.D., and Walton, T.L. (1975). Sediment transport processes in the vicinity of inlets with special reference to sand transport. *Estuary Research*, Volume II, Geology and Engineering, L.E. Cronin, ed., Academy Press, New York, 129-149.

Donnelly, C., Hung, N.M., Larson, M., and Hanson, H. (2004). One-line modelling of complex beach conditions: an application to coastal erosion at Hai Hau beach in the Red River Delta, Vietnam. *Proceedings of the 29th Conference of Coastal Engineering* (Lisbon, Portugal), PP. 2449-2461.

Donnelly, C., Ranasinghe, R., and Larson, M. (2005). Numerical of Beach Profile Change Caused by Overwash. *Proceedings of Coastal Sediments '05,* ASCE (on CD).

FitzGerald, D.M., Kraus, N.C., and Hands, E.B. (2000). Natural Mechanisms of Sediment Bypassing at tidal Inlets. *Coastal and Hydraulics Engineering Technical Note* ERDC/CHL CHETN-IV-30, U.S. Army Engineering Research and Development Centre, Vicksburg, MS.

Gaudiano, D.J., and Kana T.W. (2001). Shoal bypassing in mixed energy inlets: Geomorphic variables and empirical predictions for nine south Carolina Inlets. *Journal of Coastal Research*, 17(2) 280-291.

Gravens, M.B., Scheffner, N.W., and Hubertz, J.M. (1989). Coastal Processes from Asbury Park to Manasquan, New Jersey. *Miscellaneous Paper* CERC-89-11, U.S. Army Engineer Waterways Experiment Station, Coastal Engineering Research Center, Vicksburg, MS.

Hanson, H. (1987). GENESIS: A generalized shoreline change numerical model for engineering use. Lund, Sweden: Department of Water Resources Engineering, Lund University, Ph.D. thesis, 206p.

Hanson, H. (1989). GENESIS - A Generalized Shoreline Change Numerical Model. *Journal of Coastal Research*, Vol 5(1), pp 1-27.

Hanson, H., and Kraus, N.C. (1986). Forecast of Shoreline Change Behind Multiple Coastal Structures. *Coastal Engineering in Japan*, Vol, 29, pp 195-213.

Hanson, H., and Kraus, N.C. (1989). GENESIS: Generalized Model for Simulating Shoreline Change. Report 1. Technical Reference. *Technical Report* CERC-89-19, US Army Engineer Waterways Experiment Station, Coastal Engineering Research Center, Vicksburg, MS.

Hanson, H., Kraus, N.C., and Nakashima, L. (1990). Shoreline Change Behind Transmissive Detached Breakwaters - Shoreline Change and Storm-Induced Beach Erosion Modeling: A collection of Seven Papers. *Miscellaneous Paper* CERC-90-2, U.S. Army Engineer Waterways Experiment Station, Coastal Engineering Research Center, Vicksburg, MS.

Hanson, H., and Larson, M. (1993). Sand Transport and Coastal Development at Skanör/Falsterbo. Report No. 3166. Department of Water Resources Engineering, Lund Inst. of Technology, Lund University, Lund, Sweden. (In Swedish.)

Hanson, H., Larson, M., and Kraus, N.C. (2001). A new approach to represent tidal currents in the one-line model concept. *Proceedings of Coastal Dynamics '01*, American Society of Civil Engineers.

Hanson, H., Larson, M., Kraus, N.C., and Gravens, M.B. (2006). Shoreline response to detached breakwaters and tidal current: Comparison of numerical and physical models. *Proceeding of the 30th Coastal Engineering Conference*, World Scinetific, pp. 3357-3369.

Hanson, H., and Militello, A. (2005). Representation of Non-Erodible (Hard) Bottom in Two-Dimensional Morphology Change Models. *Technical Note* ERDC/CHL CHETN-

IV-63, US Army Engineer Research and Development Center, Coastal and Hydraulics Laboratory, Vicksburg, MS.

Häglund, M., and Svensson, P. (2002). Coastal erosion at Hai Hau Beach in Red River Delta, Vietnam. Lund, Sweden: Department of Water Resources Engineering, Lund University, Master's thesis, 80p.

Hicks, D.M., and Hume, T.M. (1996). Morphology and size of ebb tidal deltas at natural inlets on open-sea and pocked-bay coasts, North Island, New Zealand. *Journal of Coastal Research*, 12(1), 47-63.

Inman, D.L., and Bagnold, R.A. (1963). Littoral Processes in the Sea. In: Hill, M.N. (Ed.), Vol. 3. Interscience, New York, pp. 529–533.

Jarrett, J.T. (1976). Tidal prism – inlet area relationships. U.S. Army Engineer Waterways Experiment Station, Vickburg, MS., 60p.

Kana, T.W. (1995). A mesoscale sediment budge for Long Island, New York. *Marine Geology*, 126(1), 87-110.

Kana, T.W., Hayter, E.J., and Work, P.A. (1999). Mesoscale sediment transport at southeastern U.S. tidal inlets: Conceptual model applicable to mixed energy settings. *Journal of Coastal Research*, 15(2), 303-313.

Kana, T.W., Williams, M.L., and Stevens, D. (1985). Managing shoreline changes in the presence of nearshore shoal migration and attachment. *Proceedings Coastal Zone '85* (ASCE, New York), pp. 1277-1294.

Keulegan, G.H., and Hall, J.V. (1950). A formula for the calculation of tidal discharge through an inlet. *U.S. Army Corps of Engineering, beach Erosion board Bulletin,* vol. 4, 15-29.

Kraus, N.C. (1998). Inlet cross-section area calculated by process-based model. *Proceeding of the 26th Coastal Engineering Conference*, ASCE, pp. 3265-3278.

Kraus, N.C. (1999). Analytical model of spit evolution at inlets. *Proceeding of Coastal Sediments '99*, ASCE, pp. 1739-1754.

Kraus, N.C. (2000). Reservoir model of ebb-tidal shoal evolution and sand bypassing. *Journal of Waterway, Port, Coastal, and Ocean Engineering*, 126(3), 305-313.

Kraus, N.C. (2002). Reservoir model for calculating natural sand bypassing and change in volume of ebb-tidal shoals, part I: Description. *Coastal and Hydraulics Engineering Technical Note* ERDC/CHL CHETN-IV-39, U.S. Army Engineering Research and Development Centre, Vicksburg, MS.

Kraus, N.C., Hanson, H, and Harikai, S. (1984). Shoreline Change at Oarai Beach, Japan: Past, Present and Future. *Proceedings of 19th Coastal Engineering Conference*, American Society of Civil Engineers, pp 2107-2123.

Kraus, N.C., Scheffner, N.W., Hanson, H., Chou, L.W., Cialone, M.A., Smith, J.M., and Hardy, T.A. (1988). Coastal Processes at Sea Bright to Ocean Township, New Jersey,

Volume 1: Main Text and Appendix A. *Miscellaneous Paper* CERC-88-12, U.S. Army Engineer Waterways Experiment Station, Coastal Engineering Research Center, Vicksburg, MS.

Kraus, N.C., and Seabergh, W.C. (2002). Inlet spit and Maintenance of navigation channels. *Coastal and Hydraulics Engineering Technical Note* ERDC/CHL CHETN-IV-44, U.S. Army Engineering Research and Development Centre, Vicksburg, MS.

Kraus, N.C., and Wise, R.A. (1993). Simulation of January 4, 1992 Storm Erosion at Ocean City, Maryland. *Shore and Beach*, 61(1), 34-41.

Kriebel, D.L. (1982). Beach and Dune Response to Hurricanes. M.S. Thesis, University of Delaware, Newark, DE, 163p.

Kriebel, D.L., and Dean., R.G. (1985). Numerical Simulation of Time-Dependent Beach and Dune Erosion. *Coastal Engineering*, Vol. 9, 221-245.

Larson, M., Capobianco, M., and Wise, R.A. (1999). Modeling Cross-Shore Sediment Transport at Different Scales Using Equilibrium Beach Profile Theory. *Proceedings of Coastal Sediments '99*, American Society of Civil Engineer, pp 1371-1386.

Larson, M., and Kraus, N.C. (1989). SBEACH: Numerical Model for Simulating Storm-Induced Beach Change, Report 1: Empirical Foundation and Model Development. *Technical Report* CERC-89-9, U.S. Army Engineer Waterways Experiment Station, Coastal Engineering Research Center, Vicksburg, MS.

Larson, M., and Kraus, N.C. (1998). SBEACH: Numerical Model for Simulating Storm-Induced Beach Change, Report 5: Representation of Non-Erodible (Hard) Bottoms. *Technical Report* CERC-89-9, U.S. Army Engineer Waterways Experiment Station, Coastal Engineering Research Center, Vicksburg, MS.

Larson, M., and Kraus, N.C. (2003). Modeling Regional Sediment Transport and Coastal Evolution along the Delmarva Peninsula. *Proceedings Coastal Sediments '03*, ASCE (on CD).

Larson, M., Kraus, N. C., and Byrnes, M. (1990). SBEACH: Numerical Model for Simulating Storm-Induced Beach Change. Report 2: Numerical Formulation and Model Tests. *Technical Report* CERC-89-9, U.S. Army Engineer Waterways Experiment Station, Coastal Engineering Research Center, Vicksburg, MS.

Larson, M., Kraus, N.C., and Connell, K.L. (2006). Modeling sediment storage and transfer for simulating regional coastal evolution. *Proceeding of the 30th Coastal Engineering Conference* (California, USA), World Scientific, pp. 3924-3936.

Larson, M., Kraus, N.C., and Hanson, H. (2002a). Simulation of regional longshore sediment transport and coastal evolution- the Cascade model. *Proceeding of the 28th Coastal Engineering Conference*. World Scientific Press, 2002.

Larson, M., Hanson, H., and Kraus, N.C. (1987). Analytical Solutions of the One-Line Model of Shoreline Change. *Technical Report* CERC-87-15, U.S. Army Engineer

Waterways Experiment Station, Coastal Engineering Research Center, Vicksburg, MS.

Larson, M., Rosati, J.D., and Kraus, N.C. (2002b). Overview of regional coastal processes and controls. *Coastal and Hydraulics Engineering Technical Note* CHETN XIV-4, U.S. Army Engineer Research and Development Center, Vicksburg, MS.

Larson, M., Wise, R. A., and Kraus, N. C. (2004). Modeling Dune Response due to Overwash Transport. *Proceedings 29th Coastal Engineering Conference*, World Scientific Press, pp. 2133-2145.

Luettich, R.A., Westerink, J.J., and Scheffner, N.W. (1992). ADCIRC: an Advanced Three-Dimensional Circulation Model for Shelves, Coasts, and Estuaries. Report 1: Theory and Methodology of ADCIRC-2DDI and ADCIRC-3DL. *Technical Report* DRP-92-6, U.S. Army Engineer Waterways Experiment Station, Vicksburg, MS.

Mase, H. (2001). Multi-directional random wave transformation model based on energy balance equation. *Coastal Engineering Journal*, 43(4), 317-337.

Militello, A., and Kraus, N.C. (2001). Shinnecock Inlet, New York, site investigation, Report 4, Evaluation of flood and ebb shoal sediment source alternatives for the west of Shinnecock Interim Project, new York, *Technical Report* CHL-98-32, U.S. Army Corps of Engineers, Engineer Research and Development Centre, Vicksburg, MS.

Militello, A., Reed, C.W., Zundel, A.K., and Kraus, N.C. (2004). Two-Dimensional Depth-Averaged Circulation Model M2D: Version 2.0, Report 1, Technical Documentation and User's Guide. *Technical Report* ERDC/CHL TR-04-02, Coastal and Hydraulics Laboratory, Vicksburg, MS.

Pelnard-Considere, R. (1956). Essai de theorie de l'evolution des forms de rivage en plage de sable et de galets. 4th Journees de l'Hydraulique, Les Energies de la mer, Question III, Rapport No. 1, pp. 289-298 (in French).

Pruszak, Z., Szmytkiewicz, M., Hung, N.M., and Ninh, P.V. (2002). Coastal Processes in the Red River Delta area, Vietnam. *Coastal Engineering Journal*, 44(2), 97-126.

Psuty, N.P., Grace, M., and Pace, J.P. (2005). The coastal geomorphology of Fire Island, A portrait of continuity and change. *Technical Report* NPS/NER/NRTR-2005/021. U.S. Department of the Interior, National Park Service, Northeast Region, Boston, Massachusetts.

Rosati, J.D., Gravens, M.B., and Smith, W.G. (1999). Regional sediment budget for Fire Island to Montauk Point, New York, USA. *Proceeding of Coastal Sediment Conference* -1999. pp. 803-817.

Smith, W.G., Watson, K., Rahoy, D., Rasmussen, C., and Headland, J.R. (1999). Historic geomorphology and dynamics of Fire Island, Moriches and Shinnecock Inlets, New York. *Proceedings of Coastal Sediment'99*, ASCE, pp. 1597-1612.

Soulsby, R. (1998). Dynamics of Marine Sands, Thomas Telford Ltd., London, U.K.

Swart, D.H. (1974). A Schematization of Onshore-Offshore Transport. *Proceedings of 14th Coastal Engineering Conference*, American Society of Civil Engineers, pp. 884-900.

Swart, D.H. (1976). Predictive Equations Regarding Coastal Transport. *Proceedings of 15th Coastal Engineering Conference*, American Society of Civil Engineers, pp. 1113-1132.

Van Rijn, L.C. (1993). *Principles of sediment transport in rivers, estuaries and coastal seas*. University of Utrecht, Department of Physical Geography, Aqua Publications.

Vellinga, P. (1982). Predictive Computational Model for Beach and Dune Erosion During Storm Surge. *Proceedings of Coastal Structures '83*, American Society of Civil Engineers, pp. 806-819.

Vogel, M.J., and Kana, T.W. (1984). Sedimentation patterns in a tidal inlet system, Moriches inlet, New York. *Proceeding of the 19th Coastal Engineering Conference.* World Scientific. pp. 3017-3033.

Watanabe, A., Shimizu, T., and Kondo, K. (1991). Field application of a numerical model of beach topography response. *Proceedings of Coastal Sediments '91*, ASCE, pp. 1814-1828.

Wijdeven, B. (2002). Coastal Erosion on a Densely Populatated Delta Coast, the interactions between man and nature: a case study of Nam Dinh province, Red River delta, Vietnam. Delft, the Netherlands: Faculty of Civil Engineering and Geosciences, Delft University of Technology, M.S. thesis, 163p.

Williams, G.L., Morang, A., and Lillycrop, L. (1998). Shinnecock Inlet, New York, site investigation, Report 2, Evaluation of sand bypass options. *Technical Report* CHL-98-32, U.S. Army Corps of Engineers, Waterways Experiment Station, Vicksburg, MS.

Williams, M.L., and Kana, T.W. (1987). Inlet shoal attachment and erosion at Isle of Palms, South Carolina: A replay. *Proceedings of Coastal Sediment'87*, (Columbia, SC), pp. 1174-1187.

Wise, R.A., and Kraus, N.C. (1993). Simulation of Beach Fill Response to Multiple Storms, Ocean City, MD. *Proceedings of Coastal Zone '93*, American Society of Civil Engineers, pp. 133-147.

Wise, R.A., Smith, S.J., and Larson, M. (1996). SBEACH: Numerical Model for Simulating Storm-Induced Beach Change. Report 4. Cross-Shore Transport Under Random Waves and Model Validation with SUPERTANK and Field Data. *Technical Report* CERC-89-9, U.S. Army Engineer Waterways Experiment Station, Coastal Engineering Research Center, Vicksburg, MS.

Appendix

Hoan, L.X., Hanson, H., Larson, M., Donnelly, C., and Nam, T.P. (2010). Modeling Shoreline Evolution at Hai Hau Beach, Vietnam. *Journal of Coastal Research,* 26(1), 31-43.

Journal of Coastal Research	26	1	31–43	West Palm Beach, Florida	January 2010

Modeling Shoreline Evolution at Hai Hau Beach, Vietnam

Le Xuan Hoan[†‡], Hans Hanson[†], Magnus Larson[†], Chantal Donnelly[†], and Pham Thanh Nam[†‡]

[†]Lund University
Department of Water Resources Engineering
Box 118, SE-221 00 Lund
Sweden
Hoan.Le_Xuan@tvrl.lth.se

[‡]Vietnamese Academy of Science and Technology
Institute of Mechanics
264 Doi Can, Hanoi
Vietnam

ABSTRACT

HOAN, L.X.; HANSON, H.; LARSON, M.; DONNELLY, C., and NAM, P.T., 2010. Modeling shoreline evolution at Hai Hau Beach, Vietnam. *Journal of Coastal Research,* 26(1), 31–43. West Palm Beach (Florida), ISSN 0749-0208.

The coastline of Hai Hau District, located on the northeast coast of Vietnam with about 30 km of shoreline, is chronically eroding. Previous studies have tried to highlight the main causes of the erosion along this coastline, and several hypotheses exist. To examine the hypothesis that gradients in the longshore sediment transport rate and cross-shore fine sediment lost offshore are the main causes generating the serius erosion at Hai Hau Beach, a newly developed numerical model of shoreline change based on the one-line theory was applied and compared with data. Sea dike segments, reinforced by stones and mortar, were modeled using a seawall boundary condition, and the sediment continuity equation was modified to take into account the offshore transport of fine-grained sediment. The simulated shorelines agreed well with the measured shorelines, both for the calibration and validation periods. The calculated sediment budget shows that the net sediment transport is in the southward direction and that a large amount of fine-grained sediment is lost into deep water. These two sinks of sediment are believed to be the main causes of the serious erosion at Hai Hau Beach.

ADDITIONAL INDEX WORDS: *Hai Hau Beach, Ba Lat Mouth, shoreline evolution, sediment transport, fine sediment, shoreline modeling.*

INTRODUCTION

The Red River system laden with alluvia forms a flat fertile plain and 165 km of coastline, mainly belonging to the coastal Nam Dinh and Thai Binh Provinces in the northeast coast of Vietnam. The annual amount of sediment transported by the Red River system is about 100×10^6 tn (Ninh, Quynh, and Viet Lien, 2001; Pruszak *et al.,* 2002; Van Maren and Hoekstra, 2004), discharging into the Gulf of Tonkin through seven active mouths (from north to south): Van Uc, Thai Binh, Diem Dien, Tra Ly, Ba Lat, Lach Giang, and Day (Figure 1). These major river mouths represent very rapid accretion zones where the shoreline is expanding at a rate of about 15–100 m/y (Do *et al.,* 2007; Van Maren and Hoekstra, 2004).

The main portion of the coastline of Nam Dinh and Thai Binh Provinces, particularly at the seven active river mouths, is stable or accreting, while the coastline segment of Hai Hau District, the area of interest between Ha Lan and Lach Giang estuaries, is seriously eroding. According to several recent studies, the erosion rate averaged along the coastline is about 5–10 m/y (Donnelly *et al.,* 2004; Wijdeven, 2002), with a maximum rate reaching 19–35 m/y (Pruszak *et al.,* 2002).

Several studies have postulated hypotheses for the cause of the erosion at Hai Hau Beach. Saito (2001), Thanh *et al.* (2005), and Quynh Le *et al.* (2007) analyzed measured data of suspended sediment carried by the Red River system and showed that the total suspended load has significantly decreased (about 20–40%) after the construction of the Hoa Binh dam (built in 1983) and the Thac Ba dam (built in 1968) in the upstream part of the river. This implies that the total sediment supply to Hai Hau Beach has significantly diminished, which is suggested to be one of the main causes of the serious erosion there. Pruszak (1998) suggested that the construction of the Hoa Binh dam and/or the cutting off of the Ha Lan River (Figure 1) in 1955 caused a deficit in the sediment supply to the Hai Hau coast, resulting in serious erosion. Other proposed causes include deforestation (Pruszak, 1998), the reduction in sediment from river training, and sea level rise (Huan, 1996). However, satellite images and measured data on shoreline change show that the erosion at Hai Hau Beach started in the beginning of the 20th century, and it seems to have slowed down after 1966, well before these interferences with the natural river system (that is, the cutting off of the Ha Lan River and the building of the Hoa Binh and Thac Ba dams) occurred. Thus, these interferences cannot be the main reasons for the persistent erosion problems (Vinh *et al.,* 1996).

Do *et al.* (2007) analyzed the grain-size trends and transport vectors of the Red River Delta and showed that the dominant transport directions are perpendicular to the depth contours to a depth of about 25 m, and alongshore in the southward direction in coastal waters shallower than 5 m. Because the headland of the Ba Lat Estuary protrudes well from the mainland and the shoreline of Hai Hau runs in the NE-SW

DOI: 10.2112/08-1061.1 received 17 April 2008; accepted in revision 28 July 2008.

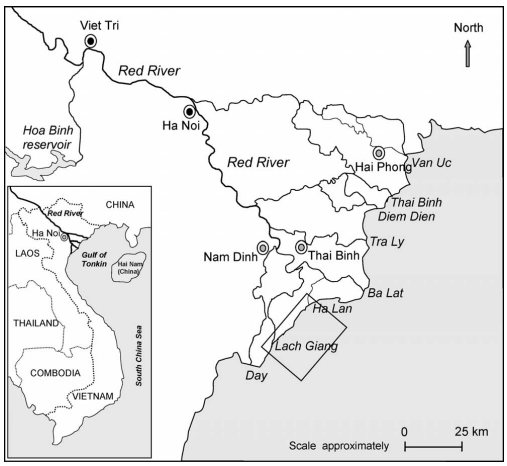

Figure 1. Study site and the distributaries of the Red River system.

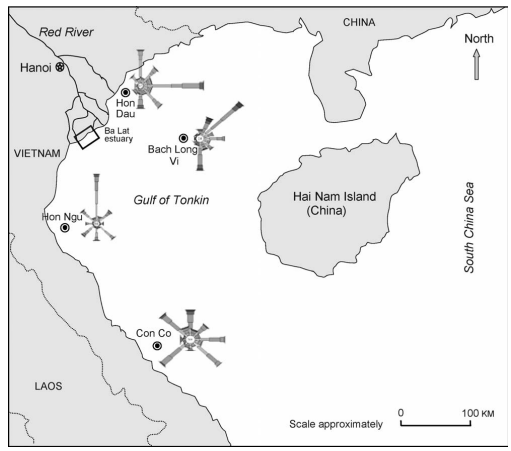

Figure 2. Wind roses at the stations around Hai Hau Beach, based on time series of 20 years (from 1976 to 1996) with four records a day and converted to 10 m above mean sea level.

direction (Figure 1), southward sediment transport from the Ba Lat falls into the deep water off Hai Hau Beach. Thus, this erosional beach is not supplied with sediment from the Ba Lat Mouth. Donnelly *et al.* (2004), Häglund and Svensson (2002), and Wijdeven (2002) suggested that coastal erosion at Hai Hau Beach is caused by net longshore sediment transport (LST) rates or, more specifically, gradients in the LST, and fine-grained-size sediment from the beach lost into deep water. This is believed to be the most likely cause for the retreat of Hai Hau Beach. However, none of the previous studies have been able to conclusively prove this.

The main objectives of the present study were to establish the cause of the erosion at Hai Hau Beach and to estimate the recession rate. A new numerical model based on the one-line theory of shoreline change was used to quantify the gradients in LST, to determine the cause of these gradients, and to model the shoreline response. In the future, the calibrated and validated model may assist in determining remediation measures to stabilize the shoreline. Measured shoreline positions in 1910, 1965, and 2000 were used to calibrate and validate the model.

ENVIRONMENTAL CONDITIONS AT THE SITE

Winds

The wind climate in the northern part of Vietnam is clearly distinguished by two main monsoons, the winter monsoon and the summer monsoon. The winter monsoon (November to March) is characterized by strong winds blowing from the north, lower temperature, and lower precipitation. The summer monsoon (May to September) is characterized by moderate winds blowing from the south, higher temperature, and higher precipitation. In addition, there is a transition period between the two main monsoons (April and October), characterized by light eastern trade winds with cool weather.

The wind roses at four stations around Hai Hau Beach (Figure 2) show that the wind field within the Gulf of Tonkin is markedly affected by the topography. Since the Bach Long Vi (BLV) station is located in the middle of the Gulf of Tonkin (on Bach Long Vi Island), away from the mainland, wind data recorded at this station are expected to be most representative for calculating offshore waves at Hai Hau Beach (Pruszak *et al.,* 2002; Wijdeven, 2002).

Nearshore Topography

The nearshore region of Hai Hau Beach has a very gentle slope, creating a relatively wide zone for wave transformation and energy dissipation (Pruszak *et al.,* 2002). A bathymetry map of the site extracted from a Vietnamese navy map with bathymetry corrections from 1980 shows that the depth contours at Hai Hau Beach are more or less parallel with the shoreline and that the offshore slope is rather constant (Figure 3). However, seaward of the Ba Lat Mouth, the slope is steeper and a more complex topography occurs, creating losses of alluvial sediment to offshore locations (Wijdeven, 2002). The mean beach slopes, based on cross-shore profiles measured in 2001, determined from the offshore distance to a depth of 7–8 m, are about 1.0–1.6%. Near the Ba Lat Mouth, the sea floor has a slope of 4.0% (Wijdeven, 2002). The results of a least-square fit with the equilibrium beach profile (EBP) shape introduced by Dean (1977) against four measured cross-shore profiles (profile numbers MC12, MC13, MC21, and MC22; see Figure 3) produced values of the scale parameter (A) in the range 0.063–0.081 $m^{1/3}$. This corresponds to a median grain size (D_{50}) of about 0.14–0.18 mm (see Figure 4 and Table 1).

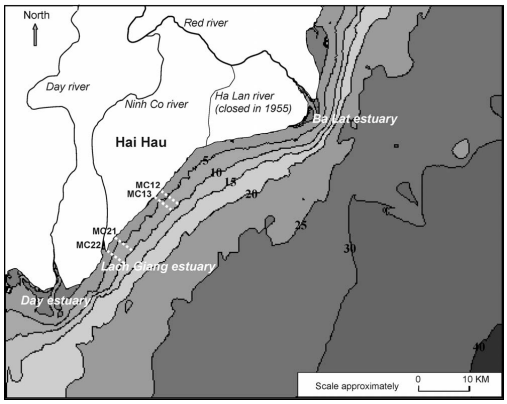

Figure 3. Bathymetry map of the site and locations of the measured cross-shore profiles.

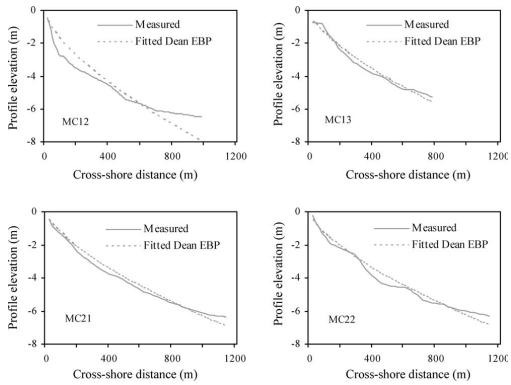

Figure 4. Comparison of measured profiles and fitted EBP at four cross-shore sections.

Wave Climate

Because of the prevailing wind climate, the deepwater wave regime in the Gulf of Tonkin has clear seasonal features. Based on the data from visual buoy observations at Hon Dau station, Pruszak *et al.* (2002) and Vinh *et al.* (1996) showed that in the winter the prevailing waves arrive from the northeast, whereas in the summer the waves come from the east and southeast (in deep water). Wind velocities during the winter monsoon are stronger than during the summer monsoon, generating higher waves in deep water relative to the summer monsoon. The estimated average wave height in deep water is in the range of 1.8–2.0 m for winter and 1.2–1.4 m for summer. However, the most pronounced seasonal difference is probably the frequency of occurrence of significant wave height, H_s: an H_s of 3 m is exceeded 10% of the time in the winter, whereas an H_s of 2 m is exceeded 10% of the time in the summer (Van Maren, 2004).

In the northern part of Vietnam, storms and typhoons mainly occur in July and August (during the summer period). On average two storm or typhoon events per year hit the coastline in the northern provinces of Vietnam. During storms or typhoons the deep water wave height can reach up to 8–10 m and the storm surge up to 2 m (Ninh, Quynh, and Viet Lien, 2001; Pruszak *et al.,* 2002; Sundstrom and Soderval, 2004; Vinh *et al.,* 1996).

For Vietnam in general and Hai Hau Beach in particular, long time series of wave measurements are not available. Within the framework of a program funded by the Swedish International Development Cooperation Agency (SIDA), four field campaigns were carried out at anchored stations off Hai Hau Beach in 2005 and 2006 (Hung *et al.,* 2006; Sjödahl and Kalantari, 2005). However, this field work was performed in moderate weather conditions and for short-term periods (around 10 d). The frequency of occurrence of significant wave heights, based on the measured data at the anchored station at a 20-m depth (Station S1; see Figure 5), show that in winter, measured wave heights were higher than in summer (Figure 6). In the winter, H_s exceeds 1.0 m during 10% of the measurement time, whereas in the summer H_s exceeds 0.6 m during 10% of measurement time.

Because the Gulf of Tonkin connects to the South China Sea through a large opening in the southeast direction (Figure 2), swell waves will occur in the Gulf of Tonkin when strong wave conditions exist in the South China Sea; for example, during strong monsoons, tropical storms, or typhoons. Recently, simultaneous measurements of wave and wind parameters at anchored stations around Hai Hau Beach indicate that swell wave height higher than 1.0 m occurred, even when wind conditions were calm (Hung *et al.,* 2006). Thus, tropical storms and typhoons occurring in the southern part of the South China Sea may damage the Hai Hau coast through the swell waves they generate.

Tides

Field observations show that astronomical tides are of a regular diurnal type. Tidal waves enter from the South China Sea and are partly reflected in the northern enclosure of the Gulf of Tonkin. With a length of approximately 500 km and a depth of 50 m, the resonance time of the basin is about 25 hours (Van Maren and Hoekstra, 2004), which is close to the period of the diurnal tides. Therefore, the diurnal components

Table 1. *Results of least-square fit to the measured profiles, with EBP shape introduced by Dean (1977).*

Profile Number	A ($m^{1/3}$)	D_{50} (mm)	E_{rms}[1]
MC12	0.081	0.18	0.72
MC13	0.063	0.14	0.23
MC21	0.063	0.14	0.25
MC22	0.064	0.14	0.33

[1] Root-mean-square deviation.

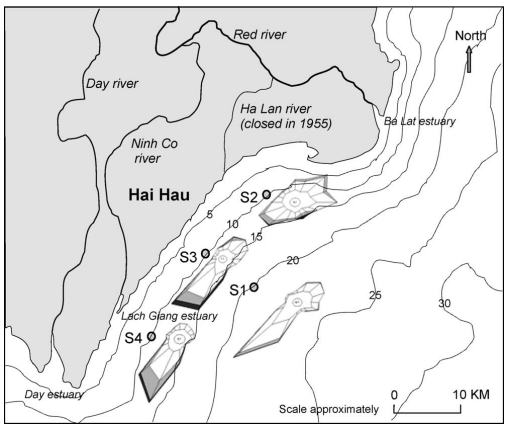

Figure 5. Current prisms based on short-term series of measured data in 2005 and 2006 at four anchored stations.

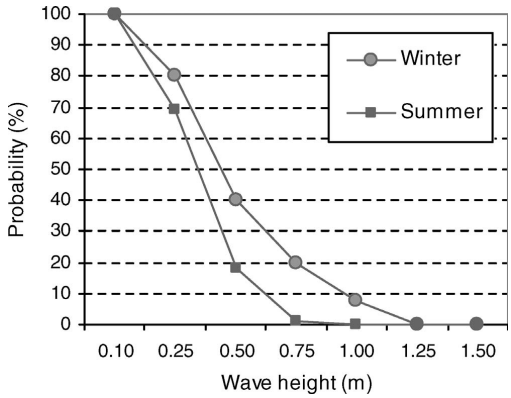

Figure 6. Frequency of occurrence of significant wave height, based on the short-term series of measured data in 2005 and 2006 at a depth of 20 m off Hai Hau Beach.

O1 and K1 are near resonance mode, and the amplitude of these components increases northward along the Vietnamese coastline (Guohong *et al.,* 1999). Tidal range in the study area varies from 0.5 m during neap tide to 3.2 m during spring tide.

Current Regime

The major current components in the nearshore zone include wave-induced currents, tidal currents, wind-driven currents, and river outflow (near the river mouths). These current components interact with the dynamic morphology and generate complicated nearshore current circulation patterns (Pruszak *et al.,* 2002).

Since the shoreline of Hai Hau Beach runs in the NE-SW direction, dominant wave directions in both winter and summer are largely oblique to the shoreline, resulting in strong wave-generated currents alongshore. At Hai Hau Beach, wave-induced currents are expected to be the dominant currents for generating sediment transport and morphological change.

The tidal currents play a primary role in the formation of tidal flats and tidal channels in the coastal low-lying wetland area. In the Gulf of Tonkin, tidal waves propagate from south to north, resulting in tidal currents that are northward during flood tide and southward during ebb tide. The average tidal flow in the nearshore zone, at a depth of about 5 m, has a velocity of 25–40 cm/s. The maximum tidal velocity may reach 60–80 cm/s (Pruszak *et al.,* 2002). Due to the asymmetry of tidal currents in the nearshore regions, the period of flood tide is shorter than that of ebb tide, 42% and 58% of the time, respectively, resulting in south-directed net tidal currents in the coastal zone (Van Maren and Hoekstra, 2004).

It is noteworthy that, based on measured data and numerical models, Ninh, Quynh, and Viet Lien (2001) and Van Maren and Hoekstra (2004) showed that the wind-driven current circulation is rotating counterclockwise, and its center is located in the middle of the Gulf of Tonkin during both the winter and summer monsoons. Therefore, in the nearshore zone of Hai Hau Beach, the residual current is consistently in the southward direction. However, as mentioned above, wind velocity during winter is stronger than that during summer, and the consistent wind current in winter is stronger than that in summer (Van Maren, 2004).

Long-term current measurements do not exist in Vietnam in general; field campaigns have mainly lasted from 2 to 7 days. Within the SIDA program, as mentioned above, four anchored stations of current measurements were set up off Hai Hau Beach (Figure 5). The field campaigns were carried out in 2005 and 2006, in January (typical winter month) and August (typical summer month), each campaign lasting about 10 days. The current prisms based on the integrated measurement data show that the residual currents are clearly in the southward direction in both winter and summer, except at station number 2 (S2) located at the northernmost point. Average current velocities occurring during the field campaign periods were about 30 cm/s, and maximum values were about 50–80 cm/s.

Riverine Budgets

The Red River brings a huge amount of sediment that is discharged into the Gulf of Tonkin through the seven active river mouths. The annual sediment load discharged to the sea has a clear seasonal variation. Rainfall in summer is much higher (about 80% of total annual rainfall) than in winter, resulting in most of the sediment load being discharged in summer (around 91–96% of the total of annual sediment load; see Van Maren and Hoekstra, 2004). The total sediment load discharged to the sea by the Red River is estimated in the range of 75–100 million tn per year. About 30% of the

total sediment load remains in the nearshore zone and develops sandy ridges and tidal flats (depths below 2 m); the remaining material passes the intertidal plain and goes offshore to deep water areas (depths of 2 m to 30 m; Do *et al.,* 2007; Pruszak *et al.,* 2002). Percent relative river discharge load per distributary of the Red River system are (from north to south in Figure 1): Van Uc, 19%; Thai Binh, 6%; Tra Ly, 9%; Ba Lat, 21%; Lach Giang, 6%; Day, 19%; and 20% for all smaller distributaries (Van Maren and Hoekstra, 2004).

Sea Dikes

In order to secure the coastal areas and to protect the inhabitants during storms or typhoons, sea dike defense systems have been constructed. At Hai Hau District the system comprises two parallel dikes with a distance of about 200–250 m in between. Their purpose is to withstand attacks by heavy storms or typhoons. During a storm or typhoon attack, if the first dike facing the sea fails, resulting in some dike sections being breached and the land between the two dikes inundated, then the second dike diminishes effects of flooding on the inhabitants and agricultural land behind this dike. When breaching at the first dike takes place, the land in between the two dikes is considered lost, and a new dike will be built behind the former second dike.

Overall, sea dike defense systems in Vietnam, including in the Hai Hau District, are made purely of soil or soil core covered by a revetment layer of stones. These sea dikes, therefore, often fail during heavy attacks such as storms or typhoons. Since the first dike in the Hai Hau District directly faces heavy attacks from the sea, it has been upgraded with stones and mortar. In a 5-year (1995–2000) project funded by the French government to upgrade the sea dike system of Nam Dinh Province, some dike sections at Hai Hau District were reinforced. However, these dike sections can only survive moderate weather conditions and may still fail during heavy attacks. This dike system is not capable of stopping the erosion, but it seems to decrease the erosion rate. The erosion of the sea dike system at Hai Hau does not depend only on the structure of the revetment; scours developing at the dike toe is another issue. The dike toe is gradually undermined even during moderate weather conditions, resulting in a series of cavelike features penetrating into the dike body. Thus, scours create favorable conditions for breaching and subsequent sea dike collapse when heavy attacks occur.

MODELING OF SHORELINE CHANGE

Offshore Wave Climate Estimation

In general, the main challenge in modeling of a coastal process is to estimate accurately the offshore wave climate. Long-term time series of offshore wave data are not available in Vietnam or at Hai Hau Beach. Therefore, offshore waves were hindcasted from wind data recorded at the wind stations around the study area. As mentioned previously, wind data at BLV station (see Figure 2) were preferred to estimate offshore waves (Pruszak *et al.,* 2002; Wijdeven, 2002). However, by comparing measured wave data with predictions from winds at Con Co (CC) station, Häglund and Svensson (2002) realized that the wind at CC station may significantly control the wave climate at Hai Hau Beach under certain circumstances. In order to derive a more representative wind climate for the waves, they suggested the approach of combining wind data at BLV and CC. In the present study, a long-term time series of waves (20 y from 1976 to 1996) was estimated by combining wind data at BLV and CC. The procedure for combining wind data postulated by Häglund and Svensson (2002) was applied. Wind data at BLV are mainly used to estimate the offshore waves, except when the wind comes from the angle band between SE and SW. In those cases, the offshore waves at Hai Hau Beach are approaching from the south, and thus they are partly controlled by the wind climate at CC station (see Figure 2). Therefore, within this angle band, wind data at CC was included in estimating the offshore waves by using the wind direction at CC and a weighted average value of the measured wind speeds at BLV and CC.

A commonly applied wave hindcasting method was used to calculate the offshore wave parameters. The Sverdrup-Munk-Bretschneider (SMB) method described in USACE (1984) was verified by comparing the wave climate hindcast with visually observed wave records at BLV station during 1 year, 1984 (Donnelly *et al.,* 2004; Häglund and Svensson, 2002). Thus, in this study the waves were calculated using the SMB method and used as input data to a nearshore wave transformation model.

In order to estimate the waves generated during extreme storms or typhoons, in the absence of measurements, a numerical model for storm- and typhoon-generated waves is most reliable. Here, for simplicity, the parametric wave model developed by Young in 1987, described in USACE (2002), based on results from simulations with a numerical spectral model, was used to estimate waves generated by extreme storms or typhoons.

Nearshore Wave Transformation

Some earlier studies (Häglund and Svensson, 2002; Pruszak *et al.,* 2002; Wijdeven, 2002) used one-dimensional wave transformation models to estimate the nearshore wave characteristics. However, the bathymetry offshore of Hai Hau Beach is complex, and in this case, a one-dimensional transformation is insufficient to account for the changes in wave angle that can have a significant effect on the sediment transport direction (Donnelly *et al.,* 2004). Donnelly *et al.* (2004), Hung, Hanson, and Dien (2006), and Sjödahl and Kalantari (2005) used the 2-D STeady State spectral WAVE (STWAVE) transformation model to calculate the inshore wave climate. STWAVE is a steady-state finite-difference model based on the wave-action balance equation (Smith, Sherlock, and Resio, 2001). Advantages of using STWAVE include the ability to model wave transformation over complicated bathymetry quickly and efficiently for many different wave spectra.

In the present study, another 2-D Energy Balance Equation with a Diffraction term (EBED) transformation model was applied to calculate the inshore wave climate. The EBED model was developed by Mase (2001) based on the energy-balance equation for multidirectional random waves, taking

into account wave shoaling, refraction, diffraction, and wave breaking. Advantages of using the EBED model include the ability to reproduce wave transformation over complicated bathymetry and the facilities for setting up the input and output for many different wave spectra. The 20-year-long hindcast time series of offshore waves was used as input data for the EBED model in order to reproduce the nearshore wave climate at Hai Hau Beach.

The shoreline of Hai Hau Beach runs in the NE-SW direction, whereas the shoreline around the Ba Lat Mouth primarily runs in the N-S direction (Figure 1). Thus offshore waves coming from N and NNE occur in deep water when wind blows from these directions, and a part of this wave energy is transported to the nearshore region of Hai Hau Beach via diffractive and refractive effects of the headland of the Ba Lat Estuary. Data from recent wave observations at Hai Hau Beach also indicate that inshore waves exist in the nearshore zone, while offshore waves as well as winds at BLV station are coming from the N or NNE direction. Offshore wave energy coming from both N and NNE constitutes a considerable amount, about 31%, of the total offshore wave energy. Therefore, it is necessary to take the waves coming from these directions into account. In principle, wave transformation models can reproduce waves with incoming angles of $-90°$ to $+90°$, referring to the offshore axis of the orthogonal coordinate system used. This implies that if the orthogonal coordinate system of the studied domain is rotated so that the x-axis is parallel with the shoreline (NE-SW direction), only incoming waves from NE to SW will be reproduced. Because a basic assumption is that waves are entering through the offshore boundary, it was decided that the wave grid should only be used for waves with incoming angles of $-45°$ to $+45°$. Thus, in order to represent all wave directions from N to SW, it was necessary to establish three orthogonal coordinate systems (Figure 7). On each coordinate system, incoming wave angles from $-45°$ to $+45°$ referring to the vertical axis (offshore-pointing y-axis) were simulated. The first system is rotated so that the y-axis is parallel to the NE direction (called System-NE), the second one is rotated so that the y-axis is parallel to the SE direction (called System-SE), and the third one is rotated so that the y-axis is parallel to the SW direction (called System-SW). Thus, the incoming wave angles from N to ENE, encompassing 75.7% of total offshore wave energy, are simulated on System-NE; the incoming wave angles from E to SSE, encompassing 13.8% of total offshore wave energy, are simulated on System-SE; and the incoming wave angles from S to SW, encompassing 8.1% of total offshore wave energy, are simulated on System-SW. Through this procedure, most of the offshore wave energy, up to 98%, was taken into account. The wave model domain was expanded in the northward direction over the Ba Lat Mouth (Figure 1) to examine the effects of the Ba Lat Estuary headland on the wave climate in the nearshore zone of Hai Hau Beach.

It is useful to investigate the difference in the simulated results of wave propagation between the respective coordinate systems. Two cases were examined, corresponding to the two borders between the coordinate systems (Figure 7). The first border, between System-NE and System-SE, is direction

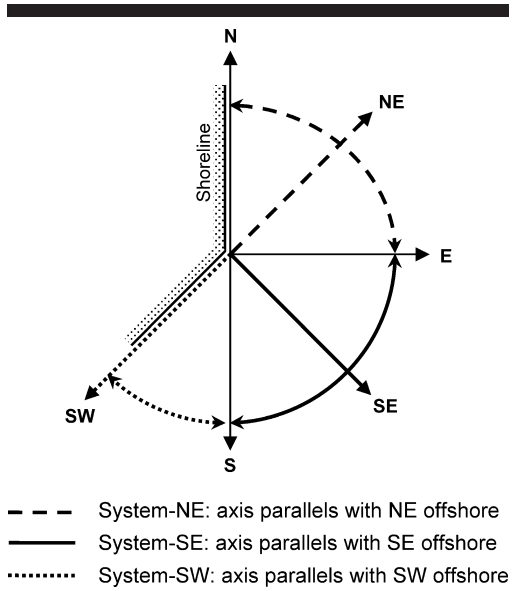

Figure 7. Sketch illustrating the rotation of the calculated coordinate system to simulate waves coming from N to SW.

E. The incoming wave angles from this direction correspond to $-45°$ in System-NE, whereas they correspond to $+45°$ in System-SE. The second border, between System-SE and System-SW, is direction S. The incoming wave angles from this direction correspond to $-45°$ and $+45°$ in System-SE and System-SW, respectively. Because only the nearshore wave climate is used as input data for the shoreline change model, wave parameters along the 7-m depth contour, outside the breaker line, were taken into consideration. Input offshore wave parameters for the wave propagation model used to test at the first border were as follows: significant wave height H_s = 2.3 m, and significant wave period T_p = 6.0 s. The average absolute differences along the 7-m depth contour with respect to wave height and wave angle are 0.06 m and 1.5°, respectively (Figures 8a and 8b). Consequently, the average relative difference in LST is 2.3% (Figure 8c). At the second border, input offshore wave parameters for the wave propagation model were H_s = 1.3 m and T_p = 5.0 s. The average absolute differences along the 7-m depth contour with respect to wave height and wave angle are 0.02 m and 1.9°, respectively (Figures 9a and 9b). Consequently, the average relative difference in LST is 2.6% (Figure 9c). These tests show that differences in simulated results for the wave climate in the nearshore zone between the different coordinate systems are not significant for the present application.

Shoreline Data

Shoreline data were obtained from maps and satellite images. Several difficulties were encountered when digitizing

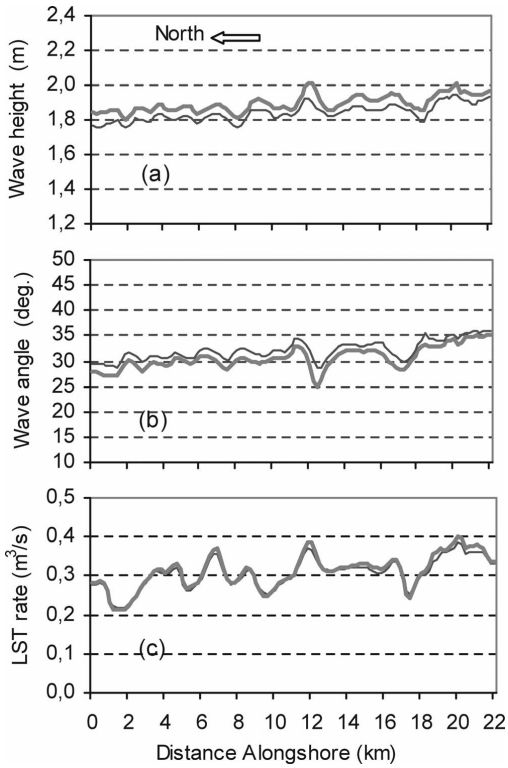

Figure 8. Comparison of simulated results of wave transformation and LST in the System-NE system (thin line) and the System-SE system (thick line) along the 7-m depth contour. (a) Wave height, (b) wave angle, (c) average relative difference in LST.

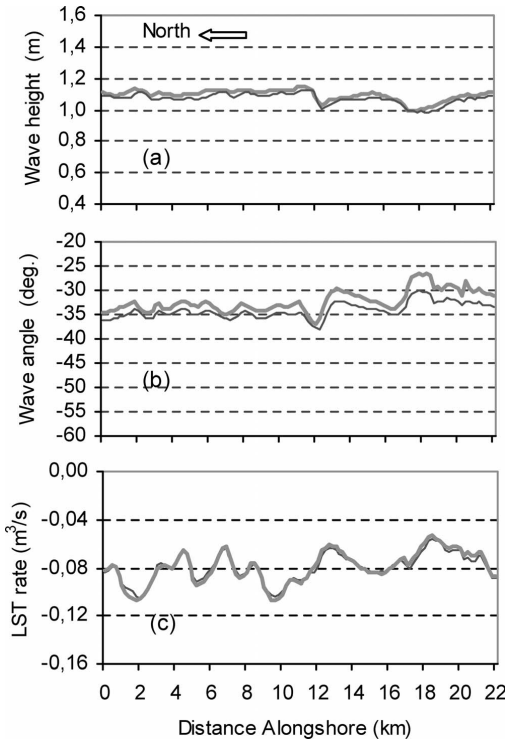

Figure 9. Comparison of simulated results of wave transformation and LST in the System-SW system (thin line) and the System-SE system (thick line) along the 7-m depth contour. (a) Wave height, (b) wave angle, (c) average relative difference in LST.

the map and satellite image data sets. Owing to the age of the maps and the different mapping authorities, the available maps employed different mapping projections based on different geographical ellipsoids and ellipsoidal data, and the shoreline was given at varying tidal data. It was therefore not possible to find full sets of coordinate transformation parameters to match the maps. The tidal data used for shoreline mapping was also unclear on the older maps. Donnelly *et al.* (2004) further investigated and determined that the accuracy of the shoreline digitization was in a range of ±8.5 to ±18.0 m, depending on the scale of the map.

Comparisons of historical shorelines from the past century showed an estimated coastline retreat of up to 14 m/y in some areas, with an alongshore average of 7 m/y. These figures, however, have reduced to a maximum of 8 m/y and an alongshore average of only about 1 m/y between 1992 and 2000. This is probably because by 1992, dikes were built to extend the full length of the shoreline, and 75% of these were upgraded between 1995 and 2000. Table 2 compares the shoreline erosion rates calculated in various earlier studies. As can be seen, the erosion rates calculated by Pruszak *et al.* (2002) differ substantially from those calculated by Wijdeven (2002) and Donnelly *et al.* (2004). This is probably because the data used for the shoreline comparisons of Pruszak *et al.* (2002) were not referenced geographically, nor was the tidal datum consistent. The larger erosion rates observed by Wijdeven (2002) for the period 1955–1965 can be explained because the 1955 French map was plotted using a different tidal datum to the other maps. The results of Wijdeven (2002) for the periods 1912–1955 and 1965–1995 are similar to the new rates from Donnelly *et al.* (2004).

Digitizing the shoreline required some simplifications to arrive at a shoreline suitable for one-line modeling. There are several minor estuaries and some sand spits along the Hai Hau coast. These were smoothed over in order to create a continuous, well-defined shoreline that could be modeled with one-line theory (Hanson, 1989). The estuaries, which were more significant in the first half of the century, were anticipated not to have significant influence on the overall

Table 2. *Calculated shoreline recession rates.*

Pruszak *et al.* (2002)		Wijdeven (2002)		Donnelly *et al.* (2004)	
Period (y)	Erosion Rate (m/y)	Period (y)	Erosion Rate[1] (m/y)	Period (y)	Erosion Rate[2] (m/y)
1905–1927	34.7	1912–1955	5.5–9.5	1910–1992	7.0 (14.0)
1927–1966	18.7	1955–1965	20.0–24.0	1992–2000[3]	1.0 (8.0)
1966–1992	3.6	1965–1995	6.0–9.0	—	—

[1] Erosion rates indicated are lower and upper boundary rates.
[2] Erosion rate averaged along the shoreline. Figure in parentheses is the maximum.
[3] This figure may not reflect mapping accuracy, but it indicates that erosion rates have decreased.

shoreline development because of their limited size. In the second half of the century, these estuaries were sealed off from the ocean by dikes and sluices, and hence they had an even lesser effect on the shoreline development. The longshore dike line in the latter part of the century was quite complicated, and spits could be seen building up across the recessed sections of the dike. The digitized shoreline was drawn across the seaward edge of such spits, so that the beach was assumed solid behind that stretch of shoreline.

In this study, the best available maps were from 1910 (Service Geographique de l'Indochine, the French colonial mapping service), 1965 (USACE Army Map Service), and 2000 (various Vietnamese mapping authorities). The shoreline of Hai Hau Beach was modeled between the Ha Lan Estuary in the north and the Lach Giang Estuary in the south (Figure 1). The shoreline appears to have been fairly stable at these locations. The section modeled varied therefore between 18 and 22 km in length (different stable shoreline points were identified as lateral boundaries for the calibration and validation periods of the modeling).

Sediment Transport and Shoreline Change Modeling

Some earlier investigations used varying methods to quantify the longshore sediment transport and shoreline change in the study area. The Coastal Engineering Research Center (CERC) formula (USACE, 1984) was used by Häglund and Svensson (2002) to calculate the longshore gradients in sediment transport. A one-dimensional wave transformation model was used to reproduce the inshore wave data with differing shoreline orientations to calculate a value for the sediment transport rate. Thus, this approach does not take into account gradients in breaking wave height along the shoreline. The BIJKER formula (Bijker, 1971) was used by Pruszak *et al.* (2002) and Wijdeven (2002) to calculate discrete values for sediment transport at various sites along the modeled coastline. The shoreline change model, GENESIS (Hanson, 1989), was used by Donnelly *et al.* (2004) and Hung, Hanson, and Dien (2006) to calculate sediment transport rates and shoreline evolution. In this approach, sediment transport rates at each cell are calculated based on a modified version of the CERC formula to take into account the longshore gradients in breaking wave height.

In this study, the shoreline change modeling is based on the theory of one-line model of shoreline change. The algorithms for the numerical modeling were developed by Hanson (1987). The general equation of shoreline change was derived from conservation of sediment volume. The continuity equation with respect to a local coordinate system, where the y-axis points offshore and the x-axis is oriented parallel to the trend of the shoreline, is expressed as

$$\frac{\partial y}{\partial t} + \frac{1}{(D_B + D_C)}\left(\frac{\partial Q}{\partial x} + q\right) = 0 \tag{1}$$

where x = longshore coordinate (m); y = cross-shore shoreline position (m); t = time (s); D_B = average berm elevation (m); D_C = depth of closure (m); Q = longshore sand transport rate (m^3/s); and q = source or sink of sand (m^3/s/m).

The empirical predictive formula for LST is expressed as (Hanson, 1987)

$$Q = (H^2 C_g)_b \left[a_1 \sin(2\theta_{bs}) - a_2 \cos\theta_{bs} \frac{\partial H}{\partial x}\right]_b \tag{2}$$

where H = wave height (m); C_g = wave group celerity given by linear wave theory (m/s); b = subscript denoting the breaking wave condition; θ_{bs} = angle of breaking waves to the local shoreline; and

$$a_1 = \frac{K_1}{16(\rho_s/\rho - 1)(1 - p)(1.416)^{(5/2)}} \tag{3}$$

$$a_2 = \frac{K_2}{8(\rho_s/\rho - 1)(1 - p)\tan\beta(1.416)^{(5/2)}} \tag{4}$$

where K_1 and K_2 = empirical coefficients, treated as calibration parameters; ρ_s = density of sand (kg/m^3); ρ = density of water (kg/m^3); p = porosity of sand on the bed; and $\tan\beta$ = average bottom slope from the shoreline to the depth of active longshore transport.

The hypotheses for the causes of erosion at Hai Hau Beach were introduced above. Under wave influence, eroded material is picked up from the seabed and transported in two directions: the longshore direction and the cross-shore direction. The former is expected to contain coarser sediment that is transported alongshore. This component is represented by the term $\partial Q/\partial x$ in Equation (1). The latter contains a larger amount of fine-grained sediment that is transported offshore and deposited further out in the Gulf of Tonkin. Such cross-shore sediment losses may be expressed in the one-line modeling through the term q (Equation [1]). Because classical one-line models of shoreline change do not include more complex relationships for q, it was necessary to develop such a relationship. In this study, the cross-shore loss of fine sediment depends on the rate of erosion, directly proportional to the gradient of LST rate through an offshore loss parameter α, which specifies the ratio of fine material in the eroded

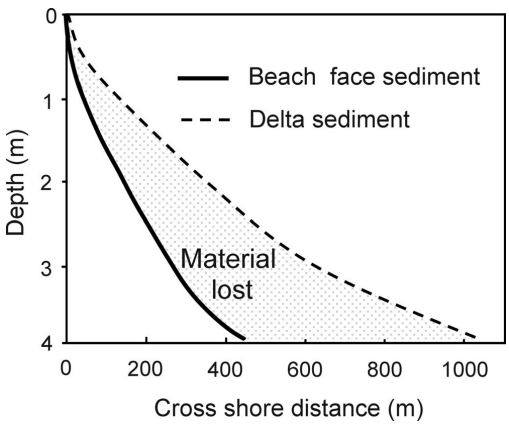

Figure 10. Comparison of equilibrium beach profiles behind the dikes and in the surf zone (Donnelly *et al.,* 2004).

sediment. The relationships employed are given by (Donnelly *et al.,* 2004)

$$q = \frac{\alpha}{1-\alpha}\frac{\partial Q}{\partial x}, \qquad \frac{\partial Q}{\partial x} > 0 \tag{5}$$

$$q = 0, \qquad \frac{\partial Q}{\partial x} \leq 0. \tag{6}$$

Equations (5) and (6) state that the loss of fine sediment only occurs during erosive conditions when the resident sediment is being mobilized. These equations were substituted into Equation (1) such that the sediment continuity equation is expressed in terms of α:

$$\frac{\partial y}{\partial t} + \frac{1}{(D_B + D_C)}\frac{1}{(1-\alpha)}\frac{\partial Q}{\partial x} = 0. \tag{7}$$

The value of the loss parameter was estimated by comparing equilibrium beach profiles for sediment samples taken behind the dikes and in the surf zone. Sediment behind the dikes consists of deltaic deposits laid down by the Red River distributaries. Sediment sampling shows the median grain size in this region, D_{50}, to be about 0.085 mm (Donnelly *et al.,* 2004). On the other hand, sediment in the surf zone, where finer sediments are put into suspension and carried offshore, is coarser, and samples gave D_{50} values of 0.15 to 0.20 mm (Donnelly *et al.,* 2004; Häglund and Svensson, 2002; compare with Table 1). If an equilibrium beach profile, as defined by Dean (1977), is constructed for each of these sediment samples (Figure 10), it may be assumed that α, the material loss, is the area difference in percent between the two profiles. This can then be expressed as (Donnelly *et al.,* 2004)

$$\alpha = 1 - \left(\frac{A_{delta}}{A_{surf}}\right)^{3/2} \tag{8}$$

where A_{delta} is the shape parameter in the equilibrium beach profile equation for deltaic sediments and A_{surf} is the shape parameter for the surf zone sediments. For the samples taken at Hai Hau Beach, α varied around 0.6–0.7. When calibrating the model, α was varied within this range.

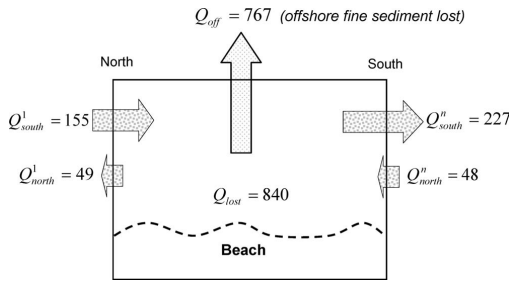

Figure 11. Sketch of calculated sediment budgets (values are multiplied by 10^3 m^3/y).

Sediment Budget Estimation

To obtain an overall view of the sediment entering and exiting the study area, a sediment budget was developed (see Figure 11). The sources and sinks in the sediment budget for the study area are defined as follows (particular values will be shown in the section "Modeled Sediment Budget"): At the north boundary (cell number 1), sediment enters through the southward longshore transport rate (Q^1_{south}) and exits through the northward transport (Q^1_{north}). Similarly, at the southern boundary (at cell number n), sediment enters through the northward transport (Q^n_{north}) and exits through the southward transport (Q^n_{south}). The fine sediment transported into deep water is denoted by Q_{off}.

Figure 12 illustrates how the offshore loss of sediment was computed. At each time step, the offshore loss is calculated as a function of the longshore transport gradient ($Q_{i+1} - Q_i$), as expressed by Equations (5) and (6). In Figure 12, erosion occurs in cells 1 and 2 because $Q_3 > Q_2 > Q_1$. Thus, these cells will experience offshore losses, q_1 and q_2. In cell 3 there is no erosion ($Q_4 < Q_3$) and, thus, no offshore losses. The total rate of offshore loss of fine sediment $q^{(t)}_{tot}$ at time step (t) was calculated as

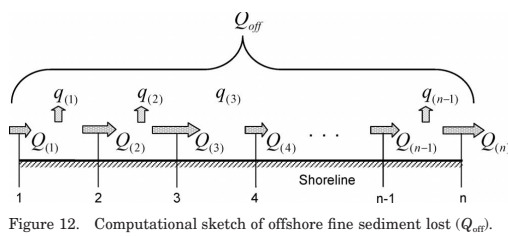

Figure 12. Computational sketch of offshore fine sediment lost (Q_{off}).

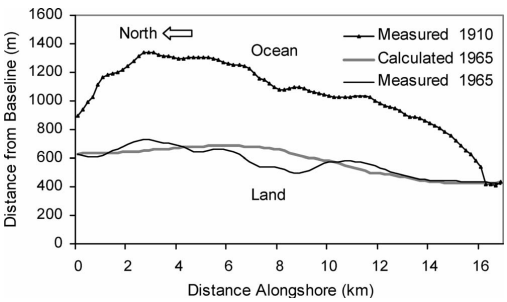

Figure 13. Measured and modeled shorelines from the period 1910 to 1965.

$$q_{\text{tot}}^{(t)} = \sum_{i=1}^{n-1} q_i. \tag{9}$$

The average loss of fine sediment over the simulation period was estimated from

$$Q_{\text{off}} = \frac{1}{T} \sum_{t=0}^{T} q_{\text{tot}}^{(t)} \Delta t \Delta x \tag{10}$$

where Δt is the time step and T is the total simulated time.

MODELING RESULTS

An implicit solution scheme was used to solve the coupled Equations (1) and (2) with space and time steps of 200 m and 1 hour, respectively. A stability parameter (R_s) of the calculation scheme is estimated on the basis of the Courant Criterion (Hanson and Kraus, 1989), where values of $R_s < 10$ are suggested. The model calculates values of R_s at each time step at each grid point alongshore and determines the maximum value. For both the calibration and validation period, the calculated maximum value of R_s is 4.8. In addition, depending on the interval of time series of input wave hindcast (DTW), the time step must be opted so that the model receives the input wave data at a specific time corresponding to DTW. To satisfy this requirement, the time step must be a proper fraction (*e.g.,* 1/2, 1/3) of DTW. Thus, with 6 hours of DTW and the maximum value of R_s mentioned above, the time step of 1 hour satisfies all critical conditions for the calculation scheme.

The model was calibrated and validated using the measured shorelines from 1910, 1965, and 2000 at Hai Hau Beach. Note that the Ha Lan Estuary, at the northern end of the beach (Figure 1), migrated during this period; hence a stable shoreline point at the northern end of Hai Hau Beach was not found. The northern boundary of the model was therefore simulated as a moving boundary. The average value of the shoreline movement at this boundary was estimated from the measured shoreline positions to be 4.4 m/y. This value is used for both the calibration and validation period.

To estimate how well the modeled shorelines agreed with the measured shorelines, two kinds of error were employed:

Table 3. *Summary of errors and erosion rates in calibration and validation.*

	Max Absolute Error (m)	% Average Relative Error	Max Erosion Rate (m/y)	Average Erosion Rate (m/y)
Calibration	133.7	9.0	12.1	8.7
Validation	123.4	9.1	12.7	6.8

maximum absolute error (in m) and average relative error (%). The maximum absolute error is defined as the maximum absolute difference between measured and modeled shorelines. The average relative error is estimated using the following formula:

$$\%\ \text{error} = \frac{\frac{1}{n}\sum_{i=1}^{n} \left| y_{\text{modeled}}^{(i)} - y_{\text{measured}}^{(i)} \right|}{\frac{1}{n}\sum_{i=1}^{n} \left| y_{\text{eroded}}^{(i)} \right|} \times 100 \tag{11}$$

where n = the number of cells alongshore; $y_{\text{modeled}}^{(i)}$ = the modeled shoreline position of cell i; $y_{\text{measured}}^{(i)}$ = the measured shoreline position of cell i; and $y_{\text{eroded}}^{(i)}$ = the distance between the measured initial and final shorelines, respectively, in cell i.

Model Calibration and Validation

The measured shorelines from 1910 and 1965 were used to calibrate the model. The parameter values during calibration were optimized based on error minimization (Figure 13). The calibration parameters obtained are $\alpha = 0.7$, $K_1 = 0.89$, and $K_2 = 0.50$. The maximum absolute error and average relative error for the calibration period are 133.7 m and 9.0%, respectively (Table 3).

Employing the above calibration parameters, the model was validated from 1965 to 2000 using the 1965 measured shoreline as the initial shoreline. For the period from 1995 to 2000, two sea dike segments reinforced by stones and mortar that were constructed in 1995 were represented using a seawall boundary condition (Figure 14). Maximum absolute error and average relative error for the validation period are 123.4 m and 9.1%, respectively (Table 3). The difference in the maximum rate of shoreline retreat between the calibration and validation periods is negligible, with values of 12.1 m/y and 12.7 m/y, respectively. However, the average rate of shoreline retreat shows a greater difference, with 8.7 m/y for the calibration period and 6.8 m/y for the validation period (Table 3).

Modeled Sediment Budget

The calculated values for the components in the sediment budget show that the total amount of sediment from sources is $Q_{\text{source}} = Q_{\text{south}}^{\text{l}} + Q_{\text{north}}^{n} = 203 \times 10^3$ m^3/y, and the total amount of sediment from sinks is $Q_{\text{sink}} = Q_{\text{north}}^{\text{l}} + Q_{\text{south}}^{n} + Q_{\text{off}} = 1043 \times 10^3$ m^3/y, where fine sediment lost offshore is 767×10^3 m^3/y (70% of total sink volume). Thus, the annual sediment volume lost from the area is $Q_{\text{lost}} = Q_{\text{sink}} - Q_{\text{source}} = 840 \times 10^3$ m^3/y.

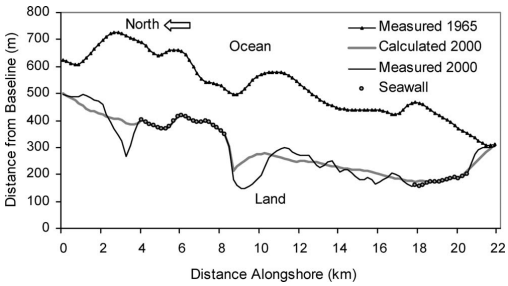

Figure 14. Measured and modeled shorelines from the period 1965 to 2000.

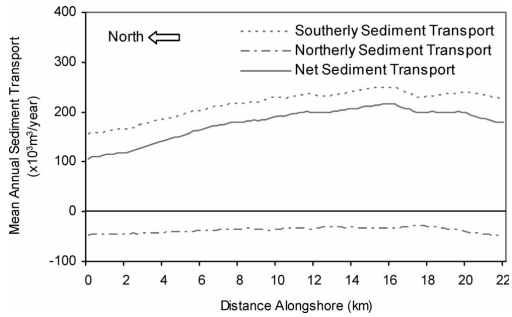

Figure 15. Spatial distribution of annual longshore sediment transport rates.

There is a large difference in the LST rates between the southward and northward directions. Overall, the southerly directed sediment transport rate is around 150×10^3 to 250×10^3 m^3/y, whereas the northerly sediment transport rate is only about 30×10^3 to 50×10^3 m^3/y, constituting about 15% of the gross sediment transport rate. The result is a significant net sediment transport rate in the southward direction with values in the range of 100×10^3 to 200×10^3 m^3/y (Figure 15). It should be stressed that the curves in Figure 15 and the block arrows in Figure 11 represent averages and that the net local transport gradients in space that determine the offshore sediment transport are not shown. As previously discussed, the offshore losses are proportional to the transport gradient during erosive conditions and without such gradients there will be no offshore losses.

DISCUSSION

This model does not simulate the fine details of the shoreline shape; however, the general trend and magnitude of shoreline change are well reproduced during both the calibration and the validation periods, including the influence of the seawalls through the boundary conditions (Figures 13 and 14). Average relative errors for the calibration and validation periods are 9.0% and 9.1%, respectively, and maximum absolute errors are 133.7 m and 123.4 m, respectively (Table 3). Annual shoreline retreat rates estimated from the measured shorelines decreased from 8.7 m during the calibration period to 6.8 m during the validation period. This shows that the average erosion rate at Hai Hau Beach has been slowing down during recent decades.

As mentioned above, the sea dike system in Hai Hau District was constructed purely of soil, and then, before 2000, only some segments were reinforced with stones and mortar. Even though these sea dike segments may fail during heavy storm or typhoon attacks, in the present model they were treated as seawalls because they survived during the simulating period. However, these seawalls were subsequently completely destroyed by heavy typhoon attacks in 2005. Based on a report on the state of the sea dikes in Hai Hau District (Lam *et al.,* 2005), there were two reinforced sea dike segments that were described with the seawall boundary condition during the validation period. The first one belongs to Hai Loc Commune in the northern part of the area and faces attacks from the sea resulting in higher erosion intensity at the two ends of the seawall. The second one belongs to Hai Hoa Commune in the southern part; it does not face the sea, and therefore no effects have been observed. Due to the net sediment transport in the southward direction, higher intensity of erosion takes place at the south end of the northern reinforced sea dike.

Because of the different wind energy supply between winter and summer, offshore wave energy in the winter (coming from the north) is much greater than that in the summer (coming from the south). Estimates of the offshore wave energy from the wave hindcast show that in winter (from November to March) about 52.2% of the total offshore wave energy is supplied, while in summer (from May to September) only 29.3% is supplied. On the other hand, since the shoreline of Hai Hau Beach runs in the NE-SW direction (about 40° with respect to the N direction), incoming wave angles from N to ESE, generating the LST in the southward direction, encompass about 81% of the total offshore wave energy. Incoming wave angles from SE to SW, generating the LST in the northward direction, encompass only about 17% of the total offshore wave energy (Table 4). Thus, the southward sediment transport, encompassing about 85% of the gross transport, is much higher than the northward sediment transport, making up only about 15% of the gross transport (Figure 15); this results in a large net sediment transport to the south. In addition, gradients in the LST rates to the south (in winter) are higher than in the transport to the north (in summer), and therefore there is a large amount of fine sediment being transported into deep water during the winter (Figure 11). This implies that the serious erosion at Hai Hau Beach mainly occurs during the winter period.

According to previous studies, river outflow and riverine sediment from the Red River seldom reach the Hai Hau coastline (Do *et al.,* 2007; Pruszak *et al.,* 2002; Van Maren, 2004). The sediment from the Red River is mainly deposited within a 10-km area around the river mouth (Van Maren, 2004), and the remaining finer sediment is transported to

Table 4. *Distribution of offshore wave energy estimated from the wave hindcast.*

Direction	N	NNE	NE	ENE	E	ESE	SE	SSE	S	SSW	SW	WSW	W	WNW	NW	NNW
% energy	4.5	26.7	42.1	2.4	3.6	1.3	3.1	5.8	2.7	0.4	5.0	0.2	0.4	0.2	0.8	0.9

deeper water. This implies that the coastline of Hai Hau Beach is only supplied with sediment from the Red River to a limited degree. The limited sediment supply is expected to contribute to the sediment deficit and associated erosion along the Hai Hau coastline. In this study, the considered domain was expanded over the Ba Lat Mouth when running the wave propagation model to examine the effects of the river mouth and its protruding topography. The results of the wave simulations show that the headland of the Ba Lat Estuary produces significant diffractive and refractive effects on the waves approaching from the north, resulting in an alongshore variation of wave heights and angles in the nearshore zone of Hai Hau Beach. Wave height and angle along the 7-m depth contour increase from the Ha Lan Estuary (north) to the Lach Giang Estuary (south). Thus, when waves come from the northern sector, a corresponding increase appears of about 0.2–0.4 m in height and 10–15° in angle (Figure 16). Consequently, a gradient occurs in the LST when waves are coming from these directions. Thus, the Ba Lat Estuary does not only provide limited sediment for Hai Hau Beach, but it also produces gradients in the LST, causing the serious erosion at the Hai Hau coastline.

Several previous studies pointed out the existing high sediment transport alongshore and cross-shore. Pruszak *et al.* (2002) stated that the material originating from the Red River system is very mobile. About 70% of the mainly clayey material being discharged remains suspended, passes the intertidal plain, and goes offshore to deepwater areas (depths of 2 m to 30 m). The severe beach erosion suggests that relatively high sediment movement (longshore and cross-shore transport) should exist. Donnelly *et al.* (2004), by comparing the equilibrium beach profile behind the dikes and in the surf zone based on samples taken at Hai Hau Beach, found that 60–70% of the material mobilized by gradients in LST was transported to deep water. Do *et al.* (2007), using the method by McLaren and Bowles (1985) to analyze and relate grain-size trends with the net transport paths, showed that the dominant transport direction is perpendicular to the depth contours to a depth of about 25 m. Sediments are transported alongshore in a southwestward direction in coastal waters shallower than 5 m. Again, in this study, calculated results of LST and shoreline change show that fine sediment lost in the offshore direction represents a large ratio (about 60%) of the total sediment transport. Annual sediment transport in the southward, northward, and offshore directions is on the average about 220×10^3 m^3/y, 40×10^3 m^3/y, and 750×10^3 m^3/y, respectively. The net sediment transport is in the southward direction, being on the average 180×10^3 m^3/y.

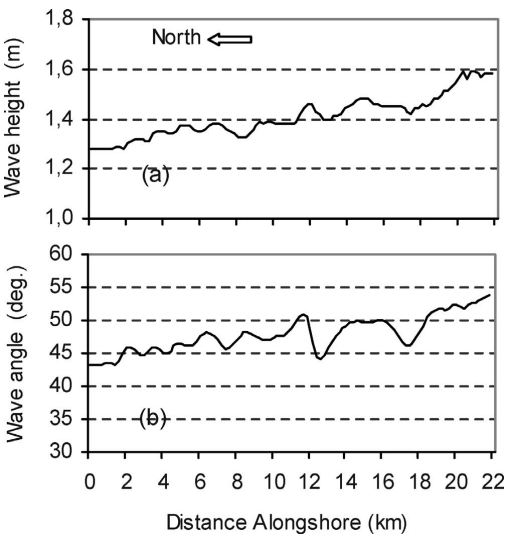

Figure 16. Distribution of wave height and angle along the 7-m depth contour for waves coming from the NE, H_s = 3.3 m, and T_p = 6 s. (a) Wave height, (b) wave angle.

CONCLUSIONS

(1) The shoreline change model successfully simulated the shoreline evolution at Hai Hau Beach, including the dike-seawall boundary condition, offshore sediment losses, and the complex morphology around the Ba Lat Mouth. The overall magnitude and trend of the simulated shoreline evolution was in good agreement with the measurements, both for the calibration and validation period. The calculated results used to establish a sediment budget showed that the net sediment transport is in the southward direction and that a large amount of fine sediment is transported offshore into deep water.

(2) Gradients in the LST and fine sediment lost into deep water are the major causes of the severe erosion at Hai Hau Beach. Gradients in the LST are generated by diffractive and refractive effects of the headland of the Ba Lat Estuary on the waves coming from the north; thus, the erosion rate of the Hai Hau shoreline is believed to have a strong relationship with the deposition rate at the Ba Lat Estuary.

(3) Incoming wave energy in the winter is much higher than in summer, resulting in a net sediment transport in the southward direction. Gradients in the LST rate are significant when the waves are coming from the north. Thus, the severe erosion at Hai Hau Beach occurs mainly in winter.

ACKNOWLEDGMENTS

The authors are grateful to Prof. Zbigniew Pruszak, Dr. Rafal Ostrowski, Dr. Grzegorz Rozynski, Dr. Shigeru Kato, Prof. Do Ngoc Quynh, Prof. Tran Gia Lich, Dr. Nguyen Thi Viet Lien, Dr. Dinh Van Manh, and Dr. Phan Ngoc Vinh for general discussions and comments on the paper; to Dr. Bas Van Maren for providing reprints of his papers; to Prof. Guohong Fang for providing tidal data; and to MS Nguyen Van Moi and MS Nguyen Thi Kim Nga for providing wind, wave, and shoreline data. This study was financed by a grant from SIDA.

LITERATURE CITED

Bijker, E.W., 1971. Longshore transport computations. *Journal of Waterways,* 97(4), 687–701.

Dean, R.G., 1977. Equilibrium Beach Profiles: U.S. Atlantic and Gulf Coasts. Newark, Delaware: University of Delaware, Department of Civil Engineering, Ocean Engineering Report No. 12, 45p.

Do, M.D.; Mai, T.N.; Chu, V.N.; Tran, N.; Dao, M.T.; Van Weering, Tj., C.E., and Van Den Bergh, G.D., 2007. Sediment distribution and transport at the nearshore zone of the Red River delta, Northern Vietnam. *Journal of Asian Earth Sciences,* 29(4), 558–565.

Donnelly, C.; Hung, N.M.; Larson, M., and Hanson, H., 2004. One-line modelling of complex beach conditions: an application to coastal erosion at Hai Hau beach in the Red River Delta, Vietnam. *In: Proceedings of the 29th Conference of Coastal Engineering* (Lisbon, Portugal), pp. 2449–2461.

Guohong, F.; Yue-Kuen, K.; Kejun, Y., and Yaohua, Z., 1999. Numerical simulation of principal tidal constituents in the South China Sea, Gulf of Tonkin and Gulf of Thailand. *Continental Shelf Research Journal,* 19(7), 845–869.

Hanson, H., 1987. GENESIS: A Generalized Shoreline Change Numerical Model for Engineering Use. Lund, Sweden: Lund University, PhD dissertation, 206p.

Hanson, H., 1989. GENESIS—A generalized shoreline change numerical model. *Journal of Coastal Research,* 5(1), 1–27.

Hanson, H. and Kraus, N.C., 1989. GENESIS: Generalized Model for Simulating Shoreline Change, Report 1, Technical Reference. Washington: Department of the Army, U.S. Army Corps of Engineers, 185p.

Häglund, M. and Svensson, P., 2002. Coastal Erosion at Hai Hau Beach in Red River Delta, Vietnam. Lund, Sweden: Lund University, Master's thesis, 80p.

Huan, N.N., 1996. Vietnam Coastal Zone Vulnerability Assessment. Hanoi, Vietnam: Center for Consultancy and Technical Support of Meteorology, Hydrology and Environment, Report of Vietnam VA Project, 5p.

Hung, N.M.; Hanson, H., and Dien, D.C., 2006. Simulation of shoreline evolution at Hai Hau beach, Red River Delta with the GENESIS model. *In: Proceedings of the First Scientific Workshop on "Coastline Evolution"* (Thinh Long, Vietnam), pp. 97–107.

Hung, N.M.; Moi, N.V.; Them, N.Q.; Dat, N.T.; Donnelly, C., and Grahn, L., 2006. Field measurements on nearshore processes in the Red River Delta coastal zone. *In: Proceedings of the First Scientific Workshop on "Coastline Evolution"* (Thinh Long, Vietnam), pp. 29–42.

Lam, N.X.; Ha, L.T.; Bon, T.V., and Phan, N.V., 2005. Report of the Current State of the Sea Dikes in Hai Hau District. Nam Dinh, Vietnam: Department of Natural Resources and Environment, Technical Report of CCP-2005 Project, 65p.

Mase, H., 2001. Multi-directional random wave transformation model based on energy balance equation. *Coastal Engineering Journal,* 43(4), 317–337.

McLaren, P. and Bowles, D., 1985. The effects of sediment transport on grain-size distributions. *Journal of Sedimentary Petrology,* 55(4), 457–470.

Ninh, P.V.; Quynh, D.N., and Viet Lien, N.T., 2001. The Scientific Foundation and Technical Parameters in the Coastal Zone of Vietnam for Nearshore Designed Constructions. Hanoi, Vietnam: Institute of Mechanics, NCST, Final Report of the National Marine Project, 99p.

Pruszak, Z., 1998. Coastal Processes in the Red River Delta with Emphasis on Erosion Problems. Gdansk, Poland: Institute of Hydroengineering, Polish Academy of Science, Internal Report, 18p.

Pruszak, Z.; Szmytkiewicz, M.; Hung, N.M., and Ninh, P.V., 2002. Coastal processes in the Red River Delta area, Vietnam. *Coastal Engineering Journal,* 44(2), 97–126.

Quynh Le, T.P.; Garnier, J.; Gilles, B.; Sylvain, T., and Minh, C.V., 2007. The changing flow regime and sediment load of the Red River, Viet Nam. *Journal of Hydrology,* 334(2), 199–214.

Saito, Y., 2001. Deltas in Southeast and East Asia: their evolution and current problems. *In: Proceedings of APN/SURVAS/LOICZ Joint Conference on Coastal Impacts of Climate Change and Adaptation in the Asia-Pacific Region, APN* (Kobe, Japan), pp. 185–191.

Sjödahl, M. and Kalantari, Z., 2005. Nearshore Hydrodynamics at Hai Hau Beach, Vietnam: Field Measurements and Wave Modeling. Lund, Sweden: Lund University, Master's thesis, 83p.

Smith, J.M.; Sherlock, A.R., and Resio, D.T., 2001. *STWAVE: Steady-State Spectral Wave Model, User's Guide for STWAVE Version 3.0.* Vicksburg, Mississippi: U.S. Army Corps of Engineers, 66p.

Sundstrom, A. and Sodervall, E., 2004. The Impact of Typhoon on the Vietnamese Coastline—A Case Study of Hai Hau and Ly Hoa Beach. Lund, Sweden: Lund University, Master's thesis, 70p.

Thanh, T.D.; Saito, Y.; Dinh, V.H.; Nguyen, H.C., and Do, D.C., 2005. Coastal erosion in Red River Delta: current status and response. *In: Proceedings of an International Conference on Geological Evolution and Human Impact* (Beijing, China), pp. 98–106.

USACE (U.S. Army Corps of Engineers), 1984. *Shore Protection Manual (SPM).* Washington: U.S. Government Printing Office, 1088p.

USACE, 2002. *Coastal Engineering Manual (CEM), Part II, Chapter 2.* Washington: U.S. Government Printing Office, 77p.

Van Maren, D.S., 2004. Morphodynamics of a Cyclic Prograding Delta: The Red River, Vietnam. Utrecht, the Netherlands: Utrecht University, PhD dissertation, 167p.

Van Maren, D.S. and Hoekstra, P., 2004. Seasonal variation of hydrodynamics and sediment dynamics in a shallow subtropical estuary: the Ba Lat River, Vietnam. *Estuary, Coastal and Shelf Sciences,* 60(3), 529–540.

Mouth, T.T.; Kant, G.; Huan, N.N., and Pruszak, Z., 1996. Sea dike erosion and coastal retreat at Nam Ha province, Vietnam. *In: Proceedings of the 25th Conference of Coastal Engineering* (Orlando, Florida, ASCE), pp. 2820–2828.

Wijdeven, B., 2002. Coastal Erosion on a Densely Populated Delta Coast, the Interactions between Man and Nature: A Case Study of Nam Dinh Province, Red River Delta, Vietnam. Delft, the Netherlands: Delft University of Technology, Master's thesis, 163p.

Appendix

II

Hoan, L.X., Hanson, H., Larson, M., and Nam, T.P. (2010). Modeling regional sediment transport and shoreline response in the vicinity of tidal inlets on the Long Island coast, United States. *Coastal Engineering.* (Submitted)

Modeling regional sediment transport and shoreline response in the vicinity of tidal inlets on the Long Island coast, United States

Le Xuan Hoan[a,b], Hans Hanson[a], Magnus Larson[a], Pham Thanh Nam[a,b]

[a] *Water Resources Engineering, Lund University, Box 118, 22100 Lund, Sweden.*
[b] *Institute of Mechanics,Vietnam Academy of Science and Technology, 264 Doi Can, Hanoi, Vietnam.*

Abstract

A new numerical model was developed to simulate regional sediment transport and shoreline response in the vicinity of tidal inlets based on the one-line theory combined with the reservoir concept for volumetric evolution of inlet shoals. Sand bypassing onshore and sheltering effects on wave action from the inlet bar and shoals were taken into account. The model was applied to unique field data from the south coast of Long Island, United States, including inlet opening and closure. The simulation area extended from Montauk Point to Fire Island inlet, including Shinnecock and Moriches Inlets (Fig. 1). A 20-year time series of hindcast wave data at three stations along the coast were used as input data to the model. The capacity of the inlet shoals and bars to store sand was estimated based on measured cross-sectional areas of the inlets as well as from comprehensive surveys of the inlet area. Several types of sediment sources and sinks were represented, including beach fills, groin systems, jetty blocking, inlet bypassing, and flood shoal and ebb shoal feeding. The model simulations were validated against annual net longshore transport rates reported in the literature, measured shorelines, and recorded sediment volumes in the flood and ebb shoal complexes. Overall, the model simulations were in good agreement with the measured data.

Key words: *Numerical modeling, sediment transport, shoreline response, tidal inlet, inlet shoal.*

1. Introduction

Morphology change and shoreline response in the vicinity of tidal inlets are controlled by both dynamic and static factors. Dynamic factors include net longshore transport rate, tidal prism, and wave regime, whereas properties of structures, angle of ebb jet related to the local shoreline, general offshore and nearshore bathymetry, size and shape of the back bay, sediment grain size, and artificial beach fills are static factors (Carr and Kraus, 2001). The dynamic factors can play a role in regional coastal processes, whereas the static factors often act at the scale of the local processes. Engineering activities around tidal inlets, such as creation and maintenance of navigation channels, require comprehensive knowledge of regional and local processes as well as the interactions between them. Regional sediment transport and shoreline evolution models that include local processes at tidal inlets are to a large degree lacking at present.

Kraus (2000, 2002) introduced a mathematical aggregate model of volume change and sand bypassing at tidal inlets, based on a reservoir analogy approach. In this model, the ebb shoal, bypassing bar, and attachment bar were included, but the flood shoal and main channel were neglected. Larson *et al.* (2002a) introduced a numerical model to simulate sediment transport and coastal evolution at regional scale, named Cascade. This model can simultaneously simulate different spatial and temporal processes at scales from regional to local. Regional sediment transport and shoreline change extending hundreds of kilometers and covering several inlets were represented. The model also includes inlet phenomena such as inlet creation, ebb shoal development, and bypassing bars between beaches and inlets. Larson *et al.* (2006) further developed the inlet reservoir model to include flood shoal development, based on the model introduced by Kraus (2002). This model was then included in Cascade after which the sediment transport and shoreline response in the vicinity of Shinnecock Inlet and Moriches Inlet on the south coast of Long Island, United States, were simulated. However, in these simulations the shoreline change downdrift the inlets were not well reproduced. The reasons for this discrepancy between calculations and measurements are attributed to sand moving onshore from the attachment bars, as well as the sheltering effects on wave action from the inlet shoals and bars. These processes have not been included in any previous model. Thus, in order to develop a general model for regional coastal evolution with regard to the effects of inlets, sand bypassing onshore from the attachment bars and the sheltering effects of the inlet morphological elements on the downdrift shoreline were described in the present model.

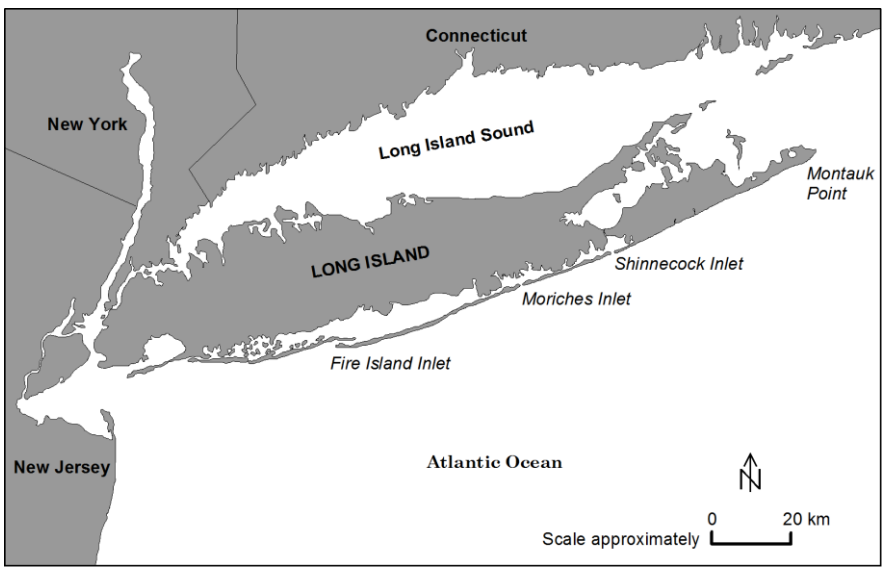

Fig. 1. Study site and locations of the inlets on the south Long Island coast, New York.

In this study, a new numerical model of regional sediment transport and shoreline change, combined with the inlet reservoir model, is introduced. The shoreline change model was based on one-line theory following basic formulations and algorithms developed by Hanson (1987). The predictive formula for longshore transport rate as modified by Larson *et al.* (2002a) to include shoreline characteristics at the regional scale was employed. Measured data by Gaudiano and Kana (2001) were used to model the onshore movement of a portion of the attachment bar volumes. Sheltering effects on the wave action from the inlet shoals and bars were represented by an attenuation coefficient affecting the breaking wave height in the sheltered area. Distances from the centerline of the inlets to the attachment bars were calculated using the empirical formulas introduced by Carr and Kraus (2001). The model was employed to simulate the coastal evolution of the Long Island coast covering the inlets at Shinnecock and Moriches. Measured shorelines in 1983, net longshore transport rates estimated by Rosati *et al.* (1999), and measured volumes of the flood and ebb shoal complexes (the ebb shoal complex includes ebb shoal, bypassing bar, and attachment bar) were used to validate the model.

2. Methodology

The model development focused on simulating regional sediment transport and local shoreline response in vicinities of the tidal inlet as well as development of the tidal shoal volumes. Regional sediment transport and shoreline evolution was simulated based on the shoreline change model developed by Hanson (1987). The inlet reservoir model based on a reservoir analogy approach developed by Kraus (2000, 2002) was employed. For this model, relationships between tidal morphological units and pathway of sand bypassing must be specified. The basics of the model components are described below with some of the components were developed as a part of this study, whereas other components were based on previous work.

2.1 Shoreline change model

The shoreline change modeling is based on the one-line theory (Pelnard-Considere, 1956), employing algorithms for the numerical solution developed by Hanson (1987). Conservation of sediment volume yields the fundamental equation to be solved for obtaining the shoreline change. Employing a local coordinate system, where the y-axis points offshore and the x-axis is oriented parallel to the trend of the shoreline, this equation is expressed as,

$$\frac{\partial y}{\partial t} + \frac{1}{(D_B + D_C)}\left[\frac{\partial Q}{\partial x} + q\right] = 0 \qquad (1)$$

where: x = longshore coordinate; y = cross-shore shoreline position; t = time; D_B = average berm elevation; D_C = depth of closure; Q = longshore sand transport rate; q = source or sink of sand.

The empirical predictive formula for the total longshore sand transport developed by Hanson *et al.* (2006) was used,

$$Q = \frac{\varepsilon}{8(\rho_s/\rho - 1)(1-p)w_s} H_b^2 C_{gb} \cos\alpha_0 \left[K_1 \left(a_1 \sin\alpha_0 + \overline{V_{ex}} \right) - K_2 a_2 \right] \quad (2)$$

in which, $a_1 = \frac{5}{32}\frac{\pi\chi}{C_f}\sqrt{g}A^{\frac{3}{2}}$; $a_2 = \frac{\pi}{C_f\chi^2}\sqrt{gd_b}\frac{\partial H_b}{\partial x}$ and $A = 2.25\left(\frac{w_s^2}{g}\right)^{\frac{1}{3}}$

where: H = wave height; d = water depth; C_g = wave group celerity; b = subscript denoting breaking wave condition; K_1, K_2 = empirical coefficients (treated as calibration parameters); ρ_s = density of sand; ρ = density of water; p = porosity of sand on the bed; w_s = fall velocity; $\overline{V_{ex}}$ = external surf-zone average longshore current velocity generated by tide or/and wind; A = shape parameter; χ = breaker index; g = acceleration due to gravity; C_f = bottom friction coefficient; ε = transport coefficient expressing efficiency of the waves keeping sand grains in suspension, which can be estimated through physical parameters as (Bayram *et al.*, 2007), $\varepsilon = \left(4.0 + 9.0\frac{H_b}{w_s T_p}\right)\times 10^{-5}$; T_p = peak wave period; and α_0 = angle of breaking waves to the local shoreline orientation given by,

$$\alpha_0 = \alpha_b - \arctan\left(\partial y/\partial x\right) \quad (3)$$

The effect of a regional shoreline shape enters in Eq. (3) by assuming that the local shoreline evolves with respect to the regional shoreline (Larson *et al.*, 2002a), yielding a new expression for α_0,

$$\alpha_0 = \alpha_{br} + \alpha_b - \arctan\left(\partial y/\partial x\right) \quad (4)$$

where $\alpha_{br} = \arctan\left(\partial y_r/\partial x\right)$ and y_r denotes the regional shoreline, which is taken to be constant in time.

2.2 Tidal prism and equilibrium volume of ebb shoal complex

Jarret (1976) summarized the state of knowledge on the relationship between cross-sectional area and tidal prism for inlets in the United States. Separate relationships were developed for the Atlantic, Gulf, and Pacific Ocean coasts classified according to whether the inlets have two, one, or no jetties. The relationship for the Atlantic Ocean coast and inlets with two jetties is (Militello and Kraus, 2001),

$$A_c = 14.74\times 10^{-5} P^{0.95} \quad (5)$$

where A_c = minimum cross-sectional area of the entrance channel below mean sea level (in m^2), and P = spring tidal prism (in m^3).

Walton and Adams (1976) developed predictive empirical formulas for the equilibrium volume of an ebb tidal shoal depending on the tidal prism and the amount of wave

exposure of the coasts classified into groups of highly exposed, moderately exposed, and mildly exposed coasts. The formula for moderately exposed coasts is most applicable to the inlets along the southern shore of Long Island (Millitello and Kraus, 2001), and thus it was used in this study,

$$V_E = 6.44 \times 10^{-3} \times P^{1.23} \tag{6}$$

where V_E = volume of ebb shoal complex at equilibrium (in m^3).

2.3 Inlet Reservoir Model

Larson *et al.* (2006) refined the inlet reservoir model by Kraus (2002) through the introduction of the flood shoal and associated coupling coefficients, which analytically describe the transfer of sediment between the morphological units. The inlet morphology is schematically divided into distinct morphology units including ebb shoal, bypassing bars, attachment bars, and flood shoal (Fig. 2). Each morphological unit is assumed to have a certain equilibrium volume for fixed hydrodynamic and sediment conditions.

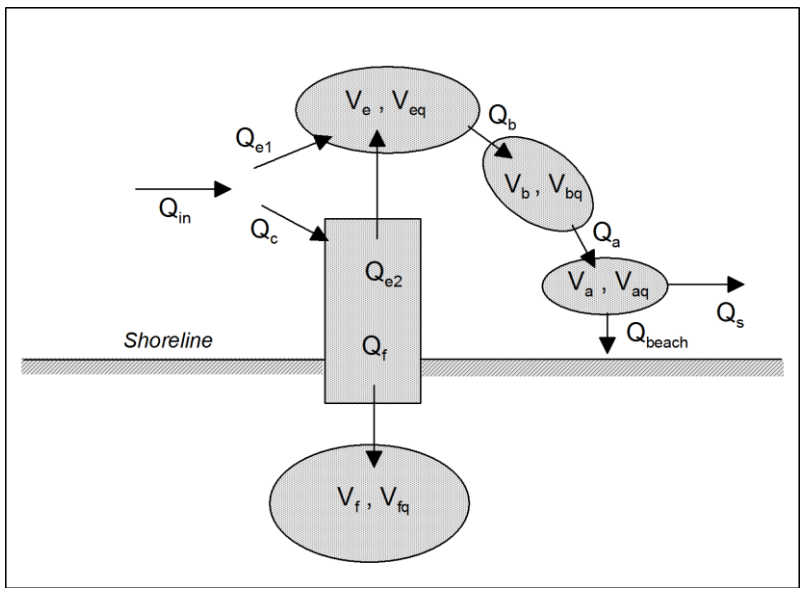

Fig. 2. Definition sketch for inlet morphological units with sediment transport occurring from the left-hand side (after Larson *et al.*, 2002a).

In order explain the inlet model employed in the present study, the simple case of sediment being transported from left-to-right is considered here, where Q_{in} is the incoming sediment transport rate around the jetty (if such a structure is present). The transport Q_{in} is split into

one portion that goes to the ebb shoal, Q_{e1}, and one portion that goes into the channel, Q_c. Once in the channel, the sediment might be transported to the ebb shoal, Q_{e2} or to the flood shoal, Q_f. Sediment at a rate Q_b is leaving the ebb shoal and feeding the bypassing bar. The volume of the ebb and flood shoal at any given time is V_e and V_f, respectively, with the corresponding equilibrium values of V_{eq} and V_{fq}.

The mass conservation equation of sediment for the ebb shoal is,

$$\frac{dV_e}{dt} = Q_{e1} + Q_{e2} - Q_b \tag{7}$$

and for the flood shoal,

$$\frac{dV_f}{dt} = Q_f \tag{8}$$

Transport out of the ebb shoal is,

$$Q_b = \frac{V_e}{V_{eq}}\left(Q_{e1} + Q_{e2}\right) \tag{9}$$

Transport rates between elements are defined through the coupling coefficients,

$$Q_{e1} = \delta Q_{in} \;;\; Q_c = (1-\delta)Q_{in} \tag{10}$$

$$Q_{e2} = \beta\left(1-\delta\right)Q_{in} \;;\; Q_f = \left(1-\beta\right)\left(1-\delta\right)Q_{in} \tag{11}$$

where δ and β are coupling coefficients defined as follows (Larson *et al.*, 2006),

$$\delta = \frac{V_e + V_f}{V_{eq} + V_{fq}},\; \beta = \frac{1 - V_e/V_{eq}}{2 - V_e/V_{eq} - V_f/V_{fq}} \tag{12}$$

Sediment at rate Q_a is leaving the bypassing bar and feeding the attachment bar. The volume of the bypassing and attachment bars at any given time is V_b and V_a, respectively, with the corresponding equilibrium values V_{bq} and V_{aq}.

The sediment volume conservation equation for the bypassing bar is,

$$\frac{dV_b}{dt} = Q_b - Q_a \tag{13}$$

whereas the transport from the bypassing bar is given by,

$$Q_a = \frac{V_b}{V_{bq}} Q_b \tag{14}$$

The transport out from the attachment bar and further along the shore, Q_s, is:

$$Q_s = \frac{V_a}{V_{aq}} Q_a \tag{15}$$

In the area of the bypassing and attachment bars, incident wave energy greatly exceeds ebb-directed tidal energy, allowing a portion of the ebb shoal to migrate towards the shore under accretionary wave conditions (Kana *et al.*, 1999; Rosati *et al.*, 1999; Gaudiano and Kana, 2001). Thus, shoal bypassing is a natural form of beach nourishment (Gaudiano and Kana, 2001). This process is believed to contribute partly in the generation of a salient-type feature commonly observed on beaches downdrift inlets. In order to describe the process of onshore sand transport from the attachment bar to the shoreline in the numerical model, a macroscopic approach is taken where it is assumed that a certain fraction of the transport supplying the attachment bar volume is transferred to the beach at each calculation time step. Thus, sediment moves at a rate Q_{beach} from the attachment bar to the shoreline, expressed through a fraction, γ, of the total net sand transport being supplied to the attachment bar at any given time,

$$Q_{beach} = \gamma\left(Q_a - Q_s\right) = \gamma Q_a\left(1 - \frac{V_a}{V_{aq}}\right) \tag{16}$$

The sediment volume conservation equation for the attachment bar is:

$$\frac{dV_a}{dt} = Q_a - Q_s - Q_{beach} = \left(1-\gamma\right)\left(Q_a - Q_s\right) \tag{17}$$

Larson *et al.* (2002a) introduced a nonlinear relationship for releasing sediment from the ebb shoals when the inlet cross-sectional area is decreasing or closes completely. Thus, the above equations, (9), (14), (15) and (16) were changed to a nonlinear form, that is, $Q_{out} = Q_{in}(V/V_q)^n$, where Q_{out} and Q_{in} are sediment transport rates going out and entering a morphological unit, respectively, V and V_q are the volumes at a given time and at equilibrium of the unit, and n is an empirical power. By specifying a value of $n<1$ for situations where sediment is released back to the beach, the release will be slower than for the linear model. Larson *et al.* (2002a) suggested a value of n between 0.1 and 0.2 when the shoal experienced reduction in volume.

2.4 Distance to attachment bars

According to Hicks and Hume (1996) and Carr and Kraus (2001), the tidal prism is expected to control the size and location of the ebb shoal. Carr and Kraus (2001) developed an empirical relationship between tidal prism and the distance from the centerline of the inlet to the downdrift and updrift attachment bars by examining 108 tidal inlets in the United States. The inlets were classified according to whether the inlets had two, one or no jetties. For inlets with two jetties, the empirical relationships governing distance to the attachment bar was found to be,

for downdrift attachment bars: $Wd = 0.50 \times P^{0.451}$ (18)

for updrift attachment bars: $Wu = 0.16 \times P^{0.495}$ (19)

where Wd and Wu = distance from centerline of the inlet to the downdrift and updrift attachment points where the ebb shoal complex attaches to the shoreline (in m), respectively.

The angle between the orientation of the ebb jet and the shoreline affects the size and shape of the delta (Hicks and Hume, 1996); thus, the above relationships could be modified for improved predictability by including the ebb jet angle. If the ebb jet is perpendicular to the local shoreline trend, the morphological asymmetry is mainly controlled by the magnitude and direction of net longshore transport, as well as wave refraction and diffraction over the bathymetry and ebb shoal. Thus, a straight channel is expected to promote morphological symmetry and a reduced distance to the downdrift attachment point (Carr and Kraus, 2001). However, if the ebb jet angle becomes more acute, the tidal and wave energy oppose each other less. An ebb jet flow more parallel to the wave crests implies that the waves can more efficiently return shoreward sand deposited from the ebb jet (Hicks and Hume, 1996), but at a location further downdrift. Thus, a more acute ebb jet angle is expected to promote more sand being transferred to the downdrift beach and a longer distance to the attachment bar. These effects are believed to act at Shinnecock Inlet as well as at Moriches Inlet (Carr and Kraus, 2001), where the ebb shoal is attached to the updrift shoreline close to the jetty with an extended distance to the downdrift attachment bar. Thus, Eqs. (18) and (19) were modified by including the angle between the ebb jet and the local shoreline, ψ, expressed as,

for downdrift attachment bars: $Wd = 0.50 \times P^{0.451}(1+\cos\psi)$ (20)

for updrift attachment bars: $Wu = 0.16 \times P^{0.495}(1-\cos\psi)$ (21)

For the case where the ebb jet is perpendicular to the shoreline, ψ takes on a value of 90 deg, implying no asymmetry due to ebb jet orientation.

2.5 Wave sheltering effects from attachment bar

Beach erosion typically occurs along the shoreline on both sides of the attachment bar, whereas accretion occurs in its lee (Dean and Walton, 1975; Williams and Kana, 1987; Gaudiano and Kana, 2001) (see Figs. 3 and 4). The sheltered area behind the bar is gradually filled in, and finally the shoal attaches to the shore resulting in alongshore spreading of the bar in both directions from the point of attachment (Gaudiano and Kana, 2001). Thus, there are two mechanisms that cause sediment to gradually feed sand to the area behind the bar. The first mechanism is the onshore bypassing process of sand from the attachment bar due to landward flow associated with the waves (Williams and Kana, 1987; FitzGerald *et al.,* 2000). The second mechanism is due to the sheltering from the wave activity provided by the bar, which produces a zone of low energy in which alongshore currents can deposit transported material (Dean and Walton, 1975). The onshore bypassing process is described through the coefficient, γ, which represents the fraction of the transport supplied to the attachment bar build-up that is transferred to the shore (see Eq. (16)). The decrease in wave energy in the lee of the bar is expressed through a reduction in

breaking wave height. In the numerical model, a calibration parameter for reduction of the breaking wave height in the lee of the bar was introduced. In principal, the value of this parameter depends on the size and shape of the bar, which are different on the downdrift and updrift sides of the inlet due to asymmetry in inlet morphology. The breaking wave height in the lee of the bar was multiplied by a spatially varying attenuation parameter, η, and thus, H_b in Eq. (2) was replaced with ηH_b, where $0 \le \eta \le 1$. The value of η is less than 1.0 behind the bars, and equals 1.0 outside the sheltered areas. In principal, η has a minimum value at the centre point of the sheltered area, and its value increases towards both sides of the bar. As a simplification for this study, the values of η within the sheltered areas were obtained by linearly interpolating between a minimum value at the centre point of the respective sheltered area and 1.0 in areas not sheltered by the bar. The minimum values inside the bars were determined through a calibration procedure.

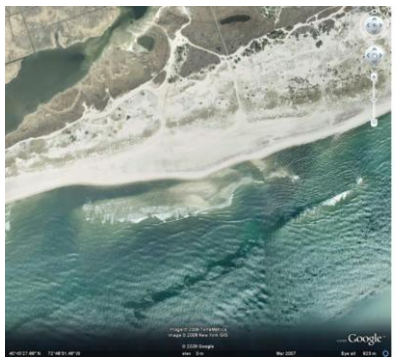

Fig. 3. Onshore migration of sediment from attachment bar at Moriches Inlet.

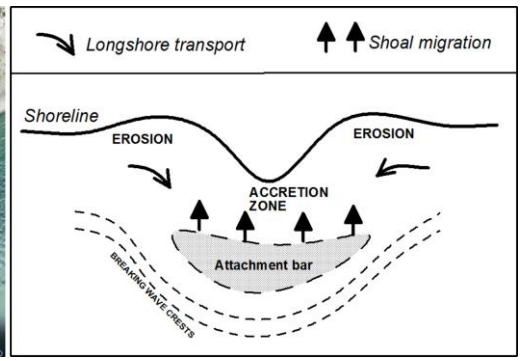

Fig. 4. Depiction of sand movement (after Kana *et al.*, 1985).

3. Study area and model setup

The Long Island coast, New York, was selected as a suitable location for validating the capability of the model to simulate regional sediment transport and development of tidal inlet shoal volumes. The study area extended from Fire Island Inlet to Montauk Point because the most available information originated from this coastal stretch (Larson *et al.*, 2002a). The stretch includes many coastal features and processes such as sediment transport and evolution at regional scale, the cross-sectional areas of the inlets varied substantially with time including opening and closure of the inlets, substantial shoreline response in vicinities of the jettied inlets, large amount of beach fill volumes placed at several locations along the coast (Larson *et al.*, 2002a), and a system of groins constructed to protect the beach.

Two types of simulations were performed with the new numerical model for the study area: (1) simulating the overall annual net longshore transport and regional shoreline evolution; and (2) simulating shoreline response in vicinities of the inlets and the tidal inlet shoal development in connection with varying cross-sectional area of the inlets. The objectives of these simulations were to validate the capability of the model to simulate shoreline response in the vicinity of the inlets and tidal inlet shoal development at local scale in combination with longshore sediment transport and shoreline evolution at regional scale.

The Long Island shoreline has a length of about 135 km and it is oriented in a direction of about 67.5 deg northeast. A model coordinate system was defined with a similar orientation for the *x*-axis. The lateral boundary conditions for the modeling consisted of "no shoreline change" specified based on shoreline measurements covering a period from 1830 to 1995 (Larson *et al.*, 2002a). Suitable locations for such a boundary condition were identified approximately 10 km west of Montauk Point and 15 km east of Fire Island Inlet.

Hindcast wave data (a 20-years time series at an interval of 3 hours from 1976 to 1995) from three WIS Stations along the coast was used as input data for the modeling. The spatial step was set at 100 m, and the input wave parameters were linearly interpolated based on the three stations corresponding to this spatial interval. The time step was set at 3 hours, coinciding with the interval of measured wave data. Following Larson *et al.* (2002a), the depth of closure was chosen to 8 m and the representative median grain size 0.3 mm. The regional shoreline shape was determined from spatial filtering of the shoreline measured in 1870 when no inlets existed using a window length of 7 km (Larson *et al.,* 2002a).

Measurements of inlet cross-sectional areas at Shinnecock and Moriches Inlets were performed at several occasions between 1931 and 1998, which includes the closure and subsequent opening of Moriches Inlet in the 1950's. These data were used to calculate the equilibrium volumes of the ebb shoal complexes, from which the equilibrium volumes of the individual morphological units at the inlets could be estimated (Larson *et al.*, 2002a). Equilibrium volume of the flood shoals were set to 4.10^6 m^3 for both inlets (Larson *et al.*, 2006).

Several structures were included in the simulations. Jetty lengths on each side of the inlets and the time of construction were specified according to information from the literature. The lengths of the east and west jetties at Moriches Inlet are 258 m and 445 m, respectively, and the jetties were constructed in 1953 (Vogel and Kana, 1984). For Shinnecock Inlet, the lengths of the east and west jetties are 280 m and 450 m, respectively, with construction carried out in 1953 (Smith *et al.*, 1999). Changes in the jetty lengths were not modeled, but they were kept constant during the simulation time after completion. The 15 groins comprising the Westhampton groin field were constructed in three phases, from March 1965 to October 1966, from 1969 to 1970, and in 1998 (Rosati *et al.*, 1999). These groins were included in the model at the proper times and the lengths and locations of the groins were specified based on available data.

Dredged material has typically been placed along adjacent beaches or within nearshore areas east and west of the inlets (Smith *et al.*, 1999). These beach fill volumes were included in the model as source terms in the sediment conservation equation that vary in time and space. A total volume of about 800,000 m^3 was placed west of Shinnecock Inlet between 1949 to 1983, and another 1,115,000 m^3 was put in this area between 1983 and 1995 (Larson *et al.*, 2002a). From 1955 to 1969, a total volume of about 661,000 m^3 was placed east of the inlet. Total quantities placed at Moriches Inlet between 1953 to 1996 were approximately 2.5 million cubic meters in which about 1.3 million cubic meters (52%) and 0.75 million cubic meters (30%) were placed to the east and west of the inlet, respectively (Smith *et al.*, 1999). Smaller beach fills have been placed at other locations, but they were neglected in the present modeling study.

In order to employ Eqs. (20) and (21), the angle between the ebb jet and the local shoreline must be specified. At Shinnecock Inlet, after completion of the jetties, the inlet opening rotated to conform to the jetty orientation which were in a north-south direction (Smith *et al.*, 1999), and at Moriches Inlet, the channel was oriented slightly east of north entering the inlet (Psuty *et al.*, 2005). The ebb jets are generally oriented parallel to the jetties. Based on satellite images, the angle between the ebb jet and local shoreline at Shinnecock and Moriches Inlet were set to 60 deg and 67 deg, respectively.

The equilibrium volumes, V_{eq}, V_{bq} and V_{aq}, of each morphology unit must be specified in Eqs. (7) to (17). Limited information exists on the equilibrium size of the individual morphological units described in the reservoir model. To simplify, the units are determined as being a constant fraction of the volume of the ebb shoal complex, which in turn is a function of inlet cross-sectional area (tidal prism). Militello and Kraus (2001) estimated sand bypassing to the attachment bar at a rate of about 19,000 m^3/yr for Shinnecock Inlet. The rate of ebb shoal growth, which is estimated to 117,000 m^3/yr (Williams *et al.*, 1998), implies that the ratio between the attachment bar and the ebb volume growth is 0.16. The ratio between bypassing bar and the ebb shoal volume is assumed to be 0.25 following Larson *et al.* (2002a). In the present study, the same ratios were employed for the both inlets.

To employ Eqs. (16) and (17), the fraction of the transport causing deposition on the attachment bar transferred to the shore at any given time must be specified. Gaudiano and Kana (2001) analyzed nine tidal inlets in South Carolina on the Atlantic Coast, which revealed that only a small fraction of the entire ebb shoal complex are transferred to the shore during bypassing events. The mean volume percentage is about 3.1. Taking into consideration the ratio between the attachment bar and the ebb shoal complex volume, the sand volume percentage transferred to the shore is about 20.0. Thus, the coefficient γ in the Eqs. (16) and (17) was set to 0.20.

The length of the attachment bars must be specified when modeling the alongshore distribution of the onshore sand transport from the attachment bar. This term could be expressed through the distances from inlet to the attachment bars, which is a function of the tidal prism. The assumption is made here that the length of the attachment bar corresponds to half the distance from the inlet to the attachment bar center.

4. Results and discussion

4.1. Shoreline evolution

The model was first run for the period 1933 to 1983 to compare with the measured shoreline in 1983. The simulated and measured shorelines, as well as the initial shoreline, are plotted in Fig. 5, in which Fig. 5a gives an overview and Fig. 5b and 5c the details at Shinnecock and Moriches Inlet, respectively. The shoreline plots provide a view "standing on shore" looking towards the ocean with Montauk Point on the left side and Fire Island Inlet on the right side. The transport coefficients were chosen based on the best fit between simulated and measured shorelines to be $K_1 = 0.15$ and $K_2 = 0.04$, respectively. The value of the transport coefficient was held constant for the entire study domain. The wave height attenuation coefficient was set to $\eta = 0.85$, implying that the breaking wave height at centre point of the lee of the attachment bars decreases 15% compared to the height outside the sheltered areas. This value was held constant during the entire simulation time, as well as for the downdrift and updrift bars. In general, η depends on the size and shape of the attachment bar, the incident wave energy relative to the tidal energy, and the wave refraction and diffraction around the bar. Ebb shoal volumes vary over time and differ between downdrift and updrift sides due to the morphological asymmetry of tidal inlet. However, for long-term simulation performed here, the attenuation coefficient is regarded as an average value.

The simulated shoreline is overall in good agreement with the measured shoreline, particularly on the updrift side of the jetties and in the downdrift area where the salient-type feature appears. However, at Shinnecock Inlet, on both sides of this feature, the shoreline retreat was overestimated by the model, and south of the downdrift attachment bar at Moriches Inlet, the simulated shoreline retreat was underestimated. The reason for this discrepancy may be due to several factors, at regional and local scale, that were not included in the model. Overwash by storm waves could produce shoreward displacement of the shoreline, which may have been the case west of Moriches Inlet. During storm surge, waves may overtop the island, and overwash of sediment occurs. This sediment is deposited on the back of the island and it is lost from the nearshore system or transported back at a low rate by wind (Larson *et al.*, 2002b). Large storm events have contributed to significant alteration of the Fire Island shoreline. These storms generally cause rapid beach erosion, dune displacement, and coastal flooding (Psuty *et al.*, 2005).

A local transport process, not described in the model, is a part of the transport system that is formed when sediment moves around the inlet, being bypassed through the shoals and bars (Kana *et al.*, 1999). In this system, a portion of the bypassing sand cycles back to the inlet (Williams and Kana, 1987; Kana *et al.*, 1999) due to flood tidal currents and wave refraction around the ebb shoal. This process is expected to produce erosion in the area close to the jetties. In addition, there are a number of other factors expected to cause the difference between the modeled and measured shorelines that were not included the model, such as wind-blown sand, inlet channel dredging, and sea level rise.

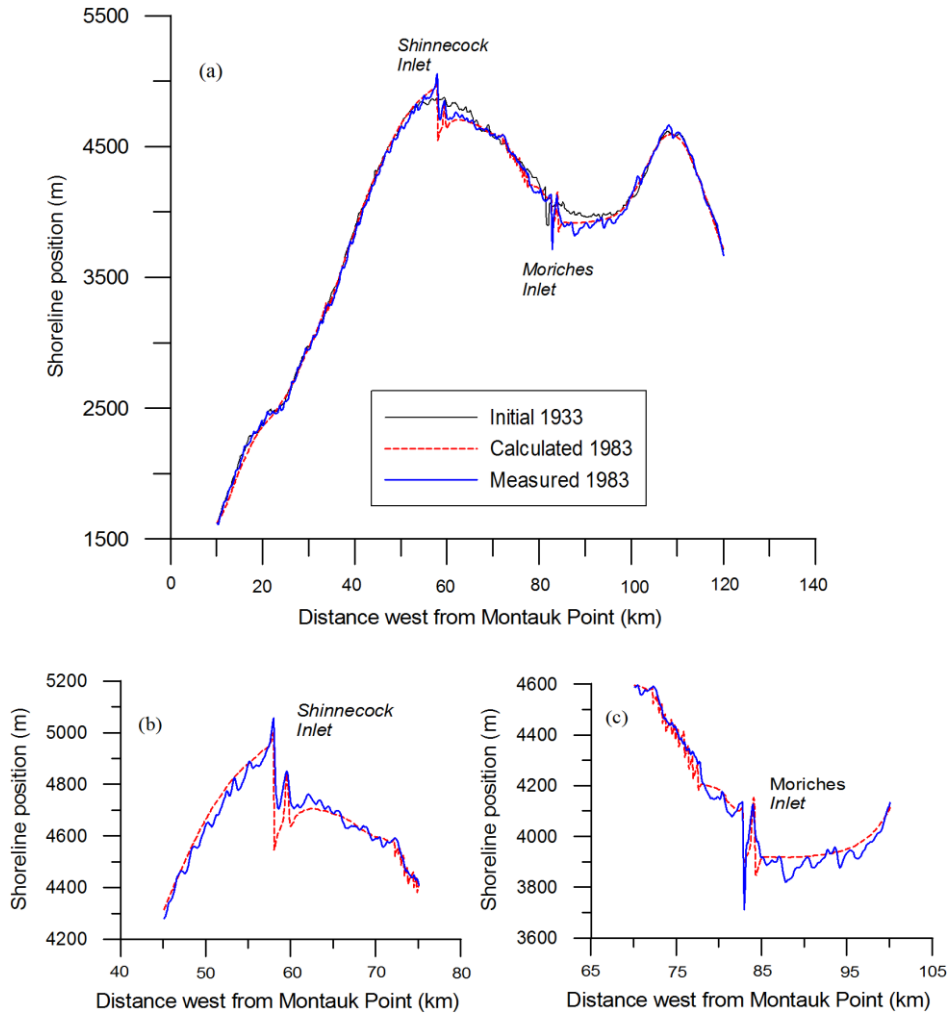

Fig. 5. Comparison between the measured and simulated shoreline in 1983 (a): Overview and detail from (b) Shinnecock Inlet and (c) Moriches Inlet.

4.2 Longshore transport rate

The simulated net transport rate together with the derived transport data reported by Rosati *et al.* (1999) is plotted in Fig. 6. The simulated annual net longshore transport rates were in good agreement with the analyzed data, except at Montauk Point where the rate was underestimated. The data from Rosati *et al.* (1999), for Montauk Point, included several important sinks and sources not described in the model, such as offshore losses due to sea

level rise (76,000 m^3/yr), beach fill placement (from zero to 170,000 m^3/yr), and bluff erosion (from 33,000 to 203,000 m^3/yr). This will affect net transport rates and cause a difference between the modeled and analyzed results at Montauk Point.

The net annual longshore transport rate exhibits an increasing trend from Montauk Point to Fire Island Inlet. Since the tidal inlets act as sinks to the longshore transport as they evolve towards their equilibrium state, the net transport rate decreases significantly across the inlets. The average annual longshore net transport rate obtained in this study is 108,000 m^3/yr.

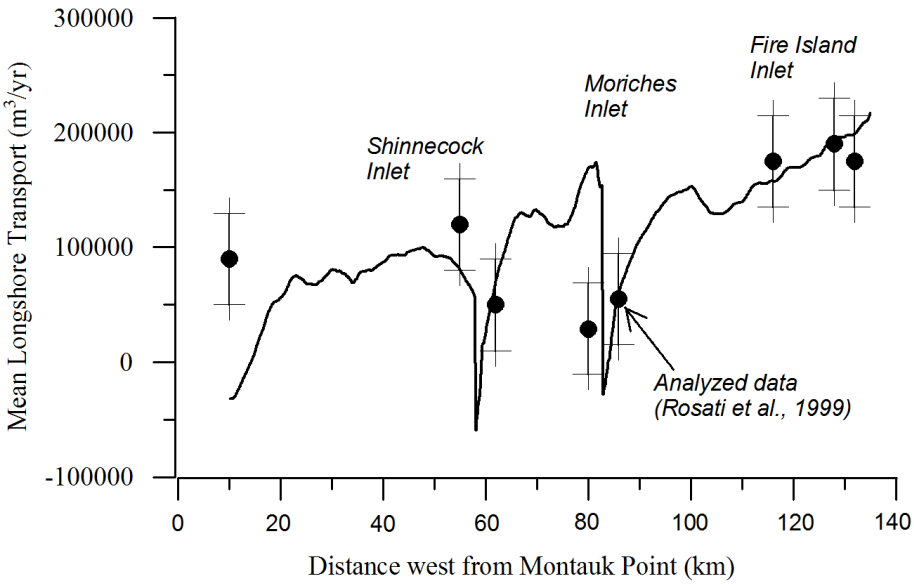

Fig. 6. Comparison between annual net transport rate and estimated data from measurements.

4.3 Flood and ebb shoal growth

The model was also run for the period 1933 to 2000 to compare with the measurements of ebb and flood shoal volume growth. Comparison between the calculated and measured ebb and flood shoal volumes are plotted in Figs. 7 and 8, respectively, where the total volume of the ebb shoal complex is displayed. Overall, the calculated and measured data are in good agreement, although specific individual points show more discrepancy.

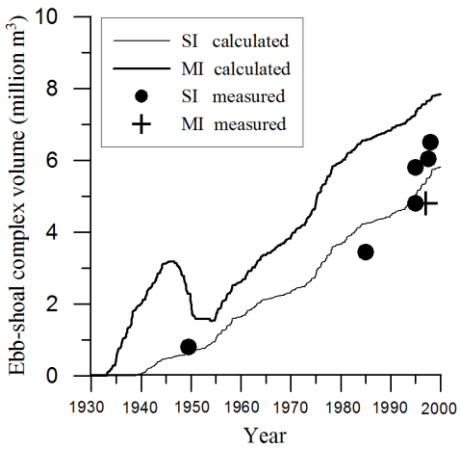

Fig. 7. Comparison between the measured and calculated volume of ebb-shoal complex (SI = Shinnecock Inlet, MI = Moriches Inlet).

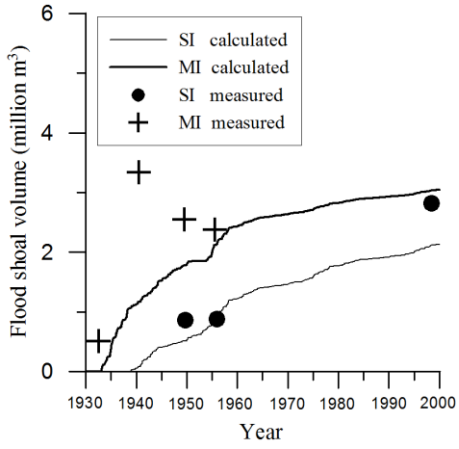

Fig. 8. Comparison between the measured and calculated volume of flood shoal (SI = Shinnecock Inlet, MI = Moriches Inlet).

5. Conclusions

A new numerical model of regional sediment transport and shoreline change combined with the inlet reservoir model was developed and successfully applied to simulate the evolution of the south shore of the Long Island coast, New York. The model was employed to simulate the period from 1933 to 2000, which included inlet opening and closure. The simulations covered a stretch of coastline from Montauk Point to Fire Island Inlet that includes two tidal inlets and other complex conditions involving a wide range of structures and activities such as jetties, groins, and beach fill. Model calculations were compared with measured shoreline evolution, annual net longshore transport rates reported in the previous literatures, and measured flood shoal and ebb shoal complex volumes. The simulated shoreline agreed well with the measured shoreline, including the accumulation updrift the inlets, the overall erosion downdrift the inlets, and the formation of salient-type features downdrift the inlets. The annual net longshore transport rates were overall in good agreement with the reported data, showing an increase in transport rate going west from Montauk Point. The growth of the flood and ebb shoal complexes at the inlets was also well predicted.

In order to realistically simulate the erosion and development of the salient-type feature downdrift the inlets, the predictive formula for the longshore transport rate was modified by introducing an attenuation coefficient for breaking wave height in the lee domain of the attachment bars. Also, sand bypassing from the bar to the shore was included in the inlet reservoir model. This modeling approach was indirectly validated through the improved agreement between the simulated and measured shoreline change downdrift of the inlet, in

comparison with the previous model by Larson *et al.* (2002a), which failed to capture the details of the shoreline response downdrift the inlets.

The empirical formulas for calculating the distance from centerline of an inlet to the attachment bars based on the tidal prism, developed by Carr and Kraus (2001), were modified by including the angle between ebb jet and the local shoreline trend. The average calculated distances from the inlet to updrift and downdrift attachment bars are, respectively, 252 m and 1150 m for Shinnecock Inlet, and 310 m and 1073 m for Moriches Inlet. These values are close to reported field data, implying that the updrift attachment bars are close to the jetties at both inlets, but the downdrift attachment bars extend to about 1200 m at Shinnecock Inlet (Williams *et al.*, 1998) and approximately 1100 m at Moriches Inlet (Psuty *et al.*, 2005). The calculated results show that the empirical formulas proposed, Eqs. (20) and (21), which include the angle between the ebb jet and the local shoreline, work reasonably well for the study site.

Application of the model to the Long Island coast shows the capability of the model to simulate regional sediment transport and shoreline evolution for complex conditions. Thus, a simulation domain may extend over hundreds of kilometers and cover several inlets including opening and/or closure, development of flood shoal and ebb shoal complexes, different shore protection measures, and shoreline response in the vicinity of inlets.

Acknowledgements

This work was partly funded by the Swedish International Development Cooperation Agency (Sida/SAREC) in the framework of the Project VS/RDE/03 “The evolution and sustainable management in the coastal areas of Vietnam” (LXH and PTN), and partly by Coastal Morphology Modeling and Management (Cascade) work unit, System-wide Water Resources Program conducted at the U.S. Army Engineer Research and Development Center (ML and HH). Support from Sida/SAREC project SWE-2007-123 is also appreciated.

References

Bayram, A., Larson, M., and Hanson, H. (2007). A new formula for the total longshore sediment transport rate. Coastal Engineering, 54, 700-710.

Carr, E.E., and Kraus, N.C. (2001). Morphologic Asymmetries at Entrances to Tidal Inlet. Coastal and Hydraulics Engineering technical Note IV-33, U.S. Army Engineer Research and Development Centre, Vicksburg, MS.

Dean, R.D., and Walton, T.L. (1975). Sediment transport processes in the vicinity of inlets with special reference to sand transport. Estuary Research, Volume II, Geology and Engineering, L.E. Cronin, ed., Academy Press, New York, 129-149.

FitzGerald, D.M., Kraus, N.C., and Hands, E.B. (2000). Natural Mechanisms of Sediment Bypassing at tidal Inlets. Coastal and Hydraulics Engineering Technical Note

ERDC/CHL CHETN-IV-30, U.S. Army Engineering Research and Development Centre, Vicksburg, MS.

Gaudiano, D.J., and Kana T.W. (2001). Shoal bypassing in mixed energy inlets: Geomorphic variables and empirical predictions for nine south Carolina Inlets. Journal of Coastal Research, 17(2) 280-291.

Hanson, H. (1987). GENESIS: A generalized shoreline change numerical model for engineering use. Lund, Sweden: Department of Water Resources Engineering, Lund University, Ph.D. thesis, 206p.

Hanson, H., Larson, M., Kraus, N.C., and Gravens, M.B. (2006). Shoreline response to detached breakwaters and tidal current: Comparison of numerical and physical models. Proceeding of the 30th Coastal Engineering Conference, World Scientific, pp. 3357-3369.

Hicks, D.M., and Hume, T.M. (1996). Morphology and size of ebb tidal deltas at natural inlets on open-sea and pocked-bay coasts, North Island, New Zealand. Journal of Coastal Research, 12(1), 47-63.

Jarrett, J.T. (1976). Tidal prism – inlet area relationships. U.S. Army Engineer Waterways Experiment Station, Vickburg, MS, 60p.

Kana, T.W. (1995). A mesoscale sediment budge for Long Island, New York. Marine Geology, 126(1995) 87-110.

Kana, T.W., Hayter, E.J., and Work, P.A. (1999). Mesoscale sediment transport at southeastern U.S. tidal inlets: Conceptual model applicable to mixed energy settings. Journal of Coastal Research, 15(2), 303-313.

Kraus, N.C. (2000). Reservoir model of ebb-tidal shoal evolution and sand bypassing. Journal of Waterway, Port, Coastal, and Ocean Engineering, 126(3), 305-313.

Kraus, N.C. (2002). Reservoir model for calculating natural sand bypassing and change in volume of ebb-tidal shoals, part I: Description. Coastal and Hydraulics Engineering Technical Note ERDC/CHL CHETN-IV-39, U.S. Army Engineering Research and Development Centre, Vicksburg, MS.

Larson, M., Kraus, N.C., and Connell, K.L. (2006). Modeling sediment storage and transfer for simulating regional coastal evolution. Proceeding of the 30th Coastal Engineering Conference (California, USA), World Scientific, pp. 3924-3936.

Larson, M., Kraus, N.C., and Hanson, H. (2002a). Simulation of regional longshore sediment transport and coastal evolution- the Cascade model. Proceeding of the 28th Coastal Engineering Conference. World Scientific Press, 2002.

Larson, M.; Rosati, J.D. and Kraus, N.C. (2002b). Overview of regional coastal processes and controls. Coastal and Hydraulics Engineering Technical Note CHETN XIV-4, U.S. Army Engineer Research and Development Center, Vicksburg, MS.

Militello, A., and Kraus, N.C. (2001). Shinnecock Inlet, New York, site investigation, Report 4, Evaluation of flood and ebb shoal sediment source alternatives for the west

of Shinnecock Interim Project, new York, Technical Report CHL-98-32, U.S. Army Corps of Engineers, Engineer Research and Development Centre, Vicksburg, MS.

Pelnard-Considere, R. (1956). Essai de theorie de l'evolution des forms de rivage en plage de sable et de galets. 4th Journees de l'Hydraulique, Les Energies de la mer, Question III, Rapport No. 1, pp. 289-298 (in French).

Psuty, N.P., Grace, M., and Pace, J.P. (2005). The coastal geomorphology of Fire Island, A portrait of continuity and change. Technical Report NPS/NER/NRTR-2005/021. U.S. Department of the Interior, National Park Service, Northeast Region, Boston, Massachusetts.

Rosati, J.D., Gravens, M.B., and Smith, W.G. (1999). Regional sediment budget for Fire Island to Montauk Point, New York, USA. Proceeding of Coastal Sediment Conference -1999. pp.803-817.

Smith, W.G., Watson, K., Rahoy, D., Rasmussen, C., and Headland, J.R. (1999). Historic geomorphology and dynamics of Fire Island, Moriches and Shinnecock Inlets, New York. Proceedings of Coastal Sediment'99, ASCE, 1597-1612.

Vogel, M.J., and Kana, T.W. (1984). Sedimentation patterns in a tidal inlet system, Moriches inlet, New York. Proceeding of the 19th Coastal Engineering Conference. World Scientific. pp. 3017-3033.

Walton, T.L., and Adams, W.D. (1976). Capacity of inlet outer bars to store sand. Proceeding of Coastal Engineering-1976, pp. 1919-1937

Williams, G.L., Morang, A., and Lillycrop, L. (1998). Shinnecock Inlet, New York, site investigation, Report 2, Evaluation of sand bypass options. Technical Report CHL-98-32, U.S. Army Corps of Engineers, Waterways Experiment Station, Vicksburg, MS.

Williams, M.L., and Kana, T.W. (1987). Inlet shoal attachment and erosion at Isle of Palms, South Carolina: A replay. Proceedings of Coastal Sediment'87, (Columbia, SC), 1174-1187.

Appendix

III

Hoan, L.X., Hanson, H., and Larson, M. (2010), A mathematical model of spit growth and barrier elongation. *Marine geology*. (Submitted)

A mathematical model of spit growth and barrier elongation

Le Xuan Hoan[1,2], Hans Hanson[1], and Magnus Larson[1]

1. *Water Resources Engineering, Lund University, Box 118, S-22100, Lund, Sweden.*
2. *Institute of Mechanics, Vietnam Academy of Science and Technology, 264 Doi Can, Hanoi, Vietnam.*

Abstract

A mathematical model of spit growth and barrier elongation adjacent to an inlet (of arbitrary width), supplied by sediment coming from longshore sediment transport, was developed based on the spit growth model proposed by Kraus (1999). The fundamental governing equation is the conservation equation for sand, where the width of the spit is assumed constant during growth. The portion of the longshore sediment transport feeding the spit is estimated based on the ratio between the depth of the inlet channel and the depth of active longshore transport. Sediment transport out from the channel due to the inlet flow, as well as other sinks of sand (e.g. dredging), are taken into account. Measured data on spit elongation at Fire Island Inlet, United States, and at Badreveln spit, Sweden, were used to validate the model. The simulated results are in good agreement with the measured data at both study sites, where spit growth at Fire Island was restricted by the inlet flow and the growth at Badreveln spit was unrestricted. The model calculation for Fire Island Inlet indicates that the dredging to maintain channel navigation is the major reason for the stable period observed from 1954 to 1994 at the Fire Island barrier. The average annual net longshore transport rate at the eastern side of the Fire Island inlet obtained in this study was about 220,000 m^3/yr, in which approximately 165,000 m^3/yr (75% of the net longshore transport) is deposited in the inlet feeding the spit growth, whereas the remaining portion (25%), is bypassed downdrift through the ebb shoal complex.

Key words: *Mathematical model*, *numerical modeling, sediment transport, spit growth, barrier elongation, tidal inlet, inlet shoal.*

1. Introduction

Spits are common morphological features at tidal inlets, entrances, river mouths, and barrier islands. A primary mechanism for spit development is accretion by longshore sediment transport (LST) in the shelter of a promontory, structure, or island. A second mechanism for spit elongation is associated with the migration of a tidal inlet where one spit elongates and the other spit shortens as the inlet migrates (Aubrey and Gaines, 1982; Petersen *et al.*, 2008). These mechanisms require an active LST in combination with proper hydrodynamic conditions at the inlet. In addition, some other mechanisms may form a spit, independently of LST, under a restricted combination of wave climate, tidal conditions and geological setting in the area where the spit is formed (Aubrey and Gaines, 1982). In some cases, a spit may be found where the coast makes a sudden change in its orientation (Petersen *et al.*, 2008). In the present study, however, only spit growth by accretion of sand coming from LST is investigated.

Spit growth is often categorized into restricted and unrestricted growth. In many cases, spits form at a tidal inlet or river mouth, where a significant net LST exists and/or a considerable amount of sediment is transported from the landmass or river mouth to the water body (Kraus, 1999). Depending on magnitude and direction of the net LST, the spit may form on one side or both sides of the inlet. Spit development can result in changes of the hydrodynamic conditions and geomorphological features at the tidal inlet, such as decreasing the cross-sectional area of the inlet and consequently causing the tidal jet to become gradually stronger. Therefore, the spit growth is, in turn, modified by the hydrodynamic forces. Under these conditions, the spit is expected to develop towards an equilibrium state, where the entire sediment feeding the spit is removed by the inlet flow. In this case, the spit elongation will be limited by the presence of the channel (Kraus, 1999). If the spit forms at an inlet with weak hydrodynamic forcing, the tidal channel may close due to the spit elongation. Thus, the spit growth will eventually be limited by the facing coast or by the opposite spit (if spit growth on both sides of the inlet prevails). In this study, spit elongation limited by the presence of an inlet channel or by an obstacle is classified as a restricted spit growth. A spit may also form in the shelter of headlands, barrier islands, or structures, where the spit growth is oriented towards an open area and growing without any restriction during the period under consideration. In such cases, spit elongation is classified as an unrestricted spit growth.

Kraus (1999) developed a mathematical model of spit growth due to LST. The model of Kraus was based on the continuity equation for the sediment under the assumption that the width and shape of the spit are constant during growth. In the work of Kraus, an attempt was made to estimate the amount of sediment bypassing the spit in the two cases of restricted and unrestricted spit growth. For an unrestricted spit growth, he assumed that no sediment was lost from the spit, implying that the entire LST from the updrift side feeds the spit. In a more complex situation, a time-varying LST (e.g., seasonal variation) was included through a sinusoidally fluctuating rate. For a restricted spit growth, Kraus analyzed a case of spit growth influenced by the presence of an inlet channel. The amount of sediment bypassing the spit is calculated based on a reservoir analogy using the ratio of the spit length at a particular time to that at equilibrium. Thus, an initial location of the spit must be specified to quantify the spit length. As one simple type of boundary condition, Kraus assumed that the initial location of a spit is far updrift of the channel, where the transport is unrestricted (no sediment bypasses the spit). Since there is no explicit expression to locate the initial position of spit, specifying the initial conditions for the model by Kraus is one of its greatest challenges. In addition, several factors expected to modify the spit growth rate are not included in the model, such as the channel depth (adjusts the sediment transport bypassing the spit), channel scour by tidal and river flow, and dredging works to maintain channel navigation.

Petersen *et al.* (2008) developed a simple analytical model based on the one-line concept suggested by Pelnard-Consid. re (1956) to predict the dimensions and elongation rate of an unrestricted spit growth. They considered an idealized and simplified case of a spit growing due to constant supply of the LST along a straight stretch of coastline updrift of the spit. The relationship between the angle of wave incidence and direction of spit growth was investigated. Experimental results obtained with small waves and a constant angle

showed that the width of a spit is proportional to the width of the surf zone and the proportionality factor was found to be about 8-10.

In this study, the main objective is to develop a mathematical model to simulate spit elongation due to sediment coming from LST for two different cases, restricted and unrestricted spit growth. The governing equation is primarily based on the sand volume conservation equation suggested by Kraus (1999) under the assumption that the width of the spit is constant. For restricted spit growth, under a particular LST rate and hydrodynamic conditions at a tidal inlet or river mouth, the spit elongation is expected to eventually reach an equilibrium state where the LST rate feeding the spit is equal to the transport rate going out from the channel due to the channel flow. The ratio of the depth of the inlet to the depth of active LST, together with an assumption of uniform cross-shore distribution of LST suggested by Hanson (1987), are employed to estimate the amount of sediment bypassing the spit. In addition, the sediment transport going out from the channel due to the channel flow, as well as other sinks or sources of sand, were included in the model. For an unrestricted spit growth, the entire LST feeds the spit, and no sediment is lost from the channel. The model was applied to simulate the spit growth at Fire Island Inlet, New York, United States, as an example of restricted spit growth. Then, as a simplified application, an analytical solution of the model was applied to the Badreveln spit, Sweden, as an example of unrestricted spit growth.

The spit growth model requires the calculation of LST rates, which are used as input data for the model. For the Fire Island case, a shoreline change model combined with the inlet reservoir model (Hoan *et al*., 2010) was employed to represent the LST along the coastline stretch from Mountauk Point to the Fire Island Inlet, including Shinnecock and Moriches Inlets. Hindcast wave data (a 20-years time series with waves at an interval of 3 hours from 1976 to 1995) from three WIS Stations along the coast were used as input data for the shoreline change model. The inlets along the coastline were regarded as sinks for the LST and simulated by the inlet reservoir model. For Badreveln spit, since detailed information on historical shorelines as well as the incident wave data were not available, the estimation of the annual net LST employed in the analytical solution was based on existing studies.

2. Spit growth model

The governing equation of the model is primarily based on the sand volume conservation equation suggested by Kraus (1999). In this study, an attempt is made to estimate the amount of sand, coming from the LST, bypassing the spit, and take other sinks or sources of sand into account. The model mainly focuses on two typical types of spit growth. First, spit elongation is restricted by the presence of an inlet channel or by an obstacle, and second, the spit elongates without restriction over the time period of consideration.

2.1 Restricted spit growth

Under proper hydrodynamic forcing and availability of sediment, a spit may form and elongate over time. However, at inlets an equilibrium state is typically reached at some point controlled mainly by the flow through the inlet and the LST rate. Such a limitation to the spit development is known as restricted spit growth. If the inlet flow is too weak to

prevent the navigation channel from filling in completely, the inlet will eventually close. Spits can form at the ocean and bay sides of inlets (Kraus, 1999), resulting in migration of the inlet channel and changes in the dynamic conditions at the inlet. Depending on the magnitude and direction of the net LST rate, spits can form at one side or both sides of the inlet.

In general, tidal inlets act as sinks for LST, although sediment is also bypassed from the updrift to the downdrift side. The magnitude of the bypassing depends on how close the morphological units of the inlet are to their equilibrium states. Natural bypassing of sediment at inlets occurs mainly through two processes: the LST can be bypassed through the ebb shoal complex or fall into the inlet channel and then be directly flushed out of the inlet to the downdrift beach (Bruun and Gerritsen, 1959). The hydrodynamic conditions at the inlet govern the fraction of the sediment falling into to the channel. Weak hydrodynamic forces promote deposition of sediment in the channel, which may be the case at inlets or entrances with a large cross-sectional area or with a small tidal prism. This deposition results in spit development together with shoaling of the inlet channel. Spit elongation can decrease the inlet cross-sectional area, gradually increasing the hydrodynamic forces in the channel. The stability of a spit depends on the balance between the LST rate coming into the channel and the tidal (and/or river) flow that scours the channel.

In order to derive a spit growth model, the following assumptions are made (compare Kraus, 1999),

- spit growth is sustained by the LST,
- spit elongation is in the same direction as the regional shoreline trend,
- spit width is constant,
- contours of the spit move in parallel.

Assuming that the LST (Q_{LST}) is coming to the inlet in the positive x-direction (see Fig. 1), the sand volume conservation equation that governs spit growth can be expressed as,

$$\frac{d}{dt}\left[\left(h+B_s\right)x\right]=\frac{1}{W}\left(Q_{in}-Q_c+Q_s\right) \tag{1}$$

where t = time; x = spit length; h = channel depth; B_s = average berm elevation of the spit; W = spit width; Q_{in} = sediment transport entering the channel; Q_c = sediment transport going out from the channel; and Q_s = sources or sinks of sand associated with the channel.

Kraus and Seabergh (2002; see also Kraus, 1999) proposed an approach to calculate Q_{in} for spit growth restricted by the presence of an inlet channel. In their approach, the portion of the LST rate that is transported away by the channel depends on how far the spit is from the center line of the inlet channel with respect to an initial condition for the spit position

located far updrift of the channel where the LST is unrestricted. Thus, the definition of the initial condition presents some difficulties and contains an element of subjectivity.

In this study, another method is employed to calculate Q_{in} and Q_c in Eq. 1, where the sediment pathways are taken into account. The sediment that falls into the channel (Q_{in}), contributing to the spit growth, is estimated based on the relationship between the maximum depth of the channel and the depth of active LST. If the maximum depth of the channel (D_M) is deeper than the depth of active LST (D_{LT}) it is expected that the entire LST falls into the channel (Fig. 1). Otherwise, if the maximum depth of the channel is smaller than the depth of active LST, a fraction of the LST is directly transferred to the ebb shoal complex and then bypassed downdrift (or possibly lost into deep water). If the cross-shore distribution of the LST is assumed to be uniform (Hanson, 1987), Q_{in} is expressed through the ratio between D_M and D_{LT} according to,

$$Q_{in} = \frac{D_M}{D_{LT}} Q_{LST} \tag{2}$$

where D_{LT} is estimated from an empirical equation (Hanson, 1987) as $D_{LT} = 1.6H_b$, where H_b = breaking wave height.

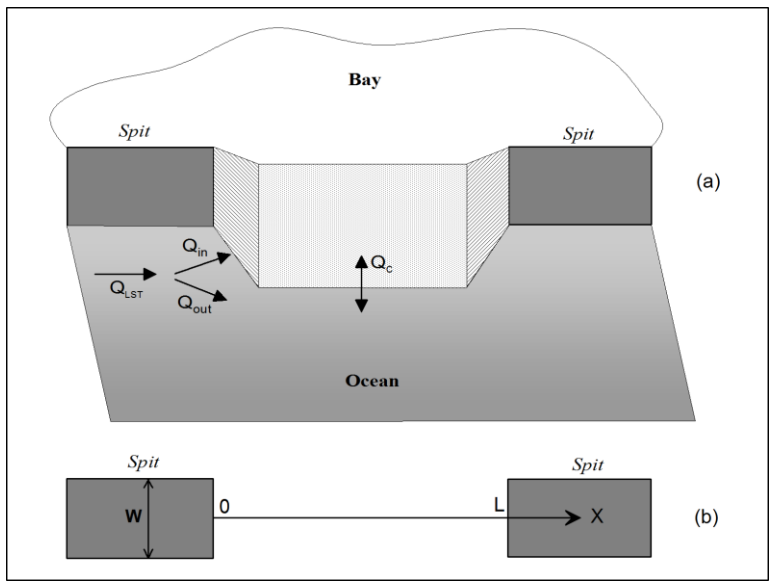

Fig. 1. Definition sketch for spit growth and sediment pathway: (a)- overview, (b)- plan view and coordinate axis.

The sediment transport rate (Q_c) produced by the inlet flow is given by (Watanabe *et al.*, 1991; Kraus, 1998),

$$Q_c = \omega \frac{(\tau_m - \tau_{cr})}{\rho g} U_c w_c \tag{3}$$

where ω = an empirical coefficient (on the order of unity); τ_m = bottom shear stress; ρ = density of water; U_c = mean velocity of the inlet channel flow; w_c = channel width; and τ_{cr} = critical shear stress for sediment transport calculated from (Van Rijn, 1993),

$$\tau_{cr} = \theta_{cr} (\rho_s - \rho) g d_{50} \tag{4}$$

where ρ_s = density of sand; d_{50} = medium grain size; and θ_{cr} = critical Shield's parameter given by (Soulsby, 1998),

$$\theta_{cr} = \frac{0.30}{1+1.2D_*} + 0.055\left[1 - \exp(-0.020D_*)\right] \tag{5}$$

where $D_* = d_{50}\left[\frac{(s-1)g}{\upsilon}\right]^{1/3}$; $s = \rho_s / \rho$; and υ = viscosity coefficient.

The bottom shear stress due to the mean current is expressed as (Kraus, 1998),

$$\tau_m = \rho c_f U_c^2 \tag{6}$$

where c_f = bottom friction coefficient, estimated following Kraus (1998),

$$c_f = g m^2 / \bar{h}^{1/3} \tag{7}$$

where g = acceleration due to gravity; m = the Manning coefficient; and $\bar{h}$ = average depth of the channel. Mean current velocity in the inlet channel is calculated based on the tidal prism (*P*), the tidal period (*T*), and the cross-sectional area of the inlet (A_c) according to Keulegan and Hall (1950),

$$U_c = \frac{\pi C_k P}{T A_c} \tag{8}$$

where C_k = a coefficient to account for a non-sinusoidal tide, having a value in the range of 0.81 to 1.0 (Kraus, 1998), and

$$A_c = \int_{x_t}^{L} h dx \tag{9}$$

where x_t = length of the spit at any given time, and L = maximum length of the spit from the initial spit position (Fig. 1).

Using Eqs. (3), (6), and (7), Eq. (1) may be written,

$$\frac{d}{dt}\left[\left(h+B_s\right)x\right] = \frac{1}{W}\left[Q_{in} - \omega U_c w_c \left(\frac{m^2}{\bar{h}^{1/3}}U_c^2 - \frac{\tau_{cr}}{\rho g}\right) + Q_s\right] \tag{10}$$

Spit elongation can gradually decrease the entrance cross-sectional area, increasing the mean current velocity in the inlet. Equilibrium conditions for the spit occur when $d/dt\left[\left(h+B_s\right)x\right] = 0$, that is,

$$Q_{in} = \omega U_c w_{ce}\left(\frac{m^2}{\bar{h}^{1/3}}U_c^2 - \frac{\tau_{cr}}{\rho g}\right) - Q_s \tag{11}$$

where w_{ce} = width of the inlet at equilibrium. Under conditions of strong inlet flow at equilibrium, τ_{cr} may be neglected (Kraus, 1998). If the channel depth is assumed to be constant, and neglecting sand sources or sinks, substituting (8) and (9) into (11), the equilibrium length of the spit is obtained as:

$$x_e = L - \frac{\omega^{1/2} m}{h^{5/3}}\left(\frac{\pi C_k}{T}\right)^{3/2}\frac{P^{3/2}}{Q_{in}^{1/2}} \tag{12}$$

Eq. (12) shows that the length of a spit at equilibrium is directly proportional to the LST rate supplied to the channel to a power 1/2 and inversely proportional to the tidal prism to a power 3/2. This means that, for the same magnitude of LST, a lower inlet flow will produce a longer spit at equilibrium than that produced by a stronger flow.

As an example of how a spit may grow depending on the tidal prism, the spit length is plotted in Fig. 2 as a function of time for different magnitude of the prism. The following input values are employed: $Q_{in} = 100{,}000\ \mathrm{m^3/year}$; $h = 5\ \mathrm{m}$; $B_s = 0$; $W = 100\ \mathrm{m}$; and $L = 1000\ \mathrm{m}$. Fig. 2 shows that during the initial stage under a weak inlet flow, spit growth is not depending on the tidal prism, but subsequently a strong channel flow develops, slowing down the spit growth. In cases with small tidal prisms (and/or small river discharge), corresponding to $P = 0$ in Fig. 2, the spit growth close the inlet.

2.2 Unrestricted spit growth

Unrestricted spit growth occurs if there is nothing preventing its elongation, for example, at a headland or a large entrance. In such cases, the cross-sectional area of the entrance is

assumed to be large enough so that the inlet current velocity is causing negligible sediment transport, implying that $Q_c \approx 0$. Thus, Eq. (1) simplifies to:

$$\frac{d}{dt}\left[\left(h+B_s\right)x\right]=\frac{1}{W}\left(Q_{in}+Q_s\right) \tag{13}$$

If a spit grows without restriction in time, the entire LST is expected to fall into the channel and feed the spit (Kraus and Seabergh, 2002), yielding $Q_{in}=Q_{LST}$, and:

$$\frac{d}{dt}\left[\left(h+B_s\right)x\right]=\frac{1}{W}\left(Q_{LST}+Q_s\right) \tag{14}$$

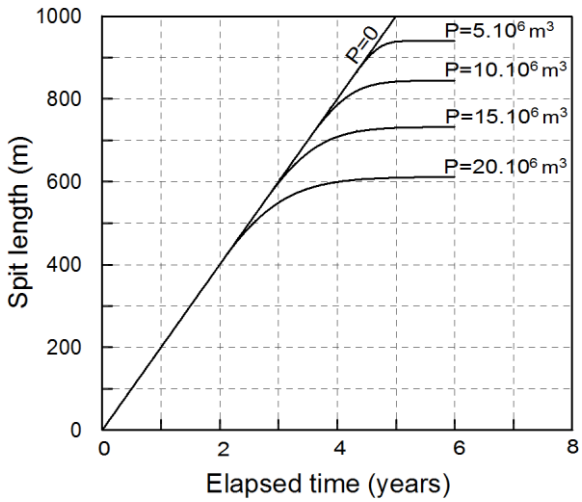

Fig. 2. Restricted spit growth for the same incoming longshore sediment transport rate with different tidal prism.

3. Sediment transport and shoreline change model

In order to simulate spit growth, the sediment transport feeding the spit at the updrift end (Q_{LST}) must be calculated. A LST and shoreline change model may be employed to compute Q_{LST} and how it varies in time, which is then used as input data to the spit model. It is important that Q_{LST} is simulated at a scale compatible with the scale determining spit growth. Over a longer time period (*i.e.*, centuries), the spit growth will be governed by the regional shoreline evolution, making it necessary to describe processes occurring at associated time and space scales. In this study, data from spit elongation at Fire Island Inlet in the United States will be used to test the spit model, and since a record of the spit

growth is available for over 150 years, a regional coastal evolution model is employed to calculate Q_{LST}.

The regional sediment transport and shoreline change model is based on the one-line theory (Pelnard-Considere, 1956), employing algorithms for the numerical solution developed by Hanson (1987). Conservation of sediment volume together with a relationship for the LST rate yield the fundamental equations to solve for obtaining shoreline change. Employing a coordinate system where the *y*-axis points offshore and the *x*-axis is oriented parallel to the trend of the shoreline, the conservation of sediment volume is expressed as,

$$\frac{\partial y}{\partial t}+\frac{1}{(D_B+D_C)}\left[\frac{\partial Q_{LST}}{\partial x}+q\right]=0 \tag{15}$$

where x = longshore coordinate; y = shoreline position; t = time; D_C = depth of closure; D_B = average berm elevation; and q = source or sink of sand.

The empirically based predictive formula for the total LST rate developed by Hanson *et al*. (2006) that exhibits sensitivity towards grain size and includes other currents than wave-generated ones was used,

$$Q_{LST}=\frac{\varepsilon}{8\left(\rho_s/\rho-1\right)\left(1-p\right)w_s}H_b^2C_{gb}\cos\alpha_0\left[K_1\left(a_1\sin\alpha_0+\overline{V_{ex}}\right)-K_2a_2\right] \tag{16}$$

in which, $a_1=\frac{5}{32}\frac{\pi\chi}{c_f}\sqrt{g}A^{\frac{3}{2}}$; $a_2=\frac{\pi}{c_f\chi^2}\sqrt{gd_b}\frac{\partial H_b}{\partial x}$ and $A=2.25\left(\frac{w_s^2}{g}\right)^{\frac{1}{3}}$

where d = water depth; C_g = wave group celerity; b = subscript denoting breaking wave conditions; K_1, K_2 = empirical coefficients (treated as calibration parameters); p = porosity of sand; w_s = fall velocity; $\overline{V_{ex}}$ = external surf-zone average longshore current velocity generated by tide or/and wind; A = shape parameter in equilibrium beach profile equation; χ = breaker index; ε = transport coefficient expressing efficiency of the waves keeping sand grains in suspension, which can be estimated through physical parameters as (Bayram *et al.*, 2007), $\varepsilon=\left(4.0+9.0\frac{H_b}{w_sT_p}\right)\times10^{-5}$; T_p = peak wave period; and α_0 = angle of breaking waves to the local shoreline orientation given by,

$$\alpha_0=\alpha_b-\arctan\left(\partial y/\partial x\right) \tag{17}$$

The effect of a regional shoreline shape may be included in Eq. (17), assuming that the local shoreline evolves with respect to the regional shoreline (Larson *et al*., 2002), yielding a new expression for α_0 according to,

$$\alpha_0=\alpha_{br}+\alpha_b-\arctan\left(\partial y/\partial x\right) \tag{18}$$

where $\alpha_{br} = \arctan\left(\partial y_r / \partial x\right)$ and y_r denotes the regional shoreline shape, which is taken to be constant over the time period studied.

4. Inlet reservoir model

Tidal inlets located along the coastline act as sinks for the LST (FitzGerald *et al*., 2000). As previously stated, the capability of an inlet to trap sand depends on how close the morphological units (*e.g*., ebb shoal complex and flood shoal) are to their equilibrium volumes (Kraus, 2000), which are functions of the tidal prism and the erosion and deposition processes in vicinity of the inlet. Thus, inlet development can produce a decrease in the LST rate on the downdrift side, reducing the LST towards a spit located further downdrift. In order represent sediment storage and transfer at inlets, the inlet reservoir model by Kraus (2000) as implemented by Larson *et al.* (2006) was employed in the present study.

Larson *et al.* (2006) refined the inlet reservoir model by Kraus (2000, 2002) through the introduction of the flood shoal and associated coupling coefficients, which analytically describe the transfer of sediment between the morphological units. The inlet morphology is schematically divided into distinct morphological units including the ebb shoal, bypassing bars, attachment bars, and flood shoal. Each morphological unit is assumed to have a certain equilibrium volume for fixed hydrodynamic and sediment conditions. Sediment is assumed to be transferred through a specific unit at a rate proportional to the ratio between actual and equilibrium volumes.

Assuming that Q_{LST} is transported towards the inlet, sediment bypasses the inlet through the ebb shoal complex at a rate Q_b, to be further transported alongshore downdrift the inlet, (Larson *et al.*, 2006),

$$Q_b = \frac{V_a}{V_{aq}} \frac{V_b}{V_{bq}} \frac{V_e}{V_{eq}} \left[\delta + \beta\left(1-\delta\right)\right] Q_{LST} \tag{19}$$

where V_a, V_b and V_e = volume of attachment bar, bypassing bar, and ebb shoal, respectively, at any given time, with the corresponding equilibrium volumes V_{aq}, V_{bq} and V_{eq}, estimated based on the tidal prism (Walton and Adams, 1976); and δ and β = coupling coefficients defined as follows,

$$\delta = \frac{V_e + V_f}{V_{eq} + V_{fq}}, \quad \beta = \frac{1 - V_e / V_{eq}}{2 - V_e / V_{eq} - V_f / V_{fq}} \tag{20}$$

where V_f, V_{fq} = volume of flood shoal at any given time and at equilibrium, respectively. The coefficient δ specifies the portion of the incoming transport (Q_{LST}) that goes directly to the ebb shoal (1-δ ends up in the channel) and β the portion of the transport deposited in the channel that is eventually transported to the ebb shoal (1-β goes to the flood shoal) (for details, see Larson *et al*., 2006).

5. Validation of the model - examples of the model application

The calculated results of spit elongation were compared with measured data at Long Island coast, New York, and at the Badreveln spit, Sweden. For the Long Island coast, the shoreline change model combined with the inlet reservoir model were used to represent the input data of LST for the spit growth model. For the Badreveln spit, estimated data on the LST from the existing literature were used as input data to an analytical solution of the model.

5.1 Study site and model setup for Long Island coast

Fire Island Inlet is one of several inlets along the south Long Island (LI) coast, New York (Fig. 3). It is located on the western side of a 130-km long stretch of the Atlantic coast that extends west of Mountauk Point, which is at the eastern most tip of LI. Fire Island inlet has existed continuously since the early 1700's (Smith *et al*., 1999), and from 1825 to 1940, the inlet migrated approximately 8 km to the west (USACE, 1999) (see Fig. 4). The migration of the inlet was temporarily halted by the construction of a jetty on the eastern side of the inlet in 1939 that was given a length of 1,525 m (USACE, 1999). However, this jetty did not provide a stable navigation channel, although it was successful in preventing inlet movement for more than a decade (Psuty *et al*., 2005). Fire Island Inlet is the major entrance to the Great South Bay, which has an estimated tidal prism of between $52 \cdot 10^6$ and $62 \cdot 10^6$ m^3, according to different sources (Jarrett 1976).

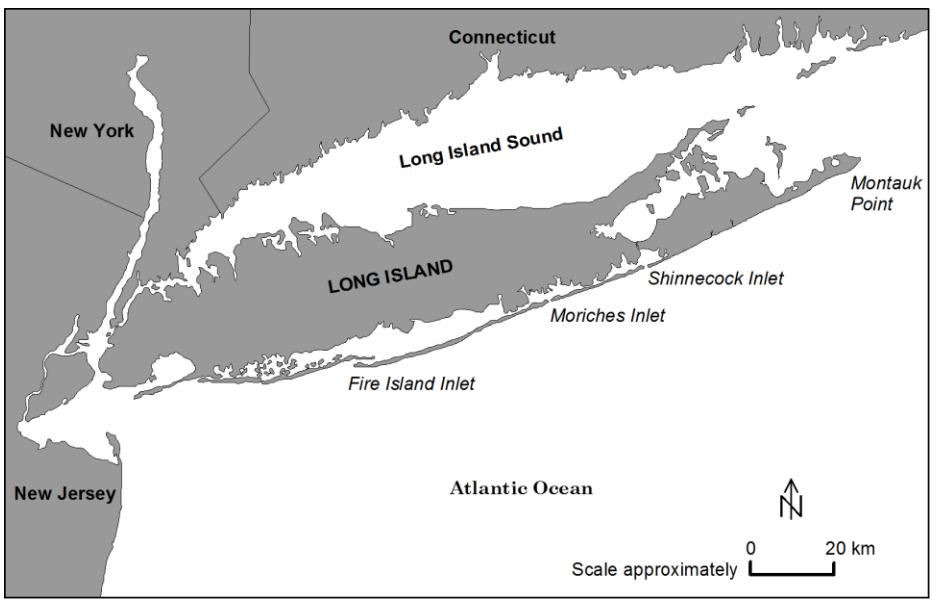

Fig. 3. Study site and locations of the inlets on the south Long Island coast, New York.

On the south coast of Long Island there are two other tidal inlets that lie between Montauk Point and Fire Island Inlet, namely Shinnecock and Moriches Inlets. Shinnecock Inlet was formed during a hurricane on the 21st of September 1938, whereas Moriches Inlet was opened during a major storm on the 4th of March 1931 (Smith *et al*., 1999). These tidal inlets together with the Westhampton groin field between Shinnecock and Moriches Inlets have been major sinks for the LST along the south coast of Long Island east of Fire Island inlet (Rosati *et al*., 1999). Inlet formation and migration at Fire Island Inlet has been influenced by the stabilization of Moriches Inlet as well as Shinnecock Inlet (USACE, 1999). These two inlets were therefore included in the modeling of the spit growth at Fire Island Inlet by using the inlet reservoir model. Measurements of inlet cross-sectional areas at Shinnecock and Moriches Inlets were performed at several occasions between 1931 and 1998, which included the closure and subsequent opening of Moriches Inlet in the 1950's. The recorded areas were used to calculate the equilibrium volumes of the ebb shoal complexes, from which the equilibrium volumes of the individual morphological units at the inlets could be estimated (Larson *et al*., 2002). The equilibrium volumes of the flood shoals were set to $4 \cdot 10^6$ m^3 for both inlets (Larson *et al*., 2006).

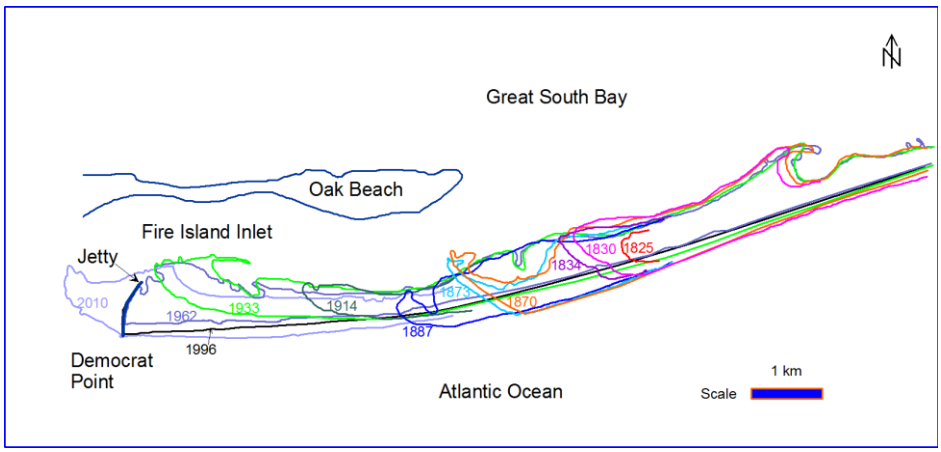

Fig. 4. Historical shoreline and spit growth at Fire Island inlet, New York (after Kana, 1995; Kraus and Seabergh, 2002; and satellite image in 2010).

The simulation area for the shoreline change model extended from Montauk Point to Fire Island Inlet, including Moriches Inlet and Shinnecock Inlet. The lateral model boundaries were placed at two stable shoreline locations, identified from historical shoreline measurements, one west of Montauk Point and the other east of Fire Island Inlet. The calibration parameter values in the empirical predictive formula for the LST rate were taken to be the same as in a previous modeling effort (Hoan *et al*., 2010), with $K_1 = 0.15$ and $K_2 = 0.04$. Following Larson *et al.* (2002), the depth of closure was set to 8 m and the representative median grain size to 0.3 mm. The regional shoreline shape was determined

from spatial filtering of the shoreline measured in 1870 when no inlets existed along the modeled stretch using a window length of 7 km (Larson *et al*., 2002).

The Fire Island Inlet is classified as a barrier overlap inlet (Kraus *et al*., 2003), indicating that the LST is large and mostly from the prevailing updrift direction, with a tidal flow sufficiently strong to maintain the inlet (Escoffier, 1977). The LST coming from the east is expected to feed the Fire Island barrier, while the LST coming from the west supplies the area west of Fire Island Inlet (Fig. 5). Thus, on the western side, the boundary condition for the shoreline change model could be set up as no sediment entering the simulation domain from the west side of Fire Island inlet, and LST from the east was used as input for the spit growth model of the Fire Island barrier.

Fig. 5. Pathway of longshore sediment transport at the Fire Island inlet, New york, based on the description of Escoffier (1977) and Kraus *et al.* (2003) for a barrier overlap inlet.

In order to employ Eqs. (8)-(10) to describe spit growth, the geometrical parameters of the spit must be specified. Based on available maps, Cedar Island to the west of Fire Island Inlet, which follows the regional shoreline trend of Fire Island, can be regarded as a stable point with respect to the Fire Island barrier elongation. Thus, the Fire Island barrier can be modeled as a spit where growth is restricted by an obstacle. The distance from the initial position to the Cedar Beach along the lengthening regional shoreline trend obtained from the Fire Island shoreline in 1825 (Kana, 1995) is about L = 10500 m. Furthermore, the average width of the Fire Island barrier is taken to be 500 m (W). Based on the measured topography reported by Smith *et al*. (1999), the depth of the entrance from the initial position to the Cedar Beach was taken as linearly decreasing from 8.5 m to 2.5 m. Tidal prism was specified to be $52 \cdot 10^6$ m^3 (Jarrett, 1976) with a semi-diurnal oscillation of about 12 hours tidal period (Psuty *et al*., 2005). The empirical coefficients, ω and C_k , were set to 1.0 and 0.9, respectively, whereas the Manning coefficient m was given a value of 0.025 (Kraus, 1998).

Hindcast wave data (a 20-years time series with waves at an interval of 3 hours from 1976 to 1995) from three WIS Stations along the coast were used as input data for the shoreline change model. The spatial step in the model was set at 100 m, and the input wave parameters were linearly interpolated alongshore based on the three stations corresponding to this spatial interval. The time step was set at 3 hours, coinciding with the interval of the measured wave data.

The jetty construction on the east side of the Fire Island inlet began in June 1939 and was completed in April 1941 (Bonisteel *et al*., 2004). The jetty intercepted the westward LST and stopped the migration of Fire Island, but by the mid-1950's it had become impounded and sand began bypassing around the tip of the jetty (Kraus *et al*., 2003; Bonisteel *et al*., 2004). This indicates that the jetty was successful to block most of the westward LST transport during the period from 1939 to the mid-1950's. Thus, a boundary condition of no sediment supply for barrier elongation was employed in the model during this period.

Dredged sand volumes were also included in the model. In order to maintain the navigational channel at Fire Island Inlet, approximately 300,000 m^3/yr of sand was dredged from 1954 to 1994 (USACE, 1999; Smith *et al.*, 1999). However, the dredging work was carried out along the length of some kilometers of the navigational channel where it is expected to include the deposited sediment coming from both sides of the channel (see Fig. 5). Roughly half of the dredged sand volume is assumed to come from the east and the other half to come from the west. Thus, in the present study, the dredged sand volume at a rate of 150,000 m^3/yr was modeled as a sink in Eq. (1).

The 15 groins comprising the Westhampton groin field were constructed in three phases, from March 1965 to October 1966, from 1969 to 1970, and in 1998 (Rosati *et al*., 1999). These groins were included in the shoreline change model at the proper times and the lengths and locations of the groins were specified based on available data.

5.2 Study site and model setup for the Badreveln spit, Sweden

The Badreveln spit is formed in the northeast part of the Falsterbo Peninsula in southern Sweden (Fig. 6). The spit started to develop in the early 1860's after the Skanör habor was constructed (Blomgren and Hanson, 2000), and extended northward from the harbor into an open area in the southwest corner of the Baltic Sea (see Fig. 6). Therefore, the Badreveln spit elongation may be modeled as an unrestricted spit growth, and it was selected as a suitable location for validating the spit growth model.

In order to employ the shoreline change model to represent the LST rate that feeds the spit, initial shoreline positions, offshore wave properties, and other boundary conditions must be specified. However, these necessary data are not available at the study site. As a simplification, the analytical solution to Eq. (14) was applied under the assumption that the sediment transport rate feeding the spit is constant (linear growth):

$$x = \frac{Q_{LST}}{\left(h + B_s\right)W} t \tag{21}$$

The input LST rate was estimated from information in existing studies. Hanson and Larson (1993) applied the numerical shoreline change model GENESIS to estimated the potential sediment transport rates along the south and west coast of the Falsterbo Peninsula. Along the Falsterbo bay coast, the average net transport rate was calculated to be 61,000 m^3/year, directed westward, and along the west coast, the average net transport rate was calculated to be 35,000 m^3/year, directed northward (see Fig. 6). The sediment transport along the west coast is expected to be partly blocked by Skanör harbor to build the south Skanör beach, and the remaining part is bypassed around the Skanör harbor to feed the Badreveln spit and the north Skanör beach. An average sediment transport rate feeding the spit was estimated to about 10,000 m^3/year. Based on the measured data, the depth of closure and the berm elevation were estimated to be 4 m and 1 m, respectively. An average width of the spit was determined based from satellite images to be 70 m. Measured data of spit elongation at several occasions from 1860 to 1994 (see Fig. 7) were used to compare with the analytical solution.

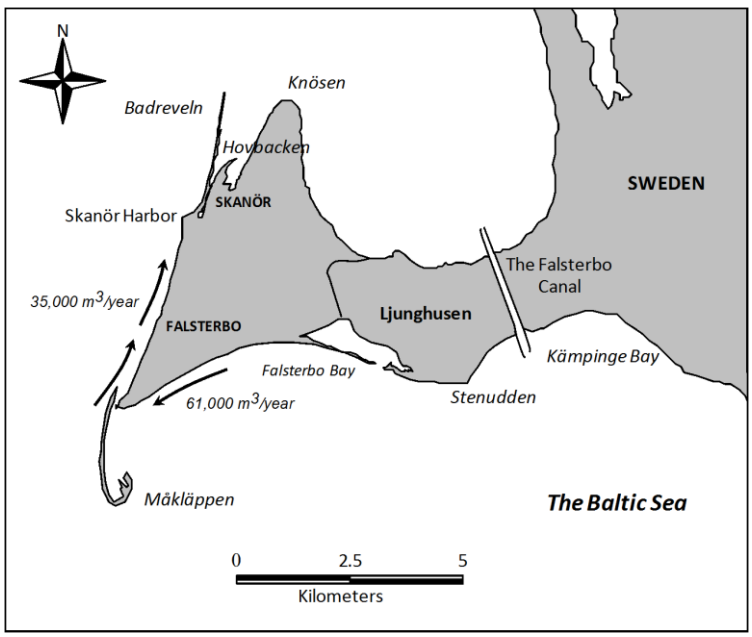

Fig. 6. Study site and calculated net sediment transport rates at the Falsterbo Peninsula in the south-west Baltic Sea (Blomgren and Hanson, 2000).

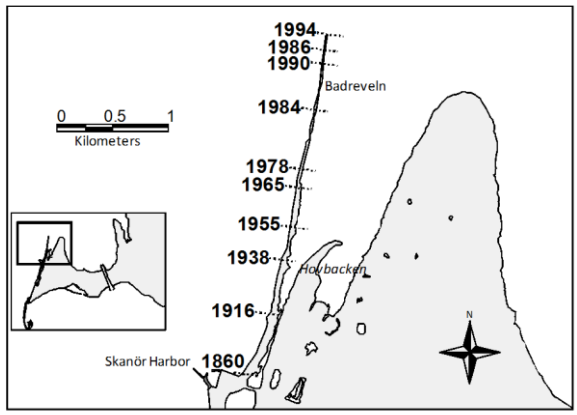

Fig. 7. The elongation of the Badreveln spit since 1860 (Blomgren and Hanson, 2000).

6. Results and discussion

The main objective of the present study is to develop a mathematical model for spit growth and validate it towards data mainly on the elongation of the Fire Island barrier. In order to provide input data on LST rates to the spit model, a regional shoreline evolution model was employed for the stretch between Montauk Point and Fire Island Inlet, including Shinnecock Inlet and Moriches Inlet. The model for the regional evolution consisted of a modified one-line model combined with the inlet reservoir model (Hoan *et al*., 2010), yielding the LST rates and information on the wave conditions needed as input at each time step to calculate spit growth.

The models were run for a period between 1825 and 2010 to reproduce the barrier elongation at Fire Island Inlet. Simulation results were compared with measured data reported by Kana (1995) and Kraus and Seabergh (2002), and the data based on satellite image in 2010 (see Fig. 8). The measured position of the Fire Island barrier in 1825 was used as the initial condition in the model. Overall, the calculated barrier elongation agreed well with the measured data, although some underestimation is observed between 1933 and 1962. These differences may be caused by lack of detailed data on dredging as well as modifications to structures during this period. Also, the actual wave conditions were not known and the simulations were performed through the repetitive use of the 20-year hindcasted time series of waves.

According to the present simulation results, the Fire Island barrier has approximately reached an equilibrium state regarding its westward extension, which is partly confirmed by the data. However, several factors have not been taken into account in the spit model, such as bottom friction effects of the long inlet channel, sediment supply from the western side (Cedar Island), and protective structures on the western side of the inlet. These factors

may significantly impact the equilibrium state of the barrier spit and the inlet cross-sectional area.

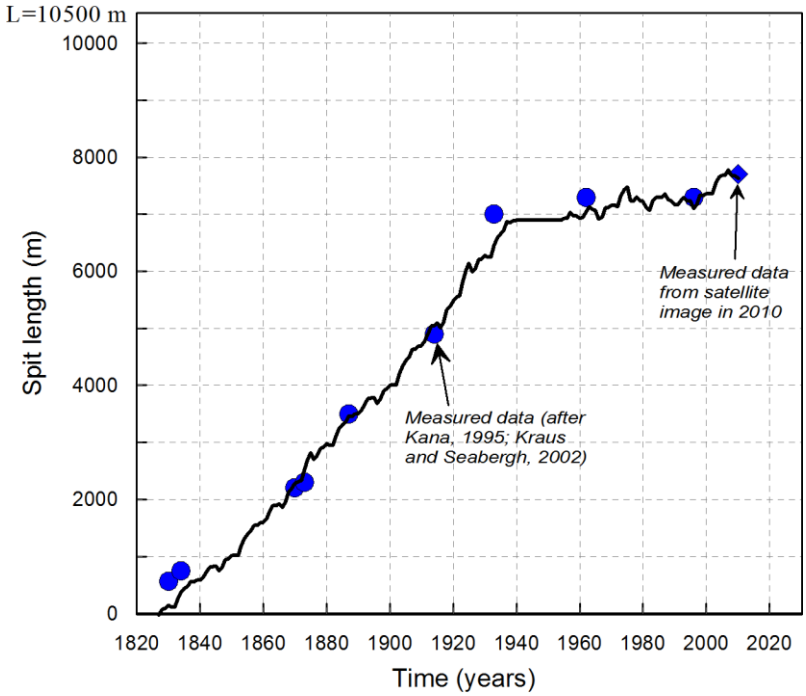

Fig. 8. Comparison between modeled and measured barrier elongation at the Fire Island inlet, New York.

The simulated net transport rate together with derived transport data reported by Rosati *et al.* (1999) are plotted in Fig. 9. The simulated annual net longshore transport rates were in good agreement with the analyzed data, except at Montauk Point where the rate was underestimated. The data from Rosati *et al.* (1999), for Montauk Point, included several important sinks and sources not described in the model, such as offshore losses due to sea level rise (75,000 m^3/yr), beach fill placement (between 0 and 170,000 m^3/yr), and bluff erosion (between 30,000 and 200,000 m^3/yr). These sources will affect the net transport rates and cause a difference between the modeled and analyzed results at Montauk Point.

The net annual LST rate shows an increasing trend from Montauk Point to Fire Island Inlet. Since the tidal inlets act as sinks to the LST when they evolve towards their equilibrium states, the net transport rate decreases significantly across the inlets. The average annual net LST rate obtained in this study is about 108,000 m^3/yr. This value is close to the estimated rate reported by Williams *et al.* (1998) being about 110,000 m^3/yr. The average annual net LST rate at the eastern side of Fire Island Inlet obtained in this study is 220,000 m^3/yr. This value is close to the estimated net LST rate reported by Rosati

et al. (1999) being in the range of 160,000 to 230,000 m^3/yr. The fraction of the net LST rate falling into the channel and feeding the spit, estimated from the Eq. (2), is about 165,000 m^3/yr (75% of net LST rate). The remaining portion of the net LST (25%) is transferred to the ebb shoal complex and/or lost into deep water.

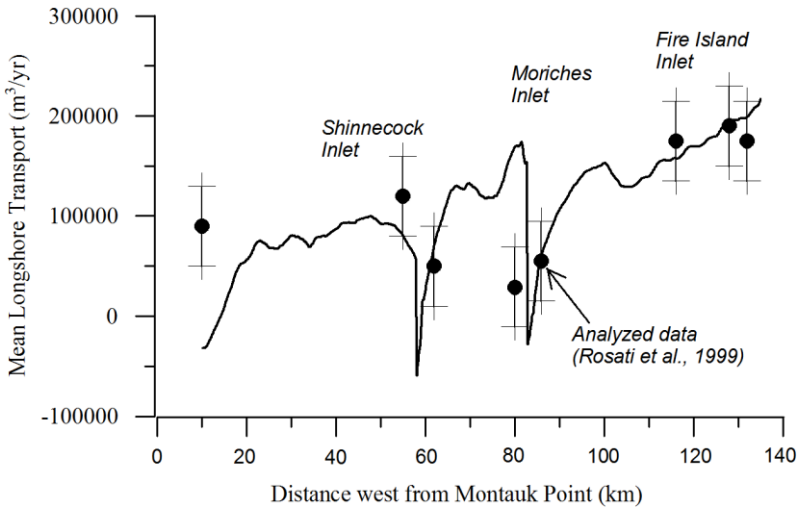

Fig. 9. Comparison between calculated annual net sediment transport rate and estimated data from measurements at Long Island coast, New York.

The westward elongation of the Fire Island barrier was halted by the jetty from 1939 to the mid-1950's, after which the jetty became impounded and sand began bypassing around the tip of the jetty (Kraus *et al*., 2003; Bonisteel *et al.,* 2004). Then, according to measured shorelines at Fire Island Inlet (Kana, 1995; Kraus and Seabergh, 2002), the Fire Island barrier was almost stable until 1996. This period is in close agreement with the period of dredging to maintain channel navigation at Fire Island Inlet reported by Smith *et al.* (1999) and USACE (1999). From 1954 to 1994 a sand volume of about 300,000 m^3/yr was dredged from the channel. However, as discussed above, the dredging work was carried out along the navigational channel where the deposited sediment is expected to come from both sides of the inlet. In this study, half of the dredged sand volume is assumed to come from the westward LST and thus, a dredging sand volume of 150,000 m^3/yr was employed in the model as a sink. This amount of dredging is close to the net LST feeding the spit. This indicates that the dredging at the inlet is the main reason for the stable period experienced at present for the Fire Island barrier.

For the Badreveln spit, comparison between the analytical solution and measured data of the spit elongation is plotted in Fig. 10. The analytical solution employed the estimated incoming net LST at a rate of 10,000 m^3/yr. Overall, the analytical solution is in good agreement with the measured data.

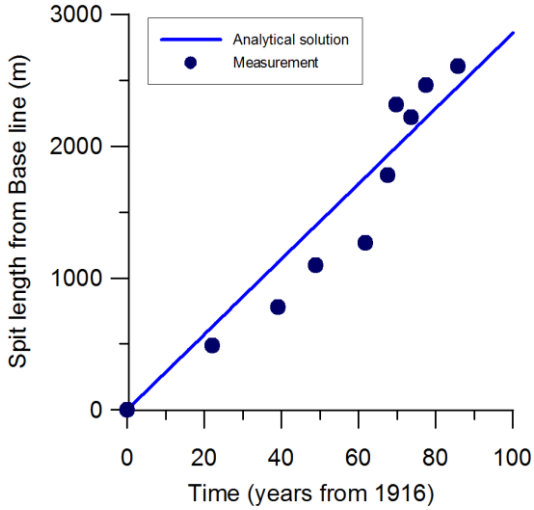

Fig. 10. Comparison between the analytical solution and measured data on spit elongation at the Badreveln spit, Sweden.

7. Conclusions

A mathematical spit model was introduced for simulating elongation of a restricted or unrestricted spit growth supplied by sediment coming from LST, under the assumptions that spit elongation is in the same direction as the regional shoreline trend, the spit width is constant, and contours of the spit move in parallel. The model requires estimates of the regional shoreline trend and maximum spatial length in which the spit elongates. Inputs for the model are the LST rate together with the breaking wave height at the incoming boundary of the spit. In this study, the ratio between maximum depth at the inlet and depth of active LST, estimated from the breaking wave height at a tip of the spit, is the main parameter governing the portion of the LST rate feeding the spit. The remaining portion of the LST rate is directly transferred to the ebb shoal complex and subsequently bypassed downdrift and/or lost into deep water. For an unrestricted spit growth, the required input of LST for an analytical solution may be the estimated net LST rate. For a restricted spit growth, tidal prism and/or river discharge are required to calculate sediment transport going out from the channel. In addition, other sinks or sources, such as sand removed by dredging or sand supplied by beach fills, are included in the model.

The model was successfully applied to simulate the barrier elongation at Fire Island inlet, New York. The model calculations were compared with measurements of the barrier elongation from 1825 to 2010 and the average annual net LST reported in previous studies. The model result of barrier elongation was in good agreement with the measured data. The calculated annual net LST rates reproduced reported data well, showing an increase in

transport rate going west from Montauk Point. The average annual net LST at the eastern side of Fire Island inlet obtained in this study is about 220,000 m^3/yr, of which 165,000 m^3/yr (75% of the entire net LST) is estimated to feed the spit growth. The remaining portion (about 25% of entire net LST) is directly bypassed through the ebb shoal complex. The calculated results show that the dredging is the main reason for stable period of the spit from 1954 to 1994.

An analytical solution to the spit model for unrestricted growth was validated through measurements at Badreveln spit, Sweden, with an estimated incoming net LST rate of about 10,000 m^3/yr. The analytical solution yielded predictions in good agreement with the measured data.

Acknowledgment

This work was partly funded by the Swedish International Development Cooperation Agency (Sida/SAREC) in the framework of the Project VS/RDE/03 “The evolution and sustainable management in the coastal areas of Vietnam” (LXH and PTN), partly funded by Coastal Morphology Modeling and Management (Cascade) work unit, System-wide Water Resources Program conducted at the U.S. Army Engineer Research and Development Center (ML and HH), and by Åke och Greta Lissheds foundation for the research project “Long-term coastal evolution” (LXH). Support from Sida/SAREC project SWE-2007-123 is also appreciated.

References

Aubrey, D.G. and Gaines, A.G. (1982). Rapid formation and degradation of barrier spits in areas with low rates of littoral drift. *Marine Geology*, 49 (3-4), 257-277.

Bayram, A.; Larson, M. and Hanson, H. (2007). A new formula for the total longshore sediment transport rate. *Coastal Engineering*, 54(9), 700-710.

Blomgren, S. and Hanson, H. (2000). Coastal Geomorphology at the Falsterbo Peninsula, Southern Sweden. *Journal of Coastal Research* 16(1), 15-25.

Bonisteel, J.M.; Peters-Snyder, M. and Zarillo, G.A. (2004). Barrier island migration and morphologic evolution, Fire island Inlet, New York, *Journal of the American Shore and Beach Preservation Association,* 72(1), 21-27.

Bruun, P. and Gerritsen, F. (1959). Natural by-passing of sand at coastal inlets. *Proceedings of the American Society of Civil Engineerings* (New York), Vol. 85, No. WW4, pp. 75-107.

Escoffier, F.F. (1977). Hydraulics and stability of tidal inlets. GITI Report 3, U.S. Army Coastal Engineering Research Centre, 75p.

FitzGerald, D.M.; Kraus, N.C. and Hands, E.B. (2000). Natural Mechanisms of Sediment Bypassing at tidal Inlets. Coastal and Hydraulics Engineering Technical Note

ERDC/CHL CHETN-IV-30, U.S. Army Engineering Research and Development Centre, Vicksburg, MS.

Hanson, H. (1987). GENESIS: A generalized shoreline change numerical model for engineering use. Lund, Sweden: Department of Water Resources Engineering, Lund University, Ph.D. thesis, 206p.

Hanson, H. and Larson, M. (1993). Sand Transport and Coastal Development at Skanör/Falsterbo. Report No. 3166. Department of Water Resources Engineering, Lund Inst. of Technology, Lund University, Lund, Sweden. (In Swedish.)

Hanson, H.; Larson, M.; Kraus, N.C. and Gravens, M.B. (2006). Shoreline response to detached breakwaters and tidal current: Comparison of numerical and physical models. *Proceeding of the 30th Coastal Engineering Conference*, World Scientific, pp. 3357-3369.

Hoan, L.X.; Hanson, H.; Larson, M. and Nam, T.P. (2010). Modeling regional sediment transport and shoreline response in the vicinity of tidal inlets on the Long Island coast, United States. *Coastal Engineering* (Submitted).

Jarrett, J.T. (1976). Tidal prism – inlet area relationships. U.S. Army Engineer Waterways Experiment Station, Vickburg, MS, 60p.

Kana, T.W. (1995). A mesoscale sediment budge for Long Island, New York. *Marine Geology,* 126(1), 87-110.

Keulegan, G.H. and Hall, J.V. (1950). A formula for the calculation of tidal discharge through an inlet. *U.S. Army Corps of Engineering, beach Erosion board Bulletin,* vol. 4, 15-29.

Kraus, N.C. (1998). Inlet cross-section area calculated by process-based model. *Proceeding of the 26th Coastal Engineering Conference*, ASCE, pp. 3265-3278.

Kraus, N.C. (1999). Analytical model of spit evolution at inlets. *Proceeding of Coastal Sediments '99*, ASCE, pp. 1739-1754.

Kraus, N.C. (2000). Reservoir model of ebb-tidal shoal evolution and sand bypassing. *Journal of Waterway, Port, Coastal, and Ocean Engineering,* 126(3), 305-313.

Kraus, N.C. (2002). Reservoir model for calculating natural sand bypassing and change in volume of ebb-tidal shoals, part I: Description. Coastal and Hydraulics Engineering Technical Note ERDC/CHL CHETN-IV-39, U.S. Army Engineering Research and Development Centre, Vicksburg, MS.

Kraus, N.C. and Seabergh, W.C. (2002). Inlet spit and Maintenance of navigation channels. Coastal and Hydraulics Engineering Technical Note ERDC/CHL CHETN-IV-44, U.S. Army Engineering Research and Development Centre, Vicksburg, MS.

Kraus, N.C.; Zarillo, G.A. and Tavolaro, J.F. (2003). Hypothetical relocation of Fire Island inlet, New York. *Proceedings of the 5th International Symposium on Coastal Engineering and Science of Coastal Sediment Processes* (Florida, USA), on CD-ROM.

Larson, M.; Kraus, N.C. and Hanson, H. (2002). Simulation of regional longshore sediment transport and coastal evolution- the Cascade model. *Proceeding of the 28th Coastal Engineering Conference*. World Scientific Press, 2002.

Larson, M.; Kraus, N.C. and Connell, K.J. (2006). Modeling sediment storage and transfer for simulating regional coastal evolution. *Proceeding of the 30th Coastal Engineering Conference* (California, USA), World Scientific, pp. 3924-3936.

Pelnard-Considere, R. (1956). Essai de theorie de l'evolution des forms de rivage en plage de sable et de galets. 4th Journees de l'Hydraulique, Les Energies de la mer, Question III, Rapport No. 1, pp. 289-298 (in French).

Petersen, D.; Deigaard, R. and Fredsoe, J. (2008). Modelling the morphology of sandy spits. *Coastal Engineering,* 55(7-8), 671-684.

Psuty, N.P.; Grace, M. and Pace, J.P. (2005). The coastal geomorphology of Fire Island, A portrait of continuity and change. Technical Report NPS/NER/NRTR-2005/021. U.S. Department of the Interior, National Park Service, Northeast Region, Boston, Massachusetts.

Rosati, J.D.; Gravens, M.B. and Smith, W.G. (1999). Regional sediment budget for Fire Island to Montauk Point, New York, USA. *Proceeding of Coastal Sediment Conference'99,* ASCE, 803-817.

Smith, W.G.; Watson, K.; Rahoy, D.; Rasmussen, C. and Headland, J.R. (1999). Historic geomorphology and dynamics of Fire Island, Moriches and Shinnecock Inlets, New York. *Proceedings of Coastal Sediment'99*, ASCE, 1597-1612.

US Army Corps of Engineers (USACE) (1999). Fire Island Inlet to Montauk Point, Long Island, New York. Main Report and Draft Environmental Impact Statement, Volume I, 1045p.

Soulsby, R. (1998). Dynamics of Marine Sands, Thomas Telford Ltd., London, U.K.

Van Rijn, L.C. (1993). Principles of sediment transport in rivers, estuaries and coastal seas. University of Utrecht, Department of Physical Geography, Aqua Publications.

Walton, T.L. and Adams, W.D. (1976). Capacity of inlet outer bars to store sand. *Proceedings of the 15th Coastal Engineering Conference*, ASCE, 1919-1937.

Watanabe, A.; Shimizu, T. and Kondo, K. (1991). Field application of a numerical model of beach topography response. *Proceedings of Coastal Sediments '91*, ASCE, 1814-1828.

Williams, G.L.; Morang, A. and Lillycrop, L. (1998). Shinnecock Inlet, New York, site investigation, Report 2, Evaluation of sand bypass options. Technical Report CHL-98-32, U.S. Army Corps of Engineers, Waterways Experiment Station, Vicksburg, MS.

Appendix

IV

Larson, M., Hoan, L.X., and Hanson, H. (2010). A direct formula to compute wave height and angle at incipient breaking. *Journal of Waterway, Port, Coastal, and Ocean Engineering*, 136(2), 119-122.

Direct Formula to Compute Wave Height and Angle at Incipient Breaking

Magnus Larson[1]; Le Xuan Hoan[2]; and Hans Hanson, M.ASCE[3]

Abstract: The purpose of this technical note is to present a new formula to compute the incipient breaking wave properties based on a simplified solution of the wave energy flux conservation equation combined with Snell's law. The execution time and calculated results of the new formula were compared with those of the iterative method which is commonly used in coastal engineering calculations, including in shoreline response modeling. The new formula could be used instead of the iterative method to save calculation time for application in coastal engineering.

DOI: 10.1061/(ASCE)WW.1943-5460.0000030

CE Database subject headings: Breaking waves; Energy; Computation; Height.

Author keywords: Breaking wave; Incipient breaking; Wave properties; Wave energy flux; Wave condition; Iterative method; New formula.

Introduction

Computationally efficient algorithms to determine the wave properties at incipient breaking from knowledge of the wave conditions in the offshore, often taken to be deep water, are required in most coastal evolution models (Kraus and Harikai 1983; Hanson 1989). The longshore sediment transport, which is the main mechanism for moving the material and causing coastline changes, is typically estimated based on the wave conditions at the break point. In coastal evolution models with a strong coupling between the waves and the coastline changes, calculations of the wave properties at the break point are made for every grid cell and every time step, implying that any reduction in computational time to obtain these properties causes significant decrease in the overall needed computer simulation time. Since long-term simulations of coastal evolution are becoming more common in engineering applications (Larson et al. 2002), reduction in computer simulation time is necessary.

The calculations of the wave properties at incipient breaking in coastal evolution models are made by employing the conservation of wave energy flux from an offshore location, where the wave conditions are known, to the break point combined with Snell's law for wave refraction. Substituting Snell's law into the energy flux conservation equation yields an equation that must be solved using some iterative numerical technique, for example, the Newton-Rhapson method. Thus, if a simplified, direct method can be developed to compute the wave properties at the break point, the simulation time can be greatly decreased.

In the following, a direct accurate formula is developed to compute the wave properties at incipient breaking based on a simplified solution of the wave energy flux conservation equation combined with Snell's law. A fourth-order polynomial equation is derived to correct the solution to the linearized equation. However, before the new formula is presented, the governing equations are first reviewed and a solution is presented for the linearized case that often yields quite accurate results. Finally, some computational tests are made with the new formula and compared to the results from solving the governing equations with an iterative technique showing the accuracy of the new formula and the savings in execution time for applications in a typical shoreline evolution model.

Governing Equations and Solution after Linearization

Assuming input wave conditions in deep water, the wave properties at incipient breaking are obtained by simultaneously solving the energy flux conservation equation and Snell's law, both equations taken from deep water to the break point. The two equations are written as

$$H_o^2 C_{go} \cos \theta_o = H_b^2 C_{gb} \cos \theta_b \tag{1}$$

$$\frac{\sin \theta_o}{C_o} = \frac{\sin \theta_b}{C_b} \tag{2}$$

where H=wave height; C_g=group speed; θ=wave angle; C=phase speed; and subscripts o and b=deep water and the break

[1]Professor, Dept. of Water Resources Engineering, Lund Univ., Box 118, 22100 Lund, Sweden.

[2]Graduate Student, Dept. of Water Resources Engineering, Lund Univ., Box 118, 22100 Lund, Sweden; and, Graduate Student, Institute of Mechanics, Vietnamese Academy of Science and Technology, 264 Doi Can, Hanoi, Vietnam (corresponding author). E-mail: Hoan.Le_Xuan@tvrl.lth.se

[3]Professor, Dept. of Water Resources Engineering, Lund Univ., Box 118, 22100 Lund, Sweden.

Note. This manuscript was submitted on December 17, 2008; approved on July 31, 2009; published online on August 3, 2009. Discussion period open until August 1, 2010; separate discussions must be submitted for individual papers. This technical note is part of the ***Journal of Waterway, Port, Coastal, and Ocean Engineering***, Vol. 136, No. 2, March 1, 2010. ©ASCE, ISSN 0733-950X/2010/2-119–122/$25.00.

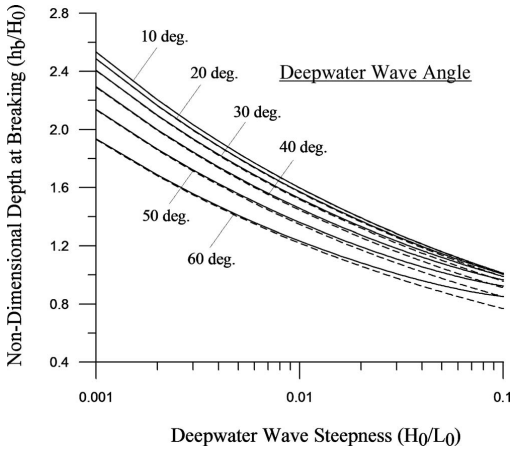

Fig. 1. Normalized depth at breaking as a function of wave steepness and angle in deep water (exact and approximate solutions)

point, respectively. The two equations are coupled and may be solved through an iterative procedure. Introducing expressions for the various wave quantities valid for deep and shallow water and substituting the unknown angle from Snell's law into the energy flux conservation equation give the following equation to solve with the water depth at breaking as the unknown:

$$\left(\frac{h_b}{L_o}\right)^{5/2}\cos\left[\arcsin\left(\sqrt{2\pi}\sin\theta_o\sqrt{\frac{h_b}{L_o}}\right)\right]=\left(\frac{H_o}{L_o}\right)^2\frac{\cos\theta_o}{\gamma_b^2 2\sqrt{2\pi}} \tag{3}$$

where h_b=water depth; L_o=deepwater wavelength; and γ_b =breaker depth ratio ($H_b=\gamma_b h_b$). Eq. (3) assumes that the long-wave theory is applicable at the break point, that is, $C_b=C_{gb}=\sqrt{gh_b}$. This approximation is typically made in shoreline evolution models, although it may introduce some errors for steep waves.

This equation shows that h_b/L_o (or equivalently h_b/H_o) is a function only of H_o/L_o and θ_o (if the input wave conditions are not in deep water, h_m/L_o will appear as another variable in the solution, where h_m is the water depth at which the wave properties are known). Once h_b is obtained, H_b and θ_b may be calculated directly from the definition of the breaker depth ratio and Snell's law, respectively. Fig. 1 illustrates the variation of h_b/H_o with H_o/L_o and θ_o (solid lines), where the governing equations were solved using the Newton-Rhapson method.

If the wave angle at incipient breaking is small ($\cos\theta_b\cong 1.0$), which is typically a good approximation, h_b can be calculated directly from

$$\frac{h_b}{L_o}=\left[\left(\frac{H_o}{L_o}\right)^2\frac{\cos\theta_o}{\gamma_b^2 2\sqrt{2\pi}}\right]^{2/5} \tag{4}$$

Fig. 1 also includes solutions after this linearization (broken lines), indicating that the error introduced by this solution is marginal for a wide range of values on H_o/L_o and θ_o (calculations showed that the error is less than 10% for all angles and steepnesses investigated). The wave angle at the break point is calculated from Snell's law

$$\theta_b=\arcsin\left(\sqrt{2\pi}\sin\theta_o\sqrt{\frac{h_b}{L_o}}\right) \tag{5}$$

The solution to the linearized equation [Eq. (4)] has previously been derived by several writers (e.g., Walton et al. 1982; Larson et al. 2002), but it is not commonly used in coastal evolution models.

New Formula for Wave Properties at Incipient Breaking

Although Eq. (4) tends to be a good approximation in general, larger deviations between the exact solution and the solution for the linearized equation may occur if the input wave conditions are not in deep water. Also, because the longshore sediment transport is quite sensitive to small changes in the breaking wave angle, accurate estimates of this angle are needed.

The equations to solve for the case of wave input at an arbitrary water depth (denoted by the subscript m) are

$$H_m^2 C_{gm}\cos\theta_m=H_b^2 C_{gb}\cos\theta_b \tag{6}$$

$$\frac{\sin\theta_m}{C_m}=\frac{\sin\theta_b}{C_b} \tag{7}$$

Assuming shallow-water wave theory at the break point and combining Eqs. (6) and (7) give

$$H_m^2 C_{gm}\cos\theta_m=\gamma_b^2 h_b^2\sqrt{gh_b}\cos\left[\arcsin\left(\sin\theta_m\frac{C_b}{C_m}\right)\right] \tag{8}$$

Introducing $\lambda=gh_b/C_m^2$ and manipulating Eq. (8) give the following result:

$$\lambda^{5/2}\left(\frac{C_m}{\sqrt{gH_m}}\right)^4\frac{C_m}{C_{gm}}\frac{\gamma_b^2}{\cos\theta_m}\cos[\arcsin(\sin\theta_m\sqrt{\lambda})]=1 \tag{9}$$

Introducing a parameter α defined as

$$\alpha=\left(\frac{C_m}{\sqrt{gH_m}}\right)^4\frac{C_m}{C_{gm}}\gamma_b^2 \tag{10}$$

into Eq. (9) and using a trigonometric relationship implies that this equation can be rewritten as

$$\lambda^{5/2}\frac{\alpha}{\cos\theta_m}\sqrt{1-\sin^2\theta_m\lambda}=1 \tag{11}$$

If the breaking wave angle is assumed small, the square root term approaches 1 and the solution to Eq. (11) simplifies to

$$\lambda_a=\left(\frac{\cos\theta_m}{\alpha}\right)^{2/5} \tag{12}$$

where subscript a denotes that it is an approximate solution corresponding to the linearized case [compare with Eq. (4)].

Employing Eq. (12) allows us to express Eq. (11) into the following form:

$$\left(\frac{\lambda}{\lambda_a}\right)^{5/2}\sqrt{1-\varepsilon\frac{\lambda}{\lambda_a}}=1 \tag{13}$$

where

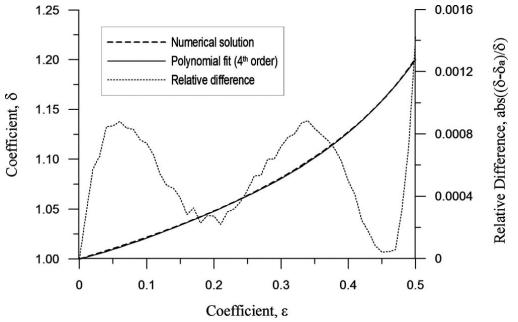

Fig. 2. Correction factor for normalized depth at breaking as a function of a nondimensional parameter that depends on input wave conditions (exact and approximate solutions)

$$\varepsilon = \frac{\sin^2 \theta_m (\cos \theta_m)^{2/5}}{\alpha^{2/5}} = \sin^2 \theta_m \lambda_a \tag{14}$$

Thus, Eq. (13) can be solved in terms of $\delta = \lambda/\lambda_a$ for different values on ε. If the relationship between δ and ε can be approximated with an empirical function, Eq. (12) can be used to compute λ_a and this value can then be corrected based on δ (predicted from ε, which may be directly computed from input data). Fig. 2 illustrates the exact solution to Eq. (13), plotting δ as a function of ε (solid line). The same figure shows a least-squares approximation by a fourth-order polynomial (broken line), which more or less falls on top of the exact solution. The polynomial is given by

$$\delta_a = 1.0 + 0.1649\varepsilon + 0.5948\varepsilon^2 - 1.6787\varepsilon^3 + 2.8573\varepsilon^4, \quad 0 \le \varepsilon \le 0.5 \tag{15}$$

where subscript a denotes an approximate solution, as before. To further illustrate how well Eq. (15) fits the exact solution, the absolute difference between δ and δ_a, normalized with δ is also plotted in the figure. The deviation from the exact value is typically below 0.1% when Eq. (15) is employed. The range of ε for which the polynomial equation was fitted should cover the input wave conditions of interest in most cases.

Evaluation of the New Formula

The new formula was evaluated by comparing the calculation speed and difference in calculated results between the new formula and the iterative method [the latter method from Hanson and Kraus (1989)]. Two computing procedures, one based on the new formula (hereafter called the new procedure) and the other based on the iterative method (hereafter called the iterative procedure), were developed and then called by a coastal evolution model. Varying values of deepwater wave properties, including T_o, H_o, and θ_o, were employed as input data for the model to test speed and accuracy of the new procedure (see Table 1).

Because the new procedure executes only one loop (direct calculation), calculation speed of this procedure for varying input wave data are not significantly different. In contrast, calculation speed of the interactive procedure depends on input deepwater wave properties and the critical value (Δ_c) of the iterative technique (used to define the accuracy of the iterative procedure). To examine the relationship between calculation speeds and the input data, the input wave properties were divided into three groups in which each group employed two constant properties and the remaining property was varied as follows: Group I where T_0 and H_0 were held constant and θ_o was varied; Group II where T_0 and θ_o were held constant and H_0 was varied; and Group III where H_0 and θ_o were held constant and T_0 was varied (see Table 1). The critical value was used as a threshold to stop the computing process when the absolute difference between the calculated breaking wave heights, at the previous step and the present step, was less than (Δ_c). Thus, accuracy of the calculated breaking wave properties is partly controlled by the values of (Δ_c). In general coastal engineering calculation, the degree of accuracy in calculated wave height is in the order of centimeters (10^{-2} m). Thus, in this study, (Δ_c) was taken to be 10^{-2}.

Table 1. Input Deepwater Wave Properties for Testing of Procedures to Compute Wave Properties at Incipient Breaking

	Number	T_0 (s)	H_0 (m)	θ_0 (deg)
Group I	1	9.0	3.0	80.0
	2	9.0	3.0	60.0
	3	9.0	3.0	40.0
	4	9.0	3.0	20.0
	5	9.0	3.0	0.0
Group II	6	6.0	2.5	40.0
	7	6.0	2.0	40.0
	8	6.0	1.5	40.0
	9	6.0	1.0	40.0
	10	6.0	0.5	40.0
Group III	11	9.0	2.0	40.0
	12	8.0	2.0	40.0
	13	6.0	2.0	40.0
	14	5.0	2.0	40.0
	15	4.0	2.0	40.0

The relative difference in calculation speed between the two methods was estimated through a ratio of calculation time of the new procedure (T_n) to those of the iterative procedure (T_i) (see Fig. 3). Fig. 3 shows that there is no clear trend in calculation speed among the groups. The relative difference in speed is in a range of 0.22 to 0.57; the average value is about 0.38. This shows that calculation time of the new formula is greatly decreased in comparison with those of the iterative method, reducing the calculation time about 40–80%.

An average relative difference in calculated breaking wave properties between the two methods was estimated through the following formula:

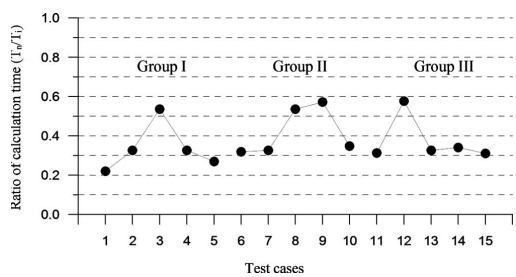

Fig. 3. Comparison of calculation speeds between the new and iterative procedures

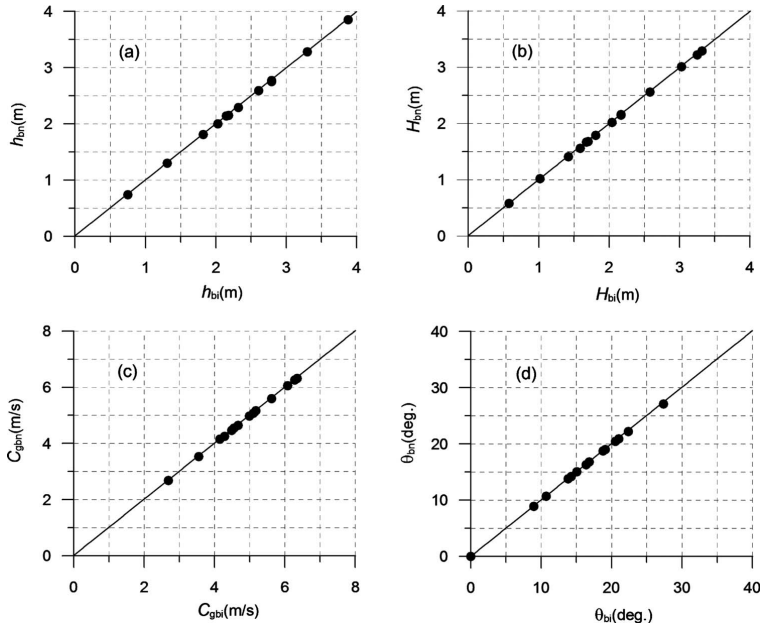

Fig. 4. Comparison of breaking wave parameters calculated by the new formula and those calculated by the iterative method with regard to (a) depth at break point; (b) breaking wave height; (c) breaking wave group velocity; and (d) breaking wave angle. Subscripts "*i*" and "*n*" denote the iterative method and the new formula, respectively.

$$ER(\%) = \frac{1}{K}\sum_{k=1}^{K}\frac{|V_{kn} - V_{ki}|}{V_{ki}} \times 100$$

where K=total number of the tested cases and V_{kn} and V_{ki} =values of each wave property calculated by the new formula and the iterative method, respectively (the subscripts "*n*" and "*i*" denote the new formula and the iterative method, respectively). The average relative difference and maximum absolute difference of h_b, H_b, C_{gb}, and θ_b are correspondingly 0.96, 0.82, 0.46, and 0.43%, and 0.04 m, 0.03 m, 0.04 m/s, and 0.28°, respectively (see Fig. 4). These values show that the differences in calculated breaking wave properties between the two methods are negligible.

Concluding Remarks

The new method involves the following calculation procedure, assuming that the wave input at an arbitrary water depth is known:

- Compute λ_a from Eq. (12) using α obtained from Eq. (10) (input wave conditions employed);
- Correct the computed λ_a by computing $\lambda = \delta\lambda_a$ with δ given by Eq. (15). In many cases, this correction will be small; and
- Compute the depth at breaking (and wave height) from the definition of $\lambda = gh_b/C_m^2$ and the angle at breaking from θ_b =$\arcsin(\sin\theta_m\sqrt{\lambda})$.

The calculation time of the new formula is significantly decreased, about 40–80%, in comparison with those of the iterative method. Relative differences in calculated results between the two methods are negligible, about 0.4–1.0%. Therefore, the new formula is recommended to be used instead of the iterative method to calculate properties at incipient wave breaking in coastal evolution models.

Acknowledgments

This work was partly funded by the Coastal Morphology Modeling and Management (Cascade) work unit, System-Wide Water Resources Program, U.S. Army Corps of Engineers (ML and HH), and partly by Sida/SAREC in the framework of the Project VS/RDE/03, "The evolution and sustainable management in the coastal areas of Vietnam" (LXH).

References

Hanson, H. (1989). "GENESIS—A generalized shoreline change numerical model." *J. Coastal Res.*, 5(1), 1–27.

Hanson, H., and Kraus, N. C. (1989). "GENESIS: Generalized model for simulating shoreline change." *Rep. No. 1*, Coastal Engineering Research Center, U.S. Army Corps of Engineers, Vicksburg, Miss.

Kraus, N. C., and Harikai, S. (1983). "Numerical model of the shoreline change at Oarai Beach." *Coastal Eng.*, 7(1), 1–28.

Larson, M., Kraus, N. C., and Hanson, H. (2002). "Simulation of regional longshore sediment transport and coastal evolution—The Cascade model." *Proc., 28th Coastal Engineering Conf.*, ASCE, Reston, Va., 2612–2624.

Walton, T. L., Birkemeier, W. A., and Weggel, J. R. (1982). "Hand-held calculator algorithms for coastal engineering." *Rep. No. 82-1*, Coastal Engineering Research Center, U.S. Army Corps of Engineers, Fort Belvoir, Va.

Appendix

V

Nam, T.P., Larson, M., Hanson, H., and Hoan, L.X. (2009). A numerical model of nearshore waves, currents and sediment transport. *Coastal Engineering* 56(2009), 1084-1096.

Coastal Engineering 56 (2009) 1084–1096

Contents lists available at ScienceDirect

Coastal Engineering

journal homepage: www.elsevier.com/locate/coastaleng

A numerical model of nearshore waves, currents, and sediment transport

Pham Thanh Nam [a,b,*], Magnus Larson [a], Hans Hanson [a], Le Xuan Hoan [a,b]

[a] Department of Water Resources Engineering, Lund University, Box 118, S-22100, Lund, Sweden
[b] Center for Marine Environment, Research and Consultation, Institute of Mechanics, Vietnamese Academy of Science and Technology, 264 Doi Can, Hanoi, Vietnam

ARTICLE INFO

Article history:
Received 29 August 2008
Received in revised form 9 April 2009
Accepted 15 June 2009
Available online 27 August 2009

Keywords:
Mathematical modeling
Random wave
Nearshore current
Swash zone
Sediment transport
Surface roller

ABSTRACT

A two-dimensional numerical model of nearshore waves, currents, and sediment transport was developed. The multi-directional random wave transformation model formulated by Mase [Mase, H., 2001. Multi-directional random wave transformation model based on energy balance equation. Coastal Engineering Journal 43(4), 317-337.] based on an energy balance equation was employed with an improved description of the energy dissipation due to breaking. In order to describe surface roller effects on the momentum transport, an energy balance equation for the roller was included following Dally and Brown [Dally, W.R., Brown, C.A., 1995. A modeling investigation of the breaking wave roller with application to cross-shore currents. Journal of Geophysical Research 100(C12), 24873-24883.]. Nearshore currents and mean water elevation were modeled using the continuity equation together with the depth-averaged momentum equations. Sediment transport rates in the offshore and surf zone were computed using the sediment transport formulation proposed by Camenen and Larson [Camenen, B., Larson, M., 2005. A general formula for non-cohesive bed load sediment transport. Estuarine, Coastal and Shelf Science 63, 249-260.; Camenen, B., Larson, M., 2007. A unified sediment transport formulation for coastal inlet application. Technical report ERDC/CHL CR-07-1, US Army Engineer Research and Development Center, Vicksburg, MS.; Camenen, B., Larson, M., 2008. A general formula for non-cohesive suspended sediment transport. Journal of Coastal Research 24(3), 615-627.] together with the advection–diffusion equation, whereas the swash zone transport rate was obtained from the formulas derived by Larson and Wamsley [Larson, M., Wamsley, T.V., 2007. A formula for longshore sediment transport in the swash. Proceedings Coastal Sediments '07, ASCE, New Orleans, pp. 1924–1937.]. Three high-quality data sets from the LSTF experimental facility at the Coastal and Hydraulics Laboratory in Vicksburg, USA, were used to evaluate the predictive capability of the model. Good agreement between computations and measurements was obtained with regard to the cross-shore variation in waves, currents, mean water elevation, and sediment transport in the nearshore and swash zone. The present model will form the basis for predicting morphological evolution in the nearshore due to waves and currents with special focus on coastal structures.

1. Introduction

Accurate predictions of waves, nearshore currents, and sediment transport play a key role in solving coastal engineering problems, especially those related to beach morphological evolution. Waves and currents mobilize and transport sediment, and gradients in the transport cause deposition or erosion of sediment, affecting the local topography. Gradients in transport rate may occur naturally or be induced by man-made structures and activities such as groins, seawalls, detached breakwaters, dredging, and beach nourishment. In order to predict the beach morphological evolution for the purpose of engineering analysis and design, a robust model of nearshore waves, currents, and sediment transport is required.

There have been a number of studies on numerical modeling of nearshore waves, currents, and sediment transport (a brief review of relevant previous work is described in the next section). However, hydrodynamic and sediment transport processes are highly complex in the nearshore and swash zone, and presently there is no general model that yields robust and reliable predictions to be used in engineering studies for a wide range of conditions. Furthermore, the lack of high-quality and synchronized experimental data makes model validation difficult.

The overall objective of this study was to develop a robust and reliable numerical model of nearshore waves, currents, and sediment transport which can be applied in coastal engineering projects. First, the present paper discusses modifications of a multi-directional random wave transformation model (EBED), which was originally developed by Mase (2001), to improve the predictive capability of wave properties in the surf zone. Then, a model for nearshore currents due to random waves in the nearshore zone is developed. In order to make this model applicable for a

* Corresponding author. Department of Water Resources Engineering, Lund University, Box 118, S-22100, Lund, Sweden.
E-mail address: Thanh_Nam.Pham@tvrl.lth.se (P.T. Nam).

0378-3839/$ – see front matter © 2009 Elsevier B.V. All rights reserved.
doi:10.1016/j.coastaleng.2009.06.007

variety of conditions including complex alongshore bathymetry, a general depth-averaged two-dimensional model of the nearshore currents due to breaking waves and tides was formulated, although in this paper the focus is on the wave-induced currents. The two-dimensional creation and evolution of the surface roller in connection with wave breaking is modeled based on a period-averaged energy balance, as proposed by Dally and Osiecki (1994), Dally and Brown (1995), and Larson and Kraus (2002). Finally, a model to calculate the sediment transport in the nearshore zone, including the surf and swash zones, is developed based on the transport formulation by Camenen and Larson (2005, 2007, 2008), Larson and Wamsley (2007), and the advection–diffusion equation. The present model will subsequently form the basis for calculating beach topography change due to waves and currents.

The paper is structured as follows: Section 2 provides a brief review of previous work relevant to the present model development. In Section 3 the model description is given, including the four sub-models: (1) the wave model; (2) the surface roller model; (3) the nearshore wave-induced current model; and (4) the sediment transport model. Section 4 briefly describes the data sets employed from the Large-Scale Sediment Transport Facility (LSTF) basin of the Coastal and Hydraulics Laboratory (CHL), U.S. Army Engineer Research and Development Center (ERDC), in Vicksburg, United States. Section 5 summarizes the results of detailed model comparison with these data sets. Section 6 encompasses a discussion on various modeling results pertaining to the wave energy dissipation, surface roller and lateral mixing effects, bottom roughness height, suspended transport obtained by advection–diffusion equation, and sediment transport in swash zone. Finally, the conclusions are given in Section 7.

2. Review of relevant previous work

Waves in coastal areas display random characteristics; thus, random wave models are needed to properly assess the wave environment. Random wave transformation models can be classified into (i) phase-resolving models, and (ii) phase-averaging models. The first type of model, for example the ones based on the Boussinesq equations, is expressed through the conservation equations of mass and momentum (Madsen and Warren, 1984, Madsen et al., 1991, 1997; Nwogu, 1993). These models describe the main physical processes in the coastal area (e.g., shoaling, diffraction, refraction, and dissipation) at the intra-wave scale. Thus, they require fine resolution in space and time and, therefore, their applications are often only suitable for small coastal areas and short-term simulations. On the other hand, phase-averaging models, commonly based on the energy balance equation, describe slowly varying wave quantities (for example, wave amplitude and wave energy) on the scale of a wavelength. Thus, they can be applied for the prediction of multi-directional random wave transformation over large coastal areas. Originally, the non-stationary wave models WAM (WAMDI group, 1988) and SWAN (Booij et al., 1996) were based on phase-averaged equations including source terms. However, diffraction was not included in these models. Then, several attempts have been made in order to include diffraction effects in the phase-averaging wave model. For example, diffraction effects were included into the characteristic velocities through the wave number containing the second derivative of wave amplitude with respect to the spatial coordinates (Booij et al., 1997; Rivero et al., 1997; Holthuijsen et al., 2003). Although these models can be applied in the coastal zone containing structures, the numerical schemes seem to be unstable, especially for the discontinuities and singularities occurring (see Holthuijsen et al., 2003).

Mase (2001) developed a random wave transformation model called EBED in which diffraction effect was included. The diffraction term was derived from a parabolic approximation of the wave equation. The numerical scheme is stable and the model can be applied for complex coastal areas with structures. In the present study, the EBED model was employed to calculate wave transformation after modifications to more accurately predict the wave conditions in the surf zone. Although, structures were not included in the investigated data of this study, the long-term objective is to model the hydrodynamics and morphological evolution in the vicinity of structures. Therefore, it is necessary to employ a wave model that includes diffraction.

There have been a number of numerical models for wave-driven currents after the concept of radiation stress was introduced by Longuet-Higgins and Stewart (1964). Early simulations of longshore current induced by regular waves, for a simple plan form beach, were carried out by Bowen (1969), Longuet-Higgins (1970), and Thornton (1970). The disadvantage of these semi-analytic models is the occurrence of an abrupt change in longshore current at the break point. By introducing an eddy viscosity term (i.e., lateral mixing) in the momentum equation for the longshore current, the physically unrealistic current distribution at the breaker-line was eliminated. Since the early models, significant progress has been made concerning nearshore currents generated by random waves. The pioneering work of Battjes (1972) illustrated that the longshore current generated by random waves is smooth in the surf zone, even though the lateral mixing term is not included. Thornton and Guza (1986) presented a model for the longshore current based on their random wave breaking model (Thornton and Guza, 1983). Van Dongeren et al. (1994, 2003), and Van Dongeren and Svendsen (2000) developed a quasi-3D nearshore hydrodynamic model named SHORECIRC, which is capable of describing several phenomena such as the edge waves, surf beats, infragravity waves, and longshore current. Kraus and Larson (1991), Larson and Kraus (2002) developed the NMLong model for computing the longshore current focusing on barred beaches. Militello et al. (2004) developed the M2D model for simulating the nearshore current due to tide, waves, wind, and rivers. Recently, Goda (2006) examined the influence of several factors on the longshore current under random waves. He demonstrated that significant differences in wave height and longshore velocity resulted depending on the employed random wave breaking model. Thus, selecting a wave model that can accurately simulate surf-zone conditions is important when computing wave-induced nearshore currents.

Much research has demonstrated that the surface roller plays an important role in generating nearshore currents. The roller was initially investigated in the laboratory by Duncan (1981) and first applied theoretically by Svendsen (1984a,b) to improve the modeling of wave setup and undertow in the surf zone. Then, the roller model, including the roller energy gradients in the energy flux balance based on the roller theory of Svendsen (1984a,b), was employed in many studies related to wave-induced currents (e.g. Nairn et al., 1990; Deigaard et al., 1991; Stive and De Vriend, 1994; Lippmann et al., 1996; Reniers and Battjes, 1997; Ruessink et al., 2001). Van Dongeren et al. (2003) extended the roller energy flux balance equation derived by Nairn et al. (1990), and they obtained calculations of longshore current that were in good agreement with the data from the DELILAH field experiment. Based on the depth-integrated and period-averaged energy balance equation, Dally and Osiecki (1994), and Dally and Brown (1995) developed a roller model for the evolution of the roller itself. Larson and Kraus (2002) applied this model in NMLong to improve longshore current simulations. In the energy balance equation, the energy dissipation per unit area after Dally et al. (1985) was used instead of the gradient in the depth-integrated time-averaged wave-induced energy flux in the x-direction. In general, the roller energy flux is only considered in the cross-shore direction in the balance equation. In the present study, the approaches by Dally and Brown (1995) and Larson and Kraus (2002) were followed, and the energy flux term in alongshore direction was included in the energy balance equation for the evolution of the roller itself.

Calculating sediment transport in the nearshore zone is a challenge because of the complexity of the hydrodynamics and the variety of governing phenomena. There are a number of nearshore sediment transport formulas that have been developed through the years for different types of applications in coastal engineering. For example, several formulas were examined and evaluated by Bayram et al. (2001), and Camenen and Larroude (2003). However, these formulas

have typically described a specific set of physical processes and been validated with limited data. Recently, Camenen and Larson (2005, 2007, 2008) developed a unified sediment transport formulation, which has been validated for a large set data on longshore and cross-shore sediment transport from the laboratory and field. Performance of the new sediment transport formulation was compared to several popular existing formulas, and the new formulation yielded the overall best predictions among investigated formulations, and therefore, it was employed in this study.

The mechanics of sediment transport in the swash zone have received less attention than the surf zone. However, the swash zone is important for the sediment exchange between land and sea, which in turn affects both the sub-aerial and sub-aqueous evolution of the beach. The limited number of studies, as well as lack of measurement data on net transport in the swash, has made it difficult to formulate mathematical models based on a detailed understanding of the governing physics. In spite of these difficulties, significant progress has been made in the last decade concerning the hydrodynamics and sediment transport conditions in the swash zone (see Elfrink and Baldock, 2002; Larson et al., 2004; Larson and Wamsley, 2007). In this study, the formulas of hydrodynamics and sediment transport rates in swash zone of Larson and Wamsley (2007) were employed. The obtained sediment transport rate at the still-water shoreline was used as boundary condition for computing the suspended load in the inner surf zone, which was derived from the advection–diffusion equation.

3. Model description

3.1. Wave model

3.1.1. The random wave model EBED

Mase (2001) developed a multi-directional random wave transformation model based on the energy balance equation with energy dissipation and diffraction terms (EBED). The governing equation, for steady state, is expressed as follows,

$$\frac{\partial(v_x S)}{\partial x}+\frac{\partial(v_y S)}{\partial y}+\frac{\partial(v_\theta S)}{\partial \theta}=\frac{\kappa}{2\omega}\left\{(CC_g\cos^2\theta S_y)_y-\frac{1}{2}CC_g\cos^2\theta S_{yy}\right\}-\varepsilon_b S \tag{1}$$

where S is the angular-frequency spectrum density, (x, y) are the horizontal coordinates, θ is the angle measured counterclockwise from the x axis, ω is the frequency, C is the phase speed, and C_g the group speed, (v_x,v_y,v_θ) are the propagation velocities given by,

$$(v_x, v_y, v_\theta)=\left(C_g\cos\theta, C_g\sin\theta, \frac{C_g}{C}\left(\sin\theta\frac{\partial C}{\partial x}-\cos\theta\frac{\partial C}{\partial y}\right)\right) \tag{2}$$

The first term on the right-hand side is added in the balance equation in order to represent the diffraction effects, and κ is a free parameter that can be optimized to change the influence of the diffraction effects. The second term represents the wave energy dissipation due to wave breaking, and ε_b is the energy dissipation coefficient. The output from the wave transformation model includes three main wave parameters: significant wave height H_s, significant wave period T_s, and mean wave direction $\bar{\theta}$.

3.1.2. The modified-EBED model

The original EBED model is stable and can be applied to the complex beach topography of coastal zones containing structures. However, the obtained output from the model often overestimates the wave parameters in the surf zone compared to measurements. The overestimation is due mainly to the algorithm describing wave energy dissipation caused by wave breaking. In the EBED model, the energy dissipation coefficient was determined by the Takayama et al. (1991) model. The calculation of this coefficient is rather complex and the coefficient does not easily lend itself to calibration.

In this study, a new approach for calculating the energy dissipation term, which was based on the Dally et al. (1985) model, was employed for improving the predictive capability of the wave model. The model is referred to as the Modified-EBED model in this paper hereafter. Thus, a modified energy balance equation is proposed as follows,

$$\frac{\partial(v_x S)}{\partial x}+\frac{\partial(v_y S)}{\partial y}+\frac{\partial(v_\theta S)}{\partial \theta}=\frac{\kappa}{2\omega}\left\{(CC_g\cos^2\theta S_y)_y-\frac{1}{2}CC_g\cos^2\theta S_{yy}\right\}-\frac{K}{h}C_g(S-S_{stab}) \tag{3}$$

where h is the still-water depth, K is dimensionless decay coefficient, S_{stab} is the stable wave spectrum density, which is determined based upon the stable wave height H_{stab} ($=\Gamma h$), with Γ being a dimensionless empirical coefficient.

Assuming that the spectrum density S and the stable spectrum density S_{stab} are functions of H_s^2 and H_{stab}^2, respectively, the dissipation term in Eq. (3) can be rewritten as,

$$D_{diss}=\frac{K}{h}C_g S\left[1-\left(\frac{\Gamma h}{H_s}\right)^2\right]. \tag{4}$$

In the Dally et al. (1985) model, the recommended values for Γ and K were 0.4 and 0.15, respectively. Goda (2006) used his formula in 1975 for determining the decay coefficient, $K=3(0.3+2.4\,s)/8$, where s is the bottom slope. In the Modified-EBED model, in order to obtain a good description of wave conditions in the surf zone for the LSTF data, the coefficients were modified according to:

$$\begin{cases}\Gamma=0.45, K=\dfrac{3}{8}(0.3-19.2s) & : s<0\\ \Gamma=0.45+1.5s, K=\dfrac{3}{8}(0.3-0.5s) & : s\geq 0\end{cases}. \tag{5}$$

The wave radiation-driven stresses were determined by the output from the wave model,

$$S_{xx}=\frac{E}{2}[2n(1+\cos^2\bar{\theta})-1] \tag{6}$$

$$S_{yy}=\frac{E}{2}[2n(1+\sin^2\bar{\theta})-1] \tag{7}$$

$$S_{xy}=S_{yx}=\frac{E}{2}n\sin 2\bar{\theta} \tag{8}$$

where $E=\rho g H_{rms}^2/8$ is the wave energy per unit area, and $n=C_g/C$ is the wave index.

3.2. Surface roller model

The wave energy balance equation for the surface roller in two dimensions is expressed as (Dally and Brown, 1995; Larson and Kraus, 2002),

$$P_D+\frac{\partial}{\partial x}\left(\frac{1}{2}MC_r^2\cos^2\bar{\theta}\right)+\frac{\partial}{\partial y}\left(\frac{1}{2}MC_r^2\sin^2\bar{\theta}\right)=g\beta_D M \tag{9}$$

where P_D is the wave energy dissipation ($=KC_g\rho g(H_{rms}^2-(\Gamma h))^2)/(8h)$), M is the wave-period-averaged mass flux, C_r is the roller speed ($\approx$C), and β_D is the roller dissipation coefficient.

The stresses due to the rollers are determined as follows:

$$R_{xx}=MC_r\cos^2\bar{\theta} \tag{10}$$

$$R_{yy} = MC_r \sin^2\bar{\theta} \tag{11}$$

$$R_{xy} = R_{yx} = MC_r \sin 2\bar{\theta}. \tag{12}$$

3.3. Nearshore current model

The governing equations for the nearshore currents are written as (Militello et al., 2004),

$$\frac{\partial(h+\eta)}{\partial t} + \frac{\partial q_x}{\partial x} + \frac{\partial q_y}{\partial y} = 0 \tag{13}$$

$$\frac{\partial q_x}{\partial t} + \frac{\partial u q_x}{\partial x} + \frac{\partial v q_x}{\partial y} + g(h+\eta)\frac{\partial \eta}{\partial x} = \frac{\partial}{\partial x}D_x\frac{\partial q_x}{\partial x} + \frac{\partial}{\partial y}D_y\frac{\partial q_x}{\partial y} + fq_y - \tau_{bx} + \tau_{Sx} \tag{14}$$

$$\frac{\partial q_y}{\partial t} + \frac{\partial u q_y}{\partial x} + \frac{\partial v q_y}{\partial y} + g(h+\eta)\frac{\partial \eta}{\partial y} = \frac{\partial}{\partial x}D_x\frac{\partial q_y}{\partial x} + \frac{\partial}{\partial y}D_y\frac{\partial q_y}{\partial y} - fq_x - \tau_{by} + \tau_{Sy} \tag{15}$$

where η is the water elevation, q_x,q_y is the flow per unit width parallel to the x and y axis, respectively, u,v is the depth-averaged velocity in x and y direction, respectively, g is the acceleration due to gravity, D_x,D_y are the eddy viscosity coefficients, f is the Coriolis parameter, τ_{bx},τ_{by} are the bottom stresses, and τ_{Sx},τ_{Sy} are the wave stresses (the latter variables are all in the x and y directions, respectively).

The depth-averaged horizontal eddy viscosity coefficient can be calculated as a function of the total water depth, current speed, and bottom roughness according to Falconer (1980),

$$D_0 = 1.154 g(h+\eta)\frac{|U|}{C_z^2} \tag{16}$$

where C_z is the Chezy roughness coefficient.

In the surf zone, the eddy viscosity is simulated as a function of the wave properties,

$$D_1 = \varepsilon_L \tag{17}$$

where ε_L represent the lateral mixing below the trough level. Kraus and Larson (1991) expressed this term as,

$$\varepsilon_L = \Lambda u_m H_{rms} \tag{18}$$

in which H_{rms} is the root-mean-square wave height, Λ is an empirical coefficient, and u_m is the wave orbital velocity at the bottom.

In the transition zone, the eddy viscosity is calculated as,

$$D_2 = (1-\alpha)D_0 + \alpha D_1 \tag{19}$$

where α is weighting parameter $(=(H_{rms}/(h+\eta))^3$, see Militello et al., 2004).

The bottom stresses under combined current and waves are determined from Nishimura (1988),

$$\tau_{bx} = C_b\left[\left(U_{wc} + \frac{\omega_b^2}{U_{wc}}\cos^2\bar{\theta}\right)u + \left(\frac{\omega_b^2}{U_{wc}}\cos\bar{\theta}\sin\bar{\theta}\right)v\right] \tag{20}$$

$$\tau_{by} = C_b\left[\left(U_{wc} + \frac{\omega_b^2}{U_{wc}}\sin^2\bar{\theta}\right)v + \left(\frac{\omega_b^2}{U_{wc}}\cos\bar{\theta}\sin\bar{\theta}\right)u\right] \tag{21}$$

in which C_b is the bottom friction coefficient, U_{wc}, and ω_b are given by,

$$U_{wc} = \frac{1}{2}\left\{\sqrt{|u^2+v^2+\omega_b^2+2(u\cos\bar{\theta}+v\sin\bar{\theta})\omega_b|} + \sqrt{|u^2+v^2+\omega_b^2-2(u\cos\bar{\theta}+v\sin\bar{\theta})\omega_b|}\right\} \tag{22}$$

$$\omega_b = \frac{\sigma H_{rms}}{\pi\sinh[k(h+\eta)]} \tag{23}$$

where σ is the wave frequency, and k the wave number.

The wave stresses are derived from the wave transformation model and the surface roller model. They are expressed by the following formulas:

$$\tau_{Sx} = -\frac{1}{\rho_w}\left[\frac{\partial}{\partial x}(S_{xx}+R_{xx}) + \frac{\partial}{\partial y}(S_{xy}+R_{xy})\right] \tag{24}$$

$$\tau_{Sy} = -\frac{1}{\rho_w}\left[\frac{\partial}{\partial x}(S_{xy}+R_{xy}) + \frac{\partial}{\partial y}(S_{yy}+R_{yy})\right]. \tag{25}$$

3.4. Sediment transport

3.4.1. Swash zone

Larson and Wamsley (2007) developed the formula for the net transport rates in the cross-shore and longshore direction, respectively, as,

$$q_{bc,net} = K_c\frac{\tan\phi_m}{\tan^2\phi_m-(dh/dx)^2}\frac{u_0^3}{g}\left(\frac{dh}{dx}-\tan\beta_e\right)\frac{t_0}{T} \tag{26}$$

$$q_{bl,net} = K_l\frac{\tan\phi_m}{\tan^2\phi_m-(dh/dx)^2}\frac{u_0^2 v_0}{g}\frac{t_0}{T} \tag{27}$$

where $q_{bc,net}$, $q_{bl,net}$ are the net transport in the cross-shore and longshore direction, respectively, K_c and K_l are empirical coefficients, ϕ_m the friction angle for a moving grain ($\approx$30°), β_e the foreshore equilibrium slope, u_0,v_0 and t_0 the scaling velocities and time, respectively, and T the swash duration (assumed that T is equal to the incident wave period). The swash zone hydrodynamics without friction, which were derived based on the ballistic theory, were employed in the model (for details see Larson and Wamsley, 2007).

3.4.2. Nearshore zone (offshore and surf zone)

Camenen and Larson (2005, 2007, 2008) developed a general transport formulation for bed load and suspended load under combined waves and current. It is referred as the Lund-CIRP formula in this paper hereafter. It can be used for both sinusoidal and asymmetric waves. To simplify calculations, the waves are assumed to be sinusoidal, having no asymmetry. Thus, the contribution to the transporting velocity from waves is negligible, implying that only the current moves the material. In such case, the bed load transport can be expressed as,

$$\frac{q_{bc}}{\sqrt{(s-1)gd_{50}^3}} = a_c\sqrt{\theta_c}\theta_{cw,m}\exp\left(-b_c\frac{\theta_{cr}}{\theta_{cw}}\right) \tag{28}$$

where the transport q_{bc} is obtained in the direction of the current, the transport normal to the current is zero, s is the relative density between sediment and water, d_{50} is the median grain size, a_c and b_c are empirical coefficients, $\theta_{cw,m}$ and θ_{cw} are the mean and maximum Shields parameters due to wave and current interaction, respectively, θ_{cr} is the critical Shields parameter, and θ_c is the Shields parameter due to current.

The suspended load is calculated based on the assumption of an exponential concentration profile and a constant velocity over the water column,

$$q_s = U_c c_R \frac{\varepsilon}{w_s}\left[1-\exp\left(-\frac{w_s d}{\varepsilon}\right)\right] \tag{29}$$

where U_c is current velocity, c_R is the reference concentration at the bottom, w_s is the sediment fall speed, ε is the sediment diffusivity, and d is the total depth ($=h+\eta$).

The bed reference concentration is obtained from,

$$c_R = A_{cR}\theta_{cw,m}\exp\left(-4.5\frac{\theta_{cr}}{\theta_{cw}}\right) \tag{30}$$

where the coefficient A_{cR} is written as,

$$A_{cR} = 3.5\,10^{-3}\exp(-0.3d_*) \tag{31}$$

with $d_* = \sqrt[3]{(s-1)g/\upsilon^2}\,d_{50}$ being the dimensionless grain size and υ is the kinematic viscosity of water.

The sediment fall speed is determined from Soulsby (1997) as:

$$w_s = \frac{\upsilon}{d_{50}}\left[\left(10.36^2 + 1.049d_*^3\right)^{1/2} - 10.36\right]. \tag{32}$$

The sediment diffusivity is related to the energy dissipation as (Battjes, 1975; Camenen and Larson, 2008),

$$\varepsilon = \left(\frac{k_b^3 D_b + k_c^3 D_c + k_w^3 D_w}{\rho}\right)^{1/3} d \tag{33}$$

where the energy dissipation from wave breaking (D_b) and from bottom friction due to current (D_c) and waves (D_w) were simply added, and k_b, k_c and k_w are coefficients (see Camenen and Larson, 2008).

Alternatively, the suspended load can be obtained by solving the advection–diffusion equation. The advection–diffusion equation is obtained from the continuity of depth-averaged suspended sediment transport as,

$$\frac{\partial(\overline{C}d)}{\partial t} + \frac{\partial(\overline{C}q_x)}{\partial x} + \frac{\partial(\overline{C}q_y)}{\partial y} = \frac{\partial}{\partial x}\left(K_x d\frac{\partial\overline{C}}{\partial x}\right) + \frac{\partial}{\partial x}\left(K_y d\frac{\partial\overline{C}}{\partial y}\right) + P - D \tag{34}$$

where $\bar{C}$ is the depth-averaged sediment concentration, K_x and K_y are the sediment diffusion coefficient in x and y direction, respectively, P is the sediment pick-up rate, and D is the sediment deposition rate.

The sediment diffusion coefficient can be calculated by Elder (1959) as,

$$K_x = K_y = 5.93u_{*c}d \tag{35}$$

where u_{*c} is shear velocity from the current only.

The sediment pick-up and deposition rates, respectively, are obtained as,

$$P = c_R w_s \tag{36}$$

$$D = \frac{\overline{C}}{\beta_d} w_s \tag{37}$$

where β_d is a coefficient calculated based on Camenen and Larson (2008); see also Militello et al., 2006),

$$\beta_d = \frac{\varepsilon}{w_s d}\left[1-\exp\left(-\frac{w_s d}{\varepsilon}\right)\right]. \tag{38}$$

The suspended transport rates in the x and y directions can be calculated from Eq. (34) as:

$$q_{sx} = \overline{C}q_x - K_x d\frac{\partial\overline{C}}{\partial x} \tag{39}$$

$$q_{sy} = \overline{C}q_y - K_y d\frac{\partial\overline{C}}{\partial y}. \tag{40}$$

The sediment transport rate is often large near the shoreline because of swash uprush and backwash processes. For example, the measurements from LSTF showed a peak in the sediment transport rate close to the shoreline that was larger than in the inner surf zone. The computed sediment transport rates obtained from currently available formulas often tend to decrease too rapidly from the swash zone towards the offshore. Thus, the interaction between the swash zone and the inner part of the surf zone is not well described. Therefore, the calculations of sediment transport may not agree with measurements in this region, unless some modifications are introduced.

In the present study, we use the sediment transport at the still-water shoreline obtained from swash zone computations as the boundary value for computing suspended load in the surf zone using the advection–diffusion equation. Furthermore, the pick-up and deposition rates described in the Eqs. (36) and (37), respectively, were also modified as follows,

$$\tilde{P} = P\left[1 + \vartheta\frac{\overline{V}}{V_0}\exp\left(-\mu\frac{d}{R}\right)\right] \tag{41}$$

$$\tilde{D} = \frac{D}{\left[1 + \vartheta\frac{\overline{V}}{v_0}\exp(-\mu\frac{d}{R})\right]} \tag{42}$$

where ϑ and μ are free non-negative coefficients, $\overline{V}$ is the mean velocity across the profile, R is the runup height. The velocity $\overline{V}$ is determined as the average longshore current across the surf zone, v_0 is obtained from swash zone computation, and R is calculated by the Hunt (1959) formula.

The total load, given by the bed load from the Lund-CIRP formula and the suspended load calculated by the advection–diffusion equation with the above modifications, is referred to as AD-Lund-CIRP hereafter. The above modifications increase the suspended sediment load near the shoreline. The empirical parameter values introduced are related to the magnitude of longshore current, scaling velocity, water depth, and runup height. Although the modifications are somewhat ad hoc, the model produces more reasonable computed sediment fluxes in agreement with the investigated measured data.

4. Large-Scale Sediment Transport Facility (LSTF) data

Five series of movable bed physical model experiments were carried out in the LSTF basin (see Hamilton and Ebersole, 2001; Wang et al., 2002) at the Coastal and Hydraulics Laboratory of the U.S. Army Engineer Research and Development Center in Vicksburg, Mississippi by Gravens and Wang (2007), and Gravens et al. (2006). The first series of experiments, referred to as "Base Cases", including four runs of approximately 160 min each on a natural beach (without structure), were aimed at generating high-quality data sets for testing and validation of sand transport formulas due to waves and currents. The

Table 1.
Measurement locations for LSTF Base Cases.

Measured locations	ADV1	ADV2	ADV3	ADV4	ADV5	ADV6	ADV7	ADV8	ADV9	ADV10
Distance to shoreline (m)	1.125	2.725	4.125	5.73	7.125	8.525	10.125	11.625	13.125	15.625

four remaining series of experiments were designed to generate data sets for testing and validation of the development of tombolos in the lee of nearshore detached breakwaters and T-head groins. Spilling breaking waves were generated by four wave generators. The beach consisted of very well-sorted fine quartz sand with a median grain size of 0.15 mm. The longshore current generated by the obliquely incident waves was circulated with twenty turbine pumps through twenty flow channels at the updrift and downdrift ends of the basin.

In this study, the Base Cases were used for validation of the model. In Base Case 1 (BC-1) the longshore current was induced by random waves and circulated by the turbine pumps. Base Case 2 (BC-2) encompassed the wave-induced current and an external longshore current which was generated by recirculating two times the wave-generated longshore flux of water. In Base Case 3 (BC-3) the wave generators were not operated so it was not used for testing the numerical model. Similar to BC-2, the external longshore current was also imposed across the model beach in Base Case 4 (BC-4) by recirculating 1.5 times the wave-generated longshore flux of water. The wave height, wave period, and wave setup were measured by thirteen capacitance gauges. However, the wave sensor at ADV10 did not work so the measured data on wave conditions at this location was not available. The data on nearshore current were collected and measured by ten Acoustic Doppler Velocimeters (ADVs). Ten wave and current sensors were collocated at ten cross-shore locations and synchronized in time for each of the eleven cross-shore sections. These locations are presented in Table 1. The remaining wave sensors, Gauge#11, Gauge#12 and Gauge#13, were located at three alongshore positions, 18.43 m seaward from the still-water shoreline, to measure wave conditions outside the toe of the movable beach (see Fig. 1). Twenty-one gravity-feed sediment traps located at the downdrift end of the movable bed model beach, in which two traps were located in the swash zone, were used to measure the magnitude and cross-shore distribution of sand transport. Beach profiles at the interval between 0.25 and 4 m were measured by rod and acoustic survey techniques after each model run.

5. Model simulation results

The computational grid for the LSTF beach was generated based on interpolation of measured beach profile data from profile Y34 to profile Y14 (see Fig. 1). The grid size was 0.2×0.2 m, and the measurements at Gauge#11, Gauge#12, and Gauge#13 were used as offshore wave conditions. The detailed information of the wave conditions at these points for cases BC-1, BC-2, and BC-4 are presented in Table 2. A TMA spectrum was assumed at the offshore boundary with the parameter values $\gamma = 3.3$, $\sigma_a = 0.07$, $\sigma_b = 0.09$, and $S_{max} = 25$. Values for the decay and stable coefficients were determined from Eq. (5). Because the beach topography of the Base Cases is fairly uniform in the alongshore direction, the variation in alongshore significant wave height and longshore current was relative small. Therefore, the comparisons between calculation and measurement in this paper were only made at the profile Y24 (center profile).

Fig. 2 shows the comparison between calculated and measured significant wave height for case BC-1. The dashed line is the calculated significant wave height obtained by the original EBED model, which overestimated the wave height in the surf zone compared to the measured data. By employing the new method for calculating wave energy dissipation due to breaking, the Modified-EBED model produced improved results. The calculated significant wave height agreed well with the measured data at all measurement locations. The root-mean-square (rms) error of the significant wave height obtained by Modified-EBED model was only 3.6%, whereas it was 13.0% for the EBED model.

The output from the Modified-EBED model, such as significant wave height, wave direction, and wave period, as well as wave-driven stresses, were employed to calculate the nearshore currents. The

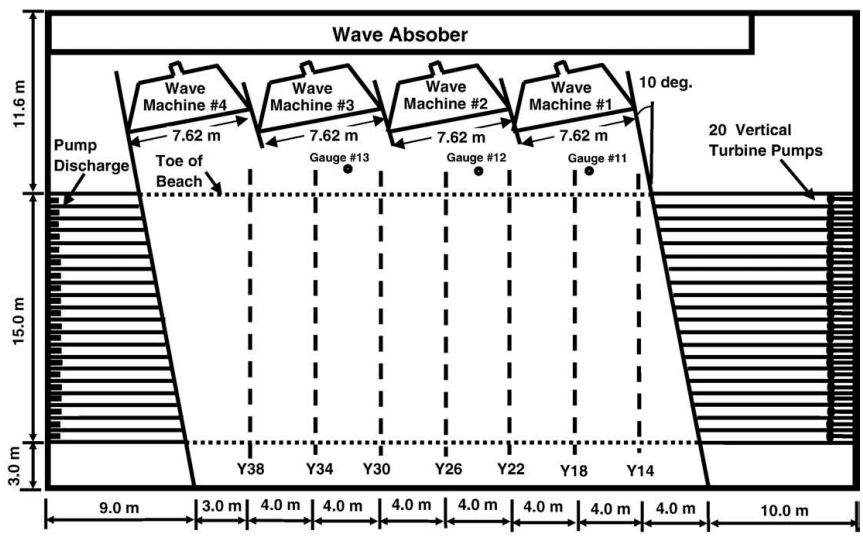

Fig. 1. Configuration of LSTF basin (Gravens and Wang, 2007).

Table 2
Offshore wave conditions for LSTF Base Cases.

Data sets	Gauges	H_{mo} (m)	T_p (s)	Θ (°)
BC-1	#11	0.220	1.444	6.5
	#12	0.225	1.468	6.5
	#13	0.228	1.465	6.5
BC-2	#11	0.213	1.439	6.5
	#12	0.226	1.469	6.5
	#13	0.228	1.460	6.5
BC-4	#11	0.216	1.447	6.5
	#12	0.221	1.472	6.5
	#13	0.222	1.460	6.5

Chezy coefficient was specified to be 40, the coefficient for lateral mixing $\Lambda = 0.5$, the roller dissipation coefficient $\beta_D = 0.1$, and the time step 0.02 s. The water fluxes on the upstream boundary were given based on measured data on longshore current at profile Y34. The downstream boundary was treated as an open boundary.

Fig. 3 illustrates the measurement data and computations of the wave-induced longshore current with and without roller. The roller effects did not only cause a shift in the longshore current towards the shoreline but also increased the maximum current in the surf zone. Although there were differences between measured and calculated longshore current with the roller at ADV3 and ADV4, the tendency after including the roller is to improve the agreement with measured data in the surf zone. The rms errors of the calculated longshore current with and without roller were 27.2% and 29.8%, respectively.

The comparison of calculated and measured wave setup is presented in Fig. 4. Both calculations of wave setup with and without roller agree well with the measurements. The setup without roller yielded slightly better agreement with the measurements compared to the setup with roller. Although the rms error of wave setup with roller (32.5%) was higher than without roller (24.3%), the difference between the computations was relatively small.

In order to calculate the scaling velocities, the runup height and wave angle prior to runup are needed. The runup height was determined by the Hunt (1959) formula. The wave angle prior to runup was given by the wave angle at the cell next to the shoreline from the Modified-EBED model output. The foreshore equilibrium slope was determined based on the observed topographical data. The values of K_c and K_I were both set to 0.0008, following Larson and Wamsley (2007).

The computed longshore sediment flux in the swash zone is presented by the dashed line in Fig. 5. There were only two measurement points in the swash zone, but the calculated longshore sediment flux is in good agreement with the measured data.

The output from the Modified-EBED model and the nearshore wave-induced currents with roller were used to determine the Shields parameters due to waves and currents. The kinematic viscosity of water υ was set to 1.36×10^{-6} m^2/s, and the density of water and sediment was given as 1000 kg/m^3 and 2650 kg/m^3, respectively. The critical Shields parameter was determined by the Soulsby and Whitehouse formula (see Soulsby, 1997). The coefficient values in the bedload transport formula a_c and b_c were given as 12 and 4.5, respectively (see Camenen and Larson, 2005). In the suspended load formula, a value of $k_b = 0.017$ was employed and k_c and k_w were calculated based on the Schmidt number (see Camenen and Larson, 2008). The coefficient values $\vartheta = 9.3$ and $\mu = 2.4$ were employed for calculating the pick-up and deposition rates. In addition, the total load formula of Watanabe (1987) with a transport coefficient equal to 1.0 was employed to compare with the Lund-CIRP and AD-Lund-CIRP.

The computations of the longshore sediment flux in the nearshore are presented in Fig. 5. There was only a slight difference in the longshore sediment flux between the Lund-CIRP and Watanabe formulas, and these calculations agree fairly well with the measured data in the offshore and outer surf zone. However, there is a significant difference between measurements and computations near the shoreline for these two formulas. Using AD-Lund-CIRP overcomes this discrepancy. Based on the calculations of longshore sediment flux in the swash zone and the modifications of pick-up and deposition rates in the advection–diffusion equation, the computed longshore sediment flux in the inner part of the surf zone also agrees with the measurements. The rms error of longshore sediment flux obtained by AD-Lund-CIRP for both swash zone and nearshore zone was 33.2%, better than those by Lund-CIRP (49.1%) and by Watanabe (49.6%).

The computations of waves, nearshore current, and sediment transport for BC-2 and BC-4 were carried out in the same manner as for BC-1. The coefficient values used for BC-1 were kept the same in the simulations for BC-2 and BC-4.

The significant wave height, longshore current, wave setup, and longshore sediment flux for BC-2 were presented in Figs. 6–9, respectively. As for BC-1, the wave predictions by the Modified-EBED model were better than those by the EBED model agreeing well with the measured data. The longshore current and wave setup were also well predicted (including roller effects). Although the overall shape of cross-shore distribution of the longshore current was in good agreement with the data, the magnitude of the current at ADV3 and ADV4 was overestimated. Sediment transport rate in the swash zone agreed well with the measured data. The difference between longshore sediment flux obtained by Lund-CIRP and Watanabe was more pronounced in the surf zone than for BC-1, especially between 0.2 m and 5.6 m seaward of the still-water shoreline. However, computations

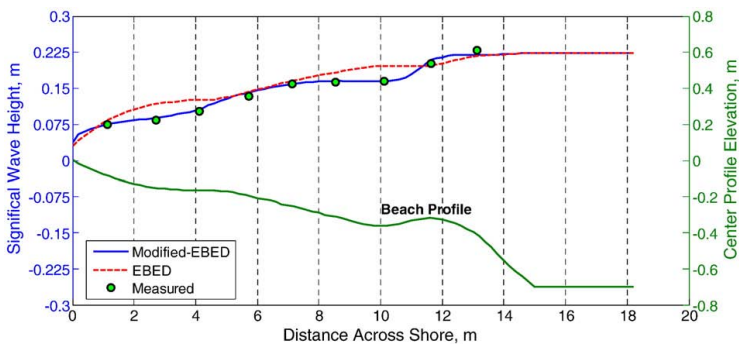

Fig. 2. Computed and measured significant wave height for LSTF BC-1.

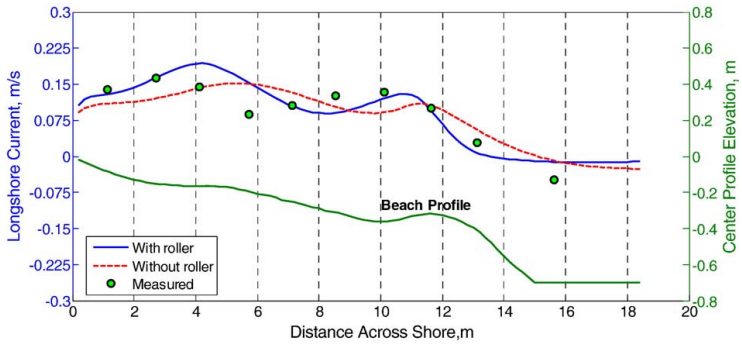

Fig. 3. Computed and measured longshore current for LSTF BC-1.

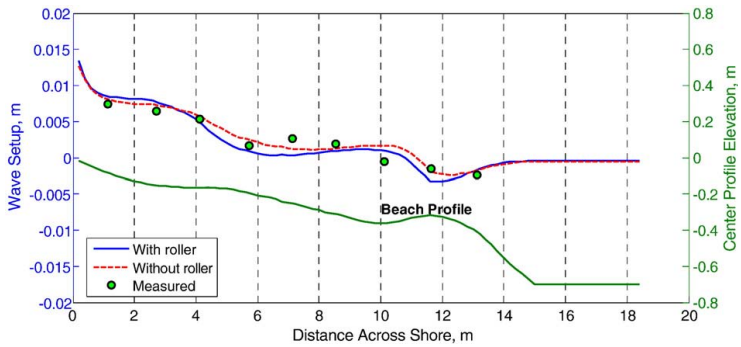

Fig. 4. Computed and measured wave setup for LSTF BC-1.

with both Lund-CIRP and Watanabe showed the same tendency of decreasing sediment flux towards the shoreline as for BC-1. Calculation with AD-Lund-CIRP, including the swash zone computation, produced reasonable sediment fluxes from the swash zone to the offshore.

Computational results and comparison with measurements for BC-4 regarding significant wave height, longshore current, wave setup, and longshore sediment flux were presented in Figs. 10–13, respectively. The significant wave height obtained by Modified-EBED agreed well with the measured data, except at ADV3 and ADV4, and the nearshore current model produced satisfactory predictions of the longshore current. However, in this run, the measured wave setup at ADV1, ADV2, ADV3, and ADV4 were too small compared to the calculated results, especially at ADV3 and ADV4 where wave setdown was observed. The mean water elevation should normally increase in the surf zone for a monotonically increasing profile, similar to what was observed in BC-1 and BC-2, so the data may contain some errors at these gauges. From ADV5 to ADV10, the calculated wave setup agrees well with the measured data. The computed longshore sediment fluxes were not as good as for BC-1 and BC-2. It was difficult to obtain good agreement between calculated and measured sediment flux in the inner surf zone near the shoreline, but AD-Lund-CIRP gave the best predictions of the longshore sediment flux compared to the Lund-CIRP and Watanabe formulas.

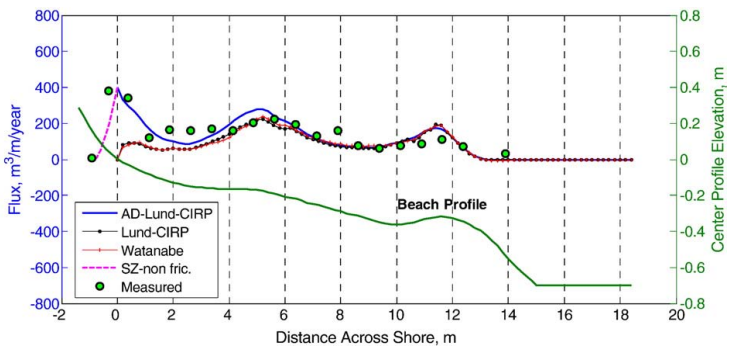

Fig. 5. Computed and measured longshore sediment flux for LSTF BC-1.

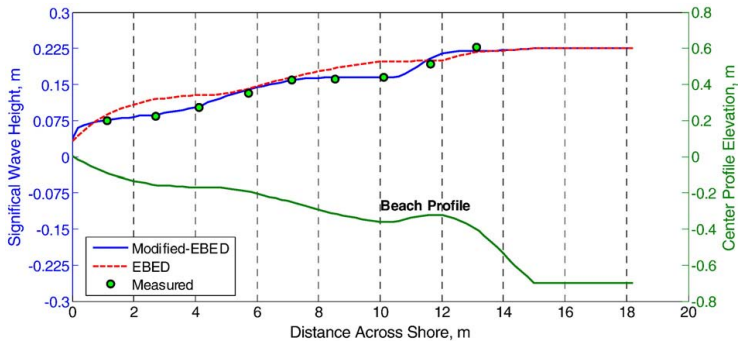

Fig. 6. Computed and measured significant wave height for LSTF BC-2.

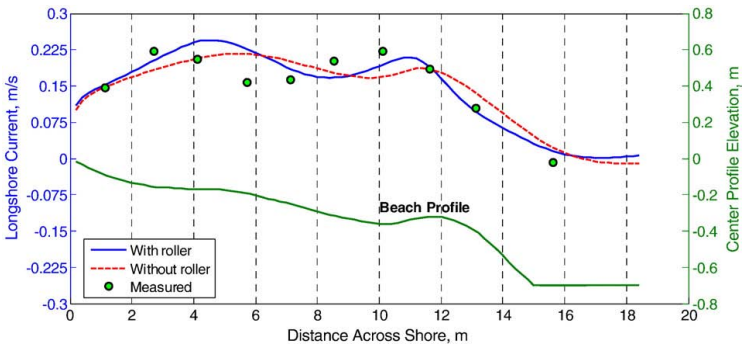

Fig. 7. Computed and measured longshore current for LSTF BC-2.

A quantitative assessment of the predictive capacity of the model was performed based on the rms error. Table 3 summarizes in detail the rms errors between computations and measurements for significant wave height obtained by the Modified-EBED and EBED model, and for the longshore current and wave setup with and without roller. Table 4 presents the quantitative assessment of the longshore sediment transport calculations in both the nearshore and the swash zone. The assessment showed that the developed model can produce reasonable computational results for the investigated data sets.

6. Discussion

In the neashore zone, energy dissipation due to wave breaking is an important process to describe in the wave model. The Takayama approach used in the original EBED model often caused an over-estimation of the wave heights in the surf zone. Thus, the modification of the energy dissipation calculations in the EBED model following Dally et al. (1985) implied a significant improvement in computing waves in the surf zone. However, appropriate values on the decay and stable coefficients should be given. The coefficient values determined

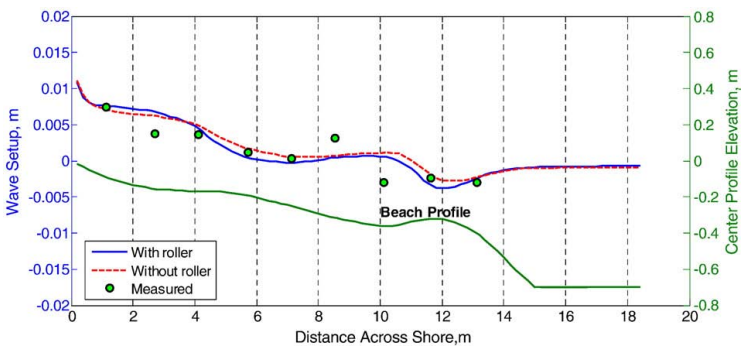

Fig. 8. Computed and measured wave setup for LSTF BC-2.

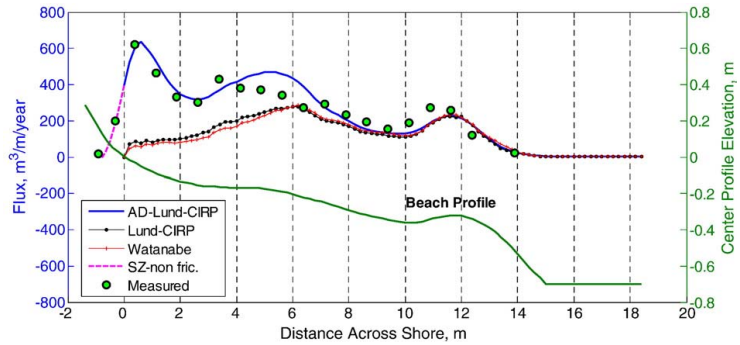

Fig. 9. Computed and measured longshore sediment flux for LSTF BC-2.

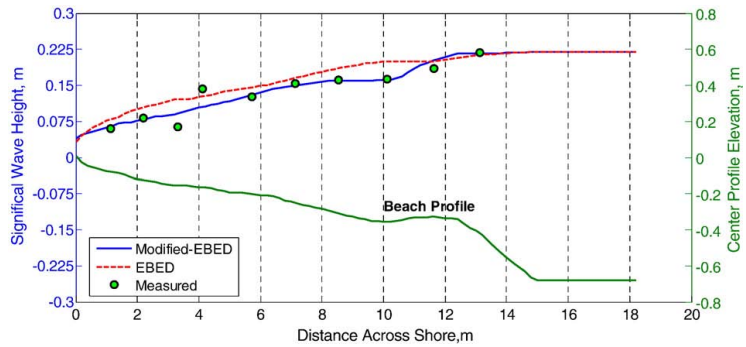

Fig. 10. Computed and measured significant wave height for LSTF BC-4.

from Eq. (5) produced good results for the Base Cases, but this equation needs to be validated with other laboratory and field data to ensure its general applicability.

Surface roller effects are necessary to include when calculating nearshore currents generated by waves. It is not only the peak of the longshore current that shifts towards the shoreline, but also the magnitude of the longshore current in the surf zone increases. The roller effects on the nearshore currents were in agreement with previously published works. By using the 2D surface roller model, energy conservation was expressed in a better manner than with the 1D model. Because the bathymetry of the LSTF basin for the Base Cases was fairly uniform, the roller energy flux alongshore in Eq. (9) was very small and could be neglected. However, this term should be included in calculations for the areas with complex bathymetry in order to obtain more accurate wave-induce currents.

Lateral mixing makes the cross-shore variation in the wave-induced longshore current smoother, and for monochromatic waves this phenomenon is needed to avoid a discontinuity at the break point. However, in the case of random waves the lateral mixing is less needed since gradual wave breaking across the profile occurs, producing a smooth forcing. Reniers and Battjes (1997) found that lateral mixing was needed to model the case of random waves breaking over a barred profile. For such a profile shape, a major portion of the waves may break on the bar and reform in the trough. In

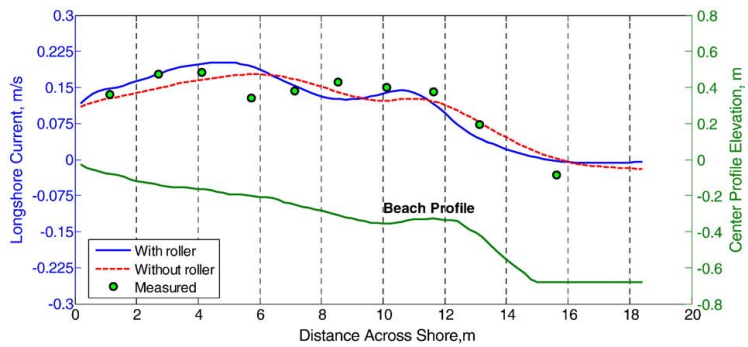

Fig. 11. Computed and measured longshore current for LSTF BC-4.

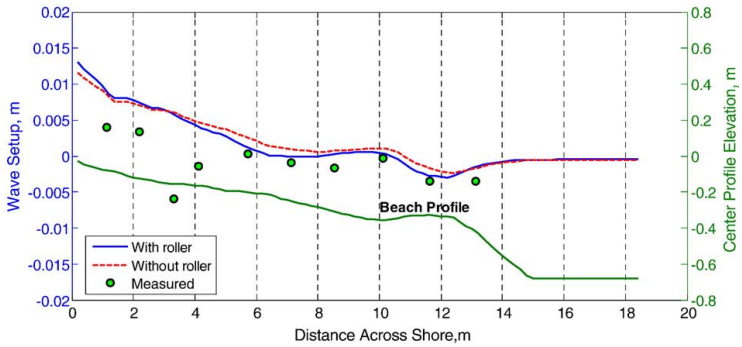

Fig. 12. Computed and measured wave setup for LSTF BC-4.

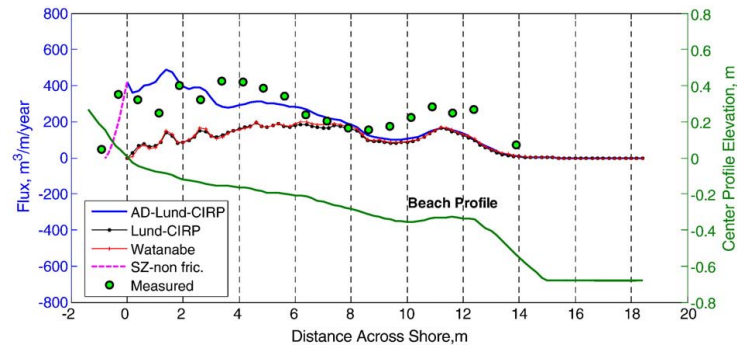

Fig. 13. Computed and measured longshore sediment flux for LSTF BC-4.

model simulations, this behavior implies little forcing in the trough and small currents here. By applying lateral mixing, this reduction in the current velocity may be counteracted. Sensitivity tests on the importance of the lateral mixing coefficient in the present study showed small effects, probably because of the profile shape changing rather gradually in the area of breaking waves.

The sediment transport typically displays great sensitivity to the roughness. Using the total roughness, including the grain-related roughness, form-drag roughness, and sediment-related roughness will produce shear stresses that may be used to calculate the sediment transport rates with some confidence. However, the formula of sediment-related roughness, which is given by Wilson (1989), is of the implicit type (for details, see Militello et al., 2006, pp. 18–20). Therefore, an iterative approach is required for solving the non-linear equation describing this roughness. In the present calculations, the Newton–Rhapson method was used for solving this equation yielding rapid convergence.

Calculating the suspended load using the advection–diffusion equation produces a smoother sediment transport rate distribution than the Lund-CIRP formula. Moreover, it can be applied to situations where suspended sediment concentration changes in time and space at a high rate, for example, at river mouths, tidal inlets, and in the vicinity of structures. Another advantage of the advection–diffusion equation is that the model uses the sediment transport rate at shoreline from the swash-zone calculations as the boundary condition for computing the suspended sediment transport in the inner surf zone.

The swash uprush and backwash occur rapidly and frequently in the swash zone, which may induce increased transport rates in the inner surf zone. If the pick-up and deposition rates were not modified ($\vartheta = 0$), the distribution of the longshore sediment transport rate would drop at a high rate seaward of the still-water shoreline, and then be similar to the calculation with the Lund-CIRP formula. Thus, it would not agree well with the investigated measured data near the shoreline. The calibration of the coefficients ϑ and μ was made for BC-1 using a range of values. The sensitivity to these coefficients is shown in Fig. 14. Based on the calibrated values for ϑ and μ, we calculated the longshore sediment flux for BC-2 and BC-4. The calibration showed that $\vartheta = 9.3$ and $\mu = 2.4$ were the most suitable values. Nevertheless, the modification of the formulas introduced and the optimal coefficient values should be validated with further data to improve the accuracy calculation of sediment transport not only for laboratory but also for field conditions.

Table 3
Root-mean-square error (%) for significant wave height, longshore current, and wave setup.

Data sets	H_s Modified-EBED	H_s EBED	v With roller	v Without roller	η With roller	η Without roller
BC-1	3.64	12.96	27.20	29.81	32.50	24.32
BC-2	3.92	14.12	17.61	19.57	51.42	52.04
BC-4	11.47	18.53	20.76	18.47	151.31	158.29

Table 4
Root-mean-square error (%) for longshore sediment transport flux.

Data sets	AD-Lund-CIRP	Lund-CIRP	Watanabe
BC-1	33.21	49.12	49.64
BC-2	18.34	59.23	62.72
BC-4	34.73	59.08	58.83

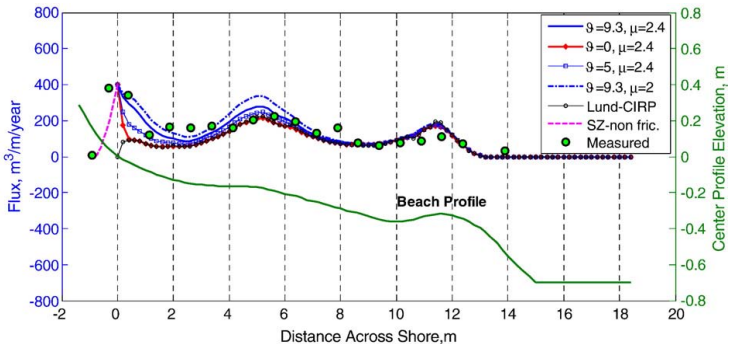

Fig. 14. Sensitive of coefficients ϑ and μ to sediment transport rate for LSTF BC-1.

7. Conclusions

A unified numerical model of nearshore waves, wave-induced currents, and sediment transport was developed. The energy dissipation due to wave breaking in the spectral wave transformation model EBED (Mase, 2001) was modified based upon the Dally et al. (1985) model, producing better predictions of the wave parameters in the surf zone. The evolution of the surface roller associated with the wave breaking after Dally and Brown (1995) was employed and enhanced, which improves the description of wave radiation stresses inside the surf zone. Including the roller shifts the nearshore current towards the shore, yielding better agreement between calculations and measurements. Newly developed formulations for the sediment transport in both swash zone and nearshore zone were applied. The modifications of pick-up and deposition rates were effective for simulating the sediment transport in the near shoreline.

The capability of model to predict the nearshore waves, wave-induced current, and sediment transport, was evaluated by comparison with three high-quality data sets from the LSTF at the Coastal and Hydraulics Laboratory. These simulations showed that the model yields reasonable predictions for the conditions studied. Thus, the model is expected to provide reliable input for calculating the morphological evolution due to waves and currents.

Acknowledgments

This work was partly funded by Sida/SAREC in the framework of the Project VS/RDE/03 "The evolution and sustainable management in the coastal areas of Vietnam" (PTN and LXH), and partly by the Inlet Modeling System Work Unit of the Coastal Inlets Research Program, U.S. Army Corps of Engineers (ML and HH). Dr. Hajime Mase at Kyoto University kindly supplied the source code for the EBED model. Dr. Ping Wang at University of South Florida and Mr. Mark Gravens at CHL provided the experimental data from their tests, which is greatly appreciated. The authors would also like to thank Dr. Nicholas C. Kraus at the U.S Army Corps of Engineers Coastal Inlet Research Program (CIRP) for the experimental data. The authors would also like to thank Dr. Nguyen Manh Hung, and the late Prof. Pham Van Ninh for their great contributions to the Project VS/RDE/03 and comments on early drafts of this paper. Finally, the authors would also like to thank the anonymous reviewers for their valuable comments.

References

Battjes, J.A., 1972. Setup due to irregular wave. Proceedings 13th International Conference on Coastal Engineering, ASCE, Vancouver, pp. 1993–2004.
Battjes, J.A., 1975. Modeling of turbulence in the surf zone. Proceedings 2nd Symposium on Modeling and Techniques, ASCE, San Francisco, pp. 1050–1061.
Bayram, A., Larson, M., Miller, H.C., Kraus, N.C., 2001. Cross-shore distribution of longshore sediment transport: comparison between predictive formulas and field measurements. Coastal Engineering 44, 79–99.
Booij, N., Holthuijsen, L.H., Ris, R.C., 1996. The 'SWAN' wave model for shallow water. Proceedings 25th International Conference on Coastal Engineering, ASCE, Orlando, pp. 668–676.
Booij, N., Holthuijsen, L.H, Doorn, N., Kieftenburg, A.T.M.M., 1997. Diffraction in a spectral wave model. Proc. 3rd Int. Symposium Ocean Wave Measurement and Analysis Wave '97, ASCE, New York, pp. 243–255.
Bowen, A.J., 1969. The generation of longshore currents on a plane beach. Journal of Marine Research 27 (2), 206–215.
Camenen, B., Larroude, P., 2003. Comparison of sediment transport formulae for the coastal environment. Coastal Engineering 48, 111–132.
Camenen, B., Larson, M., 2005. A general formula for non-cohesive bed load sediment transport. Estuarine, Coastal and Shelf Science 63, 249–260.
Camenen, B., Larson, M., 2007. A unified sediment transport formulation for coastal inlet application. Technical report ERDC/CHL CR-07-1, US Army Engineer Research and Development Center, Vicksburg, MS.
Camenen, B., Larson, M., 2008. A general formula for noncohesive suspended sediment transport. Journal of Coastal Research 24 (3), 615–627.
Dally, W.R., Osiecki, D.A., 1994. The role of rollers in surf zone currents. Proceedings 24th International Conference on Coastal Engineering. ASCE, Kobe, pp. 1895–1905.
Dally, W.R., Brown, C.A., 1995. A modeling investigation of the breaking wave roller with application to cross-shore currents. Journal of Geophysical Research 100 (C12), 24873–24883.
Dally, W.R., Dean, R.G., Dalrymple, R.A., 1985. Wave height variation across beaches of arbitrary profile. Journal of Geophysical Research 90 (C6), 11917–11927.
Deigaard, R., Justesen, P., Fredsoe, J., 1991. Modeling of undertow by one-equation turbulence model. Coastal Engineering 15, 431–458.
Duncan, J.H., 1981. An experimental investigation of breaking waves produced by a towed hydrofoil. Proc. R. Soc. London vol. A377, 331–348.
Elder, J.W., 1959. The dispersion of marked fluid in turbulent shear flow. Journal of Fluid Mechanics 5, 544–560.
Elfrink, B., Baldock, T., 2002. Hydraudynamics and sediment transport in the swash zone: a review and perspectives. Coastal Engineering 45, 149–167.
Falconer, R.A., 1980. Modelling of planform influence on circulation in harbors. Proceedings 17th International Conference on Coastal Engineering. ASCE, Sydney, pp. 2726–2744.
Goda, Y., 2006. Examination of the influence of several factors on longshore current computation with random waves. Coastal Engineering 53, 157–170.
Gravens, M.B., Wang, P., 2007. Data report: laboratory testing of longshore sand transport by waves and currents; morphology change behind headland structures. Technical Report, ERDC/CHL TR-07-8, Coastal and Hydraulics Laboratory, US Army Engineer Research and Development Center, Vicksburg, MS.
Gravens, M.B., Wang, P., Kraus, N.C., Hanson, H., 2006. Physical model investigation of morphology development at headland structures. Proceedings 30th International Conference on Coastal Engineering. World Scientific Press, San Diego, pp. 3617–3629.
Hamilton, D.G., Ebersole, B.A., 2001. Establishing uniform longshore currents in large-scale sediment transport facility. Coastal Engineering 42 (3), 199–218.
Holthuijsen, L.H., Herman, A., Booij, N., 2003. Phase-decoupled refraction–diffraction for spectral wave models. Coastal Engineering 49, 291–305.
Hunt, I.A., 1959. Design of seawalls and breakwaters. Journal of Waterways and Harbors Division 85, 123–152.
Kraus, N.C., Larson, M., 1991. NMLONG: Numerical model for simulating the longshore current; report 1: model development and tests. Technical Report DRP-91-1, U.S. Army Engineer Waterways Experiment Station, Vicksburg, MS.
Larson, M., Kraus, N.C., 2002. NMLONG: numerical model for simulating longshore current; report 2: wave–current interaction, roller modeling, and validation of model enhancements. Technical Report ERDC/CHL TR-02-22, US Army Engineer Research and Development Center, Vicksburg, MS.
Larson, M., Wamsley, T.V., 2007. A formula for longshore sediment transport in the swash. Proceedings Coastal Sediments '07. InASCE, New Orleans, pp. 1924–1937.

Larson, M., Kubota, S., Erikson, L., 2004. Swash-zone sediment transport and foreshore evolution: field experiments and mathematical modeling. Marine Geology 212, 61–79.
Lippmann, T.C., Brookins, A.H., Thornton, E.B., 1996. Wave energy transformation on natural profiles. Coastal Engineering 27, 1–20.
Longuet-Higgins, M.S., 1970. Longshore current generated by obliquely incident sea waves. Journal of Geophysical Research 75 (33), 6779–6801.
Longuet-Higgins, M.S., Stewart, R.W., 1964. Radiation stresses in water waves; a physical discussion with applications. Deep Sea Research 11, 529–562.
Madsen, P.A., Warren, I.R., 1984. Performance of a numerical short-wave model. Coastal Engineering 8, 73–93.
Madsen, P.A., Murray, R., Sorensen, O.R., 1991. A new form of the Boussinesq equations with improved linear dispersion characteristics. Coastal Engineering 15, 371–388.
Madsen, P.A., Sorensen, O.R., Schäffer, H.A., 1997. Surf zone dynamics simulated by a Boussinesq type model. Part II: surf beat and swash oscillations for wave groups and irregular waves. Coastal Engineering 32, 289–319.
Mase, H., 2001. Multi-directional random wave transformation model based on energy balance equation. Coastal Engineering Journal 43 (4), 317–337.
Militello, A., Reed, C.W., Zundel, A.K., Kraus, N.C., 2004. Two-dimensional depth-averaged circulation model M2D: version 2.0, report 1, technical document and user's guide. Technical Report ERDC/CHL TR-04-2, Coastal and Hydraulics Laboratory, US Army Engineer Research and Development Center, Vicksburg, MS.
Militello, A., Reed, C.W., Kraus, N.C., Ono, N., Larson, M., Camenen, B., Hanson, H., Wamsley, T., Zundel, A.K., 2006. Two-dimensional depth-averaged circulation model CMS-M2D: version 3.0, report 2,sediment transport and morphology change. Technical Report ERDC/CHL TR-06-9, Coastal and Hydraulics Laboratory, US Army Engineer Research and Development Center, Vicksburg, MS.
Nairn, R.B., Roelvink, J.A., Southgate, H.N., 1990. Transition zone width and implications for modeling surfzone hydrodynamics. Proceedings 22nd International Conference on Coastal Engineering. ASCE, Delft, pp. 68–81.
Nishimura, H., 1988. Computation of nearshore current. In: Horikawa, K. (Ed.), Nearshore Dynamics and Coastal Processes. InUniversity of Tokyo Press, Tokyo, Japan, pp. 271–291.
Nwogu, O., 1993. Alternative form of Boussinesq equations for nearshore wave propagation. Journal of Waterway, Port, Coastal, and Ocean Engineering 119 (6), 618–638.
Reniers, A.J.H.M., Battjes, J.A., 1997. A laboratory study of longshore currents over barred and non-barred beach. Coastal Engineering 30, 1–22.
Rivero, F.J., Arcilla, A.S, Carci, E., 1997. Analysis of diffraction in spectral wave models. Proc. 3rd Int. Symposium Ocean Wave Measurement and Analysis Wave '97. ASCE, New York, pp. 431–445.
Ruessink, B.G., Miles, J.R., Feddersen, F., Guza, R.T., Elgar, S., 2001. Modeling the alongshore current on barred beaches. Journal of Geophysical Research 106 (C10), 22451–22463.
Soulsby, R.L., 1997. Dynamics of marine sands. Thomas Telford, HR Wallingford, London.
Stive, M.J.F., De Vriend, H.J., 1994. Shear stresses and mean flow in shoaling and breaking waves. Proceedings 24th International Conference on Coastal Engineering. ASCE, Kobe, pp. 594–608.
Svendsen, I.A., 1984a. Wave heights and set-up in a surf zone. Coastal Engineering 8, 303–329.
Svendsen, I.A., 1984b. Mass flux and undertow in a surf zone. Coastal Engineering 8, 347–365.
Takayama, T., Ikeda, N., Hiraishi, T., 1991. Wave transformation calculation considering wave breaking and reflection. Rept. Port Harbor Res. Inst. 30 (1), 21–67.
Thornton, E.B., 1970. Variation of longshore current across the surf zone. Proceedings 12th International Conference on Coastal Engineering. ASCE, Washington D.C., pp. 291–308.
Thornton, E.B., Guza, R.T., 1983. Transformation of wave height distribution. Journal of Geophysical Research 88 (C10), 5925–5938.
Thornton, E.B., Guza, R.T., 1986. Surf zone longshore currents and random waves: field data and models. Journal of Physical Oceanography 16, 1165–1178.
Van Dongeren, A., Sancho, F.E., Svendsen, I.A., Putrevu, U., 1994. SHORECIRC: a quasi 3-D nearshore model. Proceedings 24th International Conference on Coastal Engineering. ASCE, Kobe, pp. 2741–2754.
Van Dongeren, A., Svendsen, I.A., 2000. Nonlinear and 3D effects in leaky infragravity waves. Coastal Engineering 41, 467–496.
Van Dongeren, A., Reniers, A., Battjes, J., 2003. Numerical modeling of infragravity wave response during DELIAH. Journal of Geophysical Research 108 (C9), 3288. doi:10.1029/2002JC001332.
WAMDI group, 1988. The WAM model-a third generation ocean wave prediction model. Journal of Physical Oceanography 18, 1775–1810.
Wang, P., Ebersole, B.A., Smith, E.R., Johnson, B.D., 2002. Temporal and spatial variations of surf-zone currents and suspended sediment concentration. Coastal Engineering 46, 175–211.
Watanabe, A., 1987. 3-dimensional numerical model of beach evolution. Proceedings Coastal Sediments '87. ASCE, pp. 802–817.
Wilson, K.C., 1989. Friction of wave-induced sheet flow. Coastal Engineering 12, 371–379.

Appendix

VI

Nam, T.P., Larson, M., Hanson, H., and Hoan, L.X. (2010). A numerical model of beach morphological evolution due to waves and currents in the vicinity of coastal structures. *Coastal Engineering.* (Submitted)

A numerical model of beach morphological evolution due to waves and currents in the vicinity of coastal structures

Pham Thanh Nam[a,b], Magnus Larson[a], Hans Hanson[a], Le Xuan Hoan[a,b]

[a] *Water Resources Engineering, Lund University, Box 118, SE-22100 Lund, Sweden*

[b] *Institute of Mechanics, Vietnam Academy of Science and Technology, 264 Doi Can, Hanoi, Vietnam*

Abstract

A numerical model was developed of beach morphological evolution in the vicinity of coastal structures. The model includes five sub-models for random wave transformation, surface roller development, nearshore wave-induced currents, sediment transport, and morphological evolution. The model was validated using high-quality data sets obtained during experiments with a T-head groin and a detached breakwater in the basin of the Large-scale Sediment Transport Facility at the Coastal and Hydraulics Laboratory in Vicksburg, Miss. The simulations showed that the model well reproduced the wave conditions, wave-induced currents, and beach morphological evolution in the vicinity of coastal structures. Both salient and tombolo formation behind a detached breakwater were simulated with good agreement compared to the measurements.

Key words: *morphodynamics, random waves, wave-induced currents, surface roller, sediment transport, coastal structures.*

1. Introduction

1.1 Background and objectives

Numerical models of beach change are useful tools in engineering projects dealing with the morphological evolution of coastal areas. Thus, a number of numerical models have been developed through the years for application in beach erosion protection, harbor construction, and navy channel dredging. However, traditionally these models have focused on a limited set of processes characterized by certain time and space scales. For example, shoreline evolution models, which were the first type of models to be used in engineering studies, describe changes in the shoreline evolution due to gradients in the longshore transport. These models typically simulate shoreline evolution over decades with limited resolution of the response on the intra-annual scale. On the other hand, profile evolution models compute changes in the profile shape due to cross-shore transport only. Such models have traditionally been used to estimate the impact of storms, implying a characteristic scale for the processes on the order of days.

Coastal structures, such as groins and detached breakwaters, are frequently utilized in coastal engineering projects to prevent beach erosion. Thus, understanding the morphological evolution in the vicinity of coastal structure is necessary to achieve an optimal functional design. There have been many attempts to develop and apply numerical models for simulating beach topography change around structures (see brief review of previous relevant studies in the following). However, the nearshore hydrodynamics and

sediment transport processes are highly complex in the vicinity of coastal structures. Moreover, the validation of numerical models against high-quality data sets is still limited. Thus, the development of models that accurately predict the morphological evolution around structures remains a challenge.

The overall aim of this study is to develop a robust and reliable numerical model to simulate beach morphological evolution under waves and currents with the emphasis on the impact of coastal structures. Preferably, the model should describe the effects of both longshore and cross-shore sediment transport over time scales from individual storms to seasonal variations. In order to facilitate this, a number of sub-models were developed and improved, including (i) a random wave transformation model, (ii) a surface roller model, (iii) a nearshore wave-induced current model, (iv) a sediment transport model, and (v) a morphological evolution model. These sub-models were coupled together and validated with detailed, high-quality data from the Large-scale Sediment Transport Facility (LSTF) basin of the Coastal and Hydraulics Laboratory (CHL) in Vicksburg, Mississippi, United States.

The paper is structured as follow: Section 1.2 presents a brief review of previous relevant work. In Section 2, the sub-models are reviewed, and Section 3 introduces the LSTF data. Section 4 describes in detail the validation of the model with the LSTF data. A discussion of the simulation results is presented in Section 5. Finally, the conclusions are given in Section 6.

1.2 Brief review of previous relevant studies

Numerical models for simulating coastal morphological evolution have developed quickly during the recent decades. Development efforts have resulted in a wide range of models at different scales, including 1D, 2D, 3D, and quasi-3D models (*e.g.*, Hanson and Larson, 1992; de Vriend *et al.*, 1993; Zyserman and Johnson, 2002; Lesser *et al.,* 2004) and several of the models have been applied in coastal engineering projects. However, here we focus our review of numerical models that have been used for coastal morphological evolution in two dimensions with the emphasis on the response of the beach topography to coastal structures, such as breakwaters, jetties, and groins.

In their pioneering work, Watanabe *et al.* (1986) investigated the beach evolution in response to a detached breakwater. The wave, current, and sediment transport fields were computed from which the topographic evolution was determined. Calculations showed that the model could rather well reproduce small-scale laboratory measurements regarding the wave height and nearshore wave-induced current around a detached breakwater, but the agreement with the measured beach evolution was mainly qualitative.

Nicholson *et al.* (1997) investigated and inter-compared five numerical models for simulating the development of a salient and a tombolo in the lee of a detached breakwater. In general, the output from these models regarding the hydrodynamics and morphological evolution was in qualitative agreement between the models (no data were employed), but differences were observed. Seven factors were identified as causing the different outputs obtained from the five numerical models, including wave type, bed roughness, eddy viscosity, wave-current interaction, refraction, smoothing, and sediment transport formula.

Steijn *et al.* (1998) applied the Delft3D model to simulate the morphological change in the vicinity of a long dam constructed at the northern end of the Texel coast. The predictions by the model were in quantitative agreement with some of the observations. A scour hole that developed in front of the tip of the dam was rather well reproduced. Nevertheless, there were large differences between the observations and computations of the morphological evolution in other areas.

Denot and Aelbrecht (1999) modeled the seabed evolution around a groin system. Two hypothetical test cases with different groin spacing and incident waves were investigated. The calculated wave and current fields around the groins were in good qualitative agreement. However, the simulated seabed evolution for both cases did not show clear areas of accumulation and erosion in the vicinity of the two groins, as expected.

Roelvink *et al.* (1999) investigated the morphological response adjacent to harbor moles and groins by using a depth-averaged morphodynamic model. Different grid sizes were applied to evaluate differences in the scour hole development around the structures. However, the wave-induced current was not considered, so the longshore transport may not have been calculated accurately.

Leont'yev (1999) developed a numerical model to simulate morphological changes due to coastal structures. Several hypothetical test cases involving groins and detached breakwaters were simulated. The model was also validated based on small-scale laboratory data and the computed result of the bed level evolution was in good agreement with the measurements.

Zyserman and Johnson (2002) applied a quasi-three dimensional model of flow, sediment transport, and bed level evolution to simulate the beach morphological evolution in the vicinity of detached breakwaters. Selected results for three test cases with different locations and sizes of the breakwater showed that the model could produce reasonable results with respect to the wave, current, and sediment transport fields, although the calculations were not compared against measurements. However, when plotting their results, the resolution in the depth contours close to the shoreline was limited; for example, only contours deeper than -2 m was shown. Thus, the topographical change near the shoreline might not have been considered in detail.

Gelfenbaum *et al.* (2003) simulated long-term morphological evolution for Grays Harbor inlet by using the Delft3D model. Filtering techniques for wave and tidal inputs were employed to reduce the number of wave conditions and flow simulations. Both the cases with and without jetties were investigated, and the model results showed quantitative agreement with observations, which indicated erosion in the inlet channel and accretion on the flood and ebb deltas. However, the simulations were only carried out for one year, whereas the measured topographic change was determined for an interval of thirty years. Thus, the comparison between the calculated and measured bed changes was not synchronized. Furthermore, the model was not successful in simulating the accumulation observed at the North Jetty.

Johnson (2004) simulated the coastal morphological evolution in the vicinity of groins by using the DHI Coastal Area Morphological Modelling System (MIKE 21 CAMS). Several important aspects of the modeling system were investigated including the effects of the

sediment transport model, offshore wave height, offshore wave direction, tidal level variation, and groin spacing.

Saied and Tsanis (2005) developed a morphological model that was called the Integrated Coastal Engineering Model (ICEM). This model was tested with some hypothetical cases including detached breakwaters and groin systems. The computations for the hypothetical test cases produced results in good qualitative agreement with the expected response. Furthermore, a case study in Ras El-Bar in Egypt was employed to validate the model, and the computed shorelines were in quite good agreement with the measurements. However, detailed comparisons between calculations and measurements of the hydrodynamics and morphological evolution in the vicinity of the groins and detached breakwaters were not presented.

Johnson *et al.* (2005) validated the MIKE 21 CAMS model based on field data from the Dubai Coast. The wave transmission, overtopping, quasi-3D sediment transport, bed friction, and a global scale factor were manipulated to achieve reasonable calibration parameter values. The calculations of the bed evolution showed quite good agreement with the measurements.

Zyserman *et al.* (2005) and Zanuttigh (2007) modeled and analyzed the morphological response induced by low-crested structures on the adjacent seabed. These studies focused on the far-field erosion in the vicinity of roundheads and gaps between structures. The model was investigated by application at two field sites, Pellestrina and Lido di Dante, where groins and low-crested breakwaters were constructed to protect against beach erosion. The obtained simulation results were in good qualitative agreement with the measurements, especially the erosion near the roundheads of the breakwaters.

Ding *et al.* (2006), and Ding and Wang (2008), developed a quasi-3D morphological model that can be applied to coastal and estuarine morphological processes. The model was validated for a complex coastal area, which included detached breakwaters and a harbor. The calculated morphological change in the lee of the breakwaters was somewhat underestimated compared to the measurements. This was possibly because the sediment transport in the swash zone was not included in the model.

Brøker *et al.* (2007) also used MIKE 21 CAMS to optimize a new layout of the main breakwaters for the Thorsminde Harbor entrance. The recommended layout was constructed in 2004. However, the validation of the model was limited. The long-term beach evolution in the vicinity of new layout was not modeled, but only short simulations for selected storm conditions were carried out.

In summary, the development of numerical models of morphological evolution around coastal structures has encompassed significant improvements through the years. However, the morphodynamical processes are extremely complex and some are beyond our current state of knowledge. Furthermore, available high-quality data for validation are limited. Therefore, many of the previous modeling efforts neither included all relevant morphodynamical processes nor were validated against high-quality data from laboratories and field surveys.

2. Model descriptions

The model that was developed includes sub-models to calculate the nearshore waves, currents, sediment transport, and the morphological change. The sub-models are briefly described in the following (for a more detailed discussion of the wave, current, and sediment transport sub-module, see Nam *et al.*, 2009; Nam and Larson, 2009 and 2010).

2.1 Modified-EBED model

Multi-directional and multi-frequency random wave transformation can be modeled based on the energy balance equation with diffraction and energy dissipation terms (Mase, 2001; Nam *et al.* 2009; Nam and Larson, 2009 and 2010) as,

$$\frac{\partial\left(v_x S\right)}{\partial x}+\frac{\partial\left(v_y S\right)}{\partial y}+\frac{\partial\left(v_\theta S\right)}{\partial \theta}=\frac{\kappa}{2\omega}\left\{\left(CC_g\cos^2\theta S_y\right)_y-\frac{1}{2}CC_g\cos^2\theta S_{yy}\right\}-\frac{K}{h}C_g\left(S-S_{stab}\right) \tag{1}$$

where S is the angular-frequency spectrum density, (x, y) the horizontal coordinates, θ the angle measured counterclockwise from the x axis, v_x, v_y, and v_θ the propagation velocities in their respective coordinate direction, ω the frequency, C the phase speed, and C_g the group speed, h the still water depth, κ a free parameter that can be optimized to change the influence of the diffraction effects, K a dimensionless decay coefficient, and S_{stab} the stable wave spectrum density, which is a function of the stable wave height H_{stab} $\left(=\Gamma h\right)$, with Γ being a dimensionless empirical coefficient. Based on Goda (2006), the coefficients K and Γ can be determined as,

$$\begin{cases}\Gamma=0.45,\ K=\dfrac{3}{8}(0.3-19.2m) & :\ m<0\\ \Gamma=0.45+1.5m,\ K=\dfrac{3}{8}(0.3-0.5m) & :\ 0\le m\le 0.6\end{cases} \tag{2}$$

where m is the bottom slope.

The output from the model includes three main parameters: significant wave height, significant wave period, and mean wave direction. The wave-driven radiation stresses can be derived based on the output of the Modified-EBED model as,

$$S_{xx}=\frac{E}{2}\left[2n(1+\cos^2\bar{\theta})-1\right];\ S_{yy}=\frac{E}{2}\left[2n(1+\sin^2\bar{\theta})-1\right];\ S_{xy}=S_{yx}=\frac{E}{2}n\sin 2\bar{\theta} \tag{3}$$

where $E=\rho_w g H_{rms}^2/8$ is the wave energy per unit area, with ρ_w the water density, g the acceleration due to gravity, and $n=C_g/C$ the wave index.

2.2 Surface roller model

The surface roller was modeled based on the energy balance equation as (Dally and Brown, 1995; Larson and Kraus, 2002),

$$P_D + \frac{\partial}{\partial x}\left(\frac{1}{2}MC_r^2 \cos^2\bar{\theta}\right) + \frac{\partial}{\partial y}\left(\frac{1}{2}MC_r^2 \sin^2\bar{\theta}\right) = g\beta_D M \tag{4}$$

where P_D is the wave energy dissipation ($= KC_g\rho_w g(H_{rms}^2 - (\Gamma h)^2)/(8h)$), M the wave-period-averaged mass flux, C_r the roller speed ($\approx C$), and β_D the roller dissipation coefficient.

The stresses due to the roller were calculated as,

$$R_{xx} = MC_r \cos^2\bar{\theta};\ R_{yy} = MC_r \sin^2\bar{\theta};\ R_{xy} = R_{yx} = MC_r \sin 2\bar{\theta} \tag{5}$$

2.3 Nearshore currents model

The nearshore currents and water elevation can be determined based on the momentum equations and continuity equation as (Militello *et al.,* 2004),

$$\frac{\partial(h+\eta)}{\partial t} + \frac{\partial q_x}{\partial x} + \frac{\partial q_y}{\partial y} = 0 \tag{6}$$

$$\frac{\partial q_x}{\partial t} + \frac{\partial uq_x}{\partial x} + \frac{\partial vq_x}{\partial y} + g(h+\eta)\frac{\partial \eta}{\partial x} = \frac{\partial}{\partial x}D_x\frac{\partial q_x}{\partial x} + \frac{\partial}{\partial y}D_y\frac{\partial q_x}{\partial y} + fq_y - \tau_{bx} + \tau_{Sx} \tag{7}$$

$$\frac{\partial q_y}{\partial t} + \frac{\partial uq_y}{\partial x} + \frac{\partial vq_y}{\partial y} + g(h+\eta)\frac{\partial \eta}{\partial y} = \frac{\partial}{\partial x}D_x\frac{\partial q_y}{\partial x} + \frac{\partial}{\partial y}D_y\frac{\partial q_y}{\partial y} - fq_x - \tau_{by} + \tau_{Sy} \tag{8}$$

where η is the water elevation, q_x, q_y the flow per unit width parallel to the *x* and *y* axis, respectively, u, v the depth-averaged velocity in *x* and *y* direction, respectively, D_x, D_y the eddy viscosity coefficients, *f* the Coriolis parameter, τ_{bx}, τ_{by} the bottom stresses, and τ_{Sx}, τ_{Sy} the wave stresses (the latter variables are all in the *x*- and *y*-directions, respectively).

In this study, we only consider the wave-induced currents. The wave stresses were determined from the output of the Modified-EBED model, and from the surface roller model as,

$$\tau_{Sx} = -\frac{1}{\rho_w}\left[\frac{\partial}{\partial x}(S_{xx} + R_{xx}) + \frac{\partial}{\partial y}(S_{xy} + R_{xy})\right] \tag{9}$$

$$\tau_{Sy} = -\frac{1}{\rho_w}\left[\frac{\partial}{\partial x}(S_{xy} + R_{xy}) + \frac{\partial}{\partial y}(S_{yy} + R_{yy})\right] \tag{10}$$

The eddy viscosity in the offshore is determined based on the work by Falconer (1980), whereas the expression by Kraus and Larson (1991) is employed for the surf zone. The bottom stresses can be calculated from Nishimura (1998).

2.4 Sediment transport model

2.4.1. Swash zone

The net transport rates over several swash cycles in the cross-shore and longshore direction can be calculated based on the formula by Larson and Wamsley (2007) as,

$$q_{bc,net} = K_c \frac{\tan\phi_m}{\tan^2\phi_m - (dh/dx)^2} \frac{u_0^3}{g}\left(\frac{dh}{dx} - \tan\beta_e\right)\frac{t_0}{T} \tag{11}$$

$$q_{bl,net} = K_l \frac{\tan\phi_m}{\tan^2\phi_m - (dh/dx)^2} \frac{u_0^2 v_0}{g}\frac{t_0}{T} \tag{12}$$

where $q_{bc,net}$, $q_{bl,net}$ are the transport in the cross-shore and longshore direction, respectively, K_c and K_l empirical coefficients, ϕ_m the friction angle for a moving grain ($\approx 30\,\text{deg}$), β_e the foreshore equilibrium slope, u_0, v_0 and t_0 the scaling velocities and time, respectively, and T the swash duration (T is set equal to the incident wave period). The swash zone hydrodynamics without friction (yields u_0, v_0 and t_0), which were derived based on the ballistics theory, were employed in the model (for details see Larson and Wamsley, 2007).

2.4.2 Nearshore zone (offshore and surf zone)

The bed load transport is determined following the work by Camenen and Larson (2005, 2007),

$$\frac{q_{bc}}{\sqrt{(s-1)gd_{50}^3}} = a_c\sqrt{\theta_c}\,\theta_{cw,m}\exp\left(-b_c\frac{\theta_{cr}}{\theta_{cw}}\right) \tag{13}$$

where the transport q_{bc} is obtained in the direction of the current (the transport normal to the current is zero), s the relative density between sediment and water, d_{50} the median grain size, a_c and b_c empirical coefficients, $\theta_{cw,m}$ and θ_{cw} the mean and maximum Shields parameters due to wave and current interaction, respectively, θ_{cr} the critical Shields parameter, and θ_c the Shields parameter due to current.

The suspended load can be obtained by solving the advection-diffusion equation. The advection-diffusion equation is obtained from continuity in the depth-averaged suspended sediment transport as,

$$\frac{\partial(\overline{C}d)}{\partial t} + \frac{\partial(\overline{C}q_x)}{\partial x} + \frac{\partial(\overline{C}q_y)}{\partial y} = \frac{\partial}{\partial x}\left(K_x d\frac{\partial\overline{C}}{\partial x}\right) + \frac{\partial}{\partial x}\left(K_y d\frac{\partial\overline{C}}{\partial y}\right) + \overline{P} - \overline{D} \tag{14}$$

where $\overline{C}$ is the depth-averaged sediment concentration, K_x and K_y the sediment diffusion coefficient in x and y direction, respectively, $\overline{P}$ the sediment pick-up rate, and $\overline{D}$ the sediment deposition rate (for details see Nam *et al.*, 2009).

2.5 Morphological evolution model

The morphological evolution is based on the sediment volume conservation equation,

$$\frac{\partial h}{\partial t} = \frac{1}{1-n_p}\left(\frac{\partial q_{tot,x}}{\partial x} + \frac{\partial q_{tot,y}}{\partial y}\right) \tag{15}$$

where n_p is the porosity, and $q_{tot,x}$ and $q_{tot,y}$ the total load in x and y directions, respectively. In the offshore and surf zone, the total load is the sum of bed load and suspended load, which are calculated based on equations (13) and (14). In the swash zone, it is based on the transport rates obtained from (11) and (12).

3. LSTF data and selected test cases

Five series of physical model experiments were undertaken in the basin of the LSTF (Gravens *et al.*, 2006; Gravens and Wang, 2007; Hamilton and Ebersole, 2001; Wang *et al.*, 2002). The main aim of these experiments was to obtain high-quality data sets for validating formulas for sediment transport, as well as investigating the beach evolution in the vicinity of coastal structures. The first series of experiments consisted of four runs approximately 160 min each that were performed on a natural beach without structures. The second and third series of experiments, referred to as "Test 1" and "Test 2", were carried out with a detached breakwater in the basin that was located between profile Y22 and Y26, at four meter distance from the initial still water shoreline (see Fig. 1). The currents in Test 1 were generated by waves only, whereas in Test 2 the currents were a combination of wave-induced currents and external currents. Both Test 1 and Test 2 included eight runs approximately 190 min each. The fourth series, referred to as "Test 3", included six runs 180 min each, performed on the natural beach with a T-head groin (see Fig. 2). The last series of experiments, referred to as "Test 4", were conducted in the basin with a detached breakwater, but its length was shorter and its location was closer to the shoreline than those in Test 1 and Test 2.

In all experimental runs, spilling breaking waves were generated by four wave-makers and the water was re-circulated by the pumping systems located up- and downstream of the basin. Wave gages and acoustic doppler velocimeters were co-located at ten cross-shore positions on the instrument bridge: 1.125 m (ADV1), 2.2 m (ADV2), 3.3 m (ADV3), 4.125 m (ADV4), 5.73 m (ADV5), 7.125 m (ADV6), 8.525 m (ADV7), 10.125 m (ADV8), 11.625 m (ADV9), and 13.125 m (ADV10) seaward from the initial shoreline. This bridge moved in the alongshore direction, thus the wave conditions and currents could be observed at specific cross-shore profiles. Three wave gages (#11, #12, and #13) were located at three alongshore positions, 18.43 m seaward of the initial shoreline, to measure the wave conditions seaward of the toe of the movable beach. A rod and acoustic survey techniques were employed to measure the beach profiles after each experimental run. The beach in the basin consisted of well-sorted sand with a median grain size of 0.15 mm.

In this study, three runs from Test 3 (T3C1, T3C4, and T3C6), and three runs from Test 1 (T1C1, T1C4, and T1C8), were selected to evaluate the predictive capability of the model regarding nearshore waves, wave-induced currents, and morphological evolution for the T-head groin and detached breakwater experiment, respectively.

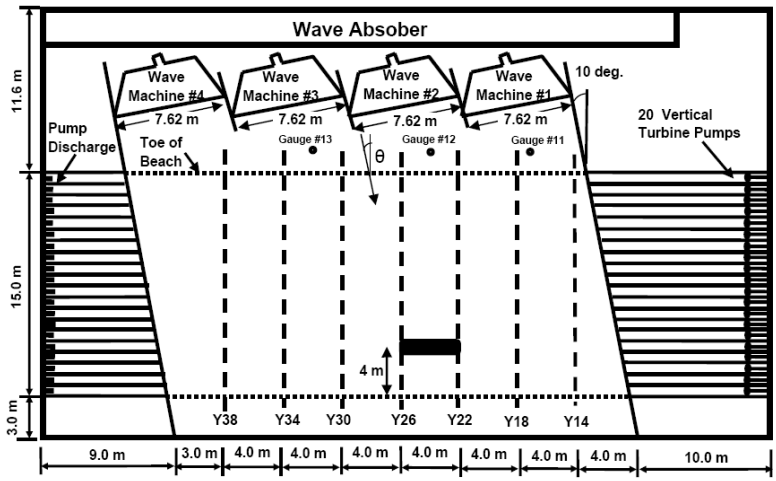

Fig. 1. Detached breakwater layout in the LSTF for Test 1 and 2 (Gravens and Wang, 2007)

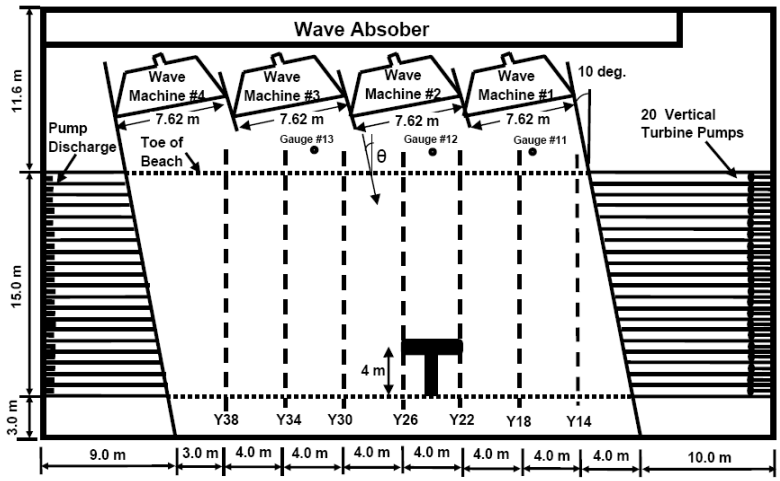

Fig. 2. T-head groin layout in the LSTF for Test 3 (Gravens and Wang, 2007)

4. Model validation against LSTF data

4.1 Model setup

The computational domain was covered by a rectangular grid with a cell size of 0.2 × 0.2 m, and interpolation was employed using the measured bathymetry data from profile Y34 to profile Y14.

The observed data at Gauges #11, #12, and #13 were used as the offshore wave conditions. Detailed information on the wave conditions at these gauges for the cases with a T-head groin and a detached breakwater is presented in Table 1. A Texel-Marsen-Arsloe (TMA)

spectrum was assumed at the offshore boundary with the parameter values $\gamma = 3.3,\ \sigma_a = 0.07,\ \sigma_b = 0.09$, and the angular spreading of the waves $S_{max} = 25$.

The decay and stable coefficients were calculated from Eq. (2), and the roller dissipation coefficient was set to $\beta_D = 0.1$. A Manning coefficient of 0.025 was used to calculate the bottom friction. The measured velocities at profile Y34 and profile Y14 were employed to specify the influx and outflux of water at the lateral boundaries for the nearshore current model. At the offshore boundary, a radiation boundary condition was given following Reid and Bodine (1968).

The coefficient values of K_c and K_l were both specified as 0.0008 for determining the net transport rates in the swash zone in the cross-shore and longshore directions, respectively (Nam *et al.*, 2009), whereas the values of a_c and b_c in the bed load formula were selected as 12 and 4.5, respectively (Camenen and Larson, 2005). In Eq. (14), the value of the diffusion coefficients were set according to Elder (1959). The pick-up and deposition rates were calculated using the formulas of Nam *et al.* (2009), and the porosity in the mass conservation equation was set to 0.4. A time step of 60 s was selected for the morphological change model.

Table 1. Offshore wave conditions

Structure types	Data sets	Gauges	H_{mo} (m)	T_p (s)	θ (deg.)
T-head groin	T3C1	#11	0.218	1.447	6.5
		#12	0.231	1.477	6.5
		#13	0.223	1.450	6.5
	T3C4	#11	0.221	1.462	6.5
		#12	0.223	1.476	6.5
		#13	0.224	1.457	6.5
	T3C6	#11	0.220	1.459	6.5
		#12	0.222	1.470	6.5
		#13	0.225	1.458	6.5
Detached breakwater	T1C1	#11	0.219	1.442	6.5
		#12	0.236	1.470	6.5
		#13	0.226	1.459	6.5
	T1C4	#11	0.222	1.452	6.5
		#12	0.232	1.472	6.5
		#13	0.225	1.464	6.5
	T1C8	#11	0.219	1.457	6.5
		#12	0.236	1.468	6.5
		#13	0.224	1.461	6.5

Fig. 3 presents a flowchart for the calculation of beach topography evolution, including the feedback loops. Based on the input data (offshore wave conditions), the Modified-EBED model is employed to calculate the wave field in the nearshore zone. The mass flux due to the roller is determined through the roller model. Thus, the wave stresses is calculated based on the random wave transformation model and the roller model. After that, the

wave-induced current field at steady state is determined from the nearshore current model. The output from the wave and current models is used to compute the Shields parameters that are employed for determining the bed load in the offshore and surf zone. The coupling between the sediment transport in the swash and inner surf zone is included. When solving the advection-diffusion equation for the offshore and surf zone, the suspended sediment concentration at the still-water shoreline (boundary between swash and surf zone) is calculated based on the sediment transport rates obtained by the swash zone computations. The beach morphological change is determined from the volume conservation equation. In order to save time in the computations, the wave, current, and sediment transport fields are only re-calculated every *n*-th morphological time step (*n*=5 in the present study). The bed level is smoothed at an interval corresponding to 15 times the morphological time step, and the smoothing coefficient is 0.25 (Johnson and Zyserman, 2002).

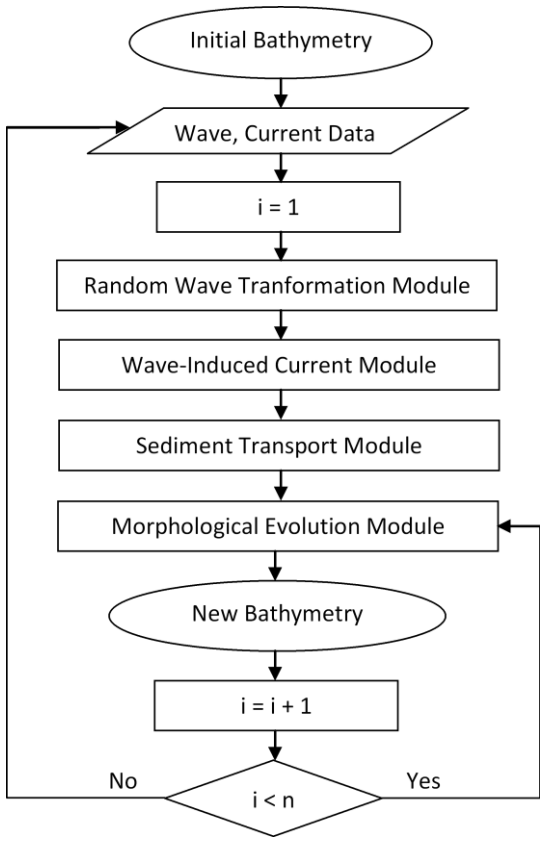

Fig. 3. Calculation procedure in the morphological evolution model

4.2 Model validation against data for T-head groin

The initial bathymetry for test case T3C1 consisted of the pre-run survey data of Test 3 in which the beach was designed to be quite uniform in the alongshore direction and the shoreline was straight. For test cases T3C4 and T3C6, the initial bathymetries were from the post-run survey data of the runs T3C3 and T3C5, respectively.

Fig. 4 shows a detailed comparison between calculations and measurements of the significant wave height along six selected profile lines in the vicinity of a T-head groin for T3C1 (see Fig. 2). The calculations obtained by the Modified-EBED model are described by the solid line, whereas the ones obtained by the original EBED model, are presented by the dashed line. As can be seen, the Modified-EBED model yielded improved predictions of significant wave height in the surf zone, resulting in more accurate wave stresses for calculating the wave-induced currents. Note that the measured data at ADV4 were not included, because the wave gage at this location did not work properly.

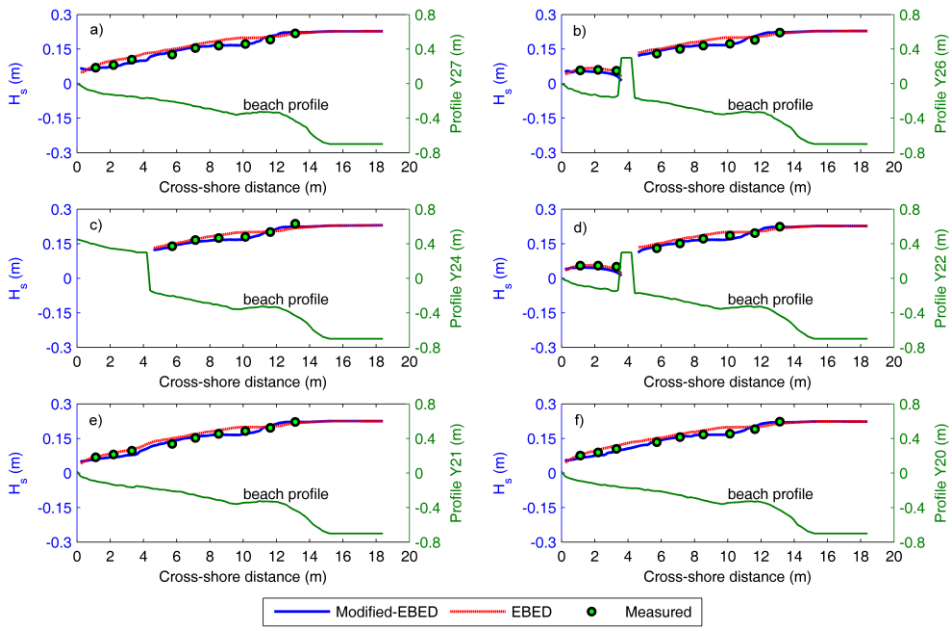

Fig. 4. Comparison of calculated significant wave height with measurements for Case T3C1

The wave-induced currents in the vicinity of the T-head groin were investigated and compared against the measurements for T3C1. Fig. 5 displays a detailed comparison between calculations and measurements of the longshore current for six selected profiles. In general, both calculated longshore currents with and without roller were in good agreement with the observations. The calculations with roller implied a current distribution that was slightly shifted towards the shoreline. The observations of longshore current at ADV9 and ADV10 were not correct (Gravens and Wang, 2009); thus, they were not employed in this comparison.

The comparison between calculated and measured cross-shore current for T3C1 is presented in Fig. 6. Calculated cross-shore currents somewhat underestimated the measurements, although they were in good agreement in the lee of the T-head groin. The calculated cross-shore currents with the roller were quite similar to those without roller. An eddy was calculated to occur around ADV3-ADV6 of profile Y20 and Y21; therefore, the cross-shore current had a shoreward direction here. Nevertheless, the measured data at these locations were relatively small and quite flat. Thus, the differences between measured and calculated cross-shore currents were significant at these locations (see Figs. 6e and f). In the present study, the undertow current was not included in the model, which is probably the main reason for these discrepancies.

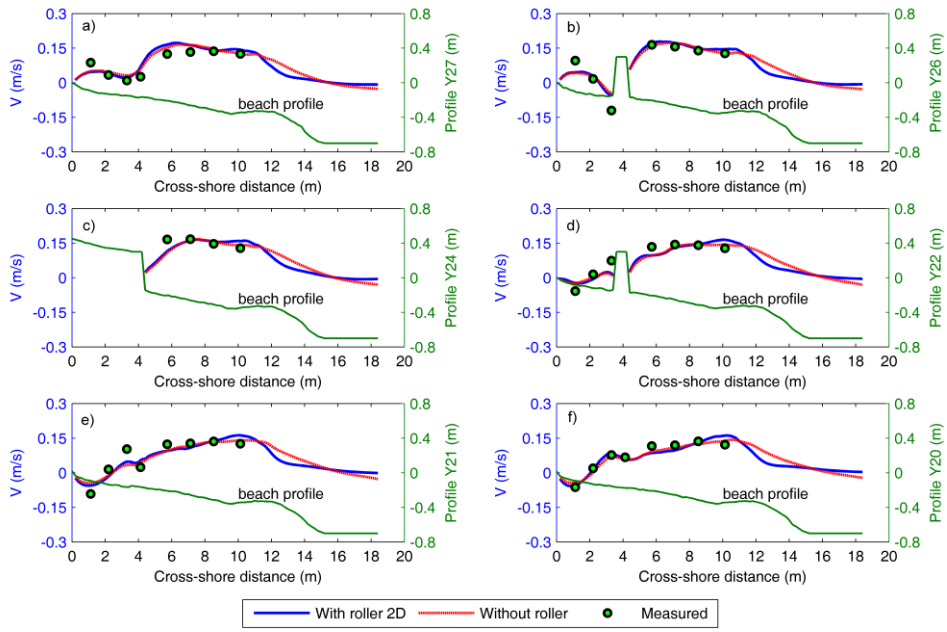

Fig. 5. Comparison of calculated longshore current with measurements for Case T3C1

The computed beach evolution after 180 min for Case T3C1 was compared with the measurements (see Fig. 7). The solid line represents the calculated bed level, whereas the dotted line shows the measurements. The calculated beach topography agreed rather well with the measurements, including the sand accumulation in the lee of T-head groin. However, there were some discrepancies between calculated and measured shoreline change up- and downdrift of the structure.

The computations of nearshore waves, wave-induced currents, and morphological evolution for T3C4 were carried out in the same manner as for T3C1. The wave conditions were also well predicted by the Modified-EBED model for this case. Although the calculations somewhat underestimated measurements, overall the Modified-EBED model reproduced well the significant wave height at all measurement locations (see Fig. 8).

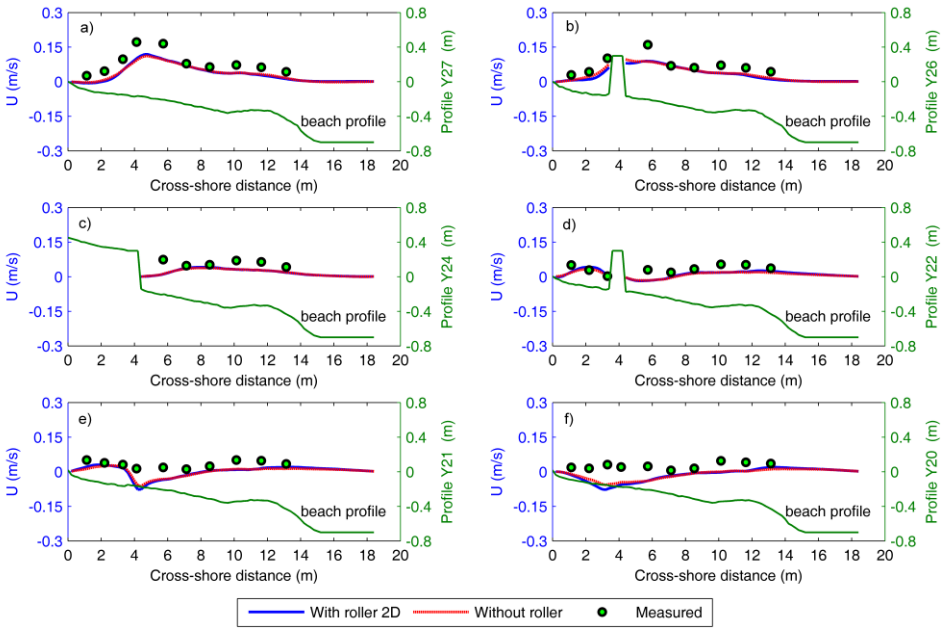

Fig. 6. Comparison of calculated cross-shore current with measurements for Case T3C1

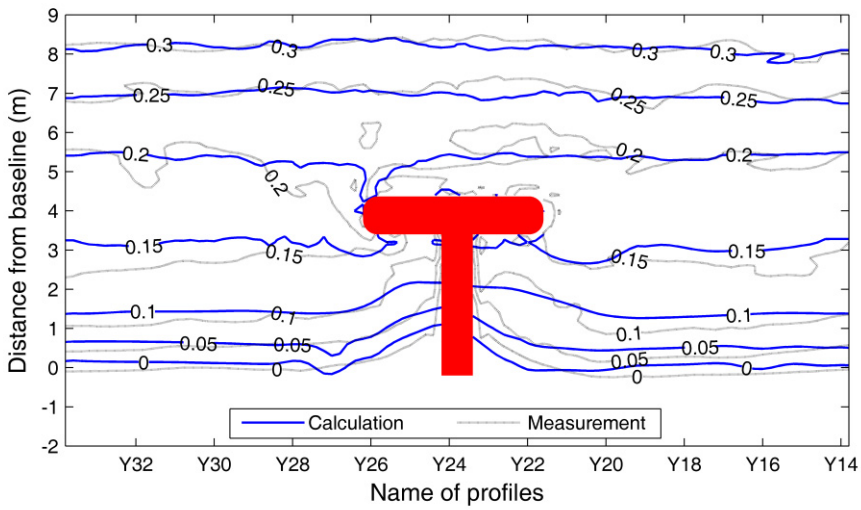

Fig. 7. Comparison of calculated bed level after 180 min with measurements for Case T3C1

Similarly to T3C1, the computed longshore current in the vicinity of the T-head groin for T3C4 was in good agreement with the measurements. As seen in Fig. 9, the computation of the longshore current with roller represented a slight improvement compared to the one without roller. The computed cross-shore current underestimated the measurements, but

the calculated eddy downstream the T-head groin was stronger than in T3C1, causing larger differences compared to the measurements in this area (see Figs. 10e and f). However, in general the calculations agreed well with the measurements in the lee of the T-head groin (Figs. 10b and d).

Fig. 11 shows the comparison between calculated bed levels after 180 min and measurements for T3C4. The computations showed that the beach evolution was fairly well predicted; especially, the shoreline changes were in good agreement with the observations. However, the calculated sand accumulation downdrift the T-head groin exceeded measured data.

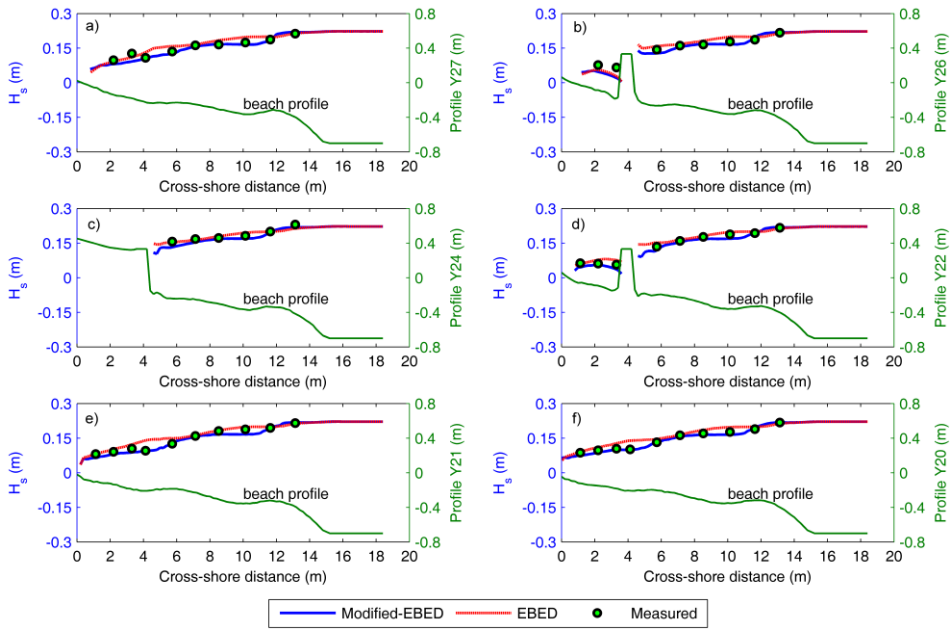

Fig. 8. Comparison of calculated significant wave height with measurements for Case T3C4

Fig. 12 shows the comparison of calculated significant wave height with the measurements for T3C6. As for T3C1 and T3C4, the wave predictions obtained by the Modified-EBED model were in good agreement with observations, and significant improvement was achieved at ADV7, ADV8, and ADV9 compared to the original EBED model.

Fig. 13 compares the measured and computed longshore current for six selected cross-shore profiles for T3C6. As can be seen, the calculations of the longshore current with roller agreed somewhat better with the measurements than the one without roller. In this case, the simulations of the longshore current were in good agreement with the observations not only in the surf zone, but also in the lee of the T-head groin.

A detailed comparison between the calculated and measured cross-shore current for T3C6 is presented in Fig. 14. As can be seen, the calculated cross-shore current with roller is quite similar to that without roller. As for the previous cases, the predicted cross-shore currents somewhat underestimated the observations. The eddy simulated downstream the T-head groin caused a significant difference between the calculated and observed cross-

shore currents at profile Y21 and Y20 (see Figs. 14e and f). However, as for T3C1 and T3C4, overall the agreement between measurements and calculations was quite good in the lee of T-head groin (see Figs. 14b and d).

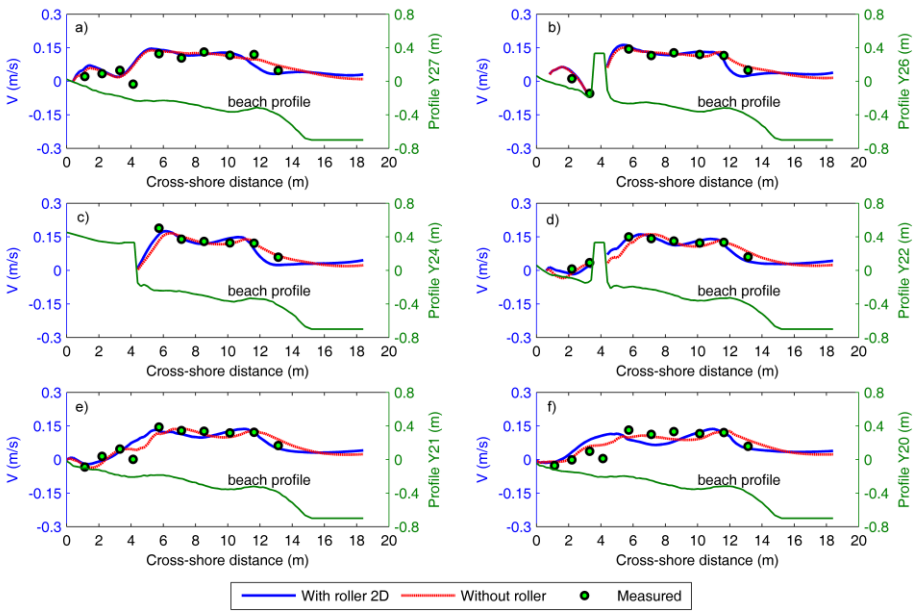

Fig. 9. Comparison of calculated longshore current with measurements for Case T3C4

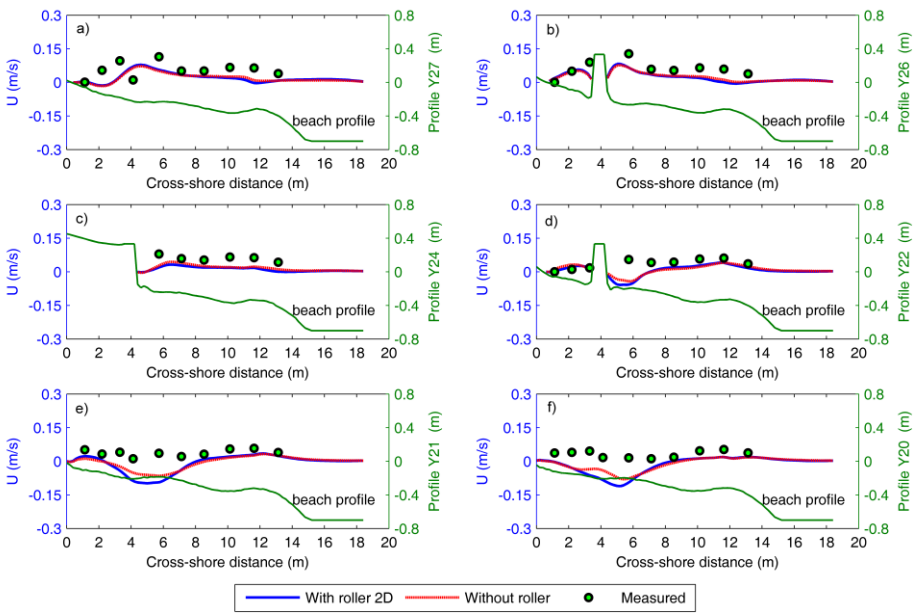

Fig. 10. Comparison of calculated cross-shore current with measurements for Case T3C4

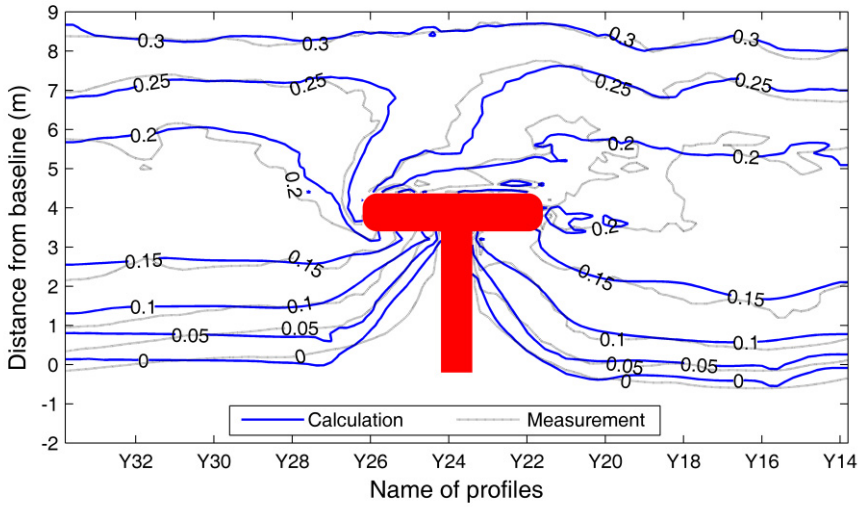

Fig. 11. Comparison of calculated bed level after 180 min with measurements for Case T3C4

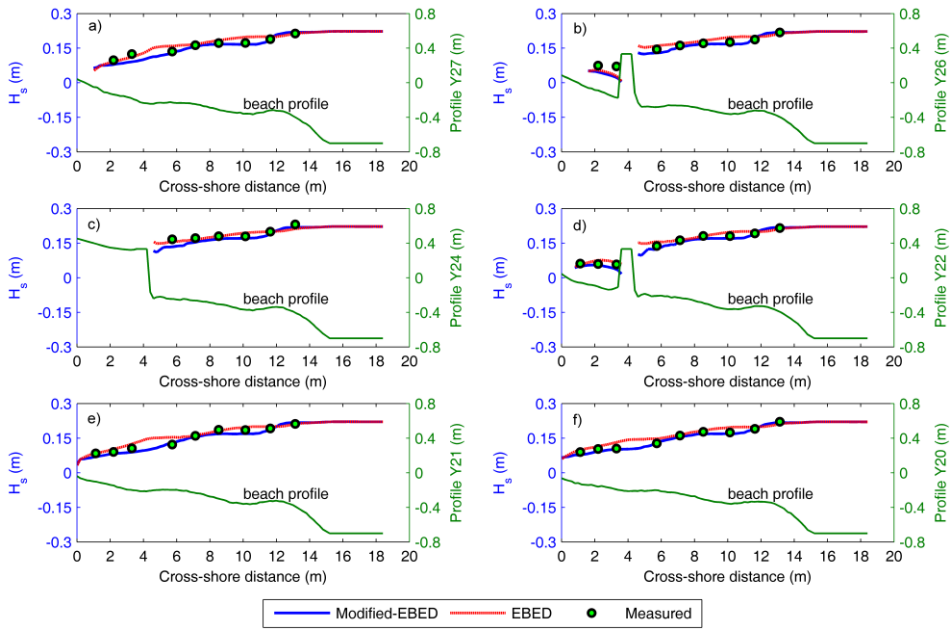

Fig. 12. Comparison of calculated significant wave height with measurements for Case T3C6

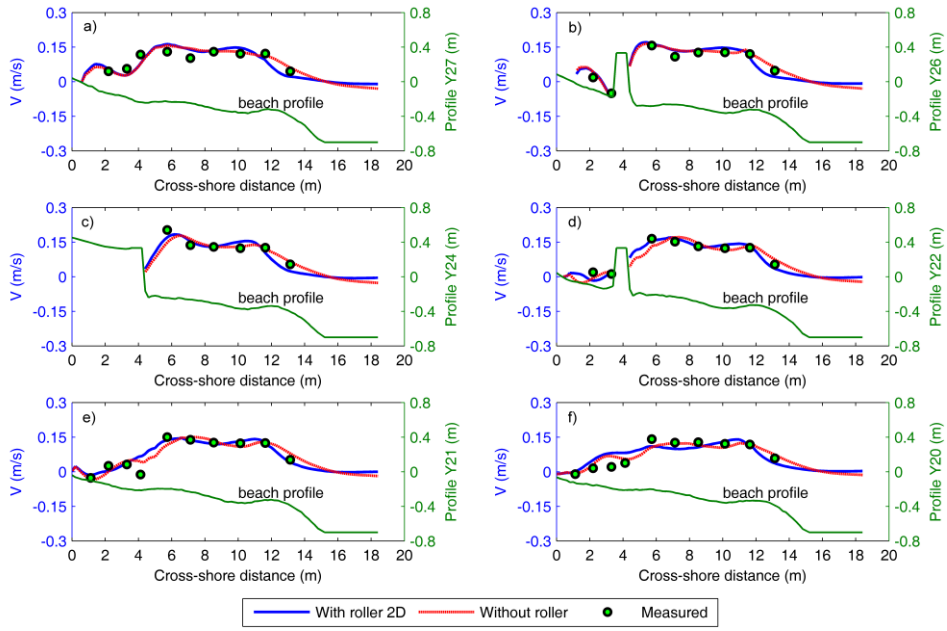

Fig. 13. Comparison of calculated longshore current with measurements for Case T3C6

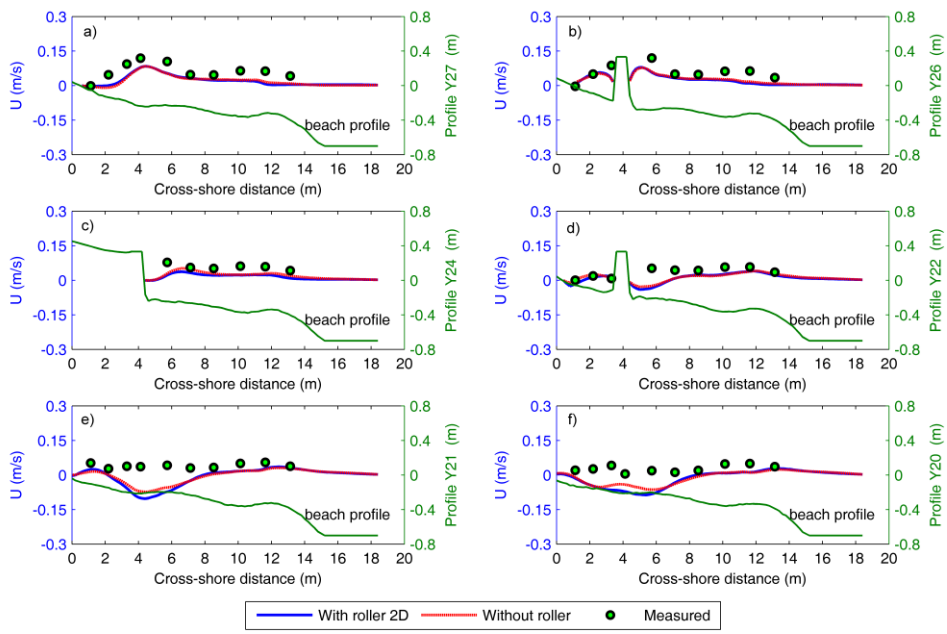

Fig. 14. Comparison of calculated cross-shore current with measurements for CaseT3C6

Fig. 15 shows the comparison between calculated and measured bed levels after 180 min for T3C6, and the simulated beach topography changes agreed well with the measurements. The salient was faithfully reproduced in the lee of T-head groin by the model. Although there were discrepancies at the updrift side, the calculated shoreline changes closely reproduced the measurements.

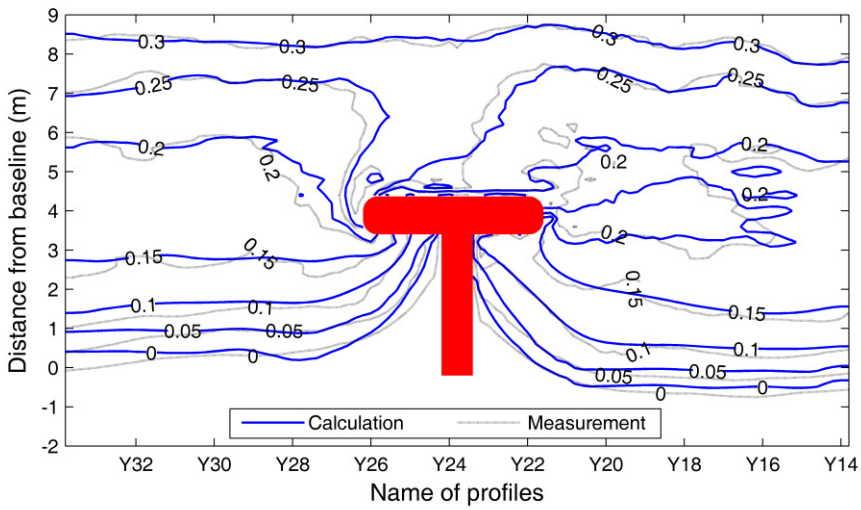

Fig. 15. Comparison of calculated bed level after 180 min with measurements for Case T3C6

4.3 Model validation against data for detached breakwater

As for T3C1, the initial bathymetry of test case T1C1 consisted of the pre-run survey data of Test 1; the beach was rather uniform in alongshore direction, and the shoreline was straight and parallel to the detached breakwater. The post-run survey data of the runs T1C3 and T1C7 were employed as initial bathymetries for the cases T1C4 and T1C8, respectively.

Model validation for Cases T1C1, T1C4, and T1C8 regarding the significant wave height, longshore current, cross-shore current, and wave setup were carried out and presented in Nam and Larson (2010). Therefore, only the validations for the beach morphological evolution are presented in the present study for these cases.

Fig. 16 shows a comparison of the calculated beach evolution after 185 min with the measurements for T1C1. The beach topography changed slightly seaward of detached breakwater. However, the salient developed significantly in the lee of the detached breakwater. The simulation showed that the calculation of the beach topographical change due to waves and currents were in good agreement with the measurements, especially concerning the salient development in the lee of detached breakwater. However, the difference between the calculated and measured downdrift shoreline was significant. The observations showed that the shoreline eroded downdrift; however, this response was not well reproduced by the model.

Fig. 17 illustrates a comparison between the calculated and measured bed levels after 190 min for T1C4. The simulated beach morphological evolution in the vicinity of detached breakwater agreed rather well with the measurements, especially regarding the salient development in the lee of the breakwater.

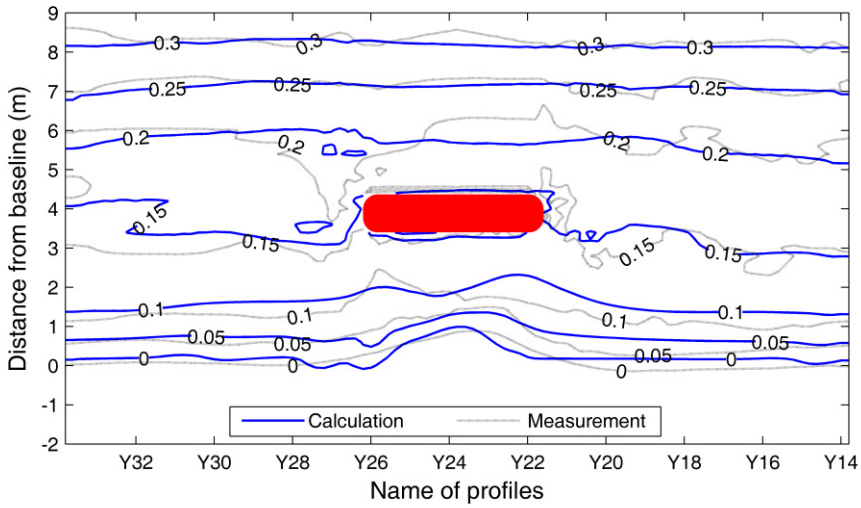

Fig. 16. Comparison of calculated bed level after 185 min against measurements for T1C1 case

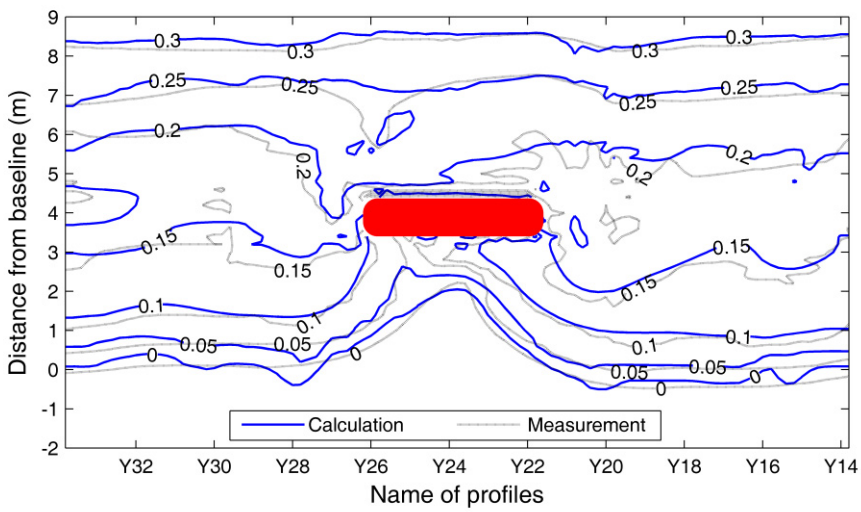

Fig. 17. Comparison of calculated bed level after 190 min with measurements for Case T1C4

The calculated bed levels after 185 min for T1C8, together with the corresponding measurements, are presented in Fig. 18. As can be seen, the beach topographical evolution

was fairly well predicted by the model, and a tombolo was predicted to develop in the lee of the detached breakwater in agreement with observations. However, the discrepancies between measurements and computations of bed level in the downdrift area were more significant than those for T1C1 and T1C4.

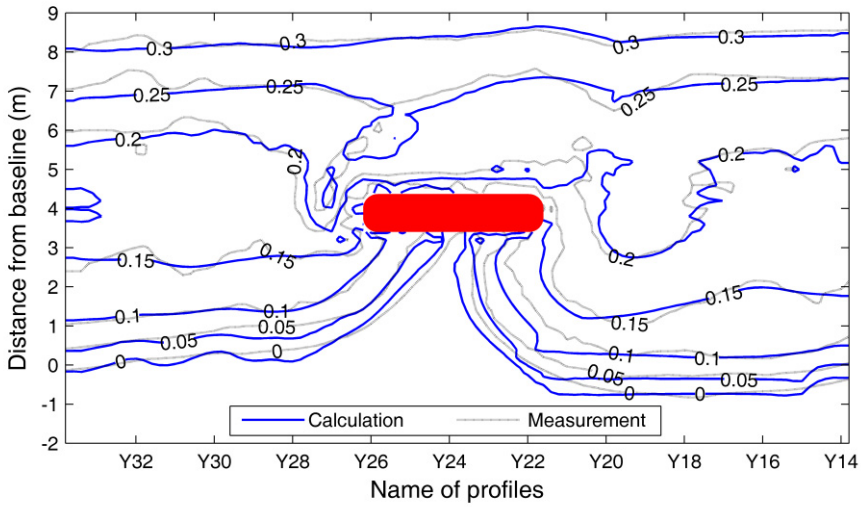

Fig. 18. Comparison of calculated bed level after 185 min with measurements for Case T1C8

5. Discussion

The wave field simulation is the crucial first step in modeling beach morphological evolution. The accuracy of the current and sediment transport fields is strongly dependent on the output from the wave model. In the present study, a diffraction term is included in the Modified-EBED model. Thus, this model can be applied to coastal areas that include structures, such as breakwaters and groins. The simulations showed that the calculations of significant wave height in the lee of detached breakwaters and T-head groins were in good agreement with the measurements, proving that the diffraction effects were well described by the model. As discussed in the previous studies of Nam *et al.* (2009) and Nam and Larson (2010), the energy dissipation due to wave breaking plays an important role in calculating the wave conditions in the surf zone. The energy dissipation is computed following the Dally *et al.* (1985) model, improving the predictions of the wave conditions in the surf zone. Thus, the Modified-EBED model can provide more accurate simulation results to be used for calculating nearshore wave-induced currents and sediment transport rates.

Calculation of wave-induced currents is also dependent on the roller effects. By including the roller, the peak of the longshore current is shifted shoreward and the magnitude of the longshore current is slightly increased in the surf zone compared to the case without roller. However, the surface roller has limited influence on the computational results for the

cross-shore current. The calculated cross-shore currents with and without roller are quite similar. The numerical model can well reproduce the longshore current. However, the calculated cross-shore current is often underestimated compared to the measurements. The undertow is not included in the model, most likely causing the differences between calculated and measured cross-shore currents.

Swash zone transport needs to be included in morphological evolution models. The sediment exchange between land and sea directly affects both the sub-aerial and sub-aquaeous evolution of the beach. In the swash zone, the frequent uprush and backwash result in high transport rates in both the cross-shore and alongshore directions. It is clearly shown in the experimental data sets obtained from the LSTF basin that the transport rate near the shoreline may be similar to the maximum values observed in the surf zone (Gravens and Wang, 2007; Nam *et al.*, 2009). Therefore, it is necessary to compute the transport rates in the swash zone, and couple those to the transport in the inner surf zone in order to realistically simulate the beach topography evolution.

The algorithm for solving the sediment volume conservation equation is an important subject. A number of numerical schemes have been introduced for solving this equation (see Callaghan *et al.*, 2006; and Long *et al.*, 2008). However, the equation is highly non-linear so it is not easy to obtain an accurate solution. For example, the Lax-Wendroff scheme was employed in many applications, but it requires that the bed celerity (Johnson and Zyserman, 2002) or bedform phase speed (Long *et al.* 2008) is determined, which may cause large errors in the calculations, if the gradient of bed forms is relatively small. Johnson and Zyserman (2002) recommended smoothing and filtering techniques to overcome the dispersion problem due to the Lax-Wendroff scheme. Recently, several high-order schemes were introduced by Callaghan *et al.* (2006) and Long *et al.* (2008) that can be applied to solve the continuity equation without resorting to smoothing or filtering techniques and that enables high accuracy solution. However, when calculating the value of the bed level at one cell, a number of values on the bed level in nearby cells need to be included. Therefore, ghost cells must be employed at open and solid boundaries (Long *et al.*, 2008), which can cause significant errors if the coastal area is complex and coastal structures are present. In this study, the first-order upwind scheme FTBS (forward in time, backward in space) was employed to solve the sediment conservation equation. Although the FTBS scheme has lower accuracy than high-order schemes, FTBS is stable and the obtained bed level changes were reasonable and in good agreement compared with the LSTF data. Furthermore, it is quite straightforward to implement and the model may be applied to complex coastal areas including structures. However, smoothing is required in the present study. In future studies, advanced numerical schemes will be continuously investigated and applied in order to obtain accurate solutions to bed level change, at the same time avoiding smoothing.

6. Conclusions

A unified numerical model of beach morphological evolution due to waves and currents was developed. It includes five sub-models, including nearshore random wave transformation, surface roller, wave-induced current, sediment transport, and morphological change models. The model was applied to simulate the beach evolution in the vicinity of coastal structures in a non-tidal environment under wave and current action.

The developed model was validated against six high-quality data sets from the experiments on the morphological impact of a T-head groin and a detached breakwater in the LSTF basin, at the Coastal and Hydraulics Laboratory, Vicksburg, Miss. The simulations showed that the model could well produce the wave field compared to the measured data. Reasonably accurate wave-induced currents were also obtained with the model, although the cross-shore currents somewhat underestimated measurements because of neglecting the undertow. The calculated beach evolution in the vicinity of the breakwater and the T-head groin agreed rather well with the measurements. Thus, it is expected that the model can be applied in coastal engineering projects for predicting the beach evolution due to waves and currents in the vicinity of coastal structures.

Acknowledgments

This work was partly funded by Sida/SAREC in the framework of the Project VS/RDE/03 "*The evolution and sustainable management in the coastal areas of Vietnam*" (PTN and LXH), partly by Lars Erik Lundberg Scholarship Foundation (PTN), partly by J. Gust. Richert Foundation (PTN), and partly by the Coastal Inlets Research Program of the U.S. Army Engineer Research and Development Center (ML and HH). Dr. Hajime Mase at Kyoto University kindly provided the source code for the EBED model. Dr. Ping Wang at Univeristy of South Florida and Mr. Mark Gravens at Coastal and Hydraulics Laboratory provided the experimental data from LSTF, which is greatly appreciated. The authors would also like to thank Dr. Nguyen Manh Hung and the late Prof. Pham Van Ninh for their great contributions to the Project VS/RDE/03. Permission was granted by Headquarters, U.S. Army Corps of Engineers, to publish this information.

References

Brøker, I., Zyserman, J., Madsen, E. Ø., Mangor, K., Jensen, J., 2007. Morphological modelling: a tool for optimisation of coastal structures. Journal of Coastal Research 23(5), 1148-1158.

Callaghan, D.P., Saint-Cast, F., Nielsen, P., Baldock, T.E., 2006. Numerical solutions of the sediment conservation law; a review and improved formulation for coastal morphological modelling. Coastal Engineering 53, 557-571.

Camenen, B., Larson, M., 2005. A general formula for non-cohesive bed load sediment transport. Estuarine, Coastal and Shelf Science 63, 249-260.

Camenen, B., Larson, M., 2007. A unified sediment transport formulation for coastal inlet application. Technical report ERDC/CHL CR-07-1, US Army Engineer Research and Development Center, Vicksburg, MS.

Dally, W. R., Brown, C. A., 1995. A modeling investigation of the breaking wave roller with application to cross-shore currents. J. Geophys. Res., 100(C12), 24873 – 24883.

Dally, W. R., Dean, R. G., Dalrymple, R. A., 1985. Wave height variation across beaches of arbitrary profile. J. Geophys. Res., 90(C6), 11917 – 11927.

De Vriend, H.J., Zyserman, J., Nicholson, J., Roelving, J.A., Péchon, P., Southgate, H.N., 1993. Medium-term 2DH coastal area modeling. Coastal Engineering 21, 193-224.

Denot, T., Aelbrecht, D., 2000. Numerical modelling of seabed evolution in the vicinity of a groin system. Proc. Coastal Structures'99, A.A. Balkema, Vol. 2, pp. 849-855.

Ding, Y., Wang, S.S.Y., Jia, Y., 2006. Development and validation of a quasi-three-dimensional coastal area morphological model. Journal of Waterway, Port, Coastal and Ocean Engineering 132(6), 462-476.

Ding, Y., Wang, S.S.Y., 2008. Development and application of coastal and estuarine morphological process modeling system. Journal of Coastal Research, Special Issue 52, 127-140.

Elder, J. W., 1959. The dispersion of marked fluid in turbulence shear flow. Journal of Fluid Mechanics 5, 544-560.

Falconer, R. A., 1980. Modelling of planform influence on circulation in Harbors. Proc., 17th Int. Conf. on Coastal Engineering, ASCE, Sydney, 2726 – 2744.

Goda, Y., 2006. Examination of the influence of several factors on longshore current computation with random waves. Coastal Engineering, 53, 157-170.

Gelfenbaum, G., Roelvink, J.A., Meijs, M., Buijsman, M., Ruggiero, P., 2003. Process-based morphological modeling of Gray Harbor inlet at decadal timescales. Proceedings of Coastal Sediments'03.

Gravens, M.B., Wang, P., 2009. Personal communication.

Gravens, M.B., Wang, P., 2007. Data report: Laboratory testing of longshore sand transport by waves and currents; morphology change behind headland structures. Technical Report, ERDC/CHL TR-07-8, Coastal and Hydraulics Laboratory, US Army Engineer Research and Development Center, Vicksburg, MS.

Gravens, M.B., Wang, P., Kraus, N.C., Hanson, H., 2006. Physical model investigation of morphology development at headland structures. Proceedings 30th International Conference on Coastal Engineering, World Scientific Press, pp. 3617–3629.

Hamilton, D.G., Ebersole, B.A., 2001. Establishing uniform longshore currents in large-scale sediment transport facility. Coastal Engineering 42 (3), 199-218.

Hanson, H., Larson, M. 1992. Overview of beach change numerical modeling. In: W. James and J. Niemczynowicz, Eds., Water, Development, and Environment, Lewis Publishers, Ann Arbor, pp 322-347.

Johnson, H.K., 2004. Coastal area morphological modelling in the vicinity of groins. Proc., 29th International Conf. on Coastal Engineering, ASCE, pp. 2646-2658.

Jonhson, H.K., Zyserman, J.A., 2002. Controlling spatial oscillations in bed level update schemes. Coastal Engineering 46, 109-126.

Johnson, H.K., Zyserman, J.A., Brøker, I., Mocke, G., Smit, F., Finch, D., 2005. Validation of a coastal area morphological model along the Dubai coast. Proceedings of Arabian Coast 2005, Dubai.

Kraus, N. C., Larson, M., 1991. NMLONG: Numerical model for simulating the longshore current; Report 1: Model development and tests. Technical Report DRP-91-1, U.S. Army Engineer Waterways Experiment Station, Vicksburg, MS.

Larson, M., Kraus, N.C., 2002. NMLONG: Numerical model for simulating longshore current; Report 2: Wave-current interaction, roller modeling, and validation of model enhancements. Technical Report ERDC/CHL TR-02-22, US Army Engineer Research and Development Center, Vicksburg, MS.

Larson, M., Wamsley, T.V., 2007. A formula for longshore sediment transport in the swash. Proc. Coastal Sediment'07, ASCE, pp. 1924-1937

Leont'yev, I.O., 1999. Modelling of morphological changes due to coastal structures. Coastal Engineering 38, 143-166.

Lesser, G.R., Roelvink, J.A, van Kester, J.A.T.M., Stelling, G.S., 2004. Development and validation of a three-dimensional morphological model. Coastal Engineering 51, 883-915.

Long, W., Kirby, J.T., Shao, Z., 2008. A numerical scheme for morphological bed level calculations. Coastal Engineering 55, 167-180.

Mase, H., 2001. Multi-directional random wave transformation model based on energy balance equation. Coastal Engineering Journal 43(4), 317-337.

Militello, A., Reed, C.W., Zundel, A.K., Kraus, N.C., 2004. Two-dimensional depth-averaged circulation model M2D: version 2.0, Report 1, Technical document and User's Guide. Technical Report ERDC/CHL TR-04-2, Coastal and Hydraulics Laboratory, US Army Engineer Research and Development Center, Vicksburg, MS.

Nam, P.T., Larson, M., Hanson, H., Hoan, L.X., 2009. A numerical model of nearshore waves, currents, and sediment transport. Coastal Engineering 56, 1084-1096.

Nam, P.T., Larson, M., 2009. A model of wave and current fields around coastal structures. Proc. Coastal Dynamics 2009, World Scientific Press, ISBN-13-978-981-4282-46-8 (with CD-ROM)

Nam, P.T., Larson, M., 2010. Model of nearshore waves and wave-induced currents around a detached breakwater. Journal of Waterway, Port, Coastal and Ocean Engineering 136 (3), 156-176.

Nicholson, J., Broker, I., Roelvink, J.A., Price, D., Tanguy, J.M., Moreno, L., 1997. Intercomparison of coastal area morphodynamic models. Coastal Engineering 31, 97-123.

Nishimura, H., 1988. Computation of neasrshore current. In: Horikawa, K. (Ed), Nearshore dynamics and coastal processes. University of Tokyo Press, Tokyo, Japan, pp. 271-291.

Reid, R.O., Bodine, B.R., 1968. Numerical model for storm surges in Galveston Bay. Journal of Waterways and Harbors Division 94 (WWI), 33-57.

Roelvink, J.A., Uittenbogaard, R.E., Liek, G.J., 1999. Morphological modelling of the impact of coastal structures. Proc. Coastal Structures'99, A.A. Balkema, Vol. 2, pp.865-871.

Saied, U.M., Tsanis, I.K., 2005. ICEM: Integrated Coastal Engineering Model. Journal of Coastal Research 21(6), 1275-1268.

Steijn, R., Roelvink, D., Rakhorst, D., Ribberink, J., Overeem, J.V., 1998. North-Coast of Texel: A comparison between reality and prediction. Proceedings 26th International Conference on Coastal Engineering, ASCE, pp. 2281-2293.

Wang, P., Ebersole, B.A., Smith, E.R., Johnson, B.D., 2002. Temporal and spatial variations of surf-zone currents and suspended sediment concentration. Coastal Engineering 46, 175-211.

Watanabe, A., Maruyama, K., Shimizu, T., Sakakiyama, T, 1986. Numerical prediction model of three-dimensional beach deformation around a structure. Coastal Engineering Journal 29, pp. 179-194.

Zanuttigh, B., 2007. Numerical modelling of the morphological response induced by low-crested structures in Lido di Dante, Italy. Coastal Engineering 54, 31-47.

Zyserman, J.A., Johnson, H.K., 2002. Modelling morphological processes in the vicinity of shore-parallel breakwaters. Coastal Engineering 45, 261-284.

Zyserman, J.A., Johnson, H.K., Zanuttigh, B., Martinelli, L., 2005. Analysis of far-field erosion induced by low-crested rubble-mound structures. Coastal Engineering 52, 977-994.